UNIVERSITY OF CALIFORNIA

Santa Barbara

N treatment performance in stormwater biofilters: Relationships between sequestered pollutants, environmental conditions, and N cycling soil bacteria.

A dissertation submitted in partial satisfaction of the

requirements for the degree Doctor of Philosophy

in Environmental Science and Management

by

Marina Feraud

Committee in charge:

Professor Patricia A. Holden, Committee Chair

Professor Arturo Keller

Professor Josh Schimel

June 2022

The dissertation of Marina Feraud is approved.

_____

Arturo Keller

_____

Josh Schimel

_____

Patricia A. Holden, Committee Chair

March 2022

N treatment performance in stormwater biofilters: Relationships between sequestered pollutants, environmental conditions, and N cycling soil bacteria.

by

Marina Feraud

ACKNOWLEDGEMENTS

I would like to thank the faculty, students and staff that have been unwavering in their support and helped me successfully complete this dissertation. To my committee: Trish Holden, Josh Schimel, and Arturo Keller, thank you for your insights, advice, and thorough reviews of my manuscripts. Thank you for challenging me to always think about the relevance of studying and answering specific scientific questions. As my advisor, Trish has always been supportive, provided thoughtful feedback, and helped steer me in the right direction. I am a better scientist thanks to her mentorship.

Funding for this research was provided by Henry Wheeler Jr. via the Urban Water Environment Project, as well as financial support extended by the Bren School of Science and Management, the Earth Research Institute, the Associated Students Coastal Fund (UCSB), The Green Initiative (UCSB), and finally the Multicampus Research Initiative (MRPI), through the project "Fighting drought with stormwater: From research to practice.

I would like to thank the staff at the Bren School and at the Earth Research Institute, who have always been patient and helped me navigate all administrative and purchasing, needs; the Cheadle Center for Biodiversity and Ecological Restoration, including Lisa Stratton, Andy Lanes, Wayne Chapman, and Ryan Lippitt, who showed me around the natural areas they managed at UCSB, and allowed me to core the soils of their bioswales; and the grounds personnel at UC Santa Barbara, UC Irvine, and UC San Diego.

To Emily Parker, Stanley Grant, Sean Ahearn, Sumant Avasarala, Andrew Mehring, Jen Le, Jessica Kurylo, Megan Rippy, Wei-Cheng Hung, Megyn Rugh, and the rest of my

MRPI colleagues, co-authors and outside collaborators, working with and learning from you has been wonderful, and I am humbled to be part of your network.

To Anne Trinh, Monika Mortimer, Dong Li, Patrick Roehrdanz, Mitchell Maier, Do Gyun Lee, Yuan Ge, John Priester, Jared Ervin, and all other Holden lab members, present or past: thanks for creating a great work atmosphere, for your invaluable help, and for always sharing your expertise. Special thanks to Laurie Van de Werfhorst, for her patience and knowledge, and for teaching me new lab skills; and to Sage Davis, who has always been ready to lend a helping hand in setting up equipment for lab classes and field research.

I am thankful for the UCSB graduate community, and especially Timnit Kefela, for being a great friend, an amazing scientist, and a talented artist to boot! To my office mates, Annette Hilton, Liviu Iancu, Becca Reynolds, Yuki Floyd, and Ying Wang, thanks for the scientific advice, talks and laughs! To the MESM and Spanish students I have had the honor to teach, thank you, I am a better teacher because of you.

Finally, none of this would have been possible without the support of my family back in Argentina, especially my parents who have stood by me every step of the way, my brother, and my extended family. I also thank my family away from home in Santa Barbara, and friends near and far (Argentina, Ireland, Germany, Switzerland, and across the world), who encouraged me when I was struggling and were always there for me. It’s taken a few long years, but I am finally ready for a new adventure!

VITA OF MARINA FERAUD

March 2022

EDUCATION

PhD	University of California, Santa Barbara, Bren School of Environmental Science & Management (2022)
MESM	University of California, Santa Barbara, Bren School of Environmental Science & Management (2012)
B.S.	Instituto Tecnológico Buenos Aires (Buenos Aires Technological Institute), Argentina. Chemical Engineering (2003)

RESEARCH INTERESTS

My research focus is bioretention systems for stormwater management. I evaluate how nitrogen cycling, and bacteria mediating N transformations are influenced by environmental conditions, and stormwater-derived pollutants, such as metals, that accumulate in soils.

GRANTS & FELLOWSHIPS

2020	Bren School Fellowship ($8000)
2017, 2016, 2015, 2014	Earth Research Institute, Summer Graduate Student Fellowship (total of 4 awards, $5200)
2015	The Green Initiative Fund, UCSB ($650)
2014	The Coastal Fund, Associated Students UCSB ($4885)
2011	Bren School, Summer Internship Fellowship ($2000)
2011	Tahoe-Baikal Institute, Financial Aid for Summer Program ($2000)

AWARDS

2016	Bren School Ph.D. Symposium, runner-up for best short talk
2012	Bren School, Academic Achievement Award (MESM program)

TEACHING EXPERIENCE

2022, 2015, 2014	Environmental Biogeochemistry
2021	Spanish 1
2019, 2015, 2014	Microbial Processes (Lab)
2018, 2016	Biological Waste Treatment
2017, 2016	Fate & Transport of Pollutants in the Environment (Lab)

PUBLICATIONS

Hung, W-C., Rugh, M., **Feraud, M**., Avasarala, S., Kurylo, K., Gutierrez, M., Jimenez, K. Truong, N. Holden, P. A., Grant, S. B., Liu, H., Ambrose, R. F., and Jay, J. A. (2022) Influence of soil characteristics and metal(loid)s on antibiotic resistance genes in green stormwater infrastructure in Southern California. J. Hazard. Mater., 424 (B), 127469.

Li, D., Van De Werfhorst, L. C., Rugh, M. B., **Feraud, M**., Hung, W-C, Jay, J., Cao, Y, Parker, E. A., Grant, S. B., and Holden, P. A. (2021). Limited bacterial removal in full-scale stormwater biofilters as evidenced by community sequencing analysis. *Environ. Sci. Technol.* 55 (13), 9199-9208.

Feraud, M. and Holden, P. A. (2021). Evaluating the relationships between specific drainage area characteristics and soil metal concentrations in long-established bioswales receiving suburban stormwater runoff. *Sci. Total Environ*., 757, 143778.

Parker, E. A., Grant, S. B., Cao, Y., Rippy, M. A., McGuire, K. J., Holden, P. A., **Feraud, M.** et al. (2021). Predicting solute transport through green stormwater infrastructure with unsteady transit time distribution theory. *Water Resour. Res*., 57 (2), e2020WR028579.

Aceves-Bueno, E., Adeleye, A. S., **Feraud, M.** et al. (2017). The accuracy of citizen science data: A quantitative review. *Bull. Ecol. Soc. Am*., 98 (4), 278-290.

Roehrdanz, P. R., **Feraud, M.,** Gyun Lee, D., … & Holden, P. A. (2017). Spatial models of sewer pipe leakage predict the occurrence of wastewater indicators in urban groundwater. *Environ. Sci. Tech*., 51 (3), 1213-1223.

Gyun Lee, D., Roehrdanz, P. R., **Feraud, M.**, … & Holden, P. A. (2015). Wastewater compounds in urban shallow groundwater wells correspond to exfiltration probabilities of nearby sewers. *Water Res.*, 85, 467-475.

Aceves-Bueno, E., Adeleye, A. S., Bradley, D., Brandt, W.T., Callery, P., **Feraud, M.** et al. (2015). Citizen science as a tool for overcoming insufficient monitoring and inadequate stakeholder buy-in in adaptive management: Criteria and Evidence. *Ecosystems*,18(3): 493-506.

MANUSCRIPTS IN PREPARATION

Feraud, M. Stormwater biofilter response to high nitrogen loading under transient flow conditions: ammonium and nitrate fates, and N_2O emissions *(In prep)*.

Feraud, M. N cycling in stormwater bioretention: Relationships between environmental conditions, surface soil metals, and N cycling bacteria *(In prep)*.

PROFESSIONAL PRESENTATIONS

2019 **Feraud, M.** & Holden, P. A. "Natural treatment systems for urban stormwater runoff: relationships between soil bacterial communities, environmental conditions and nitrogen cycling". ACS Fall Meeting 2019, San Diego, CA.

2019 **Feraud, M.** "Nitrogen cycling in natural treatment systems for urban stormwater runoff: Relationships between sequestered pollutants, environmental conditions, and soil bacterial communities". Multicampus Research Programs and Initiatives (MRPI) "Fighting drought with stormwater" Project Retreat, Costa Mesa, CA.

2016 **Feraud, M.** "Metal build-up in stormwater bioswales". Bren PhD Student Symposium, UC Santa Barbara, CA.

2015 Gyun Lee, D., Roehrdanz, P. R., **Feraud, M.** "Water Quality in Urban Areas: Evaluating shallow groundwater contamination due to leaking sanitary sewers". Bren School Annual Recognition Dinner, UC Santa Barbara, CA.

2015 Gyun Lee, D., Roehrdanz, P. R., **Feraud, M**., … & Holden, P. A. "Wastewater compounds in urban shallow groundwater wells correspond to exfiltration probabilities of nearby sewers". American Water Resources Association Spring Specialty Conference "Water for urban areas: Managing risks and building resiliency", Los Angeles, CA.

SERVICE

Engineers without borders, UCSB Chapter. Water sanitation and efficient stoves in Perú.

PROFESSIONAL EMPLOYMENT

Graduate Researcher, University of California, Santa Barbara, Bren School of Environmental Science and Management, Santa Barbara, CA (Jan 2013 – Mar 2022). Researched stormwater bioretention, within the Multicampus Research Programs and Initiatives (MRPI) project "Fighting drought with stormwater: From research to practice. Collaborated on Urban Water Environment research, assessing interactions between shallow groundwater and leaking sewers.

Lake Restoration Intern, Tahoe Baikal Institute: Lake Tahoe, CA/ Lake Baikal, Russia (Jun 2011 – Aug 2011). Volunteered in restoration projects in Lake Tahoe and Lake Baikal. Assessed erosion in cut-bank slopes in Lake Tahoe.

Nature Interpreter and English Translator, Hydrosport S. R. L.: Patagonia, Argentina (Jun 2009 – October 2009). Educated visitors on local marine flora and fauna, conservation, and sustainability during whale-watching trips in a Southern Right whale breeding area.

Quality Assurance Analyst, Merck Sharp & Dohme: Buenos Aires, Argentina (Jul 2005 – Aug 2008). Reviewed and approved packaging materials for new pharmaceutical drugs, performed quality control in the lab, released products after quality assurance checks, and completed internal and third-party Quality audits.

Safety & Environment Analyst, *Merck Sharp & Dohme*: Buenos Aires, Argentina (April 2003 – Jun 2005). Monitored water quality of drinking water network, groundwater wells and wastewater treatment plant. Implemented standard operating procedures and performed audits in safety & environmental compliance.

ABSTRACT

N treatment performance in stormwater biofilters: Relationships between sequestered pollutants, environmental conditions, and N cycling soil bacteria.

By

Marina Feraud

Stormwater runoff imposes large hydrologic and nutrient imbalances in urban areas through the delivery of large pollutant loads to surface waters. To mitigate this pollution, green stormwater infrastructure (GSI) approaches are increasingly used. Nitrogen (N) removal in GSI varies, depending on soil characteristics and plant species. However, GSI may often leach nitrate and export N. Removal of N is mediated by nitrifying and denitrifying bacteria; whether these bacteria are affected by retained soil contaminants, such as trace metals, is unknown. If accumulated soil metals reach levels that inhibit N cycling microorganisms, N treatment may be reduced. Further N treatment uncertainty arises due to limitations from prior studies, which have been mostly performed under steady-state conditions, in controlled lab environments, or have insufficiently considered transient flow conditions. A detailed understanding of the timing and magnitude of N processes across transient storms is needed to examine the role of biofilters as sources or sinks of aqueous and gaseous N, and to determine how biofilters should be managed to mitigate N export.

This doctoral research aims to address these knowledge gaps by 1) evaluating total and bioavailable metal concentrations in soils of field-scale GSI, and how accumulated metals may be predicted from drainage area characteristics, 2) assessing how soil properties, as well as total

and bioavailable metal concentrations, influence nitrifying and denitrifying bacteria across representative GSI, and 3) comprehensively assessing N fates and N transformation processes within and in between storms in a field-scale GSI receiving high-flow storm events. Results show that metals can accumulate in GSI soils, and that total metals are significantly correlated to the ratio of impervious drainage area to GSI area. Thus, monitoring efforts may prioritize soils with highest impervious ratios. Results from representative GSI show that linear regression models including soil properties and metal concentrations provide good estimates of nitrifying and denitrifying gene abundances in soils. Bioavailable fractions of Cd and Pb seem to reduce gene abundances of denitrifying microorganisms (*nir*S, *nos*Z), with implications for N_2O release. In contrast, total Cu, Ni and V appear to exert a positive influence on functional gene abundances, suggesting metal limitation in soils. Results reinforce including bioavailable metal fractions in metal risk assessments. In the final study, chemical, bacterial, and stable isotope data show that denitrification is limited even for high-frequency, large storms, and that GSI systems perform poorly, in terms of N removal, when challenged with a large transient storm, behaving as persistent N sources in subsequent storms. I propose an alternate design consisting of a treatment train of a real-time control stormwater capture system, sequentially followed by a fast-draining cell, and a slow-draining cell.

This dissertation has advanced the understanding of N processing in GSI; the potential interactions between soil nitrifying and denitrifying bacteria and accumulated soil metals has also been evaluated. Recommendations were provided to prioritize metal risk assessments, improve N treatment in GSI, and minimize N export and undesirable environmental consequences.

TABLE OF CONTENTS

Chapter 1. Introduction

1.1. Stormwater runoff pollution and green stormwater infrastructure

Currently, human nitrogen (N) inputs to the environment are beyond sustainability targets proposed in the planetary boundaries framework, so that human activities release N beyond safe environmental limits (Steffen et al. 2015). These imbalances are clearly represented in stormwater runoff in urban areas (Payne et al. 2014a). Urban runoff is larger, faster, more ephemeral, and more polluted than runoff from undisturbed areas (Walsh et al. 2004, NRC 2009, Payne et al. 2014a); runoff also delivers N (and other pollutants) to surface waters, impacting its trophic status and water quality (NRC 2009). These detrimental effects are due in part to "drainage efficiency" approaches that quickly route polluted stormwater into receiving waters, degrading urban watersheds in the process (Burns et al. 2012, Jones and Davis 2013). As storms become more frequent and intense due to climate change, watersheds may be further degraded. Thus, how to mitigate stormwater pollution in urban areas is a central challenge. There is a critical need for flexible stormwater management approaches that can adapt to changing storm conditions and increasing environmental degradation, so that anthropogenic N inputs to the environment may be minimized.

Green stormwater infrastructure (GSI) practices are flexible, nature-based solutions that are increasingly used to manage stormwater runoff. These engineered designs combine natural components like sand or soils, plants, and soil microorganisms to capture and treat runoff onsite or near the point of generation (Payne et al. 2014a). When runoff enters a GSI system, runoff volumes are reduced via infiltration and evapotranspiration, while water quality may be improved via abiotic and biotic processes that decrease pollutant loads (Ahiablame et al. 2012, Payne et al. 2014a, Ambrose and Winfrey 2015).

1.2. Pollutant removal, N cycling, and metals in GSI

Stormwater pollutants, upon entering a GSI system, may be filtered out, adsorb onto soil components, be taken up by plants, or be removed via abiotic and biotic transformations (Hsieh and Davis 2005; Davis et al. 2006). These processes remove suspended solids, fecal bacteria, and metals from stormwater runoff with varying success (Davis et al. 2003, Payne et al. 2014a). GSI systems, however, may fail to remove total nitrogen (N), often due to bacterial transformations that generate nitrate (NO_3^-), a critical and mobile water pollutant that is easily leached from GSI soils and may result in net N export (Davis et al. 2001a, Hatt et al. 2007, Bratières et al. 2008, Li and Davis 2009). Subsequent transport of exported N to surface waters is linked to eutrophication and degraded water quality (NRC 2009, Walsh et al. 2004). One approach to mitigate N pollution, is to permanently remove N from runoff by promoting denitrification in GSI soils (Zinger et al. 2013, Payne et al. 2014a). During this anaerobic process, NO_3^- is sequentially reduced to nitrite (NO_2^-), nitric oxide (NO), nitrous oxide (N_2O), and finally dinitrogen (N_2) (Zumft 1997). Incomplete denitrification, however, may occur since approximately one third of bacteria may not possess the *nos*Z gene that encodes the enzymes catalyzing the reduction of N_2O to N_2 (Philippot et al. 2011). As a result, N_2O, a potent greenhouse gas contributing to climate change (IPCC 2013), may be released. N_2O can also be emitted during nitrification, a process which warrants further study in GSI (Bateman & Baggs 2005, Butterbach-Bahl et al. 2013).

How N is processed in GSI depends largely on the prevailing environmental conditions, and the presence and activity of N cycling bacteria such as nitrifiers and denitrifiers. Prior GSI studies, however, have focused almost entirely on design features to enhance denitrification, such as including a saturated zone amended with organic carbon within GSI

soil (Kim et al. 2003, Dietz and Clausen 2006, Blecken et al. 2009, Zinger et al. 2013). These modifications provide more favorable conditions for denitrification and presumably boost the presence and activity of denitrifying bacteria (Kim et al 2003, Payne et al. 2014a). Not surprisingly, bioretention studies show increased abundance of denitrifying functional genes and potential denitrifying activities in systems that are wetter for longer times (Chen et al. 2013, Morse et al. 2017, Waller et al. 2018), and in soils with higher inorganic N and organic C concentrations (Waller et al. 2018). Denitrifying and nitrifying gene abundances in GSI may also be greater near surface soils and decrease with depth, consistent with patterns for total bacterial abundance (Chen et al. 2013, Waller et al. 2018). What is not known is how denitrifying and nitrifying bacteria are affected by other contaminants, such as trace metals that are retained in GSI soil.

Metal contaminants persist in the environment and may negatively affect soil bacteria (Giller et al. 1998, Holtan-Hartwig et al. 2002, Wang et al. 2007, Alloway 2013, Singh et al. 2014). Metals may also significantly accumulate in GSI soils (Davis et al. 2001b, Hsieh and Davis 2005, Sun and Davis 2007, Blecken et al. 2009, Lim et al. 2015, Tedoldi et al. 2016), so that there is some concern regarding long-term GSI sustainability (Jones and Davis 2013, Tedoldi et al. 2016). However, prior studies characterizing metal accumulation in GSI soils have often been short-term (Sun and Davis 2007, Li and Davis 2008), focused mostly on factors that influence metal loading (Tedoldi et al.2017), or not considered readily available metal fractions (Ingvertsen et al. 2012, Horstmeyer et al. 2016, Johnson and Hunt 2016). Overall, there is no clear rationale for prioritizing monitoring of accumulated metals. Also unknown is whether metals are accumulating to levels that may inhibit sensitive N cycling microorganisms. If accumulated soil metals preferentially inhibit nitrification, ammonium

may accumulate to toxic levels. If instead, denitrification is more strongly inhibited, nitrate may accumulate and exacerbate nitrate leaching. These potential, and so far unquantified, outcomes matter from an N removal perspective.

Further efforts to improve N removal are also hindered by the lack of comprehensive studies exploring N fates and transformations in GSI. Prior biofilter N processing studies, generally do not emulate realistic biofilter hydrology due to their small scales, isolated analysis of single storms, or use of steady state, versus more realistic transient flow conditions (Davis et al. 2007, Hatt et al. 2009, Brown and Hunt 2011, Li and Davis 2014, Payne et al. 2014b, Burgis et al. 2020).

Specifically, in lab columns dosed with a standard rate of stormwater (steady-state) there is a constant depth of pooled water over the soil surface, so that flow through the biofilter and the onset and duration of saturated soil conditions differ from usual storms. In a typical storm, runoff flow gradually increases, peaks, and then declines, so that both biofilter inflow and effluent flows are time-varying. These flow differences may produce different redox conditions, influencing the prevalence of aerobic nitrification or anaerobic denitrification. The more permanently wet soils under steady-state flow may promote more denitrification than transiently wet soils, so that many biofilter studies (e.g., Davis et al. 2001b and 2007, Hsieh and Davis 2005) may overestimate N removal.

Better N removal estimates may be derived from field studies that capture real storm events, but such studies often focus on single storms (Brown and Hunt 2011, Hatt et al. 2009, Hunt et al. 2006, Passeport et al. 2009), overlooking the effects of frequent drying and rewetting cycles on C and N processing; the influence of the antecedent dry period on nitrate formation is also disregarded. When soils are rewet, both C and N mineralization typically

increase for a short period of time. This pulse is likely due to microbial cell lysis, release of intracellular solutes, and exposure of soil organic matter that was previously physically protected (Fierer and Schimel 2002). The longer-term implications of frequent drying and rewetting cycles are reduced C mineralization, and increased activity of autotrophic nitrifiers (Fierer and Schimel 2002). Such C and N dynamics likely influence N processing and removal in biofilters. These potential effects must be evaluated via a suite of storm events because N exported during a specific storm depends on prior storm event characteristics, and weather conditions between storm events (Brown et al. 2013).

GSI studies on multiple storm events show that nitrate can be formed and accumulate during dry periods (Hatt et al. 2007, Brown et al. 2013, Li and Davis 2014), and that this accumulation increases with the antecedent dry period (Hatt et al. 2007). In these studies, N loading has followed median runoff concentrations; differences in N processing due to different N inputs have also not been evaluated. Higher nitrate loading is expected to result in higher denitrification within a storm (Payne et al. 2014b, Burgis et al. 2020), while higher N loading may export more N in subsequent storms due to nitrate formation within GSI soils (Davis et al. 2001b, Brown et al. 2013, Payne et al. 2014). Due to prior study limitations, we have an incomplete understanding for how GSI systems will process N when they receive a large, polluted storm under realistic transient flow conditions, as might be seen during a "first-flush" event. How these nutrient inputs will prime biofilter N processing in subsequent storms, and influence N treatment variability, is also unknown. Such knowledge is needed to precisely examine the role of biofilters as sources of aqueous and gaseous N, internal N processing in biofilters, and to what extent typical biofilter designs support N removal.

1.3 Dissertation focus and organization

Addressing the previously identified knowledge gaps is the focus of this doctoral dissertation research. Specifically, this research evaluates to what extent trace metals accumulate in soils of field-scale stormwater biofilters, and how these sequestered pollutants interact with soil properties and N cycling bacteria to affect N treatment. Additionally, this research advances knowledge of N fates in stormwater biofilters under realistic transient flow conditions, and provides recommendations on how N export, which is frequent in many stormwater biofilter designs, may be mitigated.

I focused on trace metals because they are common stormwater pollutants that are not readily transformed in biofilter soils and may thus accumulate. The potential harmful effects of metals on bacteria, including nitrifying and denitrifying bacteria, are well established. The effects of accumulated metals on biofilters soils, however, have not been examined through the lens of nitrifying and denitrifying bacteria, including how the N processing that these bacteria mediate is influenced by the pollutants that biofilters are designed to capture.

This dissertation describes three projects on stormwater biofilters that address research questions relating to the potential influence of trace metals on N cycling bacteria and N treatment, and on the fates of N for dynamic influent conditions.

The first project (Chapter 2) investigates soil metal accumulation in four established bioswales, addressing the questions: How do drainage area characteristics and location within the biofilter influence concentrations of soil accumulated metals? Given the observed and future projected metal accumulation, what are the risks to soil quality and soil biota? A simple model of metal accumulation was proposed based on the observed relationship between the ratio of impervious drainage area to bioswale area. The proposed model may

inform maintenance activities by identifying hot spots of metal pollution and may also guide future sampling and monitoring efforts evaluating the risk of accumulated metals to soil bacteria. This chapter has been published in the journal Science of the Total Environment (Feraud and Holden 2021).

The observation that soil metal concentrations were positively correlated to impervious drainage area served to guide biofilter site selection in the second, follow-up study (Chapter 3) performed on six representative GSI systems, addressing the question: How do soil properties and accumulated metals interactively act upon nitrifying and denitrifying bacteria, N_2O emissions, and N treatment in GSI systems? I assessed the relationships between soil properties, soil metal concentrations, the abundance and potential activity of nitrifying and denitrifying bacteria, and N_2O emissions across three time points. This analysis revealed which soil properties and soil metals most influenced nitrifiers and denitrifiers and N cycling, and whether a positive or negative influence was exerted.

The previous chapters evaluated potential effects on N treatment performance through the study of accumulated soil pollutants, and the abundance and activity of N cycling bacteria, but did not directly measure N entering and leaving a biofilter. In the third study (Chapter 4), I evaluated N fates in biofilters operating under transient flow conditions for a worst-case scenario including high-flow, high-nutrient loading storms. This study addresses the questions: How do full-scale biofilters respond to dynamic influent conditions, and what is their role as sources of aqueous and gaseous N when they are experiencing high-flow events? Embedded questions are: What are the predominant transformation processes within and in-between storms, and what is the importance of *in situ* NH_4^+, and NO_3^- generation versus influent inputs? I evaluated NH_4^+ and NO_3^- inflow and outflow data, soil properties,

greenhouse gas emissions, dual NO_3^- isotope ratios, and bacterial parameters to determine N fates, and the predominance of different N processes. Finally, I provided design recommendations to mitigate N export.

The final chapter (Chapter 5) synthesizes the major findings of this dissertation research and identifies directions for future work.

1.4 References

Ahiablame, L. M., Engel, B. A., and Chaubey, I. (2012). Effectiveness of low impact development practices: literature review and suggestions for future research. *Water Air Soil Pollut*., 223(7), 4253-4273.

Alloway, B. J. (2013). Heavy Metals in Soils, 3rd ed. Dordrecht, Netherlands: Springer Science + Business Media.

Ambrose, R. F., and Winfrey, B. K. (2015). Comparison of stormwater biofiltration systems in Southeast Australia and Southern California. *Wiley Interdiscip. Rev.: Water, 2*(2), 131-146.

Bateman, E. J., and Baggs, E. M. (2005). Contributions of nitrification and denitrification to N_2O emissions from soils at different water-filled pore space. *Biol. Fertil. Soils*, 41(6), 379-388.

Blecken, G. T., Zinger, Y., Deletic, A., Fletcher, T. D., and Viklander, M. (2009). Impact of a submerged zone and a carbon source on heavy metal removal in stormwater biofilters. *Ecol. Eng.*, 35(5), 769-778.

Bratières, K., Fletcher, T. D., Deletic, A. and Zinger, Y. (2008). Nutrient and sediment removal by stormwater biofilters: A large-scale design optimisation study. *Water Res.*, 42, 3930-3940.

Brown, R. A., and Hunt, W. F. (2011). Impacts of media depth on effluent water quality and hydrologic performance of undersized bioretention cells. *J. Irrig. Drain. Eng.*, 137(3), 132-143.

Brown, R. A., Birgand, F., and Hunt, W. F. (2013). Analysis of consecutive events for nutrient and sediment treatment in field-monitored bioretention cells. *Water Air Soil Pollut.*, 224(6), 1-14.

Burgis, C. R., Hayes, G. M., Zhang, W., Henderson, D. A., Macko, S. A., and Smith, J. A. (2020). Tracking denitrification in green stormwater infrastructure with dual nitrate stable isotopes. *Sci. Total Environ.*, 747, 141281.

Burns, M. J., Fletcher, T. D., Walsh, C. J., Ladson, A. R., and Hatt, B. E. (2012). Hydrologic shortcomings of conventional urban stormwater management and opportunities for reform. *Lands. Urban Plan.*, 105(3), 230-240.

Butterbach-Bahl, K., Baggs, E. M., Dannenmann, M., Kiese, R., and Zechmeister-Boltenstern, S. (2013). Nitrous oxide emissions from soils: how well do we understand the processes and their controls? *Phil. Trans. R. Soc. B*, 368(1621), 20130122.

Chen, X., Peltier, E., Sturm, B. S., and Young, C. B. (2013). Nitrogen removal and nitrifying and denitrifying bacteria quantification in a stormwater bioretention system. *Water Res.*, 47(4), 1691-1700.

Davis, A. P. (2007). Field performance of bioretention: water quality. *Environ. Eng. Sci.*, 24(8), 1048-1064.

Davis, A. P., Shokouhian M., Sharma H., and Minami C. (2001a). Laboratory study of biological retention for urban stormwater management. *Water Environ. Res.*, 73(1), 5-14.

Davis, A. P., Shokouhian, M., and Ni, S. (2001b). Loading estimates of lead, copper, cadmium, and zinc in urban runoff from specific sources. *Chemosphere,* 44(5), 997-1009.

Davis, A. P., Shokouhian, M., Sharma, H., Minami, C., and Winogradoff, D. (2003). Water quality improvement through bioretention: Lead, copper, and zinc removal. *Water Environ. Res., 75*(1), 73-82.

Davis, A. P., Shokouhian, M., Sharma, H., and Minami, C. (2006). Water quality improvement through bioretention media: Nitrogen and phosphorus removal. *Water Environ. Res., 78*(3), 284-293.

Dietz, M. E., and Clausen, J. C. (2006). Saturation to improve pollutant retention in a rain garden. *Environ. Sci. Technol.,* 40(4), 1335-1340.

Fierer, N. and Schimel, J. P. (2002). Effects of drying–rewetting frequency on soil carbon and nitrogen transformations. *Soil Biol. Biochem.*, 34(6), 777-787.

Giller, K. E., Witter, E., and Mcgrath, S. P. (1998). Toxicity of heavy metals to microorganisms and microbial processes in agricultural soils: a review. *Soil Biol. Biochem.,* 30(10), 1389-1414.

Hatt, B. E., Fletcher, T. D., and Deletic, A. (2007). Hydraulic and pollutant removal performance of stormwater filters under variable wetting and drying regimes. *Water Sci. Technol.*, 56(12), 11-19.

Hatt, B. E., Fletcher, T. D., and Deletic, A. (2008). Hydraulic and pollutant removal performance of fine media stormwater filtration systems. *Environ. Sci. Technol.*, 42(7), 2535-2541.

Hatt, B. E., Fletcher, T. D., and Deletic, A. (2009). Hydrologic and pollutant removal performance of stormwater biofiltration systems at the field scale. *J. Hydrol.*, 365(3), 310-321.

Holtan-Hartwig, L., Bechmann, M., Høyås, T. R., Linjordet, R., and Bakken, L. R. (2002). Heavy metals tolerance of soil denitrifying communities: N_2O dynamics. *Soil Biol. Biochem.*, 34(8), 1181-1190.

Horstmeyer, N., Huber, M., Drewes, J. E., and Helmreich, B. (2016). Evaluation of site-specific factors influencing heavy metal contents in the topsoil of vegetated infiltration swales. *Sci. Tot. Environ.*, 560, 19-28.

Hsieh, C. H., and Davis, A. P. (2005). Evaluation and optimization of bioretention media for treatment of urban storm water runoff. *J. Environ. Eng.,* 131(11), 1521-1531.

Hunt, W. F., Jarrett, A. R., Smith, J. T., and Sharkey, L. J. (2006). Evaluating bioretention hydrology and nutrient removal at three field sites in North Carolina. *J. Irrig. Drain. Eng.,* 132(6), 600-608.

Ingvertsen, S. T., Cederkvist, K., Regent, Y., Sommer, H., Magid, J., and Jensen, M. B. (2012). Assessment of existing roadside swales with engineered filter soil: I. Characterization and lifetime expectancy. *J. Environ. Qual.*, 41(6), 1960-1969.

IPCC (2013): Climate Change 2013: The Physical Science Basis. Contribution of Working Group I to the Fifth Assessment Report of the Intergovernmental Panel on Climate Change [Stocker, T.F., D. Qin, G.-K. Plattner, M. Tignor, S.K. Allen, J. Boschung, A. Nauels, Y. Xia, V. Bex and P.M. Midgley (eds.)]. Cambridge University Press, Cambridge, United Kingdom and New York, NY, USA, 1535 pp.

Jones, P. S., and Davis, A. P. (2013). Spatial accumulation and strength of affiliation of heavy metals in bioretention media. *J. Environ. Eng.*, 139, 479-487.

Johnson, J. P., and Hunt, W. F. (2016). Evaluating the spatial distribution of pollutants and associated maintenance requirements in an 11 year-old bioretention cell in urban Charlotte, NC. *J. Environ. Manage.*, 18 (2), 363-370.

Kim, H., Seagren, E. A., and Davis, A. P. (2003). Engineered bioretention for removal of nitrate from stormwater runoff. *Water Environ. Res.*, 75(4), 355-367.

Li, H., and Davis, A. P. (2008). Heavy metal capture and accumulation in bioretention media. *Environ. Sci. Technol.*, 42(14), 5247-5253.

Li, L. and Davis, A. P. (2014). Urban stormwater runoff nitrogen composition and fate in bioretention systems. *Environ. Sci. Technol*. 48(96), 3403-3410.

Lim, H. S., Lim, W., Hu, J. Y., Ziegler, A., and Ong, S. L. (2015). Comparison of filter media materials for heavy metal removal from urban stormwater runoff using biofiltration systems. *J. Environ. Manage.* 147, 24-33.

Morse, N. R., McPhillips, L. E., Shapleigh, J. P., and Walter, M. T. (2017). The role of denitrification in stormwater detention basin treatment of nitrogen. *Environ. Sci. Technol.*, 51(14), 7928-7935.

National Research Council (NRC) (2009). Urban Stormwater Management in the United States. Washington, DC: The National Academies Press.

Passeport, E., Hunt, W. F., Line, D. E., Smith, R. A., and Brown, R. A. (2009). Field study of the ability of two grassed bioretention cells to reduce storm-water runoff pollution. *J. Irrig. Drain. Eng*., 135(4), 505-510.

Payne, E. G., Fletcher, T. D., Cook, P. L., Deletic, A., and Hatt, B. E. (2014a). Processes and drivers of nitrogen removal in stormwater biofiltration. *Crit. Rev. Environ. Sci. Technol.*, 44(7), 796-846.

Payne, E. G., Fletcher, T. D., Russell, D. G., Grace, M. R., Cavagnaro, T. R., Evrard, V., Deletic, A., Hatt, B. E, and Cook, P. L. M. (2014b). Temporary storage or permanent removal? The division of nitrogen between biotic assimilation and denitrification in stormwater biofiltration systems. *PloS One, 9*(3), e90890.

Philippot, L., Andert, J., Jones, C.M., Bru, D. and Hallin, S. (2011). Importance of denitrifiers lacking the genes encoding the nitrous oxide reductase for N_2O emissions from soil. *Glob. Chang. Biol.*, 17(3), 1497-1504.

Singh, B.K., Quince, C., Macdonald, C.A., Khachane, A., Thomas, N., Al-Soud, W.A., Sørensen, S.J., He, Z., White, D., Sinclair, A. and Crooks, B. (2014). Loss of microbial diversity in soils is coincident with reductions in some specialized functions. *Environ. Microbiol.*, 16(8), 2408-2420.

Steffen, W., Richardson, K., Rockström, J., Cornell, S.E., Fetzer, I., Bennett, E.M., Biggs, R., Carpenter, S.R., De Vries, W., De Wit, C.A. and Folke, C. (2015). Planetary boundaries: Guiding human development on a changing planet. *Science*, 347(6223), 1259855.

Sun, X., and Davis, A. P. (2007). Heavy metal fates in laboratory bioretention systems. *Chemosphere*, 66(9), 1601-1609.

Tedoldi, D., Chebbo, G., Pierlot, D., Kovacs, Y., and Gromaire, M. C. (2016). Impact of runoff infiltration on contaminant accumulation and transport in the soil/filter media of sustainable urban drainage systems: a literature review. *Sci. Total Environ.*, 569, 904-926.

Tedoldi, D., Chebbo, G., Pierlot, D., Branchu, P., Kovacs, Y., and Gromaire, M. C. (2017). Spatial distribution of heavy metals in the surface soil of source-control stormwater infiltration devices – Inter-site comparison. *Sci. Total Environ.*, 579, 881-892.

Waller, L. J., Evanylo, G. K., Krometis, L. A. H., Strickland, M. S., Wynn-Thompson, T., and Badgley, B. D. (2018). Engineered and environmental controls of microbial denitrification in established bioretention cells. *Environ. Sci. Technol., 52*(9), 5358-5366.

Walsh, C.J., Leonard, A.W., Ladson, A.R., and Fletcher, T.D. (2004). Urban stormwater and the ecology of streams. Cooperative Research Centre for Freshwater Ecology and Cooperative Research Centre for Catchment Hydrology, Canberra, Australia.

Wang, Y., Shi, J., Wang, H., Lin, Q., Chen, X., and Chen, Y. (2007). The influence of soil heavy metals pollution on soil microbial biomass, enzyme activity, and community composition near a copper smelter. *Ecotoxicol. Environ. Saf.*, 67(1), 75-81.

Zinger, Y., Blecken, G. T., Fletcher, T. D., Viklander, M., and Deletic, A. (2013). Optimising nitrogen removal in existing stormwater biofilters: Benefits and tradeoffs of a retrofitted saturated zone. *Ecol. Eng.*, 51, 75-82.

Zumft, W. G. 1997. The denitrifying prokaryotes, p. 443-582. *In* A. Balows, H. G. Truper, M. Dworkin, W. Harder, and K.-H. Schleifer (ed.), The prokaryotes. Springer, Heidelberg, Germany.

.

Chapter 2. Evaluating the relationships between specific drainage area characteristics and soil metal concentrations in long-established bioswales receiving suburban stormwater runoff

This chapter has been published in the journal Sci. Tot. Environ.

Abstract

Bioswales are used to attenuate stormwater pollution, but their long-term sustainability regarding sequestered metals is relatively unknown, and a clear rationale for prioritizing soil management is lacking. Impervious areas draining into four 14-year-old suburban bioswales were delineated, for which surface soils (top 10 cm; 72 samples) were sampled; soils from 4 adjacent reference sites were also sampled. Total and water soluble metals (Cd, Cu, Pb, Zn) were quantified, and the relationships between metal concentrations and drainage area characteristics evaluated. Annual metal loads were estimated using regional runoff data to simulate current and future metal concentrations; risks to soil biota were assessed by comparing metal concentrations to ecological screening levels. The drainage areas' percent imperviousness (37–71%) and ratios of impervious drainage area to bioswale area (2.0–5.7) varied, owing to differing proportions of rooftops, paved surfaces, lawns, and natural soils. Total Cu and Zn ranged from 10.0 to 43.2 mg/kg dry soil, and 15.6 to 129.5 mg/kg dry soil,

respectively. Across all bioswales, total Zn was positively correlated to percent impervious area (r = 0.32, p = 0.0073), the ratio of connected impervious drainage area to infiltration area (r = 0.32, p = 0.0073), and percent drainage area as paved surfaces (r = 0.46, p = 5.6 E-05), but negatively correlated to percent drainage area as lawns (r = −0.48; p = 2.4 E-05). Water soluble metal concentrations were orders of magnitude lower than total metals. Given annual metal loads (0.2–0.4 mg Cu/kg dry soil; 1.5–3.1 mg Zn/kg dry soil), replacing bioswale soils to constrain metal concentrations would be unnecessary for decades. Taken together, this study proposes a transferable approach of estimating, then verifying via sampling and analysis, bioswale soil metal concentrations, such that soil management decisions can be benchmarked to ecological screening levels.

2.1. Introduction

Urbanization creates and extends impervious areas by replacing natural vegetation with paved roads, roofs, parking lots and other hard surfaces that reduce infiltration and groundwater recharge, and increase stormwater runoff (Miller et al., 2014). As runoff flows overland, it incorporates pollutants deposited during dry weather, including sediments, nutrients, and metals, which can deteriorate surface water quality (NRC, 2009). To mitigate stormwater pollution, "green" and sustainable stormwater infrastructure approaches, such as bioinfiltration using biofilters and bioswales, are increasingly implemented (Jones and Davis, 2013). Bioinfiltration systems consist of excavated basins, which may or may not be vegetated, and are filled with native soil or a specified filter media (sand, compost, mulch), that sometimes is augmented with amendments such as biochar to enhance pollutant removal (Mohanty et al., 2018; Boehm et al., 2020). Pollutants in bioinfiltration systems are removed using physical, chemical and biological processes to capture, infiltrate and remediate polluted stormwater runoff (Ahiablame et al., 2012; Ambrose and Winfrey, 2015). However, there is some concern regarding the function of bioinfiltration approaches, including the fates of stormwater-derived pollutants, such as heavy metals (Li and Davis, 2008; Jones and Davis, 2013; Tedoldi et al., 2016).

Heavy metals are of concern because they persist in the environment (Giller et al., 2009) and are effectively retained in bioinfiltration soils in lab studies (e.g. Davis et al., 2003; Blecken et al., 2009; Lim et al., 2015) and at field scales (e.g. Li and Davis, 2008; Hatt et al., 2009). Metals are largely captured near stormwater runoff inlets, so that soil metal concentrations rapidly decrease in the direction of water flow (e.g. Jones and Davis, 2013; Tedoldi et al., 2017). Metal concentrations are also typically higher in the top soil

layers (e.g. Sun and Davis, 2007; Hatt et al., 2008; Jones and Davis, 2013), sometimes reaching levels that are harmful to human health and soil biota (Sun and Davis, 2007; Li and Davis, 2008); as such, metals generally degrade soil quality (Li and Davis, 2008).

To address metal accumulation and soil quality concerns, to date, studies have characterized short-term metal accumulation in bioinfiltration systems and compared it to soil quality guidelines (e.g. Achleitner et al., 2007; Li and Davis, 2008); evaluated factors that influence metal loading to bioinfiltration systems, such as land use (e.g. Tedoldi et al., 2017; Kluge et al., 2018) and vehicular traffic (e.g. Horstmeyer et al., 2016); provided detailed soil metal contamination spatial patterns (e.g. Tedoldi et al., 2017); and assessed the effects of accumulated metals on lifetime expectancies of the systems (e.g. Ingvertsen et al., 2012). A few studies have evaluated longer term metal accumulation (e.g. Ingvertsen et al., 2012, Horstmeyer et al., 2016), but overall soil metal contamination in biofiltration systems over long time frames (> 10 years), including the potential consequences to biota and to soil management, is insufficiently understood (Tedoldi et al., 2016). To further assess potential effects on soil biota, studies should also evaluate available metal species, such as free metal cations and soluble organic and inorganic metal complexes (Young, 2013), which are more likely to interact with living organisms (Adriano, 2001). Plants and microorganisms can acquire available metal species from the soil solution; if metal concentrations are high enough, this may result in toxic effects including reduced biomass and activity in microorganisms (Giller et al., 2009), and oxidative stress damage, leaf chlorosis, poorly developed root systems, and reduced growth in plants (Adriano, 2001). In spite of these potential impacts, readily available metal species are largely uncharacterized in long-term studies of bioinfiltration systems, although they may be of use to evaluate potential

ecological risk. The nature and timing of bioinfiltration system maintenance would ideally also consider soil ecological screening levels (Eco-SSLs) that are protective of soil biota. Yet, although past evaluations of metal accumulation in bioinfiltration soils have assessed metal concentrations and estimated the years until Eco-SSLs would be reached (e.g. Johnson and Hunt, 2016; Tedoldi et al., 2017), a clear rationale for prioritizing monitoring of accumulated metals based on drainage area and bioswale characteristics, and for validating future metal accumulation predictions, has not been discussed.

Here, an approach to inform how bioinfiltration systems could be monitored long term to protect environmental and human health is proposed and initially tested. The approach attends to spatial distribution of metals in bioinfiltration systems, focusing on where most metal accumulation is likely to occur so that ecological risk based on total metal concentrations and Eco-SSLs can be performed. The approach was tested for four bioswales of similar age (>14 years), climate and design, but of varying drainage area characteristics. Soils were sampled for metals often associated with stormwater runoff (Cd, Cu, Pb, Zn) (Grant et al., 2003). Future potential soil remediation needs were estimated by predicting annual metal loads and calculating the number of years until Eco-SSLs would be reached. The objectives were to evaluate i) how drainage area characteristics, such as degree of imperviousness and impervious drainage to bioswale area ratios, relate to metal concentrations in established bioswale soils; ii) how soil metal concentrations relate to location within (e.g. side slope vs. basin bed) and along the flow-path of bioswales; iii) how water soluble metals compare to total metals in bioswale soils; and iv) the risks to soil quality and soil biota given measured and future projected metal concentrations, based on comparison to Eco-SSLs. The hypotheses were that i) metal concentrations would exceed

reference levels (i.e. those of nearby areas not receiving stormwater runoff from the built environment), and that metal concentrations would be higher in bioswales with more impervious drainage area and higher impervious drainage to bioswale area ratios; ii) metal concentrations would be higher in the basin bed rather than the side slope due to higher sedimentation; iii) metal concentrations would be higher near discrete stormwater runoff inlets due to particle association and sedimentation; iv) water soluble metal concentrations would be low since a high fraction of metals in stormwater runoff (typically 50–90%) are in particulate form (Grant et al., 2003; LeFevre et al., 2015); and v) total metal concentrations in some of the sampled soils would exceed Eco-SSLs. The hypothesized relationships between drainage areas and metal concentrations were observed but, based on those concentrations and predictions of longer-term conditions, these suburban biofilters are not expected to need soil maintenance for decades. This study builds upon previous work by examining the influence of drainage area characteristics on metal concentrations in established bioinfiltration systems, and by identifying metrics that may be predictive of soil metal concentrations.

2.2. Methods

2.2.1. Study site and bioswales

The study site, Manzanita Village, is a 4.9 ha residential university student housing complex located on the University of California, Santa Barbara (UCSB) campus, Santa Barbara, CA (N 34°24′32″; W 119°51′28″; Fig. S1). The site has a Mediterranean climate influenced by maritime winds, with monthly temperatures averaging 11.4–19.0 °C (NOAA, 2020; recorded at the proximate Santa Barbara Municipal Airport for the years 2002–2019).

Rainfall is variable, occurs mostly from November to April and, for the period 2002 to 2015, averaged 378 mm (Santa Barbara County Public Works, 2020; measured at UCSB station no. 200, N 34°24′56″; W 119°50′43″).

The four study bioswales, consisting of shallow basins separated by rock check dams, were constructed in 2001–02, as part of an ecological restoration project. The basins have average slopes of 2%, and range from 4.5 to 6 m long with trapezoidal cross sections of 2.4 m wide at the top narrowing to 1.2 m at the soil bed surface; the ponding and soil depths are approximately 15 cm (Fig. S2) and 0.9 m, respectively (CCBER, 2008). The bioswales are planted with native sedges and rushes, including *Juncus spp*. (e.g. *J. patens, J. mexicanus, J. occidentalis, J. phaeocephalus, J. textilis*) and *Carex spp*. (e.g. *C. praegracilis*), (CCBER, 2008) that are trimmed annually and weeded manually besides receiving routine spot application of glyphosate-based herbicides for weed control (personal communication, Lanes, A., June 26, 2015).

Stormwater runoff into the bioswales originates from rooftops, paved surfaces, lawns and natural soils (Fig. 1). The velocity of runoff from roof downspouts is dampened in cobble drains that are sufficiently coarse such that negligible sedimentation and pollutant removal occur therein. The contributing metal roofs are pitched (2 in 12 slope), and are comprised of aluminum, copper, and galvanized metal. Local seabirds roost on the roofs where they deposit phosphorous-rich guano; ocean aerosols also settle on roofs and thereby deposit nutrients (CCBER, 2008). Runoff from paved surfaces, lawns and natural soils enters diffusely as sheet flow into the bioswales. There are paved service roads adjacent to the bioswales used by electric powered vehicles, bicycles, and foot traffic. The otherwise unfertilized lawns are irrigated during the dry season with reclaimed water, which may be a

source of nutrients (SWRCB, 2016; Fruit Growers Lab Inc., 2020) and solids (Table S1). Reclaimed water, sourced from the reclamation facility at the Goleta Sanitary Water Resource Recovery District at Goleta, CA, consists of secondary effluent treated to tertiary standards via flocculation, filtration through anthracite coal, and chlorine disinfection (Goleta Sanitary, 2018).

Reference sites in close proximity (<10 m) to the bioswales, but not receiving stormwater runoff from built infrastructure, were used (n = 4) for comparing soil metal concentrations (Fig. S1). The natural soils in the reference sites are poorly draining, classified as Concepcion fine sandy loam (USDA Natural Resource Conservation Service's Hydrologic Soil Group C), and vegetated with native shrubs.

2.2.2. Delineation and calculation of drainage areas and degree of imperviousness

An original subwatershed map, which was the design basis of the bioswales, identified the delineation of bioswales and bioswale drainage areas (CCBER, 2003). This information was transferred into ArcMap 10.7.1, using the ESRI World Imagery layer as a basemap (ESRI, 2019), and creating shapefiles using the polygon feature to delineate the bioswales and draining areas corresponding to roofs, paved surfaces, lawns and natural soil cover. Projected areas for each of these draining surfaces were obtained from the attribute table using the "calculate geometry" option. Projected areas for the pitched roofs were adjusted using the slope (2 in 12) to estimate a roof slope multiplier of 1.038. All other areas were unmodified since the study site is relatively flat, so that projected areas from aerial images are correct representations of actual areas.

Total drainage area was computed by summing areas for roofs, paved surfaces, lawns, and natural soil cover. Total impervious area (TIA) was calculated as the sum of areas of

roofs and paved surfaces. Percent imperviousness was calculated by dividing the TIA by the total drainage area and multiplying by 100. The directly connected impervious area (DCIA) was calculated as the sum of areas of paved surfaces and roofs directly connected by cobble drains to the bioswales. Two metrics linking drainage areas and bioswale areas were computed: the ratio of TIA to bioswale area, and the ratio of DCIA to bioswale area.

2.2.3. Sampling

Soil sampling occurred between March 21st and April 4th, 2016. Eighteen soil samples were collected per bioswale at nine evenly spaced (9–12 m) locations along the flow-path: nine on the basin bed and nine on the side slope closest to nearby buildings (Fig. S3). Prior to sampling, visible rocks and vegetation were removed from the soil surface. A composite sample of approximately 700 g surface soil (0–10 cm) was obtained from each of three soil cores sampled at each location, using a cylindrical stainless-steel corer (5.08 cm diameter; 20 cm length) and collecting the soil in clean resealable plastic bags. Between uses, the corer was brushed, rinsed with Nanopure water (Barnstead Thermolyne, Ramsey, MN), and dried with a clean cloth. Four reference samples (Fig. S1), indicative of the natural background metal concentrations, were collected in the same way as bioswale soil samples. Samples were maintained on ice (4 °C) until returning to the lab for processing within 6 h. In the lab, the soil samples were sieved (2 mm) and subsampled immediately for analysis. Additional sampling (four composite samples) to characterize bioswale soils was performed in October 2018. Sieved (2 mm) soil samples were shipped (4 °C) to the Analytical Laboratory of the University of California at Davis (Davis, CA; http://anlab.ucdavis.edu/) where they were analyzed for soil texture (Sheldrick and Wang, 1993), cation exchange capacity (Rible and Quick, 1960), and total N and total C (AOAC, 1997).

2.2.4. Soil physicochemical characteristics

Gravimetric soil moisture content was determined for triplicate subsamples (3 g) of sieved soil using the mass difference before and after drying (105 °C, 24 h), following standard methods (Gardner, 1986). Dried soils (3 g) from the soil moisture analysis were combusted in a muffle oven at 450 °C for 16 h to determine soil organic matter via loss on ignition (LOI) (Nelson and Sommers, 1996). Soil pH was measured following standard methods (Thomas, 1996), including slurrying soil (10 g soil, 10 g deionized water) and settling the slurry (10 min), then measuring the pH by a pH meter (Oakton Ion 700 benchtop meter; Cole Parmer, Vernon Hills, IL). For inorganic nutrient analysis (nitrate and phosphate), soil samples (3 g, sieved) were extracted with 30 mL of 2 M KCl solution (149 g KCl Certified ACS Fisher Scientific, Pittsburgh, PA in 1 L deionized water) following standard methods (Mulvaney, 1996). Soil extracts were filtered using Whatman quantitative ashless filters, grade 42, 42.5 mm diameter (Sigma-Aldrich, St. Louis, MO) and the filtrate stored (−20 °C) until analysis, within 6 weeks. Filtrates were thawed immediately before analyzing dissolved nitrate and phosphate at the Marine Science Institute (MSI) Analytical Lab at UCSB via flow injection analysis (QuikChem8500 Series 2; Lachat Instruments, Milwaukee, WI). Extraction blanks and filter blanks were included in each inorganic nutrient analysis batch.

2.2.5. Microbial biomass by substrate induced respiration

The substrate induced respiration (SIR) method, as a metric of soil microbial biomass, was modified from West and Sparling (1986) and Fierer et al. (2003). The measurement was replicated by performing independent measures for each of two duplicate soil samples. To perform, 10 g of composite sieved soil was weighed into individual 250 mL amber glass

bottles with Teflon-taped threads, and 10 mL of autoclave-sterilized yeast extract solution (12 g autolyzed BD Difco yeast, BD Biosciences, San Jose, CA in 1 L deionized water) was added. The bottles were capped (Mininert, 24 mm, Valco Instruments Co. Inc., Houston, TX) and placed on a horizontal shaker for the duration of the 4 h incubation. Headspace gas samples (5 mL) were acquired via syringe immediately after capping, then 2 and 4 h thereafter for a total of 3 time-course measurements. To avoid pressure differentials, at each sampling time, 5 mL of air were injected into the sealed bottle via syringe prior to extracting the headspace gas sample. Additional method details are included in Appendix A – Supplementary Information. Gas CO_2 content was measured using an infrared gas analyzer (EGM-4; PP Systems, Amesbury, MA). The slope of CO_2 concentrations against time was used to calculate the rate of CO_2 production, expressed as $\mu g\ CO_2 \times g\ dry\ soil^{-1} \times h^{-1}$.

2.2.6. Metal analysis

Bioswale soil samples were analyzed for common metals found in stormwater runoff, including Cu, Pb, Zn and also Ni, Cd, and Cr (Grant et al., 2003). Total metals were quantified for strong acid-extracted soils and thus represent "pseudo-total metals", which are those that may become available under worst case environmental conditions (Link et al., 1998), and are thus suited for the scope of this study. Metals that are readily available to plants and microorganisms were evaluated by measuring water soluble metals, based on the method outlined in Seguin et al. (2004) and Rodriguez et al. (2010). To recover eluates for determining water soluble metals, one replicate of 10 g of sieved soil was weighed into 50-mL polypropylene centrifuge tubes with 10 mL chilled (4 °C) distilled water. The samples were vigorously shaken by hand (10 s) and mechanically shaken (2 h, 4 °C) in a controlled environment incubator shaker (New Brunswick Scientific Co. Inc., Edison, NJ) at 4 °C and

200 rpm. The samples were centrifuged (2500 ×*g*, 30 min, 4 °C) (Cao et al., 2008), and 1 mL of the supernatant was diluted 20-fold in 2% nitric acid (Optima ultrapure grade, Fisher Scientific, Pittsburgh, PA) before storing (4 °C) until analysis (within 4 weeks). Total metal extraction was based on EPA method 3051A and involved weighing sieved soil (one replicate, 0.5 g) into microwave quartz vessels (Anton Paar, Graz, Austria) and digesting (165 °C; 1.0 h) with 16 mL aqua regia (HNO_3 Certified ACS and HCl Certified ACS, Fisher Scientific, Pittsburgh, PA in a 1:3 ratio) in a microwave acceleration reaction system (Multiwave Eco; Anton Paar, Graz, Austria). The digested samples were transferred to acid-rinsed 50 mL PP centrifuge tubes (Corning Life Sciences, Corning, NY) and diluted to 50 mL with Nanopure water (Barnstead Thermolyne, Ramsey, MN). The acid digests were further diluted 9.4 times (1.6 mL acid digest plus 13.4 mL Nanopure water).

Water soluble and total metals were quantified via inductively coupled plasma-atomic emission spectroscopy (ICP-AES) using a TJA High Resolution IRIS instrument (Thermo Electron Corporation, Waltham, MA) based on EPA Methods 200.7 and 6010C, quantifying 11 elements (Al, Ca, Cd, Cr, Cu, Fe, Mg, Mn, Ni, Pb, and Zn) in the solution. Calibration standards were prepared using a commercial standard containing all metals (High-Purity Standard Co., Charleston, SC; 0, 1, 10, and 100 μg/L) in 2% *v*/v nitric acid. Detection limits were 7 μg/L for Pb; 10 μg/L for Cu, Fe, Mn, Zn; 12 μg/L for Mg, Ni; 14 μg/L for Cd and Cr; 22 μg/L for Ca; and 27 μg/L for Al. For quality control, one lab blank (Nanopure water, Barnstead Thermolyne, Ramsey, MN, acidified with concentrated nitric acid, Optima, Fisher Scientific, Pittsburgh, PA), and one lab duplicate were prepared for each extraction batch. Signal drift for the ICP-AES was evaluated with a quality control sample of a known standard injected every ten runs. Samples were measured in triplicate, and the precision of

signal measurement expressed as percent relative standard deviation (%RSD) was 0.1–5.0%. Good linearity was observed for all measured metals, with $R^2 > 0.9995$. No trace metals were detected in the lab blanks.

When performing statistical analysis of total Cu data, six samples that were below detection limit (DL = 10 μg/L) were substituted for a value equal to half the detection limit, a method commonly used to address censored data, which can provide an adequate estimate of summary statistics with low bias for data sets with less than 70% censored data (Antweiler and Taylor, 2008).

2.2.7. Annual metal loads and years to reach ecological soil screening levels

To simulate potential bioswale soil metal accumulation, average annual metal loads were first estimated using a simplified approach based on the method outlined in Johnson and Hunt (2016) (Eq. (1)), as follows:

$$\text{Annual metal load } \left(\frac{\text{mg metal}}{\text{kg soil}}\right) = \frac{V_R \times C_{M,\,in} \times \left(\frac{M_{rem,\,\%}}{100}\right)}{\rho_B \times A_{BSW} \times z} \qquad (1)$$

where:

V_R = Runoff volume in m^3 (Table S2)

$C_{M,\,in}$ = Mean input metal concentration in mg/m^3 (Tables S3 and S4)

$M_{rem,\,\%}$ = Median percent metal removal for bioswales

ρ_B = measured bulk density of soil media in kg/m^3 = 1200 kg/m^3

A_{BSW} = Surface area of bioswale in m^2 (Table 1)

An average median percent removal ($M_{rem,\,\%}$) of 72% for Zn, and 62% for Cu was selected, based on efficiency ratios (ER) for 59 bioswales reviewed by Fardel et al. (2019). The ER estimates overall long-term treatment performance, rather than individual storm

events, and is a measure of percent removal based on average inlet and outlet event mean concentrations. Mean input metal concentrations (Cu = 26 mg/m^3; Zn = 159 mg/m^3) were based on stormwater runoff data collected by the Santa Barbara Creeks Division in low impact development (LID) sites in Santa Barbara, CA (Tables S3 and S4). Runoff volumes (V_R) entering each bioswale were calculated via the curve number method outlined in 210-VI-TR-55 (USDA NRCS, 1986), which takes into account relative imperviousness of the drainage area, and characteristics of infiltrating soils. Further details are included in Appendix A – Supplementary Information.

To test the validity of using annual metal loads to simulate metal accumulation in the bioswales, measured and predicted metal concentrations were compared. Predicted concentrations were calculated using annual metal loads, years of operation, and the initial metal concentrations.

Since initial metal concentrations were not measured at the time of construction, concentrations representing the first decile of all measurements, and thus very low contamination levels, were used as a background value for each bioswale, following Tedoldi et al. (2017). Predicted metal concentrations were obtained as the sum of this background concentration and the product of the annual metal load and the number of years in operation. Predicted and measured metal concentrations were compared to Eco-SSLs for Cu (U.S. EPA, 2007a) and Zn (U.S. EPA, 2007b), to determine if levels of ecological concern had been reached. Eco-SSLs are average values based on reviewed ecotoxicity data, representing soil contaminant concentrations protective of four ecological receptors: plants, soil invertebrates, avian wildlife (birds), and mammalian wildlife (mammals). After verifying agreement between predicted and measured metals, metal accumulation into the future was extrapolated

to calculate how many years would have to elapse for metal concentrations to reach Eco-SSLs (Eq. (2)), as follows:

$$\text{Years to Eco-SSL} = \frac{\text{Eco-SSL-Current maximum metal concentration}}{\text{Annual metal load}} \quad (2)$$

2.2.8. Data analysis

Differences between soil physicochemical characteristics and metal concentrations across bioswales, and differences in metal concentrations between basin bed and side slope samples for each bioswale, were evaluated by one-way analysis of variance on ranks (Kruskal-Wallis) followed by post-hoc Dunn tests ($p < 0.05$) since variables were not normally distributed (Shapiro-Wilk test). Relationships between soil physicochemical characteristics and metal concentrations across all bioswales were evaluated via Spearman rank-order correlations, as were relationships between any significantly varying metal and specific drainage area characteristics. Statistical analyses were performed with R software (version 4.0.1).

2.3. Results and Discussion

2.3.1. Drainage area delineation and metrics of imperviousness

The delineation of bioswales, their respective drainage areas, and overall stormwater runoff flow direction in the study area are shown over the USGS National map topographic basemap (USGS, 2020) (Fig. 1). Bioswale and total drainage areas ranged from 274 to 762 m^2, and 1615 to 4191 m^2, respectively. Percent imperviousness in bioswale drainage areas ranged from 37 to 71%. Drainage areas in BW1 and BW2 had higher contributions from lawns (27–29%) and natural soils (27–36%), and smaller contributions from paved areas (15–19%), whereas drainage areas in BW3 and BW4 had higher contributions from paved surfaces (42%), and roofs (43%), respectively (Table 1).

Total drainage to bioswale area ratios ranged from 4.7 to 10.0 (Table 1), which is comparable to other bioinfiltration systems: drainage to bioinfiltration area ratios ranged from 8.7 to 53.3 in swales (Tedoldi et al., 2017), and from 3.5 to 14.3 in bioretention cells (Ingvertsen et al., 2012). When considering only impervious drainage area, ratios of TIA to bioswale area ranged from 2.0 to 5.7. The DCIA was equivalent to the TIA for BW1, BW3 and BW4. For BW2, the DCIA excluded roofs not adjacent to the bioswale (Fig. 1). Ratios of DCIA to bioswale area ranged from 2.0 to 5.7 (Table 1).

2.3.2. Total and water soluble metals

2.3.2.1. Total metals concentrations and distribution within and across bioswales

Soil metal concentrations in bioinfiltration systems are a reflection of the stormwater runoff inputs, the amount of infiltration, the paths stormwater runoff follows and the extent of settling processes that deposit particles and associated metals (Tedoldi et al., 2017). Bioswale soil samples were tested for metals most often associated with stormwater runoff, including Cu, Pb, Zn and also Ni, Cd, and Cr (Grant et al., 2003). Cd and Pb were below detection limit for all samples. All other metals were detected in a majority of samples, and total Zn was quantified in all samples (Appendix B – Supplementary Data). Within each bioswale, total Zn and total Cu concentrations in basin bed and side slope samples were relatively uniform (Fig. 2), and there were no significant differences for either metal based on location within each bioswale (Kruskal-Wallis, $n = 18$, $p > 0.05$). There were also no clear trends relative to sampling distance along the main direction of stormwater runoff flow (Fig. 2). Previous studies in roadside soils (e.g. Werkenthin et al., 2014) and bioretention cells (e.g. Jones and Davis, 2013, Johnson and Hunt, 2016, Tedoldi et al., 2017) have shown a radial or lateral decrease in metal concentration with distance from the inlet. Due to the

multiple inlets in the study bioswales (e.g. roof downspouts and diffuse inputs), such a trend was not observed.

Across all bioswales, total Cu and Zn soil concentrations were low and within the same order of magnitude as reference sites (Kruskal-Wallis, $n = 76$, $p > 0.05$) (Fig. 3a). Metal concentrations in the reference sites were similar to background metal concentrations reported for locations within 100 km of the study site (Appendix B – Supplementary Data). Total Zn concentrations in the study bioswales were 15.6–129.5 mg/kg dry soil, with means of 32.0–54.7 mg/kg dry soil (Fig. 2, Fig. 3a). Total Cu concentrations were above the detection limit (9.4 mg/kg dry soil) in 66 out of 72 bioswale samples and were generally below 20 mg/kg dry soil (Fig. 2, Fig. 3a). Yet there were significant differences across all bioswale samples for Zn (Kruskal-Wallis $\chi2 = 24.284$, $n = 72$, $p < 0.001$). Zn concentrations in BW2 were significantly different from BW1 (Dunn Test, $p = 0.046$), BW3 (Dunn Test, $p = 0.004$) and BW4 (Dunn Test, $p < 0.0001$) (Fig. 2). There were no significant differences for Cu across bioswales (Kruskal-Wallis $\chi2 = 8.167$, n = 72, $p > 0.05$) (Fig. 3a).

Total Zn and total Cu were significantly correlated across all bioswale samples (Spearman's $\rho = 0.58$, n = 72, $p = 8.5$ E-08) (Fig. S4), which is likely a result of these metals being associated with similar sources in residential areas, such as vehicle use and building materials (e.g. Werkenthin et al., 2014; Charters et al., 2016). Cu and Zn are known to be contributed from metal roofing and siding material via dissolution and degradation (Charters et al., 2016). Relative to published literature on metal accumulation in surface soils of stormwater infiltration systems, total Cu and Zn were within reported ranges for bioinfiltration systems between 2 and 8 years of age, but showed relatively lower metal

accumulation than reported for surface soils in residential and parking lot swales aged 6–16 years (Ingvertsen et al., 2012) (Table 2).

The relatively lower total metal concentrations may be a result of low metal loading to the bioswales due to limited vehicular traffic which is a principal contributor of Cu and Zn in stormwater runoff via tire wear and degradation of brake pad linings (Davis et al., 2001; Grant et al., 2003; Charters et al., 2016). Additionally, resuspension and release of previously sequestered pollutants during high flow events may further explain the relatively low measured metal concentrations. Further, leaching down the soil profile due to increases in salinity (e.g. Paus et al., 2014a; Lange et al., 2020), and SOM (e.g. Hatt et al., 2007; Blecken et al., 2011) cannot be excluded, even if studies on lab bioretention columns (e.g. Davis et al., 2001; Hatt et al., 2008) and field bioretention cells (e.g. Li and Davis, 2008; Jones and Davis, 2013) show that soil metal concentrations are higher at the surface. Finally, metal uptake by plants (LeFevre et al., 2015; Muerdter et al., 2018), including phytoextraction and translocation to above ground biomass, or immobilization in roots (Kidd et al., 2009), may contribute to lower soil metal concentrations, even if previous bioinfiltration studies show that some plants play a minor role in metal uptake when compared to soils (e.g. Sun and Davis, 2007; Read et al., 2008; Muerdter et al., 2018). Evaluating the extent of metal accumulation in bioswale vegetation and how plants may influence metal mobility is beyond the scope of this study.

2.3.2.2. Water soluble metals concentrations and distribution across bioswales

Water soluble Cu concentrations were below detection limit (9.4 mg/kg dry soil) for all samples. Water soluble Zn was measurable in all samples and concentrations were two orders of magnitude lower than total metal concentrations, with values between 0.12 and

3.25 mg/kg dry soil and means of 0.51–0.86 mg/kg dry soil across all bioswales. There were significant differences in water soluble Zn concentrations across sampled soils (Kruskal-Wallis $\chi 2 = 20.147$, $n = 76$, $p = 0.0005$) (Fig. 3b), and these differences occurred between BW1 and BW2 (Dunn Test, $p = 0.0004$), and BW1 and BW4 (Dunn Test, $p = 0.0061$).

Unexpectedly, total and water soluble Zn concentrations were weakly and negatively correlated (Spearman's $\rho = -0.34$, $n = 72$, $p = 0.0039$) (Fig. S5). Total metals are often not good predictors of metals in soil solution (Alloway, 2013), which have been shown to positively correlate to metal content in plant tissue (Walker et al., 2003), and in the case of Zn, positively correlate to total Zn content when sorption and mineral dissolution processes dominate over precipitation, as is typical for low Zn loading (Mertens and Smolders, 2013). The low fraction of water soluble metals is not surprising since most metals in soils are either adsorbed to soil particles or present in insoluble forms (Alloway, 2013). Although stormwater runoff carries both dissolved and particulate metals (e.g. LeFevre et al., 2015; Lindfors et al., 2017), dissolved pollutants may rapidly adsorb onto bioswale soil surfaces. Sediment aging, during which metals sorbed on particle surfaces move into smaller pores and voids within the soil matrix, which may not be accessible to living organisms (Alexander, 2000), results in a transfer of metals from labile pools where sorption is reversible to pools where desorption is slow, and further decreases the bioavailability of deposited metals (Mertens and Smolders, 2013).

2.3.3. Soil physicochemical properties, microbial biomass, and relationships to metals

The bioswale soil was classified as a sandy loam based on particle size analysis (59% sand, 28% silt and 13% clay) (UC Davis, 2018), which is within recommendations for

bioinfiltration soils (Geosyntec, 2013). The average cation exchange capacity was 17.6 meq/kg dry soil, total N was 0.2% m/m, and total C was 2.3 m/m (UC Davis, 2018).

Soil pH was determined due to its known influence on metal speciation, solubility and mobility (Young, 2013). The pH was relatively uniform across bioswales (Kruskal-Wallis, $n = 72$, $p > 0.05$), with a range of 7.2–8.6, and means ranging from 8.0 to 8.2 (Table 1). There was no significant correlation between pH and total metal content (Spearman, n = 72, p > 0.05) (Fig. S5), whereas pH was significantly and negatively correlated to water soluble metals, including Al (Spearman's $\rho = -0.183$, $n = 72$, $p = 0.01$), Fe (Spearman's $\rho = -0.169$, n = 72, $p = 0.02$), and Mg (Spearman's $\rho = -0.231$, $n = 72$, p = 0.01) (Fig. S5). The soil pH values fall within recommended values for bioinfiltration systems, which range from 5.5 to 8.5 (e.g. Geosyntec, 2011; Geosyntec, 2013; Payne et al., 2015). This pH range supports optimal retention and removal of a broad range of pollutants, including heavy metals, which tend to be immobilized at higher pH (Young, 2013). The relatively high pH in bioswale soils could be a result of the parent soil material used to construct the bioswales, since stormwater runoff is usually neutral in stormwater management systems, as observed in the National Stormwater Quality Database (Pitt et al., 2018). Further, in the study area, runoff has limited contact with surfaces that contribute alkalinity, such as calcareous building materials like concrete pavement (Ingvertsen et al., 2012).

SOM across bioswales was 2.2–14.5% (m/m), with mean values of 5.9–6.7% (m/m) (Table 1). There were no significant differences across bioswales (Kruskal-Wallis, $n = 72$, $p > 0.05$), and SOM content was not significantly correlated with total or water soluble metals (Spearman, n = 72, p > 0.05) (Fig. S5). Mean values were within design recommendations for bioinfiltration systems which typically are 5–8% for the soil mix

(e.g. State of Washington Department of Ecology, 2019), 10–12% for planting media, and >5% for topsoil (e.g. Geosyntec, 2013). These SOM values could indicate a high affinity to sorb pollutants such as heavy metals due to the presence of humic and fulvic acids (Young, 2013). Conversely, high SOM content can lead to solubilization of organic metal complexes, resulting in metal leaching during runoff infiltration (Davis et al., 2003; Lim et al., 2015), which would result in lower metal concentrations in the upper soil layer.

Nitrate concentrations across the bioswales were 0.9–62.5 mg NO_3/kg dry soil, with means values of 4.2–22.5 mg NO_3/kg dry soil (Table 1). Nitrate concentrations were significantly different across bioswales (Kruskal-Wallis $\chi2 = 44.084$, $n = 72$, $p < 0.001$) and were significantly higher in BW1 and BW2 relative to BW3 and BW4 (Dunn Test, $p < 0.0001$). BW1 and BW2 have larger drainage areas (Table 1) and receive more inputs from irrigation runoff from reclaimed water that is applied to lawns, which may explain the higher soil nutrient content since reclaimed water can potentially contribute nutrients (SWRCB, 2016; Fruit Growers Lab. Inc., 2020). Phosphate concentrations were 0.1–22.8 mg PO_4/kg dry soil, with mean values of 1.6–8.0 PO_4/kg dry soil (Table 1). The mean phosphate concentration was significantly different across bioswales (Kruskal-Wallis $\chi2 = 21.446$, $n = 72$, $p = 0.0065$). Phosphate content in BW1 and BW2 was similar and significantly higher than in BW3 (Dunn Test, $p < 0.05$). BW2 and BW4 had similar phosphate content, as did BW3 and BW4. Phosphate and nitrate were positively correlated (Spearman's $\rho = 0.60$, $n = 72$, $p = 7.2E\text{-}06$) (Fig. S5).

SIR was computed as an indicator of heavy metal stress since high levels of metal pollution can reduce microbial biomass (Giller et al., 2009). There were significant differences across bioswales (Kruskal-Wallis $\chi2 = 30.709$, n = 72, $p = 9.8$ E-07), with BW3

being higher than BW1, BW2 and BW4 (Dunn Test, $p < 0.05$). SIR values were 1.4–10.0 μg CO_2 g^{-1} h^{-1}, with mean values of 3.7–6.7 μg CO_2 g^{-1} h^{-1}, which are within reported values for semi-arid soils (e.g. Conant et al., 2004). There was no correlation between microbial biomass and total soil metal content across all bioswale samples (Spearman, $n = 72$, $p > 0.05$). However, SIR was moderately correlated with SOM (Spearman's $\rho = 0.51$, $n = 72$, $p = 4.0$ E-06) (Fig. S5), which is expected since SOM is a carbon source for heterotrophic microbial respiration. SIR was also moderately correlated with water soluble metals Al (Spearman's $\rho = 0.52$, $n = 72$, $p = 2.5$ E-06), Ca (Spearman's $\rho = 0.43$, $n = 72$, $p = 1.7$ E-04), Mg (Spearman's $\rho = 0.54$, $n = 72$, $p = 1.1$ E-06), and Fe (Spearman's $\rho = 0.49$, $n = 72$, $p = 1.2$ E-05) (Fig. S5).

2.3.4. Relationship between total metals and drainage area characteristics

Correlations between total Zn and drainage area characteristics were computed to evaluate if the degree of imperviousness in bioswales had an effect on Zn concentrations. Total Zn concentration in bioswale soils was significantly correlated to the contributing drainage basin characteristics of directly connected impervious area to bioswale area ratio (Spearman's $\rho = 0.32$, $n = 71$, $p = 0.0073$), percent impervious cover (Spearman's $\rho = 0.32$, $n = 71$, $p = 0.0073$), and paved surfaces (Spearman's $\rho = 0.46$, $n = 71$, $p = 5.6$ E-05) (Fig. 4). The correlation between total Zn and the TIA to bioswale area ratio was not significant, which is likely a result of a substantial portion of roof runoff in BW2 flowing through a large lawn area prior to entry into the bioswale (Fig. 1). The DCIA to bioswale area ratio was thus a better predictor for Zn concentrations in bioswale soil. A moderate negative correlation was observed for total Zn and percent lawns (Spearman's $\rho = -0.48$, $n = 71$, $p = 2.4$ E-05) (Fig. 4), indicating that these pervious areas may be factors in reducing metal loads to the

bioswales. Total Cu showed no significant correlation to surface area characteristics in the drainage area (data not shown), likely as a result of the generally low and uniform observed concentrations.

It should be noted that the positive correlation between total Zn and imperviousness was observed for relatively low Zn concentrations. While not studied here, such correlations might extrapolate upwards. Data reported by Tedoldi et al. (2017), which includes biofiltration systems that receive higher metal loading and/or are much smaller in size relative to their total drainage area, suggests that, on average, soil metal concentrations are higher in systems with larger drainage to bioinfiltration area ratios. However, there may be other site related factors which could obscure this relationship. This study was not confounded by spatial variations in biofilter environmental factors such as local climate, since the four bioswales are in close proximity. Further, the bioswales are similarly designed, were constructed at the same time and thus have similar soil physicochemical characteristics (Table 1). Any differences are likely a result of the types and amount of runoff that the bioswales receive, in addition to differences in vegetation in response to changes in moisture and nutrient inputs. To further test the correlation between accumulated metals and the percent imperviousness in the drainage area, and/or the ratios of impervious drainage to infiltration areas, future studies including a range of bioinfiltration designs and a broader range of impervious drainage to infiltration area ratios will be useful.

2.3.5. Estimating potential threat and the need for soil media remediation

To evaluate how long it would take for surface soil samples to reach concentrations of potential concern, annual metal loadings were computed and predicted metal concentrations at time of sampling (after 14 years in operation) were calculated and compared to measured

concentrations and Eco-SSLs. Current maximum metal concentrations were extrapolated into the future to estimate the years until Eco-SSLs were reached. Annual metal loadings were 1.7–3.1 mg/kg dry soil and 0.2–0.4 mg/kg dry soil, for Cu and Zn respectively (Table 3).

Soil metal concentrations at time of construction, or background metal concentrations, were estimated as the first decile of all measured data at time of sampling and were 10.0–11.6 mg/kg dry soil and 23.2–37.7 mg/kg dry soil, for Cu and Zn, respectively. These background metal concentrations are within the range observed for surficial (0–5 cm) soils, and below median (Cu: 14.4 mg/kg dry soil; Zn: 58 mg/kg dry soil) and mean (Cu: 17.9 mg/kg dry soil; Zn: 66 mg/kg dry soil) values for soils in the conterminous USA (Smith et al., 2013) (Table 3). Based on background concentrations, annual metal loadings and years in operation, predicted metal concentrations at time of sampling were 12.8–16.7 mg/kg dry soil and 54.6–74.1 mg/kg dry soil, for Cu and Zn respectively. Predicted metal concentrations were comparable to measured Cu concentrations, and larger than measured Zn concentrations (Table 3). Measured Zn concentrations may have been lower than predicted due to source differences between the study site, and the local sites used to estimate Zn concentrations in stormwater runoff, such that the study site had lower Zn loading. It should also be noted that model predictions did not account for future uncertainty in stormwater runoff as a result of climate change, changes in metal loading due to atmospheric deposition inputs, and the role that plants may have in effecting changes in metal mobility in soils. Future model refinement would logically include improvements on metal loading predictions that take into account these factors.

When predicted and measured Cu and Zn concentrations were considered together, there was a significant and positive linear relationship ($R^2 = 0.873$, $p = 6.78$ E-04, $n = 8$) (Fig. S6).

This relationship, though promising, should be tested with a larger number of samples experiencing a broader range of metal concentrations. Notwithstanding, this result suggests that for the studied bioswales, which are impacted by runoff from impervious surfaces (Fig. 4), if initial metal concentrations are known or can be estimated, local data of stormwater runoff metal concentrations, and drainage area characteristics such as percent imperviousness, may be used to estimate annual metal loads; metal concentrations can then be projected into the future to evaluate soil ecological risks.

Predicted metal concentrations after 14 years in operation were below all Eco-SSLs for Cu, and above at least one Eco-SSL for Zn for all study bioswales (Table 3). Total and water soluble average metal concentrations measured in the bioswales fell below most Eco-SSLs (Fig. 3, Table 3). When considering maximum concentrations, low Eco-SSLs have been reached in all bioswales in at least one location, either for Cu only, Zn only, or both Cu and Zn (Table 3, Fig. 3a). Current maximum metal concentrations were extrapolated into the future to determine the years until Eco-SSLs would be reached. All bioswales are decades away from reaching high Eco-SSLs (Table 3). Due to the inherent spatial heterogeneity in soil (Young, 2013), the existence of hot spots of contamination that exceed sediment/soil quality guidelines is not overruled, but unlikely in the studied systems where the potential for toxicity to microbes or other soil biota due to accumulated metals is likely minimal.

2.4 Conclusions

Here, for four lightly metal-contaminated suburban bioswales, which are representative of typical bioinfiltration systems, an approach that unites bioswale drainage area and bioswale characteristics is proposed, which owing to correlations with the highest

concentration metal (Zn) (Fig. 4), shows that the two types of characteristics might be predictive of metal loadings, assuming similar compositional drainage area surfaces. The validity of this approach, including extrapolation of current metal concentrations into the future, was verified by the good agreement between predicted metal concentrations based on local stormwater runoff metal concentrations from hardscape and calculated runoff (Table S2), and measured concentrations after 14 years in operation (Table 3, Fig. S6). Notwithstanding, further validation with a larger number of bioinfiltration systems experiencing a range of metal loading is required to fully test the applicability of the proposed strategy for monitoring metals in bioinfiltration soils.

For more contaminated drainage areas and bioswales, e.g. in urban settings, such relationships would be driven by higher magnitudes of metals, imperviousness, and presumably accumulation in the bioswales. However, the extrapolation of these findings to more developed areas remains to be tested. Still, this work suggests that, for other bioswale systems, a reasonable strategy for managing soils to protect resident biota could be to characterize bioswale and drainage areas relative to one another, calculate key indicators from those relationships such as DCIA to bioswale area ratios, then prioritize sampling around higher ratios, compare measured and predicted metal concentrations based on annual metal loads, and assess the trajectory to concerning Eco-SSLs (Fig. 5).

2.5. Acknowledgements

Funding for this research was provided by a gift from Mr. Henry H. Wheeler. Additional funding was provided by the UCSB Associated Students Coastal Fund (grant Fall 14-11), and Graduate Summer Fellowships from the Earth Research Institute. The writing of this

manuscript was supported by funding from by the University of California Office of the President, Multicampus Research Programs and Initiatives, Grant ID MRP-17-455083. We thank Lisa Stratton, Andy Lanes, Patrick Roehrdanz. Laurie Van der Werfhorst, Sage Davis, Do Gyun Lee, Monika Mortimer, Ying Wang, Timnit Kefela, Cruz Ortiz, Tania Gomez Ayala, and Manu Chopra for their assistance. The MRL Shared Experimental Facilities were used for ICP-AES, and are supported by the MRSEC Program of the NSF under Award No. DMR 1121053, a member of the NSF-funded Materials Research Facilities Network (www.mrfn.org).

2.6. References

Achleitner, S., Engelhard, C., Stegner, U., and Rauch, W. (2007). Local infiltration devices at parking sites – Experimental assessment of temporal changes in hydraulic and contaminant removal capacity. *Water Sci. Technol*., 55(4), 193-200.

Adriano, D. C. (2001). Trace elements in terrestrial environments: Biogeochemistry, bioavailability and risks of metals (2nd edition). Springer-Verlag, New York.

Ahiablame, L. M., Engel, B. A., and Chaubey, I. (2012). Effectiveness of low impact development practices: literature review and suggestions for future research. *Water, Air, Soil Pollut.*, *223*(7), 4253-4273.

Alexander, M. (2000). Aging, bioavailability, and overestimation of risk from environmental pollutants. *Environ. Sci. Technol*., 34 (20), 4259-4265.

Alloway, B. (2013). Sources of heavy metals and metalloids in Soils. In: Heavy metals in soils: Trace metals and metalloids in soils and their bioavailability (3rd edition), Alloway, B. (Ed.), Springer, Dordrecht, Netherlands, 11-50.

Ambrose, R. F., and Winfrey, B. K. (2015). Comparison of stormwater biofiltration systems in Southeast Australia and Southern California. *Wiley Interdiscip. Rev.: Water, 2*(2), 131-146.

Antweiler, R.C.; H.E. Taylor (2008) Evaluation of statistical treatments of left-censored environmental data using coincident uncensored data sets: I. Summary statistics. *Environ. Sci. Technol.* 42 (10), 3732-3738.

Association of Official Analytical Chemists (AOAC) (1997). Official Method 972.43, Microchemical determination of carbon, hydrogen, and nitrogen. In: Official methods of analysis of AOAC International (16th ed.), AOAC International, Arlington, VA, Chapter 12, 5-6.

Blecken, G. T., Zinger, Y., Deletic, A., Fletcher, T. D., and Viklander, M. (2009). Impact of a submerged zone and a carbon source on heavy metal removal in stormwater biofilters. *Ecol. Eng.*, *35*(5), 769-778.

Blecken, G., Marsalek, J., and Viklander, M. (2011). Laboratory study of stormwater biofiltration in low temperatures: Total and dissolved metal removals and fates. *Water Air Soil Pollut.*, 219(1–4), 303-317.

Boehm, A. B., Bell, C. D., Fitzgerald, N. J. M., Gallo, E., Higgins, C. P., Hogue, T. S., Luthy, R. G., Portmann, A. C., Ulrich, A. B., and Wolfand, J. M. (2020). Biochar-augmented biofilters to improve pollutant removal from stormwater – can they improve receiving water quality? *Environ. Sci.: Water Res. Technol*., 6, 1520-1537.

Charters, F. J., Cochrane, T. A., and O'Sullivan, A. D. (2016). Untreated runoff quality from roof and road surfaces in a low intensity rainfall climate. *Sci. Tot. Environ.*, 550, 265-272.

Cheadle Center for Biodiversity and Ecological Restoration (CCBER) (2003). Subwatershed map for Manzanita Village project site, University of California, Santa Barbara, CA.

Cheadle Center for Biodiversity and Ecological Restoration (CCBER) (2008). 5 year performance criteria monitoring report for restored wetlands at Manzanita Village, University of California, Santa Barbara, CA.

Conant, R. T., Dalla-Betta, P., Klopatek, C. C. and Klopatek, J. M. (2004). Controls on soil respiration in semiarid soils. *Soil Biol. Biochem*., 36(6), 945-951.

Davis, A. P., Shokouhian, M., and Ni, S. (2001). Loading estimates of lead, copper, cadmium, and zinc in urban runoff from specific sources. *Chemosphere, 44*(5), 997-1009.

Davis, A. P., Shokouhian, M., Sharma, H., Minami, C., and Winogradoff, D. (2003). Water quality improvement through bioretention: Lead, copper, and zinc removal. *Water Environ. Res*., 75(1), 73-82.

ESRI (2019) ArcGIS Desktop: Release 10.7 (Environmental Systems Research Institute, Redlands, CA)

Fardel, A., Peyneau, P. E., Béchet, B., Lakel, A., and Rodriguez, F. (2019). Analysis of swale factors implicated in pollutant removal efficiency using a swale database. *Environ. Sci. Pollut. Res.*, 26, 1287-1302.

Fierer, N., Schimel, J. P., and Holden, P. A. (2003). Variation in microbial community composition through two soil depth profiles. *Soil Biol. Biochem.*, 35, 167-176.

Fruit Growers Lab. Inc. (2020). General irrigation suitability analysis, reclaimed water sampled on July 15th, 2020. Lab IDs SP 2009363-005, and SP 2009363-006.

Gardner, W. H. (1986). Water content, In: Methods of soil analysis, part 1, physical and mineralogical methods (2nd edition), Klute, A. (Ed.), American Society of Agronomy, Agronomy Monographs 9(1), Madison, WI, 493-544.

Geosyntec Consultants and Larry Walker Associates (2011). Ventura County technical guidance manual for stormwater quality control measures. Manual Update 2011, Errata Update 2018. Section 6.3, BIO-3: Vegetated Swale, p. 6-149. Available at: http://www.vcstormwater.org/images/stories/NPDES_Documents/TGM/TGM_2018_Errata/Ventura-Technical-Guidance-Manual-Rev-06_29_18.pdf

Geosyntec Consultants (2013). City of Santa Barbara Stormwater BMP Guidance Manual, July 2013 (Final), Section 6.6.2 Vegetated Swale Filter, p. 6-45. Available at: https://www.santabarbaraca.gov/civicax/filebank/blobdload.aspx?BlobID=16665

Giller, K. E., Witter, E., and McGrath, S. P. (2009). Heavy metals and soil microbes. *Soil Biol Biochem*, 41, 2031-2037.

Goleta Sanitary District (2018). 2017 Reclaimed Water Annual Report. Available at: https://goletasanitary.org/downloads/category/11-reclaimed-water

Grant, S. B., Rekhi, N. V., Pise, N. R., and Reeves, R. L. (2003). A review of the contaminants and toxicity associated with particles in stormwater runoff. CTSW-RT-03-059.73.15. Prepared for California Department of Transportation. August 2003.

Hatt, B. E., Fletcher, T. D., and Deletic, A. (2007). Hydraulic and pollutant removal performance of stormwater filters under variable wetting and drying regimes. *Water Sci. Technol.*, 56(12), 11-19.

Hatt, B. E., Fletcher, T. D., and Deletic, A. (2008). Hydraulic and pollutant removal performance of fine media stormwater filtration systems. *Environ. Sci. Technol.*, 42(7), 2535-2541.

Hatt, B. E., Fletcher, T. D., and Deletic, A. (2009). Hydrologic and pollutant removal performance of stormwater biofiltration systems at the field scale. *J. Hydrol, 365*(3), 310-321.

Horstmeyer, N., Huber, M., Drewes, J. E., and Helmreich, B. (2016). Evaluation of site-specific factors influencing heavy metal contents in the topsoil of vegetated infiltration swales. *Sci. Tot. Environ.*, 560–561, 19-28.

Ingvertsen, S. T., Cederkvist, K., Regent, Y., Sommer, H., Magid, J., and Jensen, M. B. (2012). Assessment of existing roadside swales with engineered filter soil: I. Characterization and lifetime expectancy. *J. Environ Qual,* 41(6), 1960-1969.

Jones, P. S., and Davis, A. P. (2013). Spatial accumulation and strength of affiliation of heavy metals in bioretention media. *J. Environ. Eng*., 139, 479-487.

Johnson, J. P., and Hunt, W. F. (2016). Evaluating the spatial distribution of pollutants and associated maintenance requirements in an 11 year-old bioretention cell in urban Charlotte, NC. *J. Environ. Manage.*, 18(2), 363-370.

Kluge, B., Markert, A., Facklam, M., Sommer, H., Kaiser, M., Pallasch, M., and Wessolek, G. (2016). Metal accumulation and hydraulic performance of bioretention systems after long-term operation. *J. Soils Sed.* 18, 431-441.

Lange, K., Österlund, H., Viklander, M., and Blecken, G. T. (2020). Metal speciation in stormwater bioretention: Removal of particulate, colloidal and truly dissolved metals. *Sci. Tot. Environ.,* 734, 138121.

LeFevre, G. H., Paus, K. H., Natarajan, P., and Gulliver, J. S. (2015). Review of dissolved pollutants in urban storm water and their removal and fate in bioretention cells. *J. Env. Eng.*, 141(1), 0401 4050.

Li, H., and Davis, A. P. (2008). Heavy metal capture and accumulation in bioretention media. *Environ. Sci. Technol., 42*(14), 5247-5253.

Liebens, J. (2001). Heavy metal contamination of sediments in stormwater management systems: the effect of land use, particle size, and age. *Environ. Geol.*, 41(3-4), 341-351.

Lim, H. S., Lim, W., Hu, J. Y., Ziegler, A., and Ong, S. L. (2015). Comparison of filter media materials for heavy metal removal from urban stormwater runoff using biofiltration systems. *J. Environ. Manage.*, 147, 24-33.

Lindfors, S., Österlund, H., and Viklander, M. (2017). Truly dissolved and labile Cu and Zn in urban runoff from a parking lot, an industrial area and copper and zinc roofs 14th IWA/IAHR International Conference on Urban Drainage: Conference Proceedings, Prague, Czech Republic.

Kidd, P., Barceló, J., Bernal, M. P., Navari-Izzo, F., Poschenrieder, C., Shileve, S., Clemente, R., and Monterroso, C. (2009). Trace element behaviour at the root–soil interface: Implications in phytoremediation. *Environ. Exp. Bot*. 67, 243-259.

Kluge, B., Markert, A., Facklam, M., Sommer, H., Kaiser, M., Pallasch, M., and Wessolek, G. (2018). Metal accumulation and hydraulic performance of bioretention systems after long-term operation. *J. Soils Sediments* 18, 431-441.

Link, D. D., Walter, P. J., and Kingston, H. M. (1998). Development and validation of the new EPA microwave-assisted leach method 3051A. *Environ. Sci. Technol*., 32 (22), 3628-3632.

Mertens, J. and Smolders, E. (2013). Chapter 17, Zinc. In: Heavy metals in soils: Trace metals and metalloids in soils and their bioavailability (3rd edition), Alloway, B. (Ed.), Springer, Dordrecht, Netherlands, 465-493.

Miller, J.D., Kim, H., Kjeldsen, T.R., Packman, J., and Grebby, S. (2014). Assessing the impact of urbanization on storm runoff in a peri-urban catchment using historical change in impervious cover. *J. Hydrol*., 515, 59-70.

Mohanty, S. K., Valenca, R., Berger, A. W., Yu, I. K. M., Xiong, X., Saunders, T. M., and Tsang, T. C. W. (2018). Plenty of room for carbon on the ground: Potential applications of biochar for stormwater treatment, *Sci. Tot. Environ*., 625, 1644-1658.

Muerdter, C. P., Wong, C. K., and LeFevre, G. (2018). Emerging investigator series: the role of vegetation in bioretention for stormwater treatment in the built environment: pollutant removal, hydrologic function, and ancillary benefits. *Environ. Sci.: Water Res. Technol.*, 4, 592-612.

Mulvaney, R. L. (1996). Nitrogen – inorganic forms, In: Methods of Soil Analysis, Part 3 – Chemical Methods. SSSA Book Series No. 5. Sparks D. L. (Ed.), Soil Science Society of America, Madison, WI, 1129-1131.

National Climatic Data Center (2020). Climate data online search, Global summary of the year for Santa Barbara Municipal Airport, CA, US station, accessed on 06/212020, https://www.ncdc.noaa.gov/cdo-web/datasets/GSOY/stations/GHCND:USW00023190/detail

Nelson, D. W., and Sommers, L. E. (1996). Total carbon, organic carbon, and organic matter, In: Methods of Soil Analysis, Part 3 – Chemical Methods. SSSA Book Series No. 5. Sparks D. L. (Ed.)., Soil Science Society of America, Madison, WI, 1002-1005.

National Research Council (2009). Urban stormwater management in the United States. The National Academies Press, Washington, DC.

Paus, K. H., Morgan, J., Gulliver, J. S., Leiknes, T., Hozalski, R. M. (2014a). Effects of temperature and NaCl on toxic metal retention in bioretention media. *J. Environ. Eng*., 140(10), 04014034.

Paus K. H., Morgan, J., Gulliver, J. S., Leiknes, T., Hozalski, R. M. (2014b). Assessment of the hydraulic and toxic metal removal capacities of bioretention cells after 2 to 8 years of service. *Water Air Soil Pollut*., 225, 1803.

Payne, E. G., Fletcher, T. D., Cook, P. L., Deletic, A., and Hatt, B. E. (2014). Processes and drivers of nitrogen removal in stormwater biofiltration. *Crit. Rev. Env. Sci. Tech.*, 44(7), 796-846.

Payne, E. G., Hatt., B. E., Deletic, A., Dobbie, M. F., McCarthy, D. T., and Chandrasena, G. I. (2015). Adoption guidelines for stormwater biofiltration systems – Summary report. Melbourne, Australia: Cooperative Research Centre for Water Sensitive Cities.

Read, J., Wevill, T., Fletcher, T., and Deletic, A. (2008). Variation among plant species on pollutant removal from stormwater non biofiltration systems. *Water Res.*, 42(4-5), 893-902.

Rible, J. M. and Quick, J. (1960). Method S-19.0. Cation exchange capacity. In: Water soil plant tissue. Tentative methods of analysis for diagnostic purposes. Davis, University of California Agricultural Experiment Service. Mimeographed Report.

Rodriguez, S. M., Henriques, B., Coimbra, J., Kilburn, J. E., and Fey, D. L. (2010). Water-soluble fraction of mercury, arsenic and other potentially toxic elements in highly contaminated sediments and soils. *Chemosphere*, 78, 1301-1312.

Santa Barbara County of Public Works – Flood Control District (2020). Monthly and yearly rainfall record, Station: 200, Station Name: UCSB, accessed on 06/28/2020, <http://cosb.countyofsb.org/pwd/water/downloads/hydro/200dailys.pdf>

Seguin, V., Gagnon, C., and Courchesne, F. (2004). Changes in water extractable metals, pH and organic carbon concentrations at the soil-root interface of forested soils. *Plant Soil* 260, 1-17.

Sheldrick, B. H. and Wang, C. (1993). Particle-size distribution. In: Carter, M. R. (ed), Soil Sampling and Methods of Analysis, Canadian Society of Soil Science, Lewis Publishers, Ann Arbor, MI, 499-511.

Smith, D.B., Cannon, W.F., Woodruff, L.G., Solano, F., Kilburn, J.E., and Fey, D.L. (2013), Geochemical and mineralogical data for soils of the conterminous United States: U.S. Geological Survey Data Series 801, 19 p.

State of Washington Department of Ecology (2019). Stormwater management manual for western Washington. Publication No.19-10-021

State Water Resources Control Board (2016). WQ 2016-0068-DDW. Water reclamation requirements for recycled water use, accessed on 06/28/2020, <https://www.waterboards.ca.gov/board_decisions/adopted_orders/water_quality/2016/wqo2016_0068_ddw.pdf>

Sun, X., and Davis, A. P. (2007). Heavy metal fates in laboratory bioretention systems. *Chemosphere*, 66(9), 1601-1609.

Tedoldi, D., Chebbo, G., Pierlot, D., Kovacs, Y., and Gromaire, M. C. (2016). Impact of runoff infiltration on contaminant accumulation and transport in the soil/filter media of sustainable urban drainage systems: a literature review. *Sci. Total Environ.*, 569-570, 904-926

Tedoldi, D., Chebbo, G., Pierlot, D., Branchu, P., Kovacs, Y., and Gromaire, M. C. (2017). Spatial distribution of heavy metals in the surface soil of source-control stormwater infiltration devices – Inter-site comparison. *Sci. Total Environ.*, 579, 881-892.

Thomas, G. W. (1996). Soil pH and soil acidity, In: Methods of Soil Analysis, Part 3 – Chemical Methods. SSSA Book Series No. 5. Sparks D. L. (Ed.), Soil Science Society of America Madison, WI, 475-490.

UC Davis Analytical Lab, work request number 19S087, samples 1-4, accessed on 07/04/20 at https://anlab.ucdavis.edu/Results/Link/8c2afe47-3616-4738-9135-ab987c2ed980

U.S. Department of Agriculture (1986). Urban hydrology for small watersheds. Technical Release 55, 210-VI-TR-55, Second Ed., Chapter 2, accessed 07/04/2020, available at <https://www.nrcs.usda.gov/Internet/FSE_DOCUMENTS/stelprdb1044171.pdf>

U.S. Environmental Protection Agency (2007a). Ecological Screening Levels for Copper. Interim Final. OSWER Directive 9285.7-68. Washington, DC: USEPA, accessed 06/28/2020, <https://rais.ornl.gov/documents/eco-ssl_copper.pdf>

U.S. Environmental Protection Agency (2007b). Ecological Screening Levels for Zinc. Interim Final. OSWER Directive 9285.7-73. Washington, DC: USEPA, accessed 06/28/2020, <https://rais.ornl.gov/documents/eco-ssl_zinc.pdf>

USGS (2020). The National Map. Sources: Esri, HERE, Garmin, Intermap, increment P Corp., GEBCO, USGS, FAO, NPS, NRCAN, GeoBase, IGN, Kadaster NL, Ordnance Survey, Esri Japan, METI, Esri China (Hong Kong), (c) OpenStreetMap contributors, and the GIS User Community.

Walker, D. J., Clemente, R., Roig, A., and Bernal, M. P. (2003). The effects of soil amendments on heavy metal bioavailability in two contaminated Mediterranean soils. *Environ Pollut*., 122(2), 303-312.

Werkenthin, M., Kluge, B., and Wessolek, G. (2014). Metals in European roadside soils and soil solution – A review. *Environ. Pollut.*, 189, 98-110.
West, A., and Sparling, G. (1986). Modifications to the substrate-induced respiration method to permit measurement of microbial biomass in soils of differing water contents. *J. Microbiol. Methods*, 5, 177-189.
Young, S.D. (2013). Chemistry of heavy metals and metalloids in soils. In: Heavy Metals in Soils. Environmental Pollution, Vol 22. Springer, Alloway B. (ed.). Dordrecht, Netherlands, 51-95.

2.7. Figures and Tables

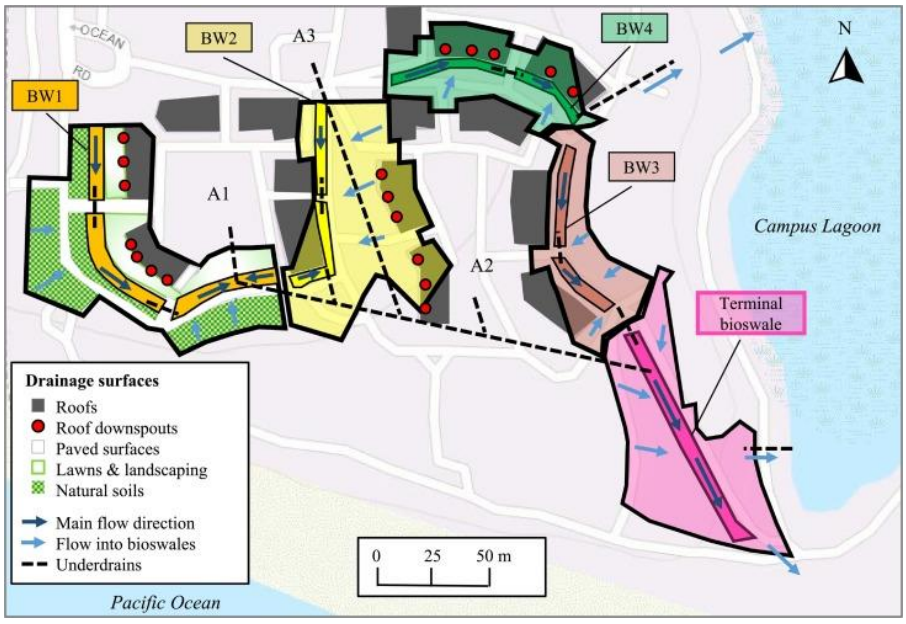

Fig. 1. Schematic of study bioswales (BW1-4) (Fig. S1) and terminal bioswale (not included in study), with the respective drainage areas outlined in black, overlaying a USGS base map (USGS, 2020). Main flow direction in the bioswales is shown as dark arrows. Flows into the bioswales are indicated by light blue arrows. Bioswale segments are connected via underdrains (dashed black lines). At the outlets of BW1, BW2 and BW3, runoff is conveyed via underdrains to a terminal bioswale, which also receives stormwater runoff from zones A1-A3. Final discharges are into the campus lagoon and the beach adjacent to the study site (southeast corner). At the outlet of BW4, an underdrain conveys runoff to a marsh which discharges into the lagoon (northeast corner). For BW1, the delineation of specific drainage areas is shown, including roofs, paved surfaces, lawns and landscaping, and natural soils. For BW2, BW3, and BW4, roofs and roof downspouts within each drainage area are shown. Except for BW1, roof color is in the background when in the drainage area. (For interpretation of the references to color in this figure legend, the reader is referred to the web version of this article).

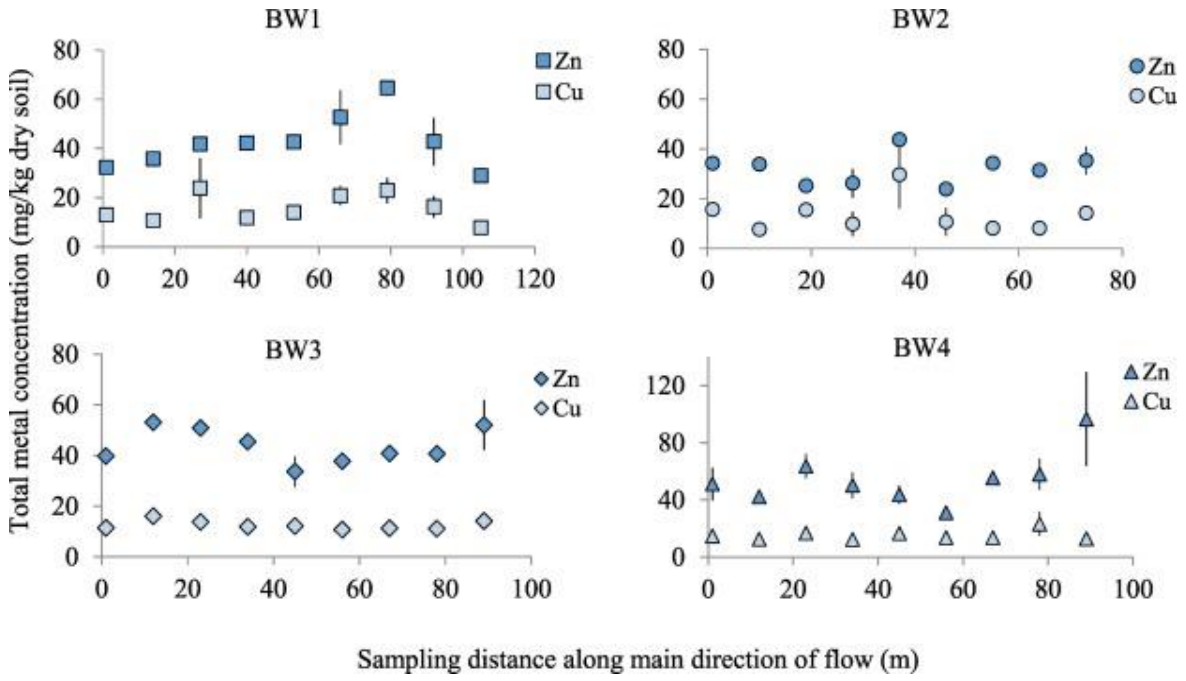

Fig. 2. Total Cu and Zn concentrations in sampled soils along bioswale flow axes. The most upstream sampling location (0 m) is at the north end for BW1, BW2, and BW3, and at the west end for BW4 (Fig. 1). Due to high vegetation density impeding access, the most downstream sampling locations in BW1 and BW2, were 30 m and 15 m in from the east end, and west end, respectively (Fig. 1). Each data point represents the average concentration across one basin bed and one side slope soil sample per sampling location (Fig. S3) for a total of 18 samples per bioswale (BW1-4) (Figs. 1 and S1). Vertical lines show the range of measured concentrations.

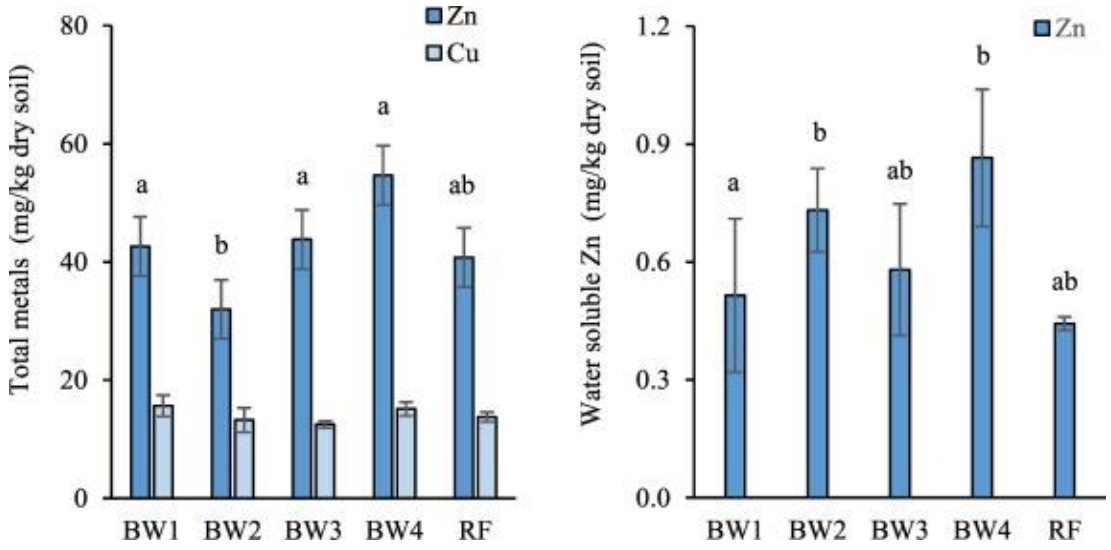

Fig. 3. Total Zn and Cu (a), and water soluble Zn (b) concentrations (mean and standard error) in sampled soils. Means are averages for basin bed and slide slope samples across nine sampling locations (Figs. 2 and S3) for the study bioswales (BW1-4) and four reference soil samples (RF) (Fig. S1). Like letters above the bars denote no significant difference for total or water soluble Zn (Kruskal-Wallis, post-Dunn test, $n = 76$, $\alpha = 0.05$). There were no significant differences for total Cu, and water soluble Cu was below detection limit in all samples.

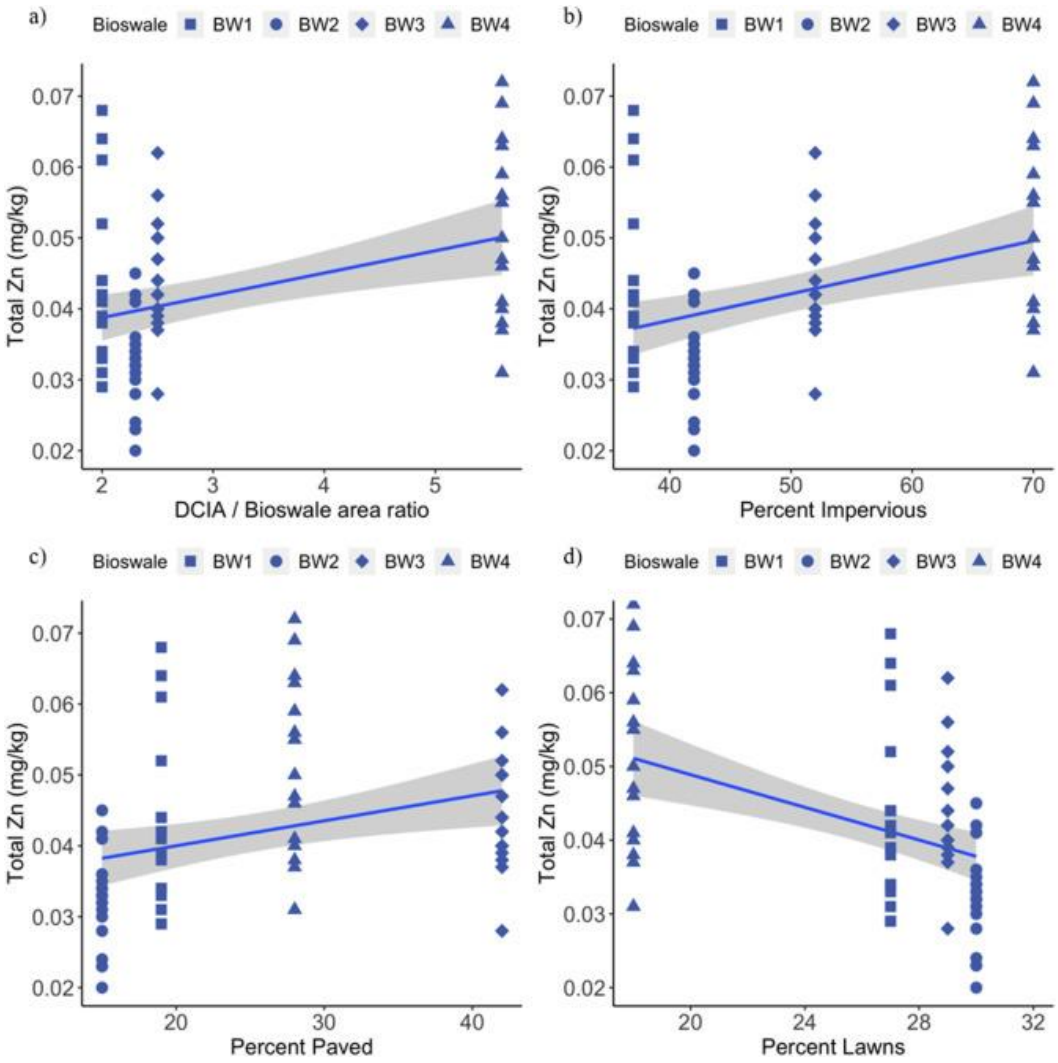

Fig. 4. Spearman correlations between the ranks of total Zn concentration and drainage area characteristics (Table 1) in sampled soils. Results from basin bed and slide slope samples for nine sampling locations (Figs. 2 and S3) for study bioswales (BW1–4) (Fig. S1). One outlier from BW4 has been removed from all data. a) Directly connected impervious area (DCIA) to bioswale area ratio ($\rho = 0.32$, $n = 71$, $p = 0.0073$); b) Percent Impervious ($\rho = 0.32$, n = 71, p = 0.0073), c) Percent Paved surfaces ($\rho = 0.46$, n = 71, $p = 5.6$ E-05); and d) Percent Lawns ($\rho = -0.48$, n = 71, $p = 2.4$ E-05). The gray shaded area represents the 95% confidence interval around the line of best fit. Significance level is $\alpha = 0.05$.

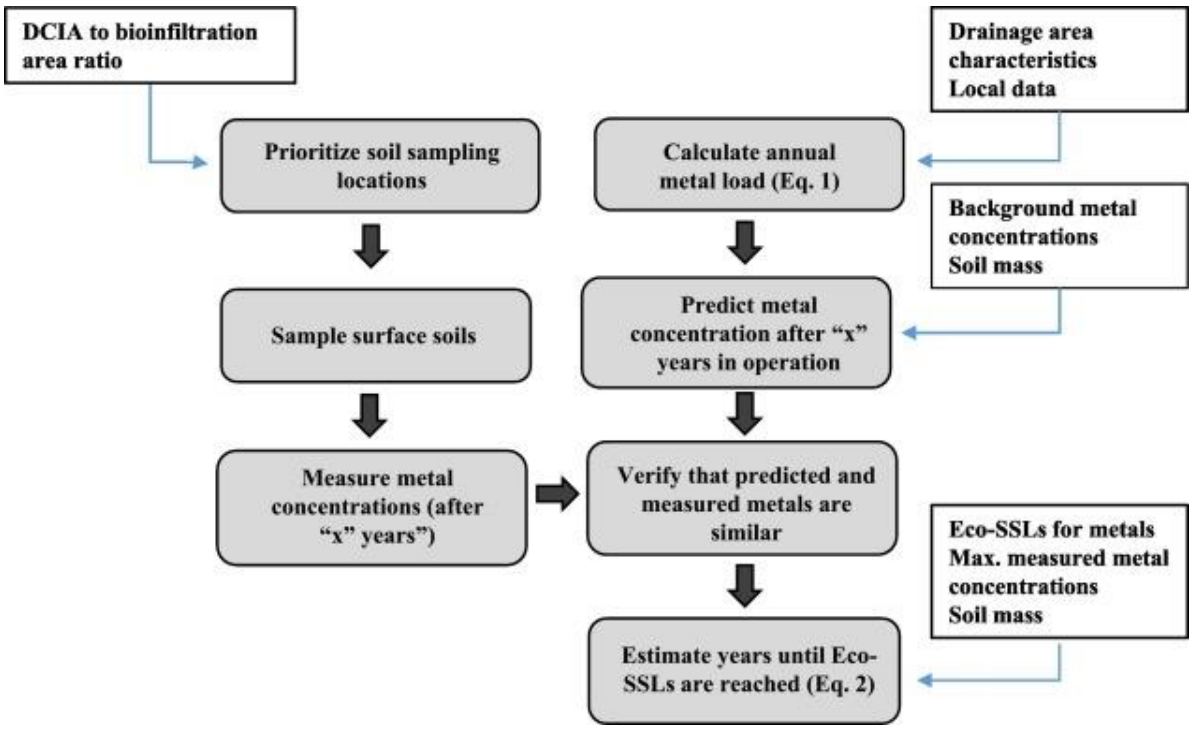

Fig. 5. Proposed strategy to manage soils to protect resident soil biota. The approach includes prioritizing sampling locations for metal analysis based on the ratio of DCIA to bioinfiltration area, calculating annual metal load to predict current soil metal concentrations, comparing predicted and measured concentrations, and projecting future metal concentrations to estimate years until Eco-SSLs are reached. Inputs required to compute the annual metal load are local data of annual precipitation and metal concentrations in stormwater runoff, and drainage area characteristics such as infiltrating soil type, percent vegetation cover, percent impervious drainage, and total drainage area. To estimate the soil mass accumulating metals, inputs are bioinfiltration area, soil depth, and bulk density. Trajectory to Eco-SSLs is estimated based on maximum metal concentrations to represent conservative estimates.

Table 1. Characteristics of drainage areas, bioswales, and soils for study bioswales (BW1 – 4) (Fig. S1).

Characteristics	**BW1**	**BW2**	**BW3**	**BW4**
Drainage Area				
Total Drainage Area (DA) (m^2)	4191	3978	1615	2231
Paved surfaces (%)	19	15	42	28
Rooftops (%)	18	29	11	43
Lawns (%)	27	29	29	18
Natural soils (%)	36	27	18	11
Impervious (%) [a]	37	44	53	71
TIA (m^2) [b]	1586	1756	850	1572
DCIA (m^2) [c]	1586	851	850	1572
Bioswale				
Bioswale Area (m^2)	762	396	345	274
DA/Bioswale Area Ratio	5.5	10.0	4.7	8.1
TIA/Bioswale Area Ratio	2.0	4.5	2.5	5.7
DCIA/Bioswale Area Ratio	2.0	2.2	2.5	5.7
Soil [d]				
Gravimetric Moisture (%)	15.8 (4.5)	21.3 (4.4)	13.6 (2.3)	16.5 (3.9)
Organic Matter (%)	6.6 (3.8)	6.2 (1.1)	6.7 (1.7)	5.9 (2.6)
Nitrate (mg/kg dry soil)	22.5 (14.4)	18.4 (6.4)	6.1 (5.3)	4.2 (3.9)
Phosphate (mg/kg dry soil)	8.0 (6.4)	3.8 (2.9)	1.6 (2.6)	2.7 (1.8)
pH	8.1 (0.4)	8.2 (0.3)	8.0 (0.2)	8.0 (0.3)

[a.] Impervious percent calculated as the sum of the percent paved surfaces and rooftops.

[b] TIA = total impervious drainage area (paved surfaces and roofs

[c] DCIA = directly connected impervious area (paved surfaces and connected roofs).

[d] Values for soil properties include mean and standard deviation (n = 18 per bioswale).

Table 2. Range of total Cu and Zn soil concentrations for the study bioswales (BW1 – 4) (Fig. S1) as compared to published data for other bioinfiltration systems, including swales, rain gardens, and bioretention cells.

Bioretention system, runoff type, and soil sampling depth	**Age (years)**	**Total Cu (mg/kg dry soil)**	**Total Zn (mg/kg dry soil)**	**Reference**
Bioswales, residential, 0 – 10 cm	> 14	10 – 43	16 - 130	This study
Swales, parking lot, 0 – 15 cm	2 – 10	26 –131	66 – 229	Achleitner et al. 2007
Swales, street and parking lot, 0 – 3 cm	10 – 25	20 – 200 [a]	50 – 850	Tedoldi et al. 2017
Swales, road, surface, 0 – 10 cm [b]	ns	2 – 50	16 – 565	Liebens et al. 2001
Swales, road, 0 – 15 cm	5 – 15	12 –100 [c]	40 – 400 [c]	Ingvertsen et al. 2012
Swales, roads, topsoil 0 – 20 cm [a]	1 – 34	3 – 730	13 – 2,520	Horstmeyer et al. 2016
Swales, roads and parking lots, 0 – 10 cm	11 – 22	6 – 210	2 – 1800	Kluge et al. 2018
Rain garden, roof runoff, 0 – 5 cm	2	15 –17	39 – 68	Dietz and Clausen 2006
Bioretention, parking lot, 0 – 10 cm	3.5 – 4.5	30 – 50	80 – 180	Li and Davis 2008
Bioretention, parking lot, 0 – 10 cm	4	8 – 50	30– 250	Jones and Davis 2013
Bioretention, street and parking lot, 0 – 10 cm	2 –8	5 – 20	45 – 88	Paus et. al. 2014b
Bioretention, parking lot, 0 – 5 cm, 5 – 10 cm	11	2 – 18	5 –228	Johnson and Hunt 2016

ns: not specified

[a] Range corresponds to 1st decile and 9th decile.

[b] Liebens et al. (2001) did not specify sampling depth; surface assumed equal to 0 – 10 cm.

[c] Mean values for studied systems.

Table 3. Initial, predicted and measured metal concentrations, annual metal loading, and years until ecological soil screening levels (Eco-SSLs) are reached based on maximum surface (0 – 10 cm) soil metal concentrations. Annual total metal loadings were calculated by multiplying the estimated average yearly runoff volume entering each bioswale (V_R, Table S2) by the average local metal concentrations in stormwater runoff (Tables S3 and S4). Eco-SSLs are guidance provided by the U.S. EPA, representing concentrations of contaminants protective of four terrestrial ecological receptors: birds, plants, mammals, and soil invertebrates (U.S. EPA 2007a).

Parameters	**Cu**				**Zn**			
Bioswale	BW1	BW2	BW3	BW4	BW1	BW2	BW3	BW4
Initial concentration (mg/kg) [a]	10.1	10.0	10.0	11.6	30.4	23.2	37.7	35.6
Annual loading (mg/kg per year)	0.23	0.41	0.20	0.36	1.73	3.13	1.53	2.75
Predicted concentration (mg/kg) [b]	13.3	15.7	12.8	16.7	54.6	67.1	59.1	74.1
Mean concentration (mg/kg) [c]	15.9	14.6	12.5	15.2	42.6	32.0	43.8	54.7
Max. concentration (mg/kg) [c]	36.0	43.2	19.4	31.6	67.8	45.2	61.8	129.5
Years to low Eco-SSL [d]	0	0	43.2	0	0	0.3	0	0
Years to high Eco-SSL [e]	195.3	90.5	10.0	135.7	53.2	36.7	64.2	11.1

[a] At time of construction, estimated from first decile data of measured metals.

[b] After 14 years in operation, based on initial concentrations and annual metal loading.

[c] Based on actual concentrations in sampled soils.

[d] Low and high Eco-SSL are 28 mg/kg soil (birds) and 80 mg/kg soil (invertebrates), respectively (U.S. EPA 2007a).

[e] Low and high Eco-SSL are 46 mg/kg soil (birds) and 120 mg/kg soil (plants), respectively (U.S. EPA 2007b).

2.8. Appendix A - Supplementary Information

2.8.1. Additional Methods

Estimation of runoff volumes to calculate annual metal loads

Runoff volumes entering each bioswale were calculated via the curve number (CN) method outlined in 210-VI-TR-55 (USDA NRCS 1986). Input parameters for the calculation include the yearly average precipitation for the period 2002 – 2015 (378 mm/yr), measured at a weather station close to the site (UCSB; station no. 200; N 34°24' 56"; W 119°50'43") (Santa Barbara County Public Works 2020), and appropriate runoff CNs for soils in hydrologic group C, which is representative of soils in the study site. Runoff (Q_R) for each bioswale was calculated as:

$$Q_R\ (mm) = \frac{(P-I)^2}{P-I+S} = \frac{(P-0.05S)^2}{P+0.95S} \qquad (S.1)$$

Where:

P = precipitation (mm)

S (in) = potential maximum retention after runoff begins (in) = [1000/CN -10]

S (mm) = S(in) x 25.4 mm/in

I = initial abstraction (mm), here defined as I = 0.05S. This is an actualization from the original formula (I = 0.2S), proposed by Woodward et al. (2003) after evaluating runoff-rainfall data from several hundred storm events.

CN = curve number (dimensionless, takes values from 0 to 100)

A composite CN is computed for each bioswale using Fig. 2.3 in 210-VI-TR-55 (USDA NRCS 1986). The directly connected impervious area, which includes paved surfaces and roofs connected to bioswales via cobble drains (Table 1), is used as the x-axis value to read

up from until intersecting the appropriate pervious CN curve, and the composite CN value is read across on the y-axis. For the study site, a pervious CN of 74 is selected, corresponding to open space in good condition for soils in hydrologic group C (Table 2.2a, 210-VI-TR-55 (USDA NRCS 1986) (Table S2). The runoff volume (V_R) entering each bioswale (Table S2) is the product of the Q_R computed in eq. S1 and the respective drainage area (Table 1).

Substrate induced respiration (SIR)

The headspace volume in the bottle used for the SIR assay was estimated by subtracting media (10 mL) and soil volumes from bottle volume (256 mL). Soil volume was estimated from the dry soil weight and a soil bulk density of 1.5 g/cm^3, appropriate for a sandy loam.

To avoid significant pressure differentials during the 3-hour incubation, at each sampling time 5 mL of air were injected into the bottle using a syringe, the headspace was mixed by pumping the syringe three times, and a well-mixed headspace sample (5 mL) was extracted. No overpressure or vacuum was observed during any of the sampling steps. To calculate the actual CO_2 concentration at each sampling point, prior to the addition of 5 mL of air, the law of additive volumes was used, assuming ideal gas behavior, such that:

$$[CO_2]_{actual} = ([CO_2]_{measured} \times V_{total} - V_{air} * [CO_2]_{air}) \times V_{headspace}^{-1}$$

Where:

$[CO_2]_{actual}$ is the CO_2 concentration in ppm (v/v), accounting for the air dilution effect

$[CO_2]_{measured}$ is the CO_2 concentration in ppm (v/v), measured by the gas analyzer

V_{total} is the sum of the headspace volume and the air addition volume, in mL

V_{air} is the volume of air addition, which is 5 mL

$V_{headspace}$ is the volume of the bottle minus the volume of soil and media

2.9. Additional Figures and Tables

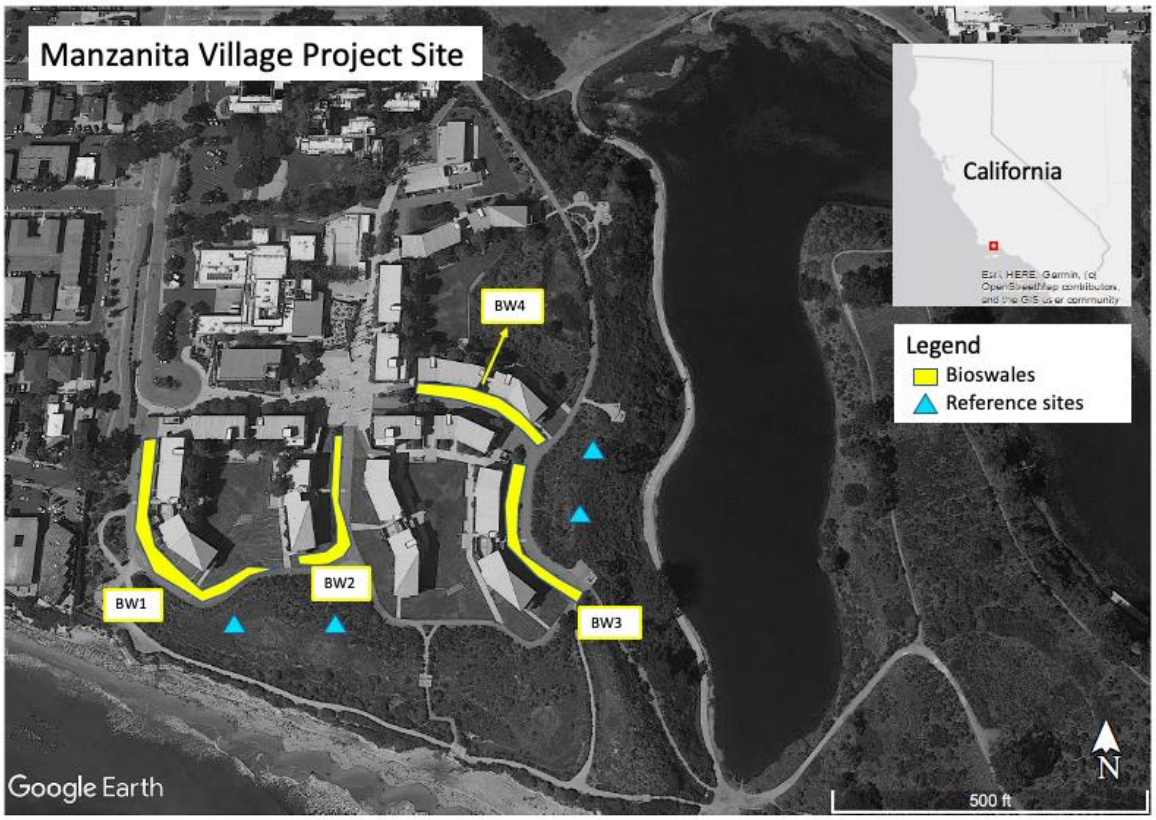

Fig. S1. Aerial image of Manzanita Village project site (N 34°24’32”; W 119°51’28”) downloaded on 06/22/2020 from Google Earth. Study bioswales (BW1-4) are delineated in yellow. Reference sites, shown via blue triangles, are areas that are close to the bioswales, and do not receive runoff from built infrastructure.

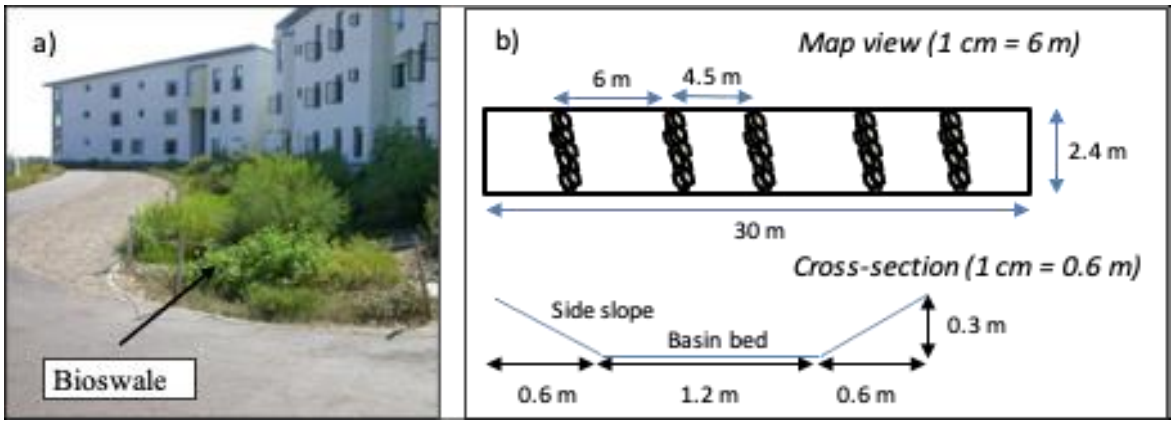

Fig. S2. a) Example photograph of one study bioswale (BW2) (Fig. S1). b) Schematic of bioswale geometry showing plan view (top) of basins separated by rock check dams, and basin cross-section (bottom), with location of basin bed and side slope.

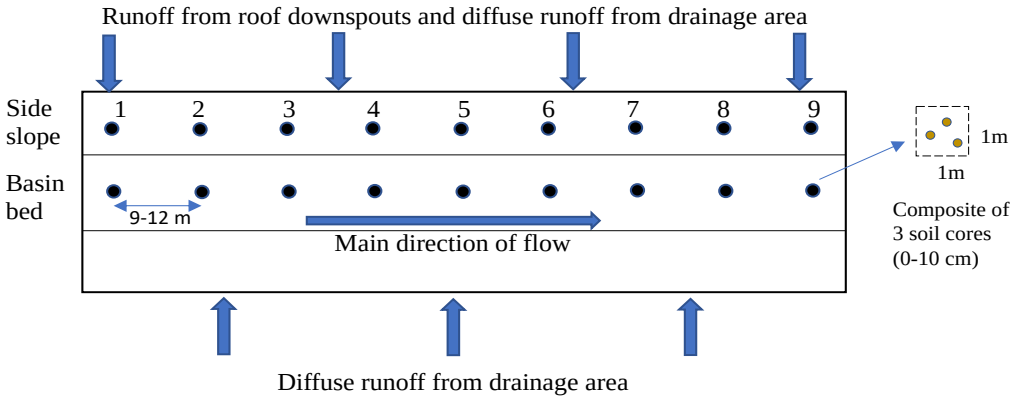

Fig. S3. Soil sampling schematic. Nine locations, equally spaced (9 to 12 meters apart depending on the total length of the bioswale), were chosen to span the length of each bioswale. At each location, soils were sampled from the basin bed and from the side slope, for a total of 18 samples per bioswale. Each sample is a composite of three soil cores, sampled to a depth of 10 cm.

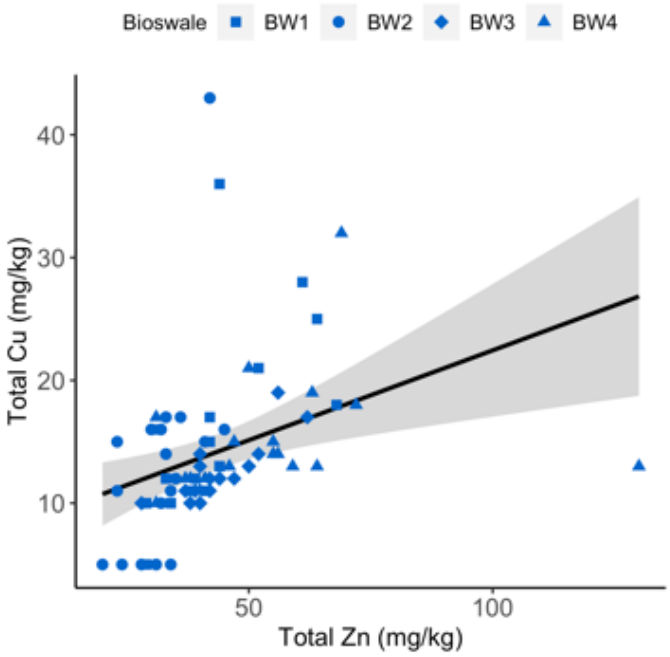

Fig.S4. Spearman correlation between the ranks of total Cu and Zn ($\rho = 0.58$, n = 72, p = 8.5 E-08) for sampled soils. Plotted data include those from the basin bed and side slope samples from nine sampling locations (Fig. 2) for study bioswales (BW1-4) (Fig. S1). The gray shaded area represents the 95% confidence interval around the line of best fit. Significance level is $\alpha = 0.05$.

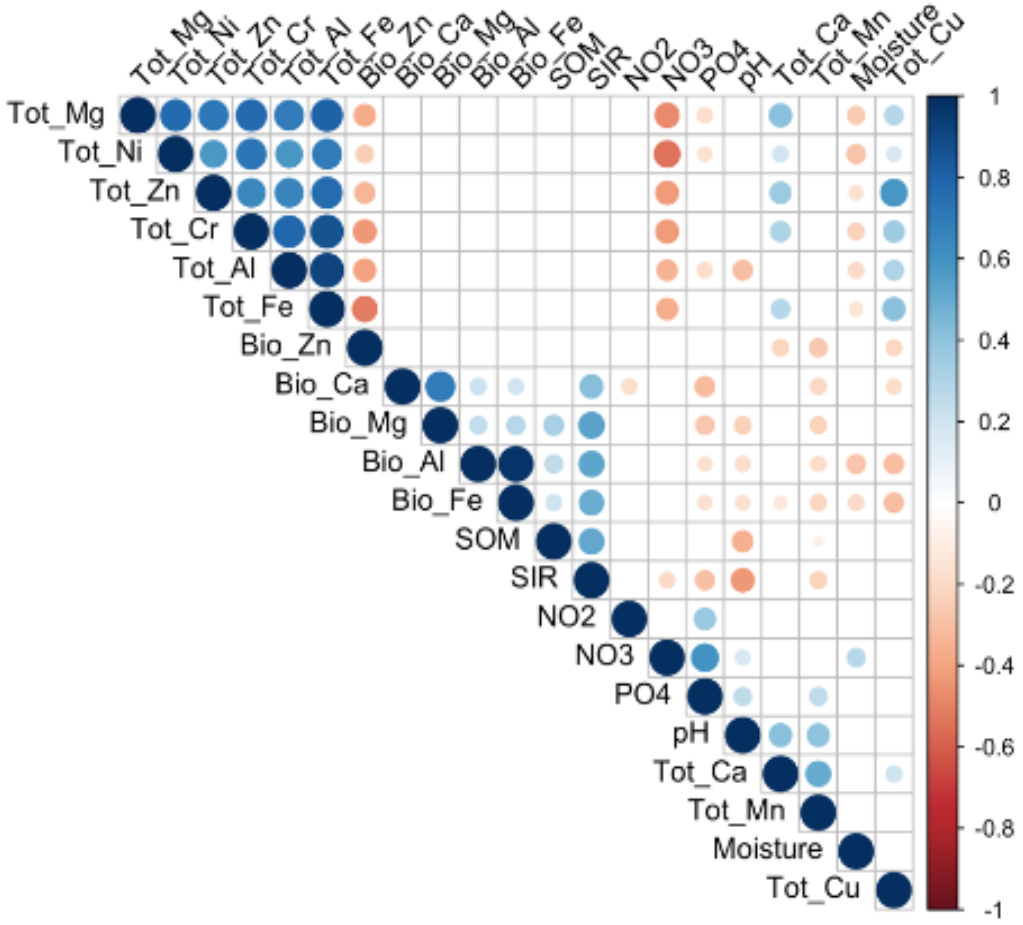

Fig. S5. Spearman correlations between the ranks of physicochemical characteristics and metal concentrations for sampled soils. Data includes soils basin bed and side slope samples for nine sampling locations (Fig. 2) of the study bioswales (BW1-4) (Fig. S1). The correlogram indicates significant correlations in blue (positive) and red (negative), where the size and color intensity of circles are proportional to the correlation coefficients. The legend (right) shows the coefficient values corresponding to the color scale. Blank spaces correspond to non-significant correlations ($\alpha = 0.05$). Total, and water soluble metals are indicated with the prefix "Tot", and "Bio", respectively.

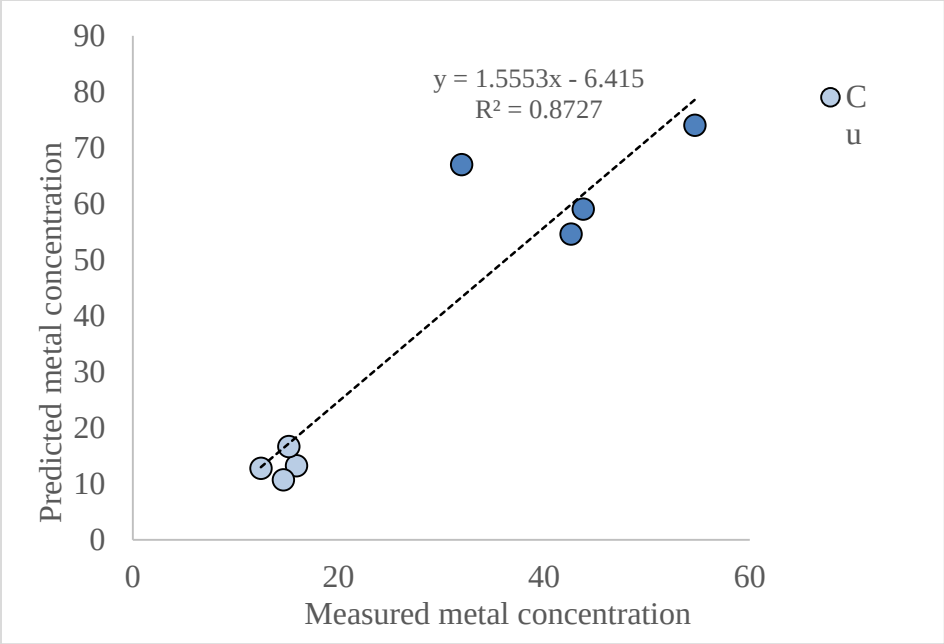

Fig. S6. Comparison between predicted and measured mean metal concentrations in sampled soils. Predicted metal concentrations were derived from the annual metal loads, years in operation, and background metal concentrations. Background metal concentrations were estimated as the first decile of all measured metal concentrations in sampled soils, including data from basin bed and side slope samples from nine sampling locations (Fig. 2) for study bioswales (BW1-4) (Fig. S1).

Table S1. Characteristics of tertiary treated and disinfected reclaimed water used for lawn irrigation in the study area. Data represents an annual average from monthly data from the Goleta Sanitary District 2017 Water Reclamation Annual Report (Goleta Sanitary 2018).

Parameter	**Value** [a]	**NPDES Limit** [b]
Turbidity, daily maximum (NTU)	1.90 (1.25)	5
Turbidity, daily average (NTU)	0.31 (0.13)	2
Total suspended solids (mg/L)	< 1.0 (0.1)	10
Biochemical oxygen demand (mg/L)	< 2 (0)	10
Settleable solids (mg/L)	< 0.1 (0.0)	0.1
pH (units)	7.0 (0.2)	6.5 - 8.4
Total coliform (MPN per 100 mL)	< 1.0 (0.0)	2.2
Chlorine residual minimum (mg/L)	15.4 (3.1)	5
Chlorine residual maximum (mg/L)	17.9 (1.8)	ns
Total dissolved solids (mg/L)	1,266 (111)	1500
Cadmium (μg/L)	0.31 (0.00)	0.01
Lead (μg/L)	2.96 (1.22)	5

[a] Values are mean and standard deviation (n = 12 for all parameters except total dissolved solids, n = 4, and cadmium and lead, n = 2).

[b] NPDES: National Pollutant Discharge Elimination System. Values represent water quality criteria in the NPDES permit for Goleta Sanitary District.

ns: not specified.

Table S2. Calculation parameters and results for yearly stormwater runoff entering study bioswales BW1-4. This calculation is derived from the average yearly precipitation and drainage area characteristics including directly connected impervious area, following the curve number method outlined in 210-VI-TR-55 (USDA 1986).

Parameter	**BW1**	**BW2**	**BW3**	**BW4**
Connected impervious area %	38	20	53	71
Pervious CN, open space > 75% cover, hydrologic soil group C[a]	74	74	74	74
Impervious CN[a], paved roads and roofs, hydrologic soil group C	98	98	98	98
Composite CN[b]	83	80	87	91
Potential maximum abstraction, S[c]	2.05	2.50	1.49	0.99
Average yearly runoff, Q (m)[d]	0.33	0.32	0.34	0.36
Average yearly runoff volume, V_R (m^3)[e]	1384	1290	553	789

[a] CN = curve number, obtained from Table 2-2a in 210-VI-TR-55 (USDA 1986)

[b] Composite curve number, obtained from Figure 2-3 in 210-VI-TR-55 (USDA 1986)

[c] S (in) = 1000/CN – 10 as per equation 2-4 in 210-VI-TR-55 (USDA 1986); S (mm) = S (in) x 25.4 mm/in

[d] Q given by equation 2-1 in 210-VI-TR-55 (USDA 1986), with I = initial abstraction = 0.05 following update suggested in Woodward et al. 2003 and converting from inches to meters.

[e] V_R = Q (m) x Drainage area (m^2) (Table 1).

Table S3. Total Cu concentrations in stormwater runoff entering low impact development (LID) sites in Santa Barbara, California. Runoff samples were collected by the City of Santa Barbara Creeks Division and tested for total recoverable metals by inductively coupled plasma-atomic emission spectroscopy (ICP-AES), following U.S. EPA method 6010B.

Station ID	Sample Type	Sample Date	Cu (mg/L)
LIDLot4	Grab	22/Jan/2009	0.049
LIDLot4	Grab	13/Oct/2009	0.090
LIDMacKen	Grab	07/Dec/2009	0.039
LIDMacKen	Grab	06/Oct/2010	0.013
LIDOakTenn	Grab	17/Nov/2012	0.010
LIDOakStag	Grab	17/Nov/2012	0.010
LIDStevePk	Grab	17/Nov/2012	0.011
LIDOakPicn	Grab	17/Nov/2012	0.016
LIDOakMain	Grab	17/Nov/2012	0.017
LIDWSNeigh	Grab	17/Nov/2012	0.031
LIDOakMain	Grab	24/Jan/2013	0.020
LIDOakPicn	Grab	24/Jan/2013	0.026
LIDOakTenn	Grab	24/Jan/2013	0.014
LIDWSNeigh	Grab	24/Jan/2013	0.026
LIDStevePk	Grab	24/Jan/2013	0.052
LIDOakMain	Composite	07/Mar/2013	0.012
LIDWSNeigh	Composite	07/Mar/2013	0.081
LIDOakTenn	Composite	07/Mar/2013	0.010
LIDStevePk	Composite	07/Mar/2013	0.011
LIDOakStag	Grab	24/Jan/2013	0.010
LIDOakPicn	Composite	07/Mar/2013	0.010
LIDOakStag	Composite	07/Mar/2013	0.010
Mean and standard deviation (mg/L)			0.026 (0.023)
Mean and standard deviation (mg/m^3)			25.8 (23.1)

Table S4. Total Zn concentrations in stormwater runoff entering low impact development (LID) sites in Santa Barbara, California. Runoff samples were collected by the City of Santa Barbara Creeks Division and tested for total recoverable metals via ICP-AES, following U.S. EPA method 6010B.

Station ID	Sample Type	Sample Date	Zn (mg/L)
LIDLot4	Grab	22/Jan/2009	0.240
LIDLot4	Grab	13/Oct/2009	0.120
LIDMacKen	Grab	07/Dec/2009	0.180
LIDMacKen	Grab	06/Oct/2010	0.084
LIDStevePk	Grab	17/Nov/2012	0.044
LIDOakPicn	Grab	17/Nov/2012	0.072
LIDOakStag	Grab	17/Nov/2012	0.082
LIDOakTenn	Grab	17/Nov/2012	0.095
LIDOakMain	Grab	17/Nov/2012	0.130
LIDWSNeigh	Grab	17/Nov/2012	0.290
LIDOakMain	Grab	24/Jan/2013	0.140
LIDOakPicn	Grab	24/Jan/2013	0.160
LIDOakStag	Grab	24/Jan/2013	0.042
LIDOakTenn	Grab	24/Jan/2013	0.084
LIDWSNeigh	Grab	24/Jan/2013	0.360
LIDStevePk	Grab	24/Jan/2013	0.310
LIDOakPicn	Composite	07/Mar/2013	0.057
LIDOakMain	Composite	07/Mar/2013	0.120
LIDOakStag	Composite	07/Mar/2013	0.027
LIDWSNeigh	Composite	07/Mar/2013	0.740
LIDOakTenn	Composite	07/Mar/2013	0.066
LIDStevePk	Composite	07/Mar/2013	0.053
Mean and standard deviation (mg/L).			0.159 (0.159)
Mean and standard deviation (mg/m^3)			159.(159)

2.10 Additional References

Goleta Sanitary District (2018). 2017 Reclaimed Water Annual Report. Accessed on 08/23/20, available at https://goletasanitary.org/downloads/category/11-reclaimed-water

U.S. Department of Agriculture (1986). Urban hydrology for small watersheds. Technical Release 55, 210-VI-TR-55, Second Ed., Chapter 2, accessed on 07/04/2020, available at https://www.nrcs.usda.gov/Internet/FSE_DOCUMENTS/stelprdb1044171.pdf

Woodward, D., Hawkins, R., Jiang, R., Hjelmfelt, A., Mullem, J., and Quan, Q. (2003). Runoff curve number method: Examination of the initial abstraction ratio. World Water and Environmental Resources Congress. 1-10. 10.1061/40685(2003)308.

2.11. Appendix B – Supplementary Data

Available at:
https://ars.els-cdn.com/content/image/1-s2.0-S0048969720373095-mmc2.xlsx

Chapter 3. Influence of soil properties and soil-sequestered metals on nitrifying and denitrifying bacteria and N_2O emissions in green stormwater infrastructure.

Abstract

Improvements in stormwater biofiltration of nitrogen (N) are hindered by lack of direct study of nitrifying and denitrifying bacteria, including in relationship to general soil properties and acquired properties such as metal accumulation in soils. We assessed surface soils and N_2O emissions from six green stormwater infrastructure (GSI) sites by field sampling with sample analysis during three events over two years. Total metal concentrations occasionally exceeded soil ecotoxicological screening levels and were overall correlated with the ratio of impervious drainage area to bioretention area in the GSI systems. Denitrifying genes (2.0×10^7 to 1.9×10^8 gc/g soil) were more abundant than nitrifying genes (4.3×10^5 to 2.5×10^7 gc/g soil), but nitrification potentials measured as enzyme activities (1.4 to 7.1 mg N kg^{-1} d^{-1}) exceeded those for denitrification (0.3 to 2.2 mg N kg^{-1} d^{-1}). This, and the correlation between N_2O emissions and bacterial *amo*A genes ($r = 0.22$, $p = 0.02$), suggested nitrification as a major N transformation process. Both nitrifying and denitrifying gene abundances were negatively correlated with total Pb, and bioavailable Cd, Ni, Pb, Se, and Zn; nitrifying and denitrifying enzyme activities were negatively correlated with total As, V, and Zn. Multiple regression modeling showed that nitrifying and denitrifying gene abundances were best explained by soil properties, system age, and total Cu, Ni and V. Total metals with biological roles were positively related, suggesting that runoff may be delivering scarce metals that support cellular functions in N processing. However, bioavailable fractions

of Cd and Pb negatively impacted normalized *nir*S and *nos*Z genes, with potential implications for N_2O release. This work provided new insights into the relationships between soil properties, accumulated metals, and bacteria mediating N removal in GSI, indicating the need for risk assessment based on bioavailable metal fractions.

3.1. Introduction

Stormwater runoff in urban areas often degrades surface water quality via large pollutant loads (Walsh et al. 2004, NRC 2009). Mitigating such pollution is increasingly done through the implementation of green stormwater infrastructure (GSI) approaches. These measures include engineered bioretention systems such as biofilters, bioswales and rain gardens, which harness soils, plants, and soil microorganisms to reduce runoff volume and improve runoff water quality (Payne et al. 2014a). When runoff enters a GSI system, pollutants may be filtered, adsorbed onto soil components, taken up by plants, and transformed abiotically or by bacteria. (Hsieh and Davis 2005; Davis et al. 2006). These processes have the combined effect of removing suspended solids, fecal bacteria, and metals from runoff (Davis et al. 2003, LeFevre et al. 2015, Li et al. 2021). However, GSI varies in how effectively it removes total nitrogen (N), because bacterial transformations can generate nitrate (NO_3^-), a critical and mobile water pollutant that can be easily leached from GSI soils and result in net N export (Hatt et al. 2007, Bratières et al. 2008, Li and Davis 2009). Subsequent N transport to surface waters is linked to eutrophication and degraded water quality (NRC 2009, Walsh et al. 2004). One approach to mitigate this N pollution, is to promote denitrification in GSI soils (Zinger et al. 2013, Payne et al. 2014b). During denitrification, NO_3^- is reduced to nitrite (NO_2^-), nitric oxide (NO), nitrous oxide (N_2O), and finally dinitrogen (N_2) (Zumft 1997); it is thus permanently removed. Approximately one third of bacteria, however, may not possess *nosZ,* the gene responsible for reducing N_2O to N_2 (Philippot et al. 2011); this may lead to incomplete denitrification and emissions of N_2O, a potent greenhouse gas (IPCC 2013). N_2O can also be emitted during nitrification; the role of nitrification in producing N_2O warrants further study in GSI.

The outcomes of N cycling in GSI depend on the environmental conditions, and the presence and activity of N cycling bacteria such as nitrifiers and denitrifiers. How biofilter soil conditions influence N cycling bacteria is well established. For example, nitrifying and denitrifying gene abundances generally decrease with soil depth (Chen et al. 2013, Waller et al. 2013), and denitrifying gene abundances correlate with average inundation time, and concentrations of inorganic N and organic C (Morse et al. 2017, Waller et al. 2018). What is not known is how bacteria mediating N removal may be affected by the pollutants that accumulate in GSI soils, such as trace metals.

Metals can potentially accumulate in GSI soils because they may be found in elevated concentrations in runoff, are efficiently retained in surface soils, and do not biodegrade (Davis et al. 2001, Hsieh and Davis 2005, Hunt et al. 2006, Sun and Davis 2007, Tedoldi et al. 2016, Muller et al. 2020). Metals are also known to inhibit bacteria when present in sufficiently high concentrations; they can reduce microbial taxa richness and diversity (Wang et al. 2007, Singh et al. 2014), and suppress specialized bacterial functions. For example, soil microorganisms exposed to 120 mg/kg dry soil of Zn and 80 mg/kg of Cu, were temporarily less able to transform N_2O into N_2, due to N_2O reductases being more sensitive to metal pollution (Holtan-Hartwig et al. 2002). We can thus hypothesize that accumulated metals in GSI soils may inhibit the N cycling microorganisms and processes that are responsible for removing N from runoff. However, we don't know whether metals reach inhibitory levels, and if so, which groups of microorganisms might be most vulnerable. If nitrifiers are specifically vulnerable, then NH_4^+ would accumulate, causing toxicity problems. If in contrast, denitrifiers are relatively vulnerable, then NO_3^- would likely accumulate and would be flushed out, enhancing downstream eutrophication. If the enzymes catalyzing N_2O

reduction were more vulnerable, then there would be more N_2O emissions, with implications for climate change. Here we set out to evaluate how accumulated soil metals, together with soil physicochemical properties, jointly influence the abundance and activity of nitrifiers and denitrifiers in GSI soils. How might the pollutants that GSI systems are designed to trap preempt proper transformation and removal of other critical pollutants such as nitrate? How do soil properties and GSI drainage area characteristics amplify or mitigate this potential influence?

We address the question: how do soil properties and accumulated metals interactively act upon nitrifying and denitrifying bacteria, N_2O emissions, and ultimately N treatment? To answer, we used multiple sampling events over two years of six full scale GSI systems in operation in Southern California. We sampled and analyzed soils and N_2O emissions in the six GSIs with differing designs and ages at times representing the dry and wet seasons, and during the dry-down following the wet season. We then developed linear models using biofilter soil characteristics and total and bioavailable soil metal concentrations to explain the variation in population sizes of nitrifiers and denitrifiers. This work provides new insights into the impacts of soil properties and stormwater pollutants on N cycling bacteria and their metabolic capabilities which can inform monitoring efforts to minimize negative N treatment outcomes, and help mitigate export of deleterious N forms (e.g., NO_3^- and N_2O) from GSI.

3.2. Material and Methods

3.2.1. Study sites and sampling

The study sites are in Southern California, and are characterized by a semi-arid climate, in which most annual rainfall occurs during the winter months (December – March) (NOAA

2019). Two GSI sites were sampled at each of three University of California campuses (Santa Barbara (UCSB), Irvine (UCI), and San Diego (UCSD)) for a total of six sites (UCSB: Manzanita (MZ) and Sierra Madre (SM); UCI: Culver (CUL) and Verano (VER); UCSD: Altman Clinical and Translational Research Institute (ACT) and Sanford (SAN) (Figure S1). All sites were sampled in the dry season (Fall: October/November 2018), the wet season (Winter: February/March 2019), and the dry-down following the wet season (Spring: April 2019) (Figure S2), as previously described in (Hung et al. 2022).

The GSI sites included bioswales and biofilters of differing sizes, drainage areas, ages, and expected soil metal pollution, receiving stormwater runoff predominantly from parking lots (Fig S1). At each site, soils were sampled using a stainless-steel coring cup (5.08 cm diameter x 10 cm length), which was attached to a slide hammer. The coring cup was fitted with a clean PVC liner, which was replaced between samples. Aboveground plant materials, rocks, and mulch were removed prior to coring. Four soil samples, spaced out over the length of the GSI system, were collected at each site; each sample consisted of three soil cores (0 to 10 cm). A total of seventy-two soil samples were collected (4 samples per site per sampling time, 6 sites, 3 sampling times). Samples were extruded from the cores and manually composited in site in a clean resealable polyethylene plastic bag. A clean metal scoopula was used to transfer approximately 1 g of field-moist soil into 15-mL conical tubes containing 3 mL of Lifeguard solution (Qiagen, Hilden, Germany) to preserve nucleic acids in the sample prior to DNA extraction (4 replicates). Soil samples were transported on ice (4 °C) to UCSB, within 6 h. Upon arrival, soil samples for DNA extraction were stored at – 20 °C. The remaining field-moist soils were sieved through a brass 2-mm mesh (No. 10) (Advantage Manufacturing, Inc., New Berlin, WI) and composited in a clean resealable polyethylene

plastic bag. Sieved soils were subsampled and stored (4 °C) for soil characterization, and bacterial and metal analyses.

Soil-atmosphere fluxes of N_2O were measured via the closed chamber method (Hutchinson and Mosier, 1981). A week prior to measurements, two metal bases (50 cm x 50 cm) were pushed flush into the ground. One base enclosed vegetation, while the second base was placed over relatively bare soil, if present. During sampling, a chamber (50 cm x 50 cm x 50 cm) was secured over a metal base to create an enclosure. Samples were collected between 7:00 am and 1:30 pm. Ancillary field measurements were air temperature and relative humidity measured with a HOBO® logger (Onset, Bourne, MA), and soil temperature and moisture. To measure N_2O fluxes, 15 mL headspace samples were collected from a sampling port at 0, 5, 10, 15, and 25 min after closure using a 20 mL syringe fitted with a stopcock valve. Gas samples were injected into 12-mL pre-evacuated Exetainers (Labco Ltd., Lampeter UK), and stored in a cool, dark place until analysis via gas chromatography (GC).

3.2.2. Soil physicochemical characterization

Soils were characterized as described before in (Hung et al. 2022). Briefly, gravimetric soil moisture and soil organic matter (SOM) by loss on ignition (LOI) were determined in triplicate by drying at 105 °C for 24 h and igniting dry soils at 550 °C for 4 h, respectively (Gardner, 1986, Nelson and Sommers, 1996). The pH was measured in a soil slurry (10 g of soil into 10 g of deionized water) with a pH meter (Oakton Ion 700 benchtop meter, Cole Parmer, Vernon Hills, IL). Soil bulk density was measured on triplicate soil cores (10.0 cm depth, 5.1 cm diameter), after drying the soil (105 °C, 24 h), by dividing the dry soil mass by the soil core volume. Soil water potential was measured via a thermocouple psychrometer, following standard methods (Or and Wraith 2000). Ammonium and nitrate were analyzed at

the UCSB Marine Science Institute Analytical Lab. Briefly, frozen soil samples (-20 °C) were thawed (4 °C) and (3 g) were extracted with 30 mL of 2 M KCl solution (Mulvaney, 1996), filtered through Whatman filtration papers (ashless, grade 42, 42.5 µm diameter, Sigma-Aldrich, St. Louis, MO), and analyzed for dissolved nitrate and phosphate using a QuikChem8500 Series 2 Flow Injection Analysis system (Lachat Instruments, Milwaukee, WI). Soil subsamples were shipped (4 °C) to the Analytical Laboratory at the University of California, Davis to determine soil texture, bulk density, cation exchange capacity (CEC), total nitrogen (TN) and total carbon (TC) using standard methods (Association of Official Analytical Chemists (AOAC), 1997, Rible and Quick, 1960, Sheldrick and Wang, 1993)

3.2.3. Bioavailable and total metal analysis

Samples were analyzed as described previously in (Hung et al. 2022). Briefly, subsamples were shipped (4 °C) to University of California, Riverside for metal analysis. Sequential extractions for bioavailable metals (soluble and exchangeable), and total acid digestions for total metal fractions, followed the methods reported by Tessier et al. (1979) and United States Environmental Protection Agency (USEPA) (USEPA, 3050B) (U.S. Environmental Protection Agency, 1996), respectively. Briefly, 2 g samples of oven-dried soil were extracted at ambient temperature with 25 mL of 1 M $MgCl_2$. Samples were shaken at 250 rpm for 2h in acid-washed and rinsed (deionized water) glassware (1.2 N HCl). The supernatants were decanted and filtered with a 45 µm syringe filter and stored until analysis of bioavailable metals. The remaining solids were air-dried for acid digestion. Dried solids were digested on a DigiPrep digestion block (95 °C for 3 h) using a concentrated nitric acid ([HNO_3], 68–70% (v/v)) and hydrogen peroxide ([H_2O_2], 30% (v/v)) solution. Digested soils were diluted to 25 mL with deionized water. Aliquots of these samples were further

diluted to 50 mL with a solution containing 6.8–7% (v/v) HNO_3, and 0.9% (v/v) H_2O_2. All reagents were analytical grade or ultra-high purity (Thermo Fisher Scientific, Waltham, MA, USA), Concentrations of arsenic (As), chromium (Cr), cadmium (Cd), copper (Cu), nickel (Ni), lead (Pb), selenium (Se), vanadium (V), and zinc (Zn), in each soil extract (bioavailable and acid-digested samples) were analyzed in triplicate via inductively coupled plasma-mass spectrometry ([ICP-MS] (7700 Series, Agilent Technologies, Santa Clara, CA, USA). Total metals were calculated by adding bioavailable and acid-digested fractions described above.

We computed the ratio of directly connected impervious area to the GSI system area, from now on referred to as ***impervious ratio*** (Chapter 2; Feraud and Holden, 2021). This ratio was used as an assessment tool, to determine if characteristics of the drainage area and the GSI system could provide an indication of relative metal accumulation. Pearson correlations and linear regressions between log-transformed total metal concentrations were calculated, and the impervious ratio calculations were then performed.

3.2.4. DNA extraction and quantitative polymerase chain reaction (qPCR)

Soil DNA was extracted in duplicate using the RNeasy PowerSoil Kit (Qiagen, Hilden, Germany), including one extraction blank per batch. Prior to extraction, the tubes containing the soil samples and LifeGuard solution (Qiagen, Hilden, Germany) were centrifuged at 7800 g for 15 min and the supernatant discarded. After this, extraction followed the manufacturer's protocol. The extracted DNA was pooled, quantified, and archived (-20 °C) until analysis.

Genes encoding bacterial 16S rRNA, and nitrifying (archaeal and bacterial *amo*A) and denitrifying (*nir*K, *nir*S, *nos*Z) functional genes, were evaluated via quantitative polymerase chain reaction (qPCR) assays in 25 µL reactions using the PowerUp SYBR Green Master Mix (Thermo Fisher Scientific, Waltham, MA) on a CFX96 real-time PCR detection system

(Bio-Rad Laboratories, Hercules, CA). Standard curves were generated by serial dilution of linearized plasmid DNA. To avoid inhibition effects during amplification, DNA extracts were diluted with nuclease free water to 3 ng/ µL. For qPCR of genes encoding 16S rRNA, DNA was diluted to 1 ng/ µL. Assays were performed in triplicate and included a positive and a negative (no template) control. Product specificity was evaluated via melt curve analysis. A subset of PCR products was further verified via gel electrophoresis on FlashGel DNA Cassettes run with a DNA Marker 100 bp - 4 kb (Lonza Group AG, Basel, Switzerland). Details for each qPCR reaction are in the Supplemental Materials (Table S1).

3.2.5. Nitrifying and denitrifying enzyme activities

Nitrifying enzyme activity (NEA) was assessed via the chlorate inhibition method, which blocks nitrite conversion to nitrate, following (Belser and Mays 1980) and (Hart et al. 1994). Duplicate soil slurries of 4 g of sieved soil and 35 mL of nitrification potential solution (0.1 mM KH_2PO4, 0.8 mM K_2HPO_4, 0.5 mM $(NH_4)_2SO_4$, and 10 mM $NaClO_3$) were prepared in 125-mL Erlenmeyer flasks and incubated on a reciprocal shaker (20 °C). Aliquots (5-mL) were removed at 15 min, 2 h, and 4 h, centrifuged, and 1 mL of supernatant transferred to a cuvette containing 1 mL of Nanopure water and 0.5 mL of nitrite color reagent (Sulfanilamide/N-Naphthyl Reagent, LabChem, Inc., Zelienople, PA). Sample absorbance was read at 543 nm with a UV spectrophotometer (UV-1800, Shimadzu Co., Kyoto, Japan). Calibration curves were developed daily using nitrite standards (0.01, 0.05, 0.1, and 0.5 ppm, ACS Analytical grade) and good linearity ($R^2 > 0.99$) was verified. The rate of nitrate production was the slope of time vs. nitrite concentration.

The denitrifying enzyme activity (DEA) assay was adapted from others (Tiedje and Smith 1979; Barnard et al. 2006). Duplicate samples of 2g of sieved soil and 20 mL of

denitrification potential media (0.72 g KNO3, 2.5g glucose, 2.2 g glutamic acid in 1L deionized water) were dispensed into amber 250-mL Boston rounds fitted with Mininert caps. The bottles were capped, and an anaerobic atmosphere was obtained by repeated evacuation (4 min) and flushing (1 min) cycles with UHP nitrogen. Acetylene was added at 10% v/v, and the bottles incubated at room temperature on a tabletop shaker (20 °C). Headspace samples (15 mL) were removed immediately, at 30 min, and 1 hour, with a syringe fitted with a stopcock valve, dispensed into evacuated Exetainers (Labco Ltd., Lampeter, UK), and analyzed within 1 week using a GC (8610C gas chromatograph (SRI Instruments)) fitted with an electron capture detector. DEA was expressed as the rate of N_2O production which was the slope of time vs. N_2O concentration.

3.2.6. N_2O analysis by gas chromatography

Gas samples from field-deployed chambers (Section 3.2.1) were analyzed within 1 week of collection with an 8610C gas chromatograph (GC) (SRI Instruments, Torrance, CA) fitted with an electron capture detector. Gas samples were stored in evacuated vials with an overpressure to avoid air intrusion, and overpressure was verified at time of GC injection. Calibration curves were obtained by triplicate injection of N_2O standards at 1 ppm, 0.1 ppm (Matheson Tri-Gas, Inc., Irving, TX), and 0 ppm (UHP N_2, Praxair, Inc., Danbury, CT). To correct for instrument drift, N_2O standards were included every 8 injections. Detection limit was 6 ug N/-N_2O m^{-2} h^{-1}.

3.2.7. Data analysis

One-way analysis of variance (Kruskal-Wallis), followed by post-hoc Dunn tests were performed to assess differences in measured parameters across sites and sampling times, since variables were not normally distributed (Shapiro-Wilk test). Spearman's rank-order

correlations or Pearson's product-moment correlations on log-transformed variables were used to assess the correlations between measured parameters. Variables were log-transformed prior to linear regression analysis. Stepwise multiple linear regression was used to assess the relationships between absolute and relative (normalized to 16 rRNA) gene abundances, metal concentrations, soil properties, and GSI system characteristics. The variance inflation factor (VIF) of each explanatory variable was computed to assess multicollinearity, and variables with VIF higher than three were excluded from the final model (Hung et al. 2022). The linear models were used to fit data and determine influential variables; models were not predictive because they utilized all measured data. To evaluate if linear models of soil properties and metal concentrations could predict functional gene abundances, we selected a data subset of three GSI systems that included the three geographical study locations (UCSB, UCI, UCSD), and showed the most variance across dependent and independent variables. Functional total gene abundances for the remaining 3 GSI systems predicted from these models were then compared to measured gene abundances as a test of the model robustness in representing the unmodeled systems. Metal concentrations below the detection limit (BDL) were manually designated at a value of half the detection limit prior to analysis. Statistical analyses were performed with R (version 4.0.1) at a level of significance of $\alpha = 0.05$.

3.3. Results and Discussion

3.3.1. GSI systems and drainage areas

GSI sites were selected to cover a range of locations, designs, and management characteristics to ensure representativeness and variability across environmental parameters

and expected metal accumulation. GSI sizes and drainage areas ranged from 103 to 1330 m^2 and from 642 to 31,883 m^2, respectively (Figure S1, Table 1). GSI drainage areas were 100% impervious, except in MZ (approximately 54% impervious). In MZ, only 20% of the impervious drainage area (796 m^2 of 3980 m^2) was directly connected to the GSI system since runoff from roofs of residential buildings first flowed across lawns. Ratios of directly connected impervious drainage area to bioretention area (defined here as impervious ratio) in the GSI system were computed as a measure of stormwater runoff loading (Chapter 2; Feraud and Holden, 2021). We expected annual metal loading to be higher in GSI systems with a higher impervious ratio, such that overall soil metal concentrations and potential risk to soil microbiota would increase with GSI system age and impervious ratio. Impervious ratios were lowest at MZ, and then ACT and SAN, with values ranging from 2.2 to 43.9, which were comparable to other GSI systems [8.7 to 53.3 in (Tedoldi et al. 2017); 3.5 to 14.3 in (Ingvertsen et al. 2012)]. In SM, CUL, and VER, the impervious ratios were higher than the recommended maximum of 16:1 (Philadelphia Stormwater Management Guidance Manual 2020). It is likely that these systems were undersized relative to their drainage area, so that for larger storms, the incoming stormwater runoff may not have been fully captured.

3.3.2. Soil characteristics of GSI systems

Soil properties that could influence metal retention and the microbial community were assessed (Table S2), and properties that varied across sites and/or seasons were used as explanatory variables in subsequent analyses (see section 3.3.8). Overall, GSI soils were most distinct at UCSD sites: soils there were sandier and had lower nutrient content and sorption capacity than UCSB and UCI sites, except for VER which was more like UCSD

sites. UCI sites had generally higher nitrate and phosphate content because fertilizers were periodically applied to GSI soils. Site-specific differences are further described below.

All soils were near-neutral to alkaline, with mean pH values ranging from 7.0 to 8.8 (Table S2). The relatively high soil pH may indicate that stormwater runoff and irrigation with reclaimed water in the drainage areas introduced base cations from calcareous building materials such as paved concrete (Ingvertsen et al. 2012) and from irrigated landscaping (Chen et al. 2013) into the GSI soils, increasing soil alkalinity. The observed pH ranges likely supported metal immobilization (Young 2013) across all GSI soils. SOM may also have aided in metal retention, with mean SOM ranging from 1.6% to 8.1%. SOM was uniform across sampling times and was lower in UCSD relative to UCSB and UCI (Kruskal-Wallis, $p < 0.0001$; Dunn's tests, $p < 0.015$) (Table S2). Mean soil moisture ranged from 9.9 to 33.2% across sites and followed similar trends as SOM; soils were typically wetter at UCSB > UCI > UCSD (Kruskal-Wallis, $p = 0.022$; Dunn's test, $p < 0.017$) (Table S2).

GSI soils were classified as sandy loams, sandy clay loam, or loamy sand, following the soil textural triangle from the United States Department of Agriculture (USDA, https://www.nrcs.usda.gov/) (Table 1, Table S2). Sand content followed the order UCSD > UCI > UCSB, whereas clay content was highest in SM and CUL (Table S2). The relative differences in particle sizes were reflected in the soil bulk density, which was highest in the sandier soils at UCSD sites (Kruskal-Wallis, $p < 0.0001$; Dunn's test, $p < 0.04$) (Table S2). These sites were expected to sorb fewer pollutants because of their soil texture indicating faster draining times, and their lower clay and organic matter content. In concordance, CEC was highest at CUL, followed by SM and MZ, then VER, and lastly the UCSD sites (Kruskal-Wallis, $p < 0.0001$; Dunn's tests, $p < 0.03$) (Table S2).

Total N and total C were highest in MZ, SM, and CUL, followed by VER, SAN, and ACT (Kruskal-Wallis, $p < 0.0001$; Dunn's tests, $p < 0.03$) (Table S2). Mean soil ammonium concentrations ranged from 0.9 to 5.7 ug N/g dry soil. Differences across sites were driven by the higher ammonium concentrations in VER and SM (Kruskal-Wallis, $p < 0.0001$; Dunn's test, $p < 0.05$) (Table S2). Mean soil nitrate ranged from 4.1 to 81.0 mg N/kg dry soil, and was highest during fall sampling for CUL, VER, and MZ (Kruskal-Wallis, $p < 0.0001$) (Table S2). High nitrate concentrations at UCI sites during fall sampling were likely due to routine fertilizer application and buildup during this dry season. Phosphate (PO_4^{3-}) concentrations ranged from 1.7 to 50.5 mg/kg dry soil. Differences in PO_4^{3-} across sites were due to high concentrations in CUL relative to SAN (Kruskal-Wallis, $p < 0.001$; Dunn's test, $p < 0.02$) (Table S2). DOC ranged from 10.9 to 103 ug C/g dry soil, and variability was mostly explained by higher concentrations in MZ and CUL, relative to SAN, and higher concentrations in Spring, relative to Fall (Table S2).

3.3.3. Total and bioavailable metals in GSI soils

Soil samples were analyzed for bioavailable and total metal concentrations (As, Cr, Cd, Cu, Ni, Pb, Se, V, and Zn) to evaluate the extent of metal accumulation in GSI soils (Table S3). Total metal concentrations were generally low and similar to background surface soil (0-5 cm) levels in the United States (Smith et al. 2013), except for As (28.8 mg/kg), Cr (96.8 mg/kg), Cu (78.8 mg/kg), Ni (83.5 mg/kg), V (150 mg/kg) and Zn (207 mg/kg), which were high at several sites. Total Cr, Ni, and Pb were within residential soil screening levels suggested by the California Department of Toxic Substance Control (DTSC), but total As was above recommended limits (0.41 mg/kg) (Cal DTSC, 2020) in all sites, which may present a concern for soil quality. Total metals were also compared to ecological soil

screening levels determined for plants, soil invertebrates or birds (Table S3), which suggested that V and Zn levels in some cases could present a risk to birds and soil invertebrates, respectively.

To assess the risk to soil microbiota, bioavailable metal fractions were considered. However, bioavailable metal concentrations were mostly a low fraction of total metals (Figure S3), with approximate percentages of 1.9% for Zn, 2.9% for Cu, 5.4% for Cr, 8.7% for Cd, 11% for Se, 14% for Ni and V, and 25% for Pb. The relatively high bioavailable Pb fraction was surprising, since Pb is mostly associated with vehicle tire and braking systems wear (Adamiec et al. 2016), and more often particle-bound, relative to other metals in stormwater runoff (LeFevre et al. 2015). Although on average bioavailable and total metal concentrations were low, they varied across sites and sampling times. Bioavailable metals were relatively uniform, except for As, Cd, and Pb. Bioavailable As was generally higher at UCSD sites (Kruskal-Wallis, $p = 0.016$), while bioavailable Cd (Kruskal-Wallis, $p < 0.0001$) and Pb (Kruskal-Wallis, $p = 0.0002$) were generally higher at UCI. Total metals varied more widely across sites, particularly for the Winter samples (Figure 1, Figures S4-5). For example, UCSD sites had higher concentrations of total Pb (Figure 1) and total As (Figure S4), while UCI sites had higher concentrations of total Cd and total Cr (Figure S4). Overall, total metal concentrations were highest during Winter sampling times, except for total Pb, which had the lowest concentrations at this time (Figure 1, Figures S4-5). The different seasonal pattern for Pb may be due to stormwater runoff resuspending previously precipitated Pb, and either washing it out or carrying it down the soil profile. This would also explain the relatively high observed bioavailable Pb fraction. This flushing out effect would be more

pronounced for metals that are particulate bound, such as Pb, than metals that are found predominantly in dissolved form.

3.3.4. Relationship between total metals, drainage area and soil properties

Correlation and linear regression analyses were performed to explore the relevance of site-specific factors such as GSI system age, drainage area, and soil characteristics on metal concentrations. Total metals, excluding As, Pb, Se, V, showed a strong positive correlation with the impervious ratio (Spearman's, r: 0.61 to 0.73, $p < 0.001$) for samples collected during the Spring (Figure S2). In contrast, total Pb was negatively correlated to the impervious ratio (Spearman's $r = -0.43$, $p = 0.036$), indicating that other sources may be influencing Pb accumulation in GSI soils. Linear regression analysis of common runoff metals Cu, Pb, and Zn, showed weak, but significant relationships between the impervious ratio and total Cu, and total Zn, but no relationship with Pb (Figure S6). Metal concentrations during dry weather sampling in the Fall were also not related to the impervious ratio. It is likely that other factors, such as direct input into GSI soils via dry deposition (Muller et al. 2020), and plant and microbial uptake of metals, are better predictors of metal accumulation when there is no significant stormwater runoff. Dry deposition would be influenced by urban factors such as traffic density, proximity to roads, and vehicle idling times (Muller et al. 2020). Also, GSI soil characteristics such as SOM, CEC, soil texture, and pH (Young 2013) would determine to what extent metals are sorbed and retained in soils.

3.3.5. Bacterial abundance, and nitrifying and denitrifying activities

Microbial biomass, measured via SIR, was evaluated as a metric of the overall health of the microbial community, where a larger population size was expected to support greater N cycling. SIR ranged from mean values of 1.9 to 11.3 mg C kg^{-1} h^{-1} and was generally higher

in UCSB and UCI sites (MZ, SM, CUL, VER) than in UCSD (ACT, SAN) (Kruskal-Wallis, $p < 0.0001$; Dunn's test's, $p < 0.01$) (Table 2). As expected, SIR was positively and significantly ($p< 0.05$) correlated with GSI system age ($r = 0.60$), SOM ($r = 0.66$), and moisture ($r = 0.75$), and negatively correlated to sand % and soil bulk density ($r = 0.70$) (Figure S7). Bacterial abundance was also assessed via 16S qPCR, which was positively correlated with SIR ($r = 0.47$, $p < 0.05$). We expected bacterial numbers to increase between Fall and Winter sampling due to moisture and nutrient inputs from storms. However, there were no seasonal variations, except in MZ where this trend was observed (Kruskal-Wallis, $p = 0.02$) (Figure 2). There were, however, significant variations across GSI sites, where bacterial population based on 16S rRNA was larger at MZ, relative to ACT, SAN, and VER.

To assess populations of nitrifiers and denitrifiers, we measured functional gene abundances. Functional gene abundances (Table 2) were comparable to other GSI (e.g., Chen et al. 2013, Waller et al. 2018). Functional genes linked to nitrification were less abundant than denitrifying genes (Figures 2-3, Table 2), which is expected in soils because nitrifying microorganisms are slow-growing and compete poorly for NH_4^+ against heterotrophic microorganisms and plants. Variations across sampling times for both nitrifying and denitrifying functional gene abundances followed the same trends as 16S rRNA, which was likely a result of the high correlation observed among all genes (Figure S7).

As an additional measure of the relative size of the nitrifying and denitrifying populations, we determined NEA and DEA. Contrary to functional gene abundance results, average nitrifying enzyme activities (1.4 to 7.1 mg kg^{-1} day^{-1}) were larger than average denitrifying enzyme activities (0.3 to 1.3 mg kg^{-1} day^{-1}) across all sites (Table 2, Figure 4). This may have indicated that nitrification was more dominant, consistent with the mostly

unsaturated conditions of GSI soils. There were no significant differences across sampling times for NEA, except in ACT, where NEA was larger in the Winter relative to the Fall (Kruskal-Wallis, $p = 0.023$). In contrast, NEA was larger at MZ than ACT, and SAN, during Fall, and Winter, and larger than ACT and VER during Spring ($p < 0.02$) (Figure 4). Overall, NEA was larger at MZ, SM, and CUL (Table 2), which are sites with greater SOM, TN, and TC (Table 2), which may support larger microbial populations. DEA was relatively uniform and low across sampling times, except in MZ, SM and SAN where DEA was higher during Winter. This increase may have been caused by higher microbial activity following re-wetting of soils, since the resulting rapid release of easily decomposable organic carbon draws down oxygen levels and primes the soil environment for denitrification (Smith and Tiedje 1979). The higher DEA at site MZ during Winter may have been caused by the water-logged soils, and the 2-3 inches of standing water observed at time of sampling. DEA was not correlated with any of the functional genes, which may reflect the high spatial and temporal heterogeneity of denitrification in soils and difficulty in sampling active denitrifiers. Small areas (hotspots) and brief periods (hot moments) often represent a high percent of the denitrification activity in terrestrial systems (Groffman et al. 2009). Based on our sampling, denitrifying activity was generally highest in sites with more SOM, and in wetter soils.

Site-specific differences, more than weather conditions, influenced NEA. Instead, DEA was relatively uniform and was more responsive to weather, which through water inputs strongly influences soil saturation and redox conditions, and thus how favorable conditions are for denitrification (Zumft et al. 1997, Payne et al. 2014 a). Both NEA and DEA were negatively correlated with soil water potential and bulk density, and positively correlated to moisture and soil organic matter (Figure S7). However, NEA and DEA are measures of potential activities

and do not reflect *in-situ* conditions. As a measure of nitrification and denitrification in the field, with relevance to GHG contributions, we assessed N_2O emissions.

3.3.6. N_2O emissions from GSI soils

N_2O emissions were evaluated as a metric for N treatment performance since emissions may occur as a byproduct of nitrification and/or incomplete denitrification. N_2O emissions from biofilters ranged from non-detectable to 61.8 N/m^2 h, with mean values across sites ranging from 16.9 to 29.9 mg N/m^2 h (Figure 5, Table S4), which were comparable to emissions from wet bioretention basins (34.3 µg N/m^2 h) (Morse et al. 2017) and parking lot biofilters (13.7 to 65.6 µg N/m^2 h) (Grover et al. 2013). There were no significant differences in average N_2O emissions across sites or sampling times. This may have been a result of distinct sampling conditions, and site differences (Table S4). For example, pulse emissions of N_2O from soils of natural and semi-natural ecosystems are frequently observed following re-wetting after periods of prolonged drought (Groffman et al. 2009). The effect is more pronounced when there is a distinct dry season and the magnitude of pulse depends on length of preceding dry period and decreases with successive rain events (Butterbach-Bahl et al. 2004, Groffman et al. 2009). Further, time of sampling may influence N_2O emissions. Samples were collected between 7 am and 2 pm, at soil temperatures ranging from 9.5 C during morning sampling in the winter to 30.8 C in an afternoon sampling in the fall (Table S4). Higher microbial activity at warmer temperatures may result in more emitted N_2O. Further, N_2O emissions depend on the activity of nitrifying and denitrifying microorganisms, which is influenced by access to ammonium or nitrate, respectively. Access to nutrients depends on site-specific characteristics such as vegetation species and density, soil organic matter, and soil moisture (Payne et al. 2014a, Muerdter et al. 2018). Wetter soils may allow

for complete denitrification of N_2O to N_2 since gas transport from the soil to the atmosphere is slower in water than in air and allows more time for reaction. As the biofilter soil dries up, N_2O may be more rapidly transported into the atmosphere. Further, as soils are reaerated, the enzymes catalyzing the reduction of N_2O to N_2 may be inhibited due to rising oxygen levels (Philippot et al. 2007). Soil reaeration depends on evapotranspiration by plants, and the speed at which water moves through the biofilter, which will be faster in soils with lower water holding capacity. As an example, the sandier soils at UCSD sites are expected to drain relatively quickly, which may act as a positive control on N_2O emissions. However, these sandier soils contain fewer nutrients, and sustain a smaller microbial biomass (Table 2), which may result in smaller N_2O emissions. There is a complex interplay between the size and activity of nitrifying and denitrifying microorganisms, the soil water status, and diffusional gas transport. To reduce some of the variability and account for the different microbial community sizes, N_2O emissions were normalized to SIR. Normalized N_2O emissions were higher at UCSD and UCI, and lower at UCSB (Figure 5). Highest normalized N_2O emissions occurred at ACT, which has sandy soils, the highest bulk density among sites, and lowest SOM (Table S2). N_2O emissions were weakly correlated with SOM and SIR ($r = 0.15$, $p = 0.04$), and were correlated with 16S rRNA genes ($r= 0.29$, $p= 0.02$). N_2O emissions were also weakly correlated with bacterial *amo*A gene abundance ($r = 0.27$, $p = 0.02$) and marginally correlated with *nir*K ($r = 0.07$, $p = 0.08$) and *nir*S ($r = 0.09$, $p = 0.07$). Although these correlations were weak, they reasonably indicated that a larger bacterial community could result in higher N_2O emissions, and that nitrification may have contributed to the measured N_2O emissions.

3.3.7. Correlations between bioavailable and total metals, and bacterial parameters

Spearman's rank correlations were performed on total metals, bioavailable metals, nitrifying gene abundances, and denitrifying gene abundances (Figure 6 and Figure S9). Nitrifying and denitrifying gene abundances were strongly correlated with each other and with measures of total bacterial population. NEA and DEA were also correlated with each other and with SIR. Interestingly, all functional gene abundances and microbial biomass as measured by SIR were negatively correlated with total Pb (Figure 6), while NEA and DEA were negatively correlated with total As, V, and Zn. Nitrifying and denitrifying genes were also negatively correlated with bioavailable Cd, Ni, Pb, Se and Zn, with the strongest negative relationships observed for *nos*Z ($r = -0.90$ to -0.97, $p < 0.05$). NEA and DEA were negatively correlated with bioavailable V ($r = -0.83$ to -0.88) (Figure S9).

The stronger correlations between bioavailable metals and functional genes indicated a potentially closer interaction with populations of nitrifiers and denitrifiers. These results reinforced the relevance of measuring bioavailable metal concentrations, as opposed to total metal concentrations, for metal risk assessment. Correlations between functional genes normalized to16S rRNA and bioavailable metals were also negative (Figure S9). Although correlations do not equate causation, the strong negative correlations between bioavailable metals and bacterial parameters suggested that dissolved or easily exchangeable metal fractions exerted a negative influence on nitrifying and denitrifying gene abundances and potential activities. In contrast, correlations between bacterial parameters and total metals were positive for metals with a biological role (Cu, Ni, Zn), and negative for metals with potential toxicity and no biological function (Pb). Care must be taken when making these comparisons, however, because other site-specific unmeasured variables may have caused

the apparent correlations. Yet, the consistent patterns for all metals, which showed different concentration ranges and accumulation patterns in the GSI sites, suggested that they exerted influence on the size and potential enzyme activities of nitrifiers and denitrifiers.

3.3.8. Stepwise multiple linear regression analysis

Multiple linear regression (MLR) was performed to determine how soil physicochemical properties, GSI system age, and soil metal concentrations jointly influenced the abundance of genes encoding 16S rRNA, and of functional genes related to nitrification (archaeal and bacterial *amo*A) and denitrification (*nir*K, *nir*S, *nos*Z). Due to the observed variability across sites and sampling times, a subset of total and bioavailable metals was considered for their influence on bacterial parameters.

We expected total metals might influence bacterial parameters more than bioavailable metals, since total metal concentrations varied more widely across measurements. The potential metal influence was considered jointly with environmental and GSI system variables. We hypothesized that metals found in higher concentrations (e.g., Cu, Ni, V) or higher bioavailable fractions (e.g., Pb) (Table S3) would explain additional variability in bacterial parameters, than environmental and GSI properties on their own. We also expected that metals with no known biological function (e.g., Pb), would exert a stronger negative influence on functional gene abundances.

3.3.8.1. Selection of explanatory variables for linear models

Initial model selection was based on soil properties and GSI area characteristics that showed seasonal and/or site variability, and could reasonably influence metal fates, and the abundance and potential activity of the soil microbial community. Models included the ratio of impervious drainage area to bioretention area in the GSI system because this ratio strongly

correlated with metals. GSI system age was included because more mature systems were expected to have developed more SOM. GSI systems initially have very little SOM, but organic matter inputs from runoff, and plant and microbial detritus will add to the SOM pool over time (Payne et al. 2014a). Soil properties used as explanatory variables were soil texture (% sand, silt, clay) and bulk density, for their influence on transport times and metal retention (Alloway et al. 2013, LeFevre et al. 2015); SOM, and DOC for their influence on metal sorption and desorption (Kalbitz et al. 2000, Davis et al. 2003, Young 2013, Lim et al. 2015); and pH, moisture, and water potential for their influence on metal speciation and mobility (Young 2013). Additionally, water availability and how water moves through soil controls redox conditions, contact times, and the extent to which microorganisms are physically connected with substrates or soil pollutants (Payne et al. 2014a).

3.3.8.2. Multiple linear regression models

We used MLR to develop linear regression equations for absolute and relative gene abundances (Table 3). From the resulting models we observed that the most influential soil properties appear to be pH, moisture, and SOM, whose influence on microbial communities are well established. For the studied soils, an increase in pH led to reduced functional gene abundances, which may have been a result of the relative soil alkalinity. GSI system age was also a significant predictor in many cases, likely due to its influence on the development of SOM. Total and/or bioavailable metals were also included in the model solutions. The adjusted R^2 values of MLR indicated that models for absolute gene abundances explained between 49% to 72% of the variance, while models for relative gene abundances explained between 41% to 69% of the variance.

Surprisingly, total Cu, Ni and V were influential variables with positive regression coefficients for at least one or several absolute gene abundances. Although we had hypothesized that these metals would influence functional gene abundances, we expected the coefficients to be negative. Water-extractable concentrations of Cu between 2 to 3.8 mg/kg, and of Ni between 2,5 to 7 may partially inhibit nitrification in sandy loams (Cela et al. 2006). These critical ranges are higher than the mean concentrations observed in this study, but similar to maximum measured values. Similarly, toxicity thresholds for V in soils were 28 mg/kg (Larsson et al. 2013). Values observed in the GSI soils frequently exceeded this threshold during Winter and Fall sampling. However, toxicity threshold values may vary widely depending on soil properties (Oorts et al. 2006, Ruyters et al. 2012). Metal concentrations observed herein were within range of background levels, which may have explained why there were no adverse effects. Co-selection for metal tolerance (Giller et al. 1998), may have also resulted in preserved microbial function, as observed in nitrifying microorganisms exposed to Cu and Zn contaminated soils (Mertens et al. 2013). A tolerant community might be better able to respond to metal stress if this stress can be managed with similar tolerance mechanisms (Bruins et al. 2000). For example, soil nitrifying population in soils contaminated with Pb, also developed co-tolerance for Zn (Rusk et al. 2004). An alternative explanation to metal tolerance is that metals with known biological roles were limited in GSI soils, so that stormwater runoff acted as a delivery mechanism and alleviated this limitation. The relatively low soil metal concentrations observed during Fall sampling (Figure 1, Figures S4-5) lend support to this scenario. Further, models for *amo*A, *nir*K, and normalized *nos*Z all included Cu, which is required by the enzymes that are encoded by these genes. The enzyme nitrous oxide reductase, encoded by *nos*Z, is a Cu-dependent enzyme, as

is the nitrite reductase encoded by *nir*K (Zumft 1997). Cu is a cofactor in many key proteins involved in metabolism in ammonia oxidizing archaea, and to a lesser extent ammonia oxidizing bacteria (Reyes et al. 2020). Cu limitation can therefore negatively impact both nitrification, and denitrification.

Unlike total metals, bioavailable metals had both positive and negative regression coefficients. One result that was unexpected was the apparent positive influence of bioavailable V on bacterial *amo*A and *nos*Z abundances (Table 3), since in non-acidic soils V exists mainly as vanadate, which has a similar structure to phosphate and may inhibit phosphate metabolism (Larsson et al. 2013). However, except in Winter samples, total V concentrations reported in this study were mostly below threshold toxicity values determined for potential nitrification in five different soils (28 to 690 mg kg^{-1} added V) (Larsson et al. 2013). The wide range in reported toxicity thresholds hinders further comparison, since soil properties such as pH, SOM, and clay content, clearly influence V bioavailability and apparent toxicity. In contrast to V, bioavailable Pb and bioavailable Cu were negatively related to normalized gene abundances of *nir*S and *nos*Z, respectively. Both metals have limited to no biological function, so this result was expected. The regression coefficient for bioavailable Pb in the equation for *nir*S/16S was low relative to the coefficients for bulk density and soil organic matter, indicating a likely minor influence on *nir*S. The coefficient for bioavailable Cd, however, was comparable to all other coefficients in the equation for *nos*Z/16S, indicating a potentially larger influence. This is concerning because inhibition of *nos*Z may lead to incomplete denitrification and N_2O release.

To verify MLR results, measured and fitted values of gene abundances were compared using scatterplots, and correlation coefficients were calculated (Figure 7). All proposed

relationships were significant ($r = 0.64$ to 0.85, $p < 0.0001$). Overall, MLR models including soil properties and metal concentrations provided a reasonable data fit for nitrifying and denitrifying gene abundances in GSI soils. The positive coefficients for total metals indicated potential positive feedback on nitrifying and denitrifying bacteria, which was contrary to what we had hypothesized. Results for bioavailable metal interaction with nitrifying and denitrifying bacteria were inconclusive since effects could be either positive or negative. However, the relatively strong negative feedback of bioavailable V on total bacteria, as assessed via gene abundance of 16S rRNA (Table 3) suggested that overall, bioavailable metals might negatively impact bacterial abundance. Further, after functional genes were normalized to 16S rRNA results indicated a negative influence for denitrifiers, with potential implications for N processing, including release of N_2O due to *nos*Z inhibition.

We used a subset of the data (3 GSI systems: MZ, CUL, ACT) to produce linear models for total gene abundances, and then used the remaining 3 GSI systems (SM, VER, SAN) to evaluate the relationship between measured and predicted functional gene abundances. The resulting linear models (adjusted R^2 values ranging from 0.55 to 0.77) (Table S5) differed, in terms of environmental and metal variables, from the models that were fitted with all the data (Table 3); they also had generally low to moderate predictive power. Significant relationships between modeled and predicted functional genes were only obtained for bacterial *amo*A, *nir*S, and *nos*Z, with adjusted R^2 values of 0.14 ($p = 0.0047$), 0.79 ($p < 0.0001$), and 0.39 ($p = 0.001$). A larger number of GSI sites may be needed to produce stronger predictive models. Also, the inapplicability of a model based on a few sites for predicting outcomes at other sites could reflect strong site-specific characteristics including which metals are most concentrated at various sites. Notwithstanding, both models using the full or partial datasets

included total metals as influential variables, so that variation in functional gene abundances was best explained by considering both intrinsic soil properties, and accumulated soil metal concentrations (Table 3, Table S5).

3.4. Conclusions

Metals were effectively retained in GSI soils, where they may impose an environmental stress on microorganisms, such as nitrifying and denitrifying bacteria, that mediate pollutant transformation processes. GSI soils occasionally exceeded ecological soil screening levels for total metals, but bioavailable metal concentrations were low. Total metal concentrations were largely explained by the ratio of directly connected impervious drainage area to bioretention area, which may serve as a predictive tool to guide monitoring efforts and metal risk assessments in a GSI system. For the studied systems, metals were not a significant threat to the abundance and enzyme activity of either nitrifying or denitrifying bacteria, although there were some significant associations. Bioavailable fractions of Cd and Pb appeared to reduce functional gene abundances of denitrifying microorganisms, with the strongest effect potentially occurring on the reduction of N_2O to N_2, which would result in N_2O release. However, total metals with known biological roles, such as metals that are enzyme co-factors (e.g., Cu), appeared to be positive controls on functional gene abundances, indicating a potential metal limitation in soils of biologically relevant metals.

Taken together these findings suggest that trace metals with a known biological role may exert a positive influence on N cycling microorganisms, but that metals that are commonly toxic such as Pb and Cd may be potentially damaging to the N processing function of GSI systems. Such relationships are likely to gain prominence in GSI sites with higher metal

pollution loads, particularly for toxic metals for which toxicity would greatly increase with increasing metal concentrations. For metal co-factors, increasing metal concentrations beyond a saturation threshold may not produce additional effect since most enzymes follow Michaelis-Menten kinetics (Tiedje et al. 1983, English et al. 2006).

Model results for MLR analysis indicated that nitrifying and denitrifying gene abundances in GSI soils were correlated with soil properties, total metals, and bioavailable metals. Our results suggest that in some cases stormwater runoff may alleviate metal limitation, rather than impose a metal stress. This positive effect is more likely in functional genes that encode enzymes that have metals as cofactors, such as Cu in *nir*K, and archaeal *amo*A. This possibility is to be considered on a site-by-site basis, depending on expected pollution levels. Still, the negative, and significant relationship between certain bioavailable metal fractions (e.g., Cd, Pb) and functional gene abundances, with regression coefficient values of similar magnitudes to those for soil environmental factors, reinforces the importance of considering bioavailable metal fractions when performing metal risk assessments in GSI soils, and of evaluating potential effects on N cycling microorganisms, and ultimately N processing, N_2O emissions, and overall N removal performance.

3.5. Acknowledgments

The performance of this research was supported by funding from by the University of California Office of the President, Multicampus Research Programs and Initiatives, Grant ID MRP-17-455083. We thank UC Grounds personnel and site managers for the use of the GSI systems. Metal analysis was performed at UC Riverside. We thank Alyson Santoro for the use of her lab for N_2O analysis via gas chromatography. Plasmid DNA standards were

provided by Dr. Alyson Santoro and Dr. Brian Badgley. Sample processing was performed with assistance by Laurie Van De Werfhorst, Dong Li, Monika Mortimer, Ying Wang, and Timnit Kefela.

3.6. References

Adamiec, E., Jarosz-Krzemińska, E. and Wieszała, R. (2016). Heavy metals from non-exhaust vehicle emissions in urban and motorway road dusts. *Environ. Monit. Assess.*, 188, 369.

Alloway, B. (2013). Sources of heavy metals and metalloids in Soils. In: Heavy metals in soils: Trace metals and metalloids in soils and their bioavailability (3rd edition), Alloway, B. (Ed.), Springer, Dordrecht, Netherlands, 11-50.

Association of Official Analytical Chemists (AOAC) (1997). Official Method 972.43, Microchemical determination of carbon, hydrogen, and nitrogen. In: Official methods of analysis of AOAC International (16th ed.), AOAC International, Arlington, VA, Chapter 12, 5-6.

Barnard, R., Le Roux, X., Hungate, B. A., Cleland, E. E., Blankinship, J. C., Barthes, L., and Leadley, P. W. (2006) Several components of global change alter nitrifying and denitrifying activities in an annual grassland. *Funct. Ecol.*, 20, 557-564.

Belser, L. W., and Mays, E. L. (1980). Specific inhibition of nitrite oxidation by chlorate and its use in assessing nitrification in soils and sediments. *Appl. Environ. Microbiol*., 39, 505-510.

Bratières, K., Fletcher, T. D., Deletic, A., and Zinger, Y. (2008). Nutrient and sediment removal by stormwater biofilters; a large-scale design optimisation study. *Water Res*., 42(14), 3930-3940.

Bruins, M. R., Kapil, S., and Oehme, F. W. (2000). Microbial resistance to metals in the environment. *Ecotoxicol. Environ. Saf.*, 45(3), 198-207.

Butterbach-Bahl, K., Baggs, E. M., Dannenmann, M., Kiese, R., and Zechmeister-Boltenstern, S. (2013). Nitrous oxide emissions from soils: how well do we understand the processes and their controls? *Phil. Trans. R. Soc. B*, 368(1621), 20130122.

Cela, S., and Sumner, M. E. (2002). Critical concentrations of copper, nickel, lead, and cadmium in soils based on nitrification. *Commun. Soil Sci, Plant Anal.*, *33*(1-2), 19-30.

Chen, X., Peltier, E., Sturm, B. S., and Young, C. B. (2013). Nitrogen removal and nitrifying and denitrifying bacteria quantification in a stormwater bioretention system. *Water Res*., 47(4), 1691-1700.

Davis, A. P., Shokouhian, M., Sharma, H., and Minami, C. (2001) Laboratory study of biological retention for urban stormwater management. *Water Environ. Res.*, 73, 5-14.

Davis, A. P., Shokouhian, M., Sharma, H., Minami, C., and Winogradoff, D. (2003). Water quality improvement through bioretention: Lead, copper, and zinc removal. *Water Environ. Res*., 75(1), 73-82.

Davis, A. P., Shokouhian, M., Sharma, H., and Minami, C. (2006) Water quality improvement through bioretention media: nitrogen and phosphorus removal. *Water Environ. Res*. 78, 284-293.

English, B. P., Min, W., Van Oijen, A. M., Lee, K. T., Luo, G., Sun, H., Cherayil, B. J., Kou, S. C. and Xie, X. S. (2006). Ever-fluctuating single enzyme molecules: Michaelis-Menten equation revisited. *Nat. Chem. Biol.*, 2(2), 87-94.

Feraud, M; Holden, P. A. (2021). Evaluating the relationships between specific drainage area characteristics and soil metal concentrations in long-established bioswales receiving suburban stormwater runoff. Sci. Tot. Environ., 757(25), 143778.

Gardner, W. H. (1986). Water content, In: Methods of soil analysis, part 1, physical and mineralogical methods (2nd edition), Klute, A. (Ed.), American Society of Agronomy, Agronomy Monographs 9(1), Madison, WI, 493-544.

Giller, K. E., E. Witter, and S. P. McGrath (1998). Toxicity of heavy metals to microorganisms and microbial processes in agricultural soils: a review. *Soil Biol. Biochem*. 30**,** 1389-1414.

Groffman, P. M., Butterbach-Bahl, K., Fulweiler, R. W., Gold, A. J., Morse, J. L., Stander, E., Tague, C., Tonitto, C. and Vidon, P. (2009). Challenges to incorporating spatially and temporally explicit phenomena (hotspots and hot moments) in denitrification models. *Biogeochemistry*, 93, 49-77.

Grover, S. P. P., Cohan, A., Chan, H. S., Livesley, S. J., Beringer, J., and Daly, E. (2013). Occasional large emissions of nitrous oxide and methane observed in stormwater biofiltration systems, *Sci. Total. Environ*., 465, 64-71.

Hart, S. C., Stark, J. M., Davidson, E. A. and Firestone, M. K. (1994). Nitrogen mineralisation, immobilisation, and nitrification. In: Methods of soil analysis: part 2 – Microbiological and biochemical properties, Bezdiecek, D. (Ed.), Soil Science Society of America, Madison, WI, 985-1018.

Hatt, B. E., Fletcher, T. D., and Deletić, A. (2007). Hydraulic and pollutant removal performance of stormwater filters under variable wetting and drying regimes. *Water Sci. Technol*., 56 (12), 11-19.

Holtan-Hartwig, L., M. Bechmann, T. Risnes Hoyas, R. Linjordet, and L. Reier Bakken. 2002. Heavy metals tolerance of soil denitrifying communities: N_2O dynamics. *Soil Biol. Biochem*. 34**,**1181-1190.

Hsieh, C. H., and Davis, A. P. (2005). Evaluation and optimization of bioretention media for treatment of urban storm water runoff. *J. Environ. Eng.*, 131(11), 1521-1531.

Hung, W.C., Rugh, M., Feraud, M., Avasarala, S., Kurylo, J., Gutierrez, M., Jimenez, K., Truong, N., Holden, P.A., Grant, S.B. and Liu, H. (2022). Influence of soil characteristics and metal (loid) s on antibiotic resistance genes in green stormwater infrastructure in Southern California. *J. of Hazard. Mater.*, 424, 127469.

Hunt, W. F., Jarrett, A. R., Smith, J. T., and Sharkey, L. J. (2006). Evaluating bioretention hydrology and nutrient removal at three field sites in North Carolina. *J. Irrig. Drain. Eng*., 132(6), 600-608.

Hutchinson, G. L., and Mosier, A. R. (1981). Improved soil cover method for field measurement of nitrous oxide fluxes. *Soil Sci. Soc. Am. J.*, 45, 311-316.

Ingvertsen, S.T., Cederkvist, K., Regent, Y., Sommer, H., Magid, J., Jensen, M.B., 2012. Assessment of existing roadside swales with engineered filter soil: I. Characterization and lifetime expectancy. *J. Environ. Qual.* 41(6), 1960-1969.

IPCC (2013): Climate Change 2013: The Physical Science Basis. Contribution of Working Group I to the Fifth Assessment Report of the Intergovernmental Panel on Climate Change [Stocker, T.F., D. Qin, G.-K. Plattner, M. Tignor, S.K. Allen, J. Boschung, A. Nauels, Y. Xia, V. Bex and P.M. Midgley (eds.)]. Cambridge University Press, Cambridge, United Kingdom and New York, NY, USA, 1535 pp.

Kalbitz K, Solinger S, Park J-H, Michalzik B, Matzner E (2000) Controls on the dynamics of dissolved organic matter in soils: a review. *Soil Sci*., 165, 277-304.

Larsson, M. A., Baken, S., Gustafsson, J. P., Hadialhejazi, G., and Smolders, E. (2013). Vanadium bioavailability and toxicity to soil microorganisms and plants. *Environ. Toxicol. Chem.*, 32(10), 2266-2273.

LeFevre, G. H., Paus, K. H., Natarajan, P., and Gulliver, J. S. (2015). Review of dissolved pollutants in urban storm water and their removal and fate in bioretention cells. *J. Env. Eng.*, 141(1), 0401 4050.

Li, H., and Davis, A. P. (2009). Water quality improvement through reductions of pollutant loads using bioretention. *J. Environ. Eng*., 135(8), 567-576.

Li, D., Van De Werfhorst, L. C., Rugh, M. B., Feraud, M., Hung, W-C, Jay, J., Cao, Y, Parker, E. A., Grant, S. B., and Holden, P. A. (2021). Limited bacterial removal in full-scale stormwater biofilters as evidenced by community sequencing analysis. *Environ. Sci. Technol.* 55(13), 9199-9208.

Lim, H. S., Lim, W., Hu, J. Y., Ziegler, A., and Ong, S. L. (2015). Comparison of filter media materials for heavy metal removal from urban stormwater runoff using biofiltration. *J. Environ. Manage.*, 147, 24-33.

Mertens, J. and Smolders, E. (2013). Chapter 17, Zinc. In: Heavy metals in soils: Trace metals and metalloids in soils and their bioavailability (3rd edition), Alloway, B. (Ed.), Springer, Dordrecht, Netherlands, 465-493.

Morse, N. R., McPhillips, L. E., Shapleigh, J. P., and Walter, M. T. (2017). The role of denitrification in stormwater detention basin treatment of nitrogen. *Environ. Sci. Technol.*, 51(14), 7928-7935.

Muerdter, C. P., Wong, C. K., and LeFevre, G. (2018). Emerging investigator series: the role of vegetation in bioretention for stormwater treatment in the built environment: pollutant removal, hydrologic function, and ancillary benefits. *Environ. Sci.: Water Res. Technol.*, 4, 592-612.

Müller, A., Österlund, H., Marsalek, J., & Viklander, M. (2020). The pollution conveyed by urban runoff: A review of sources. *Sci. Total Environ.*, 709, 136125.

Mulvaney, R. L. (1996). Nitrogen - inorganic forms, In: Methods of Soil Analysis, Part 3 - Chemical Methods. SSSA Book Series No. 5. Sparks D. L. (Ed.), Soil Science Society of America, Madison, WI, 1129-1131.

National Research Council (2009). Urban stormwater management in the United States. The National Academies Press, Washington, DC.

Nelson, D. W., and Sommers, L. E. (1996). Total carbon, organic carbon, and organic matter, In: Methods of Soil Analysis, Part 3 - Chemical Methods. SSSA Book Series No. 5. Sparks D. L. (Ed.)., Soil Science Society of America, Madison, WI, 1002-1005.

Oorts, K., Bronckaers, H., & Smolders, E. (2006). Discrepancy of the microbial response to elevated copper between freshly spiked and long-term contaminated soils. *Environ. Toxicol. Chem.*, *25*(3), 845-853.

Or, D., and Wraith, J. M. (2000). Soil water content and water potential relationships. M.E. Sumner (Ed.), Handbook of Soil Science, CRC Press, Boca Raton, pp. A53-A85.

Payne, E. G., Fletcher, T. D., Cook, P. L., Deletic, A., and Hatt, B. E. (2014 a). Processes and drivers of nitrogen removal in stormwater biofiltration. *Crit. Rev. Env. Sci. Tech*., 44 (7), 796-846.

Payne E.G., Fletcher T.D., Russell D.G., Grace M.R., Cavagnaro T.R., Evrard V., Deletic A., Hatt B.E., and Cook P.L. (2014 b). Temporary storage or permanent removal? The division of nitrogen between biotic assimilation and denitrification in stormwater biofiltration systems. *PloS One*, 9, e90890.

Philadelphia Stormwater Management Guidance Manual Version 3.2. Available at: https://www.pwdplanreview.org/manual-info/guidance-manual#

Philippot, L., Hallin, S., and Schloter, M. (2007). Ecology of denitrifying prokaryotes in agricultural soil. *Adv. Agron.*, 96, 249-305.

Philippot, L., Andert, J., Jones, C.M., Bru, D. and Hallin, S. (2011). Importance of denitrifiers lacking the genes encoding the nitrous oxide reductase for N_2O emissions from soil. *Glob. Chang. Biol.*, 17(3), 1497-1504.

Reyes, C., Hodgskiss, L. H., Kerou, M., Pribasnig, T., Abby, S. S., Bayer, B., Kraemer, S. M., and Schleper, C. (2020). Genome wide transcriptomic analysis of the soil ammonia oxidizing archaeon *Nitrososphaera viennensis* upon exposure to copper limitation. *ISME J* 14**,** 2659-2674.

Rible, J. M. and Quick, J. (1960). Method S-19.0. Cation exchange capacity. In: Water soil plant tissue. Tentative methods of analysis for diagnostic purposes. Davis, University of California Agricultural Experiment Service. Mimeographed Report.

Ruyters, S., Mertens, J., Springael, D., and Smolders, E. (2012). Co-tolerance to zinc and copper of the soil nitrifying community and its relationship with the community structure. *Soil Biol. Biochem.*, *44*(1), 75-80.

Rusk, J. A., Hamon, R. E., Stevens, D. P., and McLaughlin, M. J. (2004). Adaptation of soil biological nitrification to heavy metals. *Environ. Sci. Technol*., 38(11), 3092-3097.

Sheldrick, B. H. and Wang, C. (1993). Particle-size distribution. In: Carter, M. R. (ed), Soil Sampling and Methods of Analysis, Canadian Society of Soil Science, Lewis Publishers, Ann Arbor, MI, 499-511.

Singh, B.K., Quince, C., Macdonald, C.A., Khachane, A., Thomas, N., Al-Soud, W.A., Sørensen, S.J., He, Z., White, D., Sinclair, A. and Crooks, B. (2014). Loss of microbial diversity in soils is coincident with reductions in some specialized functions. *Environ. Microbiol.*, 16(8), 2408-2420.

Smith, M. S., and Tiedje, J. M. (1979). Phases of denitrification following oxygen depletion in soil. *Soil Biol. Biochem.,* 11(3), 261-267.

Smith, D. B., Cannon, W. F., Woodruff, L. G., Solano, F., Kilburn, J. E., and Fey, D. L. (2013), Geochemical and mineralogical data for soils of the conterminous United States: U.S. Geological Survey Data Series 801, 19 pp.

Sun, X., and Davis, A. P. (2007). Heavy metal fates in laboratory bioretention systems. *Chemosphere*, 66(9), 1601-1609.

Tedoldi, D., Chebbo, G., Pierlot, D., Kovacs, Y., and Gromaire, M. C. (2016). Impact of runoff infiltration on contaminant accumulation and transport in the soil/filter media of sustainable urban drainage systems: a literature review. *Sci. Total Environ.*, 569, 904-926

Tedoldi, D., Chebbo, G., Pierlot, D., Branchu, P., Kovacs, Y., and Gromaire, M.C., 2017. Spatial distribution of heavy metals in the surface soil of source-control stormwater infiltration devices – inter-site comparison. *Sci. Total Environ.* 579, 881-892.

Tessier, A. P. G. C., Campbell, P. G. and Bisson, M. J. A. C. (1979). Sequential extraction procedure for the speciation of particulate trace metals. *Anal. Chem.,* 51(7), 844-851.

Tiedje, J. M., Sexstone, A. J., Myrold, D. D. and Robinson, J. A. (1983). Denitrification: ecological niches, competition and survival. *Antonie van Leeuwenhoek*, 48(6), 569-583.

Thomas, G. W. (1996). Soil pH and soil acidity, In: Methods of Soil Analysis, Part 3 - Chemical Methods. SSSA Book Series No. 5. Sparks D. L. (Ed.), Soil Science Society of America Madison, WI, 475-490.

U. S. EPA. 1996. Method 3050B: Acid digestion of sediments, sludges, soils. Revision 2. USEPA.

Waller, L. J., Evanylo, G. K., Krometis, L. A. H., Strickland, M. S., Wynn-Thompson, T., and Badgley, B. D. (2018). Engineered and environmental controls of microbial denitrification in established bioretention cells. *Environ. Sci. Technol.*, 52(9), 5358-5366.

Walsh, C. J., Leonard, A. W., Ladson, A. R., and Fletcher, T. D. (2004). Urban stormwater and the ecology of streams. Cooperative Research Centre for Freshwater Ecology and Cooperative Research Centre for Catchment Hydrology, Canberra, Australia.

Wang, Y., Shi, J., Wang, H., Lin, Q., Chen, X., and Chen, Y. (2007). The influence of soil heavy metals pollution on soil microbial biomass, enzyme activity, and community composition near a copper smelter. *Ecotoxicol. Environ. Saf.*, 67(1), 75-81.

Young, S. D. (2013). Chemistry of heavy metals and metalloids in soils. In: Heavy Metals in Soils. Environmental Pollution, Vol 22. Springer, Alloway B. (ed.). Dordrecht, Netherlands, 51-95.

Zinger, Y., Blecken, G. T., Fletcher, T. D., Viklander, M., and Deletic, A. (2013). Optimising nitrogen removal in existing stormwater biofilters: benefits and tradeoffs of a retrofitted saturated zone. *Ecol. Eng.*, 51, 75-82.

Zumft, W. G. (1997). The denitrifying prokaryotes, p. 443-582. In A. Balows, H. G. Truper, M. Dworkin, W. Harder, and K.-H. Schleifer (ed.), The prokaryotes. Springer, Heidelberg, Germany.

3.7. Figures and Tables

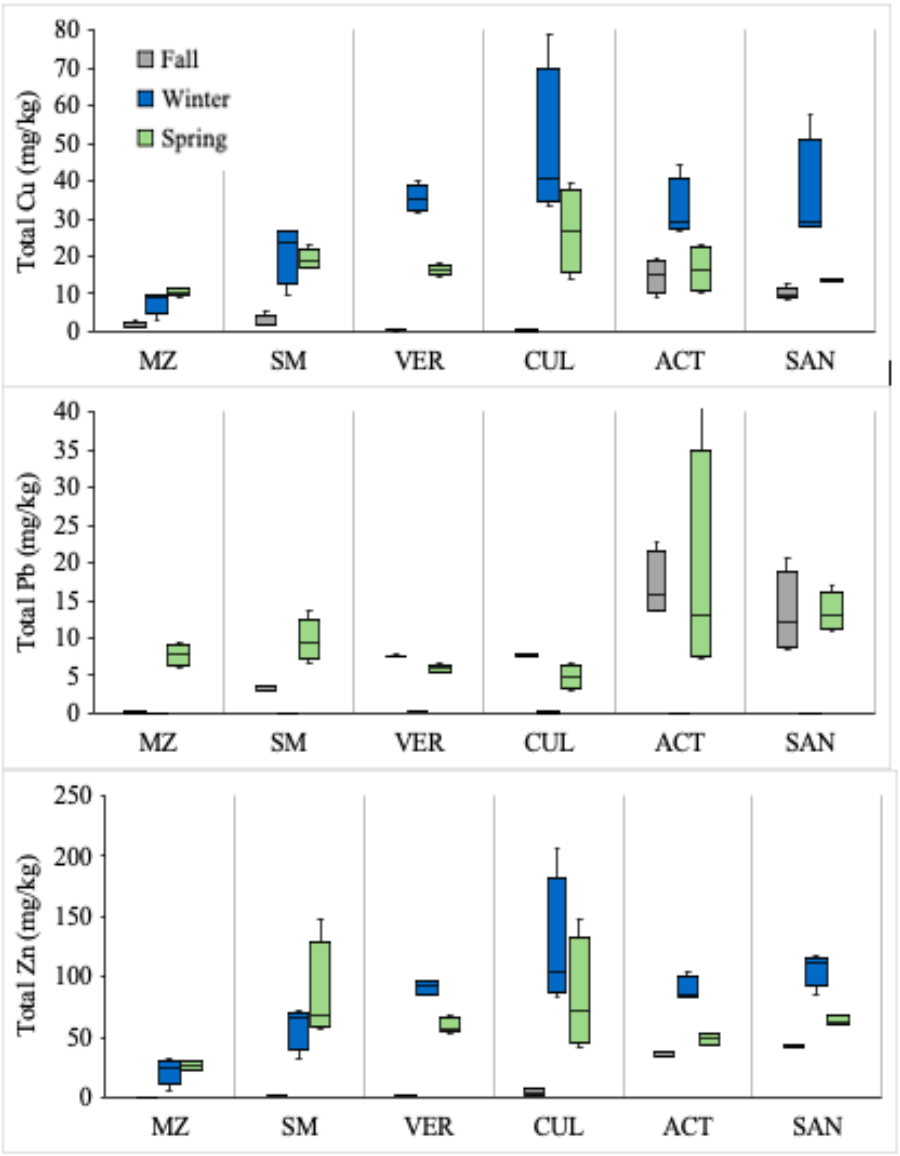

Figure 1. Total Cu, Pb, and Zn distribution across sites and sampling times for bioretention systems at UCSB (MZ and SM), UCI (VER and CUL), and UCSD (ACT and SAN) (n = 72). Boxplots show the median (solid line) and 25th (bottom) and 75th (top) percentile. The whiskers exclude outliers and extend 1.5 times the interquartile range.

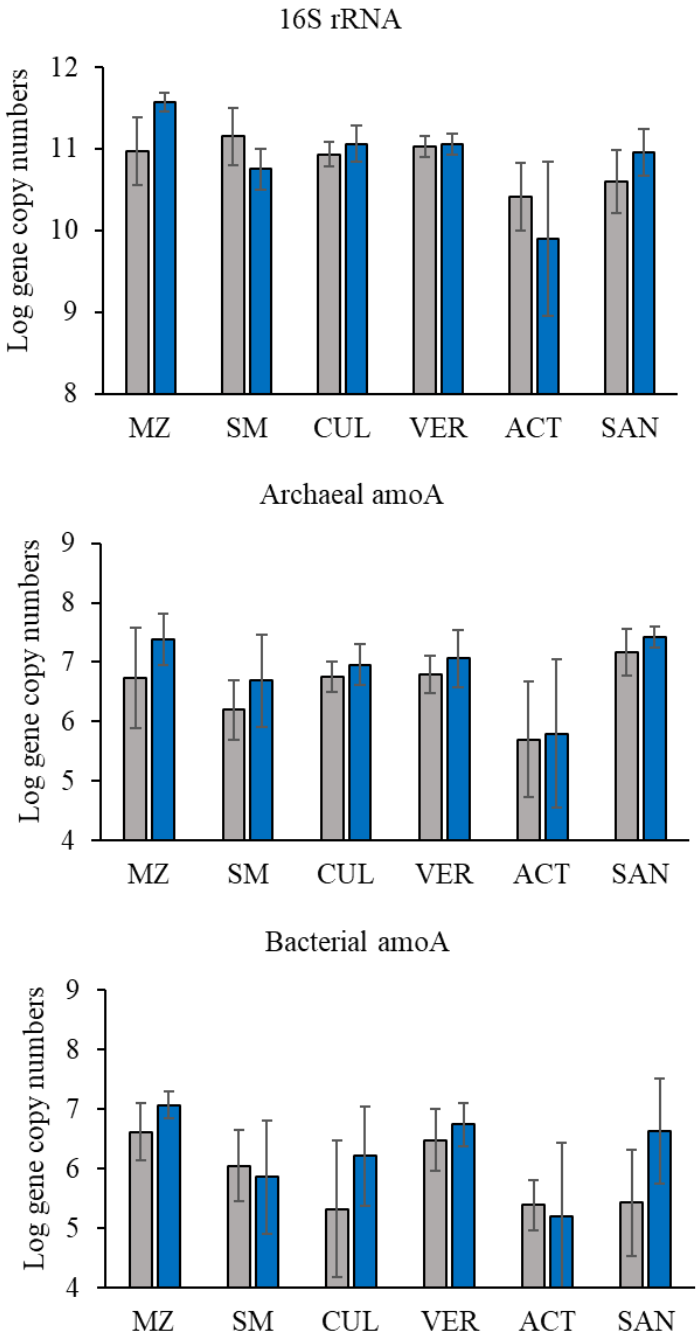

Figure 2. qPCR results for log-transformed 16S rRNA and nitrifying functional gene abundances (n = 24 for Fall sampling, n = 20 for Winter sampling). Values shown are mean and standard error. Significant differences across sites, for a given sampling time, are denoted with letters. For example, 16S rRNA gene abundance was greater in MZ than in ACT during Winter and Fall sampling.

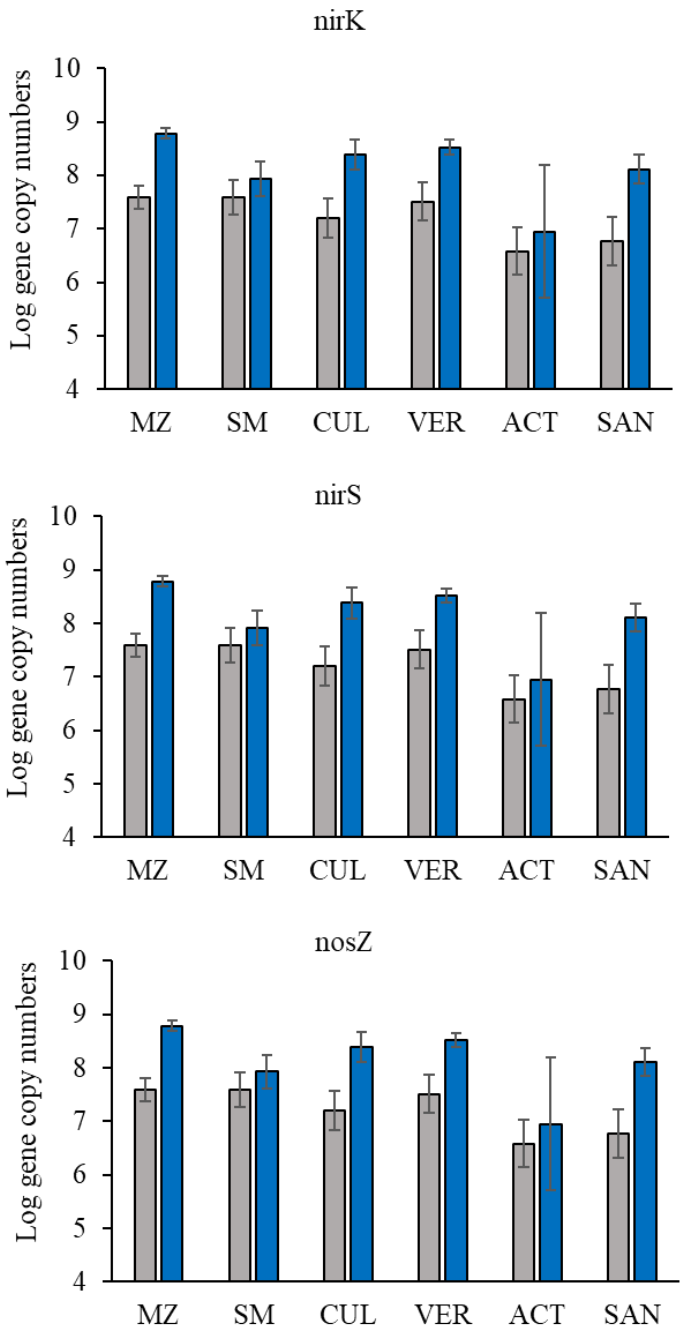

Figure 3. qPCR results for denitrifying functional gene abundances (log-transformed) Values shown are mean and standard error, and significant differences are denoted with letters (n = 24 for Fall sampling, n = 20 for Winter sampling). For example, in Fall samples, nirK gene abundance was greater in SM than ACT, but similar across all other sites. For the Winter samples, nirK gene abundances were greater in MZ, than in ACT.

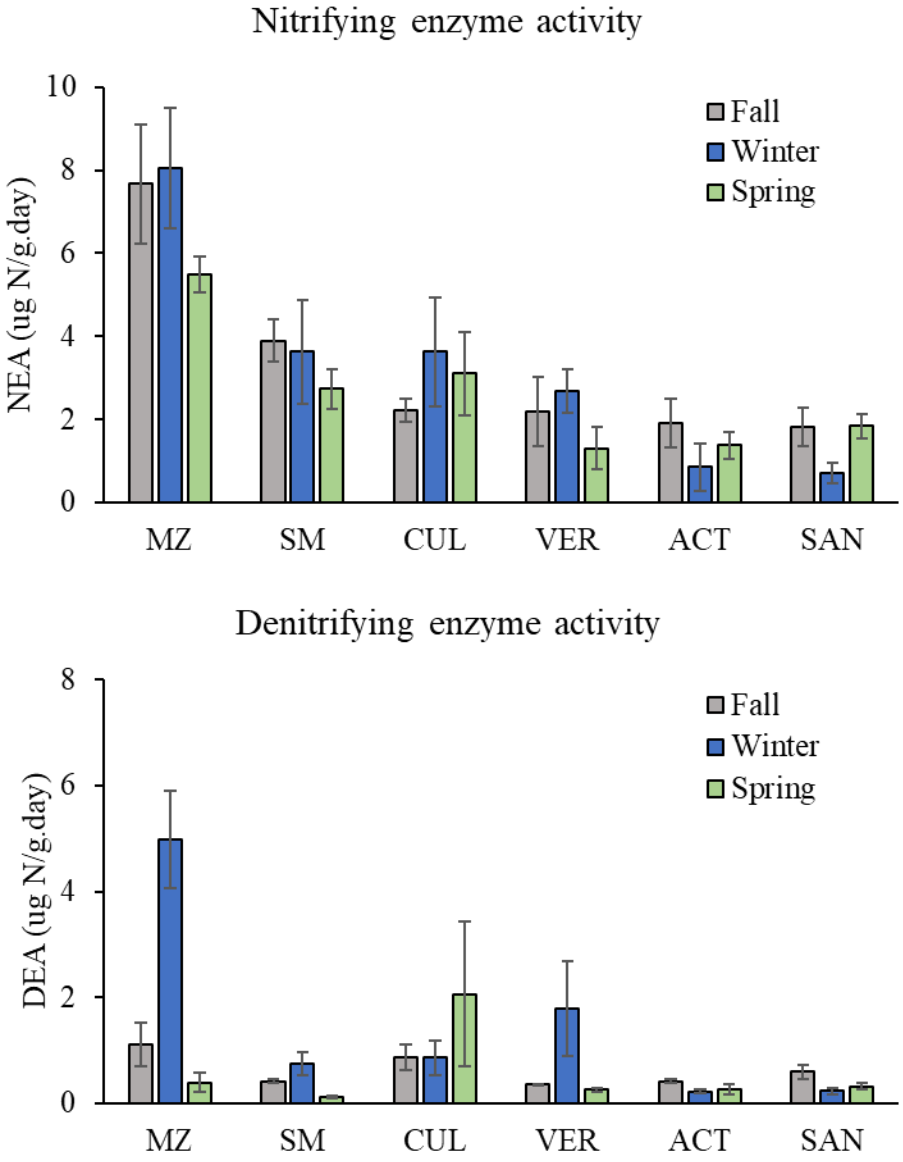

Figure 4. Nitrifying and denitrifying enzyme activities in bioretention soils (n = 72). Values shown are mean and standard error. Across sites, significant differences for each sampling time are denoted with letters. For example, NEA in MZ during the Fall is larger than in ACT and SAN, but similar to other sites.

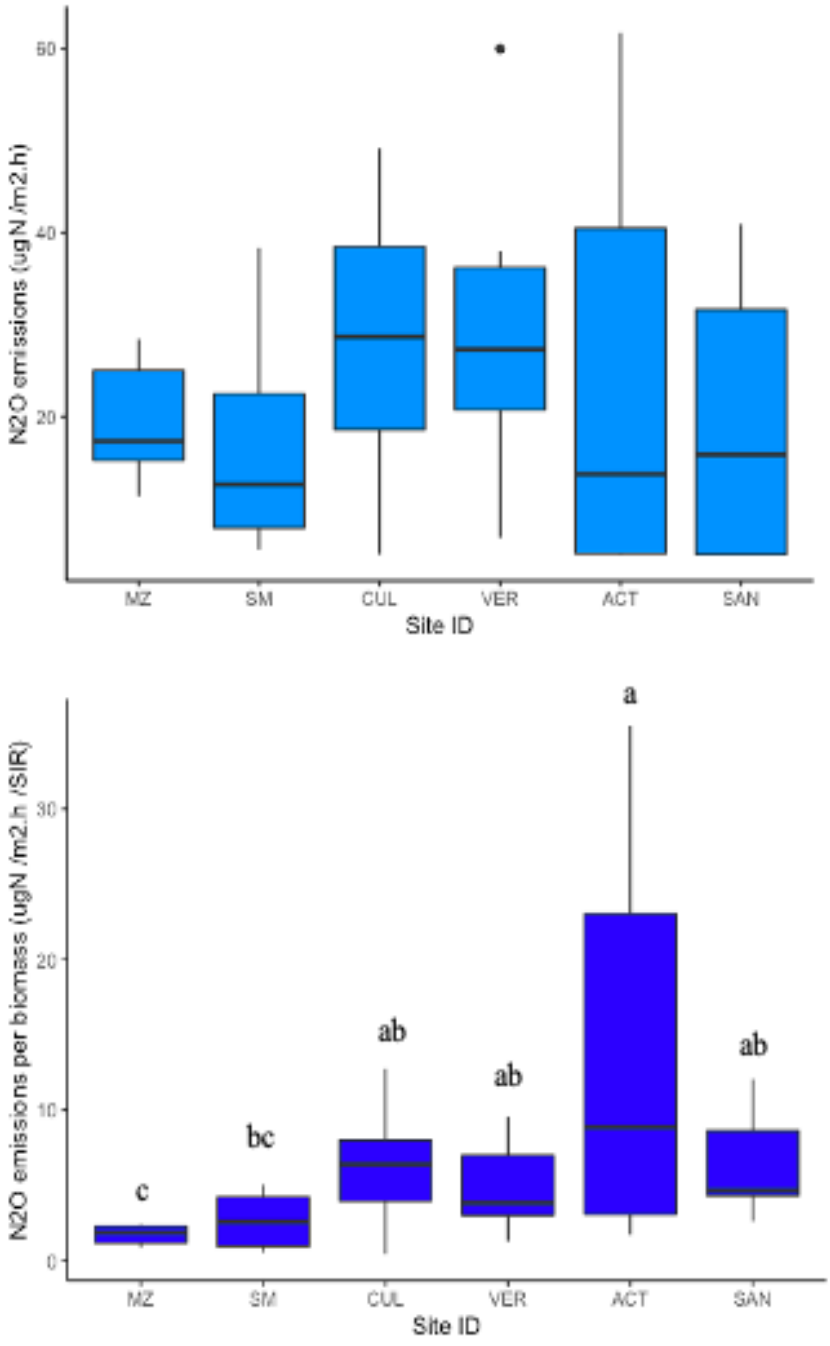

Figure 5. N_2O emissions across sites for all sampling times (Fall, Winter, and Spring). There were no significant differences in N_2O emissions across sampling times or sites. When N_2O emissions were normalized to microbial biomass (measured via SIR), ACT had higher emissions that MZ and SM, and SAN had higher emissions than MZ.

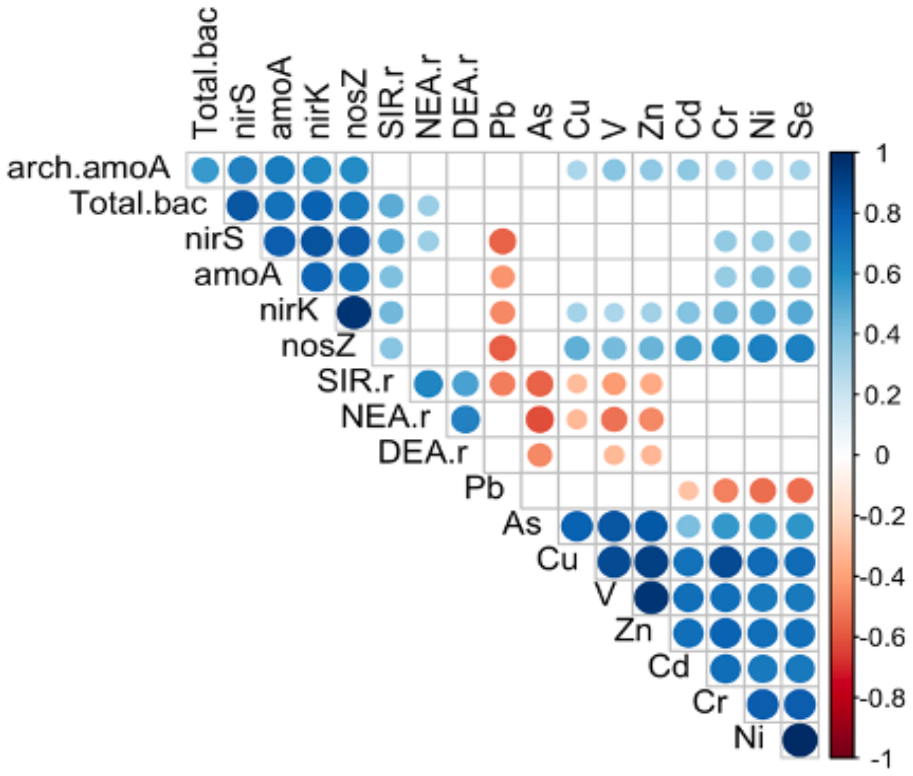

Figure 6. Spearman rank correlations between bacterial parameters and total metals (As, Cd, Cr, Cu, Ni, Pb, Se, V, Zn) across all sites for Fall and Winter Sampling (n = 44). Bacterial abundances via qPCR were not estimated for Spring samples. For Winter samples, 2 samples each (out of 4 replicates) for ACT and SAN were lost (n = 24 for Fall, n = 20 for Winter). The size of the circles is proportional to the correlation coefficient. Bacterial population sizes are represented by log-transformed gene abundances of 16SrRNA (Total.bac, total bacteria), archaeal and bacterial amoA (nitrifying bacteria), and nirK, nirS, and nosZ (denitrifying bacteria). SIR.r (substrate induced respiration) measures the microbial biomass, while NEA.r (nitrifying enzyme activity) and DEA.r (denitrifying enzyme activity) are measures of the nitrifying and denitrifying population sizes, respectively.

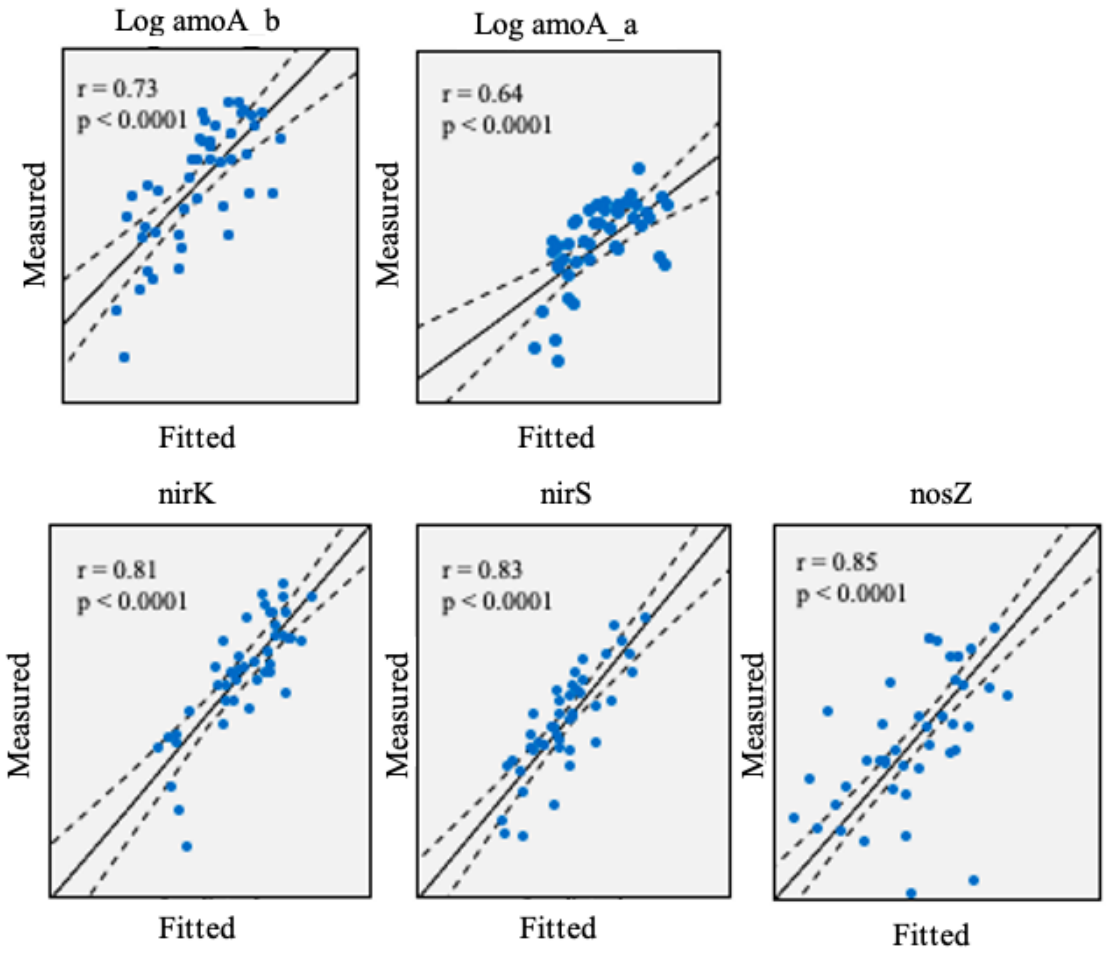

Figure 7. Pearson product-moment coefficients (*r*) between observed (measured) and fitted values of absolute abundances of archaeal and bacterial amoA genes, nirK, nirS, and nosZ based on multiple linear regression (MLR) models in GSI soils across three UC campuses (N = 44, 24 from fall sampling, and 20 samples from winter sampling).

Abbreviations: amoA_a, archaeal amoA; amoA_b, bacterial amoA.

Table 1. Site characteristics of GSI systems distributed in three UC campuses.

	MZ	SM	CUL	VER	ACT	SAN
Campus	UCSB	UCSB	UCI	UCI	UCSD	UCSD
Latitude (N)	34.40916	34.42022	33.64976	33.64571	32.87919	32.88841
Longitude (W)	119.85233	119.87016	117.82472	117.82965	117.22709	117.24468
Bioretention system	Bioswale	Biofilter	Bioswale	Bioswale	Infiltration basins	Biofilter
Bioretention area (m^2)	363	142	1330	146	1024	103
Runoff sources	Residential Building, landscape (lawns), and walkway	Parking lot driveway and parking space	Parking lot driveway and parking space	Parking lot driveway, parking space, and undeveloped land	School building (AC condensate) and walkway	Parking lot driveway, parking space, and landscape
Impervious drainage area (m^2)	1751[a]	4104	31,883	6405	6170	642
Impervious ratio [b]	2.2	28.9	24.0	43.9	6.0	6.2
Year built	2001	2015	2007	2012	2016	2011
Type of irrigation water	RW	RW	RW	PW	PW	RW
Soil classification	Sandy loam	Sandy clay loam	Sandy loam	Sandy loam	Sandy loam	Loamy sand
Soil amendments (or fertilizers)	No	Yes	Yes	Yes	Yes	Yes

Abbreviations: MZ, Manzanita; SM, Sierra Madre; CUL, Culver; VER, Verano; ACT, Altman Clinical and Translational Research Institute; SAN, Sanford; GSI, Green Stormwater Infrastructure; RW, Reclaimed Water; PW, Potable Water.

[a] Only 796 m^2 are directly connected to MZ, the other impervious surfaces correspond to roofs, where stormwater runoff flows through a manicured lawn prior to entering the bioretention system. The directly connected impervious area is used to calculate the impervious ratio.

[b] The impervious ratio is defined here as the ratio of directly connected impervious area to bioretention system area

Table 2. Microbial and bacterial community size, nitrifying and denitrifying functional gene abundance via qPCR, and nitrifying and denitrifying enzyme activities across all sites and sampling times.

Measurement	**Bioretention Site**					
	MZ	SM	CUL	VER	ACT	SAN
Potential activities						
SIR (mg C/kg h)	11.3 ± 3.2	7.7 ± 2.1	7.3 ± 5.0	5.7 ± 1.9	1.9 ± 0.9	3.0 ± 1.4
NEA mg N/kg h)	7.1 ± 2.5	3.4 ± 1.6	3.0 ± 1.9	2.1 ± 1.3	1.4 ± 1.0	1.4 ± 0.8
DEA (mg N/kg h)	2.2 ± 2.4	0.4 ± 0.4	1.3 ± 1.6	0.8 ± 1.2	0.3 ± 0.1	0.4 ± 0.2
Gene abundances [a]						
16S rRNA	2.5E+11 ± 1.6E+11	1.2E+11 ± 9.2E+10	1.1E+11 ± 5.1E+10	1.1E+11 ± 3.0E+10	3.0E+10 ± 2.5E+10	6.7E+10 ± 4.6E+10
Archaeal amoA	2.5E+07 ± 3.2E+07	7.0E+06 ± 9.3E+06	8.7E+06 ± 5.4E+06	1.2E+07 ± 8.0E+06	2.0E+06 ± 2.3E+06	2.2E+07 ± 1.2E+07
Bacterial amoA	9.3E+06 ± 5.8E+06	2.2E+06 ± 2.3E+06	2.7E+06 ± 4.4E+06	5.8E+06± 4.3E+06	4.3E+05 ± 4.7E+05	3.8E+06 ± 7.1E+06
nirK	1.1E+08 ± 8.5E+07	3.7E+07 ± 2.5E+07	5.3E+07 ± 5.8E+07	7.3E+07 ± 4.5E+07	6.9E+06 ± 7.4E+06	2.0E+07 ± 2.2E+07
nirS	4.7E+08 ± 3.3E+08	1.5E+08 ± 1.1E+08	8.4E+07 ± 6.7E+07	9.8E+07 ± 5.0E+07	2.4E+07 ± 1.8E+07	4.4E+07 ± 3.4E+07
nosZ	3.3E+08 ± 3.2E+08	7.6E+07 ± 6.4E+07	1.5E+08 ± 2.1E+08	1.9E+08 ± 1.7E+08	1.5E+07 ± 2.6E+07	5.3E+07 ± 7.8E+07

[a] Gene abundances are measured as gene copies per gram of dry soil.

Abbreviations: SIR, substrate induced respiration assay; NEA, nitrifying enzyme activity; DEA, denitrifying enzyme activity.

Table 3. Multiple linear regression models for absolute and relative abundances of functional genes in biofilter soils. Models include soil properties, and concentrations of total and bioavailable metals. Relevant explanatory variables were selected for starting models, and a stepwise method was then used to select the final models. Prior to MLR analysis, all variables were log-transformed to better approximate normal distributions.

Gene	Equation	R^2	Adj. R^2	p-value
amoA_a	Log (amoA_a) = 12.23 – 10.08 Log (pH) + 1.37 Log (Moisture) + 0.99 Log (Age) + 0.26 Log(Cu) + 0.34 Log (V_bio)	0.49	0.43	< 0.0001
amoA_b	Log (amoA_a) = 13.00 – 12.06 Log (pH) + 1.57 Log (SIR) + 1.61 Log (Silt) + 0.67 Log (V)	0.62	0.57	< 0.0001
nirK	Log (nirK) = 11.88 – 6.83 Log (pH) + 1.40 Log (SIR) + 0.24 Log (Cu) + 0.47 Log (Ni)	0.65	0.6	< 0.0001
nirS	Log (nirS) = 5.69 + 0.88 Log (Moisture) + 0.72 Log (SIR) + 0.45 Log (Age) + 0.20 Log (Cu_bio)	0.68	0.65	< 0.0001
nosZ	Log (nosZ) = 5.02 + 1.77 Log (SIR) + 0.72 Log (V) + 0.46 Log (Ni)	0.72	0.7	< 0.0001
16S rRNA	Log (16S rRNA) = 10.27 + 1.64 Log (SOM) + 0.60 Log (Age) + 0.52 Log (NH4) – 0.48 Log (V_bio)	0.55	0.5	< 0.0001
amoA_a/16S	Log (amoA_a/16S) = 1.15 – 0.16 Log (pH) + 0.12 Log (SIR) + 0.07 Log (V_bio) + 0.04 Log (Cu)	0.57	0.51	< 0.0001
amoA_b/16S	Log (amoA_b/16S) = 1.51 – 1.41 Log (pH) - 0.19 Log (W.Pot) + 0.15 Log (Silt) + 0.04 Log (V_bio) – 0.03 Log (Pb)	0.47	0.4	< 0.0001
nirK/16S	Log (nirK/16S) = 1.19 – 0.73 Log (pH) – 0.17 Log (SOM) + 0.16 Log (SIR) + 0.07 Log (Ni) + 0.05 Log (V)	0.5	0.44	< 0.0001
nirS/16S	Log (nirS/16S) = 0.65 + 0.47 Log (BulkD) – 0.11 Log (SOM) – 0.02 Log (Pb)	0.41	0.35	< 0.001
nosZ/16S	Log (nosZ/16S) + 0.41 + 0.07 Log (Age) +. 0.07 Log (DOC) 0.06 Log (Cu) – 0.05 Log (Cd_bio) + 0.05 Log (V_bio)	0.69	0.65	< 0.0001

3.8. Supplemental Materials

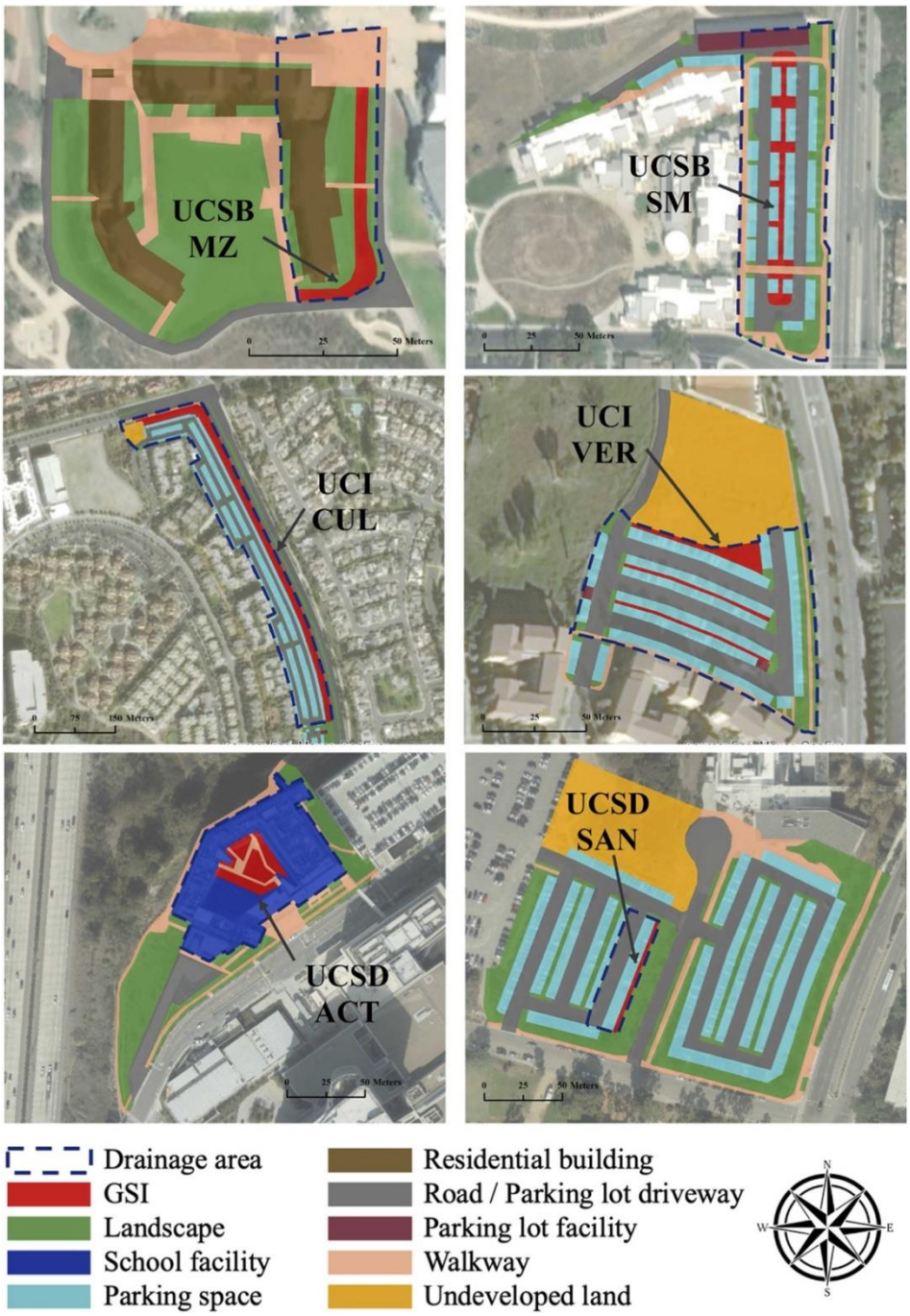

Figure S1. Bioretention sites at three Southern UC campuses (UCSB: MZ and SM; UCI: CUL, VER; UCSD: ACT, SAN), their drainage areas, and nearby land uses. Figure corresponds to Figure 1 in (Hung et al. 2022).
Abbreviations: UCSB, University of California, Santa Barbara; UCI, University of California, Irvine; UCSD, University of California, San Diego.

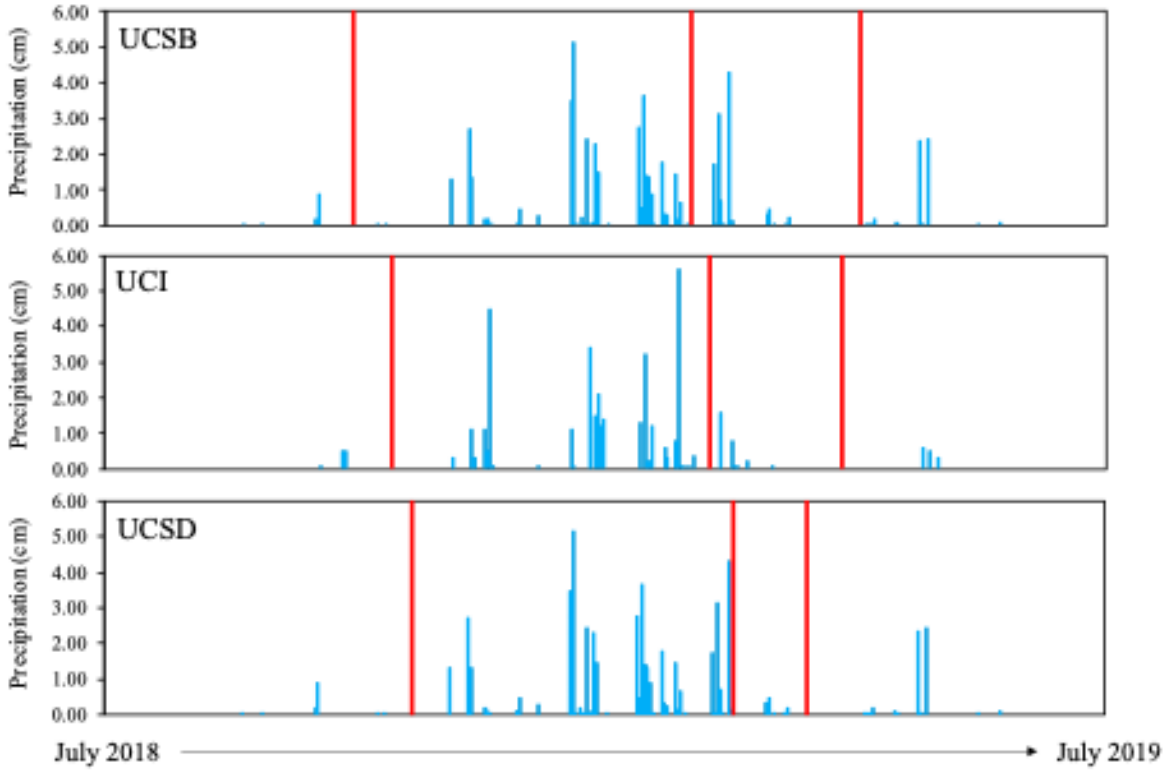

Figure S2. Daily rainfall data reported in areas close to the three study areas. Red lines indicate sampling dates in October/November 2018, February/March 2019, and April 2019. Figure corresponds to Figure S1 in (Hung et al. 2022).

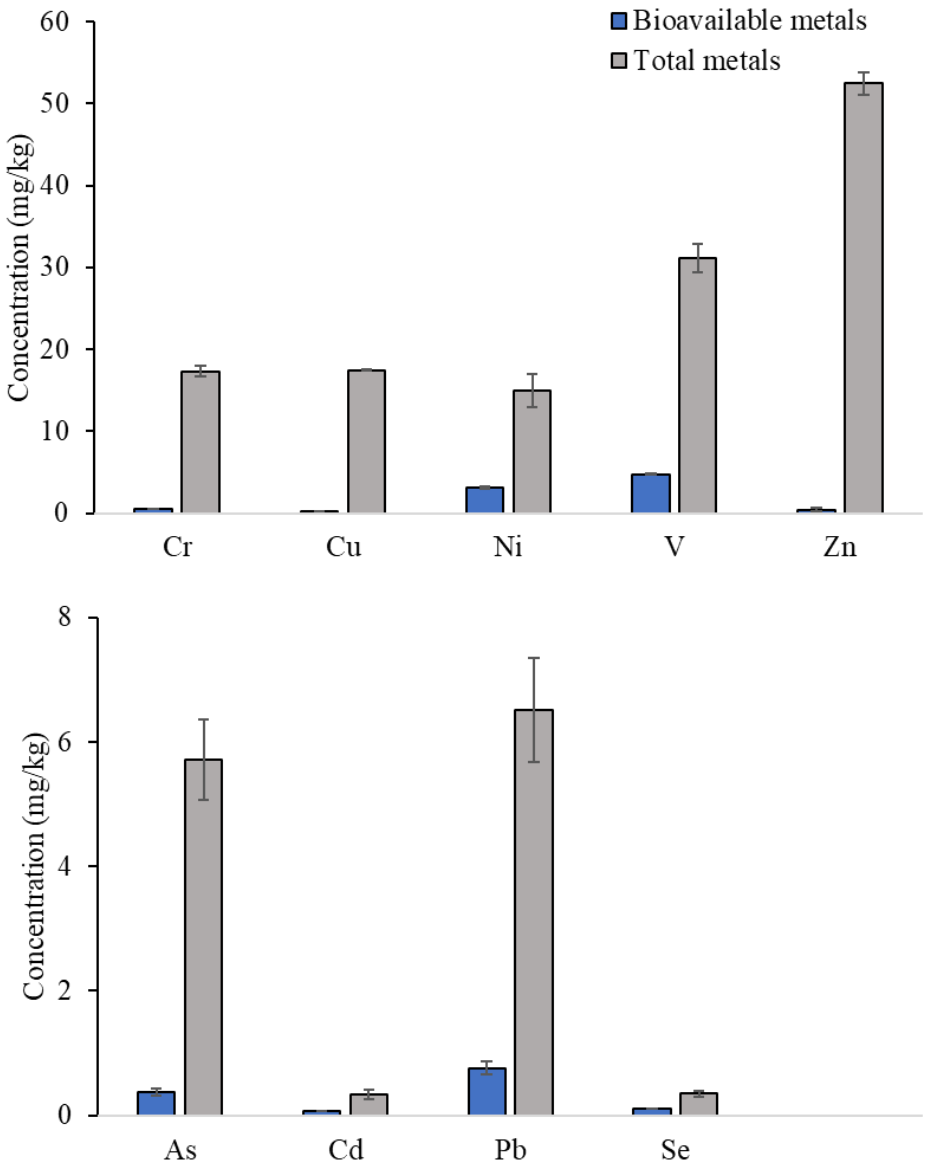

Figure S3. Bioavailable and total metals in soils collected at six GSI sites at different times. Values represent mean and standard error across all samples (n = 72). Top panel: Cr, Cu, Ni, V and Zn; bottom panel: As, Cd, Pb, and Se (note scale difference).

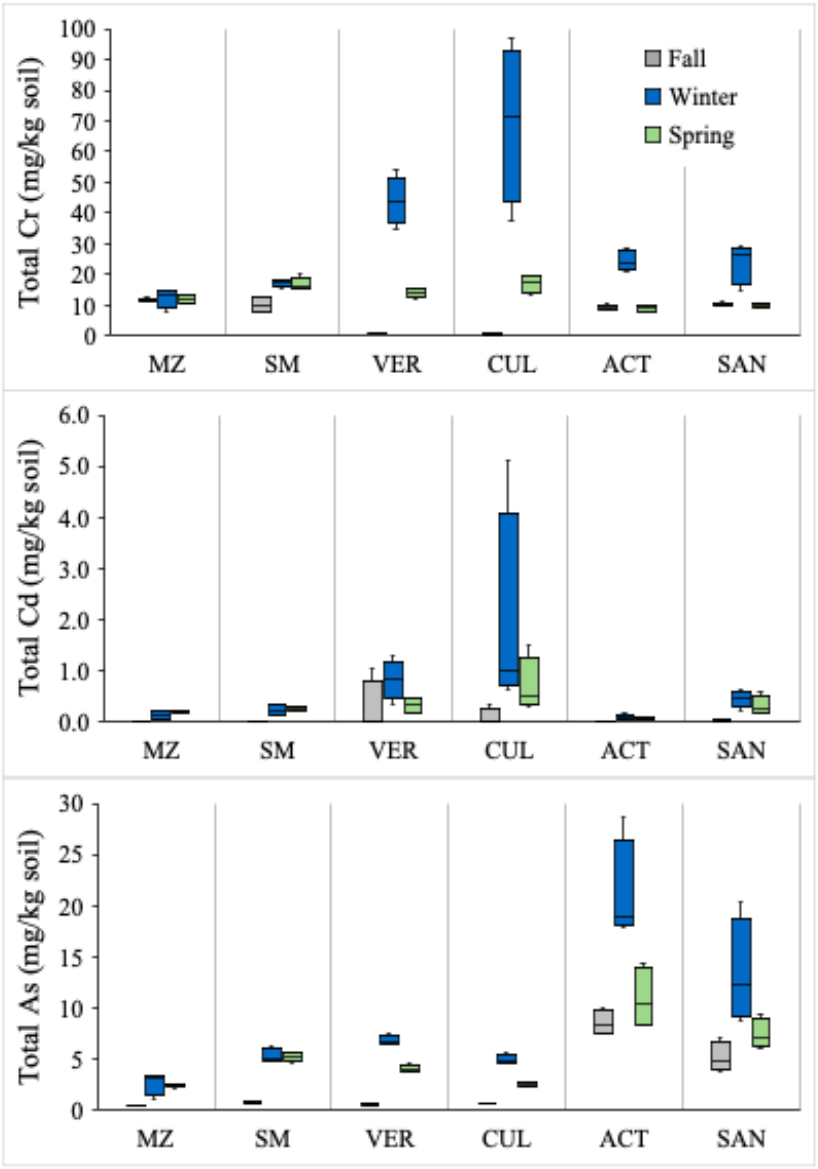

Figure S4. Total As, Cd, Cr of soils collected at six GSI sites at different times (n = 72). Boxplots show the median (solid line) and 25th (bottom) and 75th (top) percentile. The whiskers exclude outliers and extend 1.5 times the interquartile range. Sampling occurred in October/November 2018 (Fall), February/March of 2019 (Winter), and April 2019 (Spring).

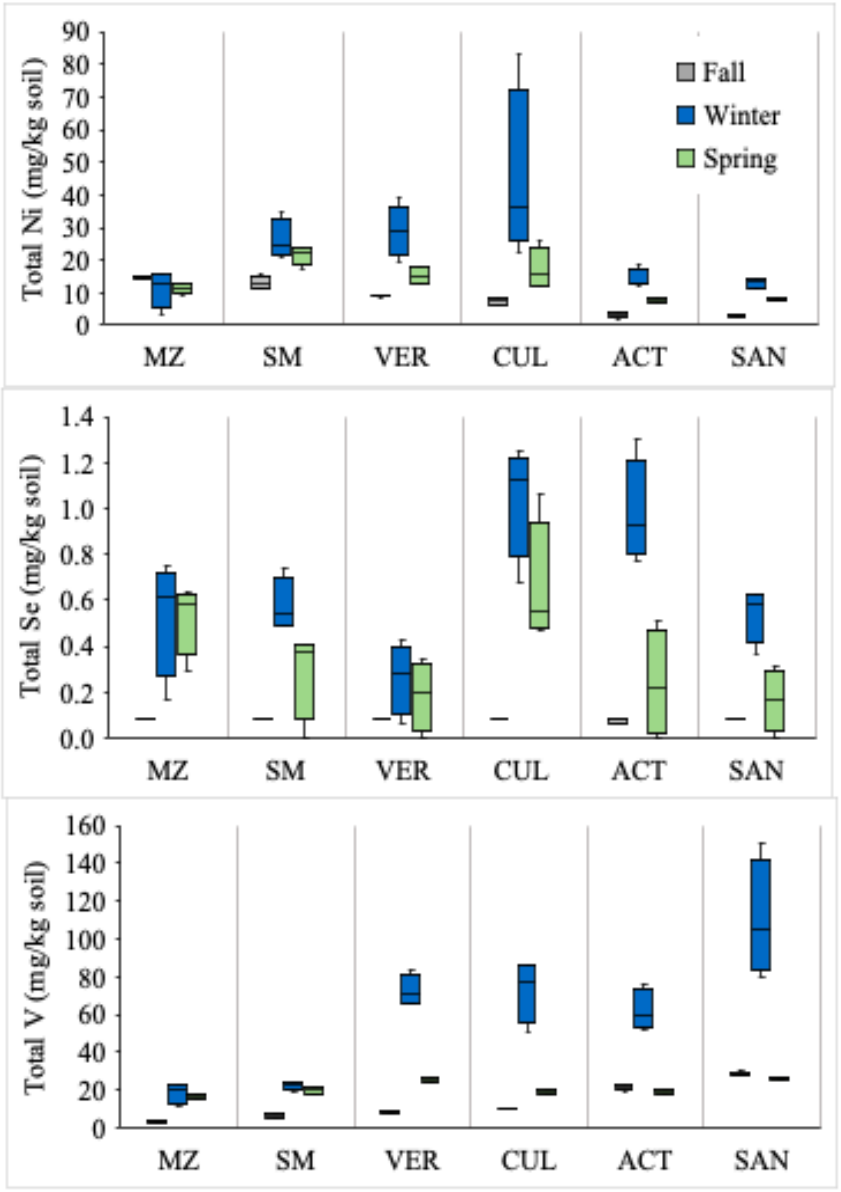

Figure S5. Total Ni, Se, V of soils collected at six GSI sites at different times (n = 72). Boxplots show the median (solid line) and 25th (bottom) and 75th (top) percentile. The whiskers exclude outliers and extend 1.5 times the interquartile range. Sampling occurred in October/November 2018 (Fall), February/March of 2019 (Winter), and April 2019 (Spring).

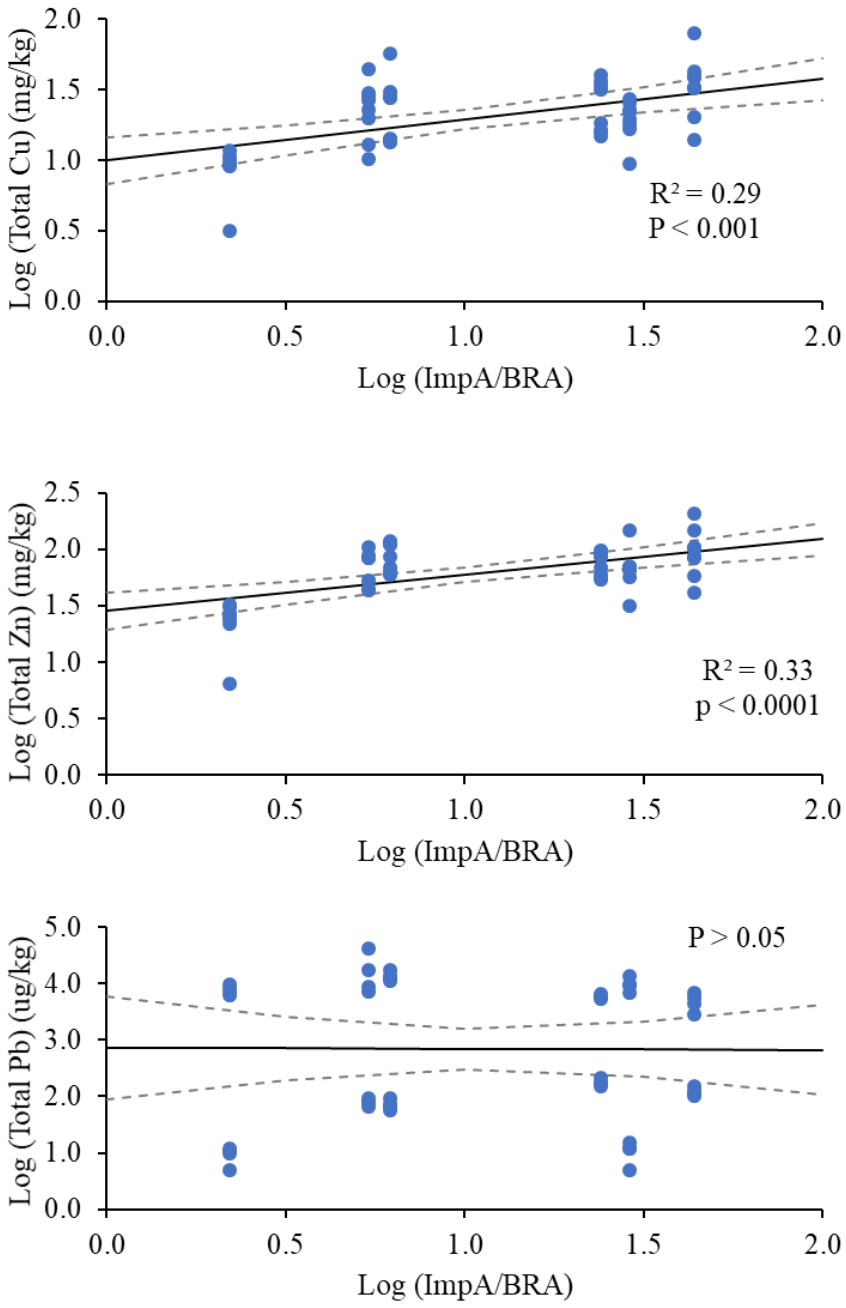

Figure S6. Linear relationship between total Cu, Zn and Pb with impervious drainage area ratio during winter and spring sampling. Mean and 95% confidence intervals are shown. Total Pb was not related to the impervious drainage area, whereas Cu and Zn were weakly, but significantly related to the ratio of impervious drainage area to bioretention area (ImpA/BRA).

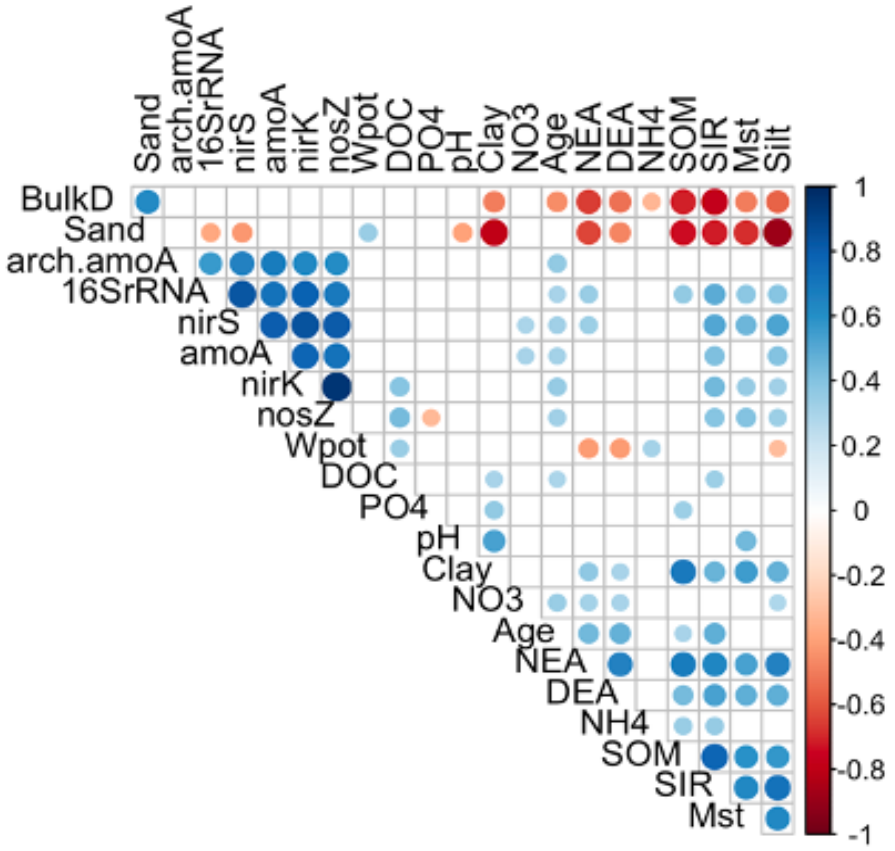

Figure S7. Significant correlations (Spearman's rank, $p < 0.05$) between environmental variables, bioretention system age, and bacterial population sizes across sites and sampling times. The size of the circles is proportional to the correlation coefficient. Bacterial population sizes are represented by log-transformed gene abundances of 16S rRNA (total bacteria), archaeal and bacterial amoA (nitrifying bacteria), and nirK, nirS, and nosZ (denitrifying bacteria). SIR (substrate induced respiration) is a measure of the microbial biomass, while NEA (nitrifying enzyme activity) and DEA (denitrifying enzyme activity) are additional measures of the population size of nitrifiers, and denitrifiers, respectively. Abbreviations: BulkD, bulk density; Wpot, water potential; PO4, phosphate; NO3, nitrate; NH4, ammonium; SOM, soil organic matter; Mst, moisture.

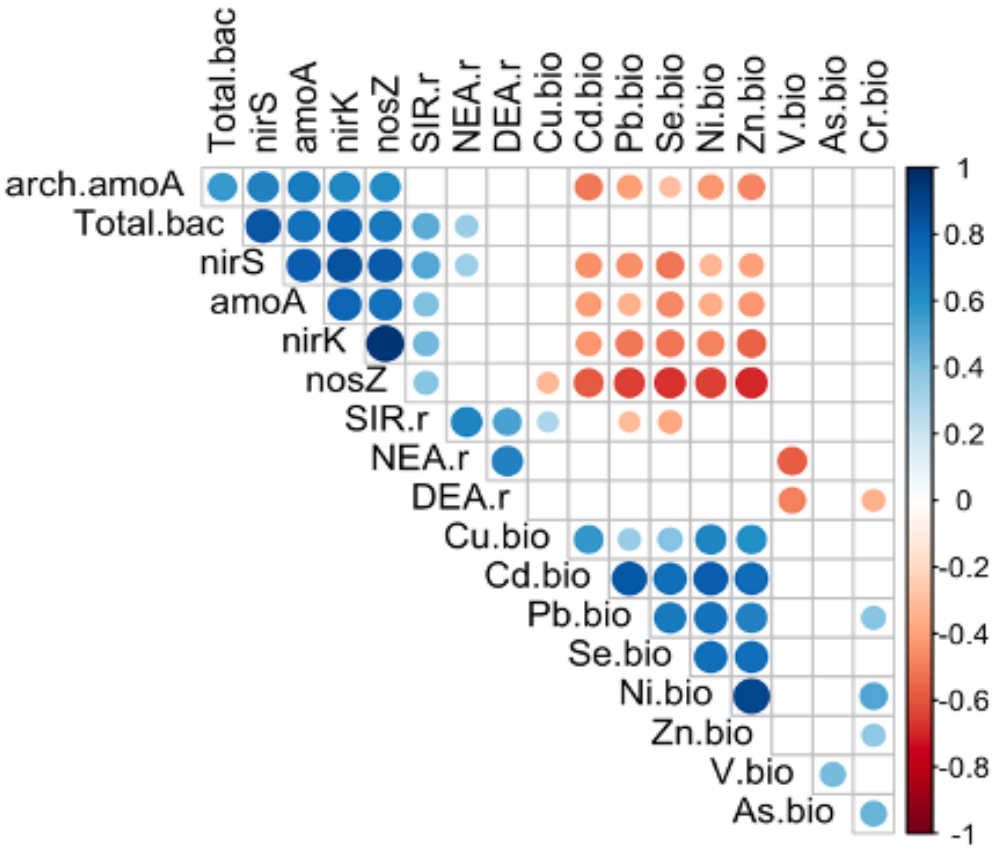

Figure S8. Spearman rank correlations between bacterial parameters and bioavailable metals (As, Cd, Cr, Cu, Ni, Pb, Se, V, Zn) across all sites for Fall and Winter Sampling. Bacterial abundances via qPCR were not estimated for Spring samples. For Winter samples, 2 samples each (out of 4 replicates) for ACT and SAN were lost (n = 44). The size of the circles is proportional to the correlation coefficient. Bacterial population sizes are represented by log-transformed gene abundances of 16S rRNA (Total.bac, total bacteria), archaeal and bacterial amoA (nitrifying bacteria), and nirK, nirS, and nosZ (denitrifying bacteria). SIR.r refers to microbial biomass measured via the substrate induced respiration method, while NEA.r and DEA.r refer, respectively, to the nitrifying, and denitrifying, enzyme activities.

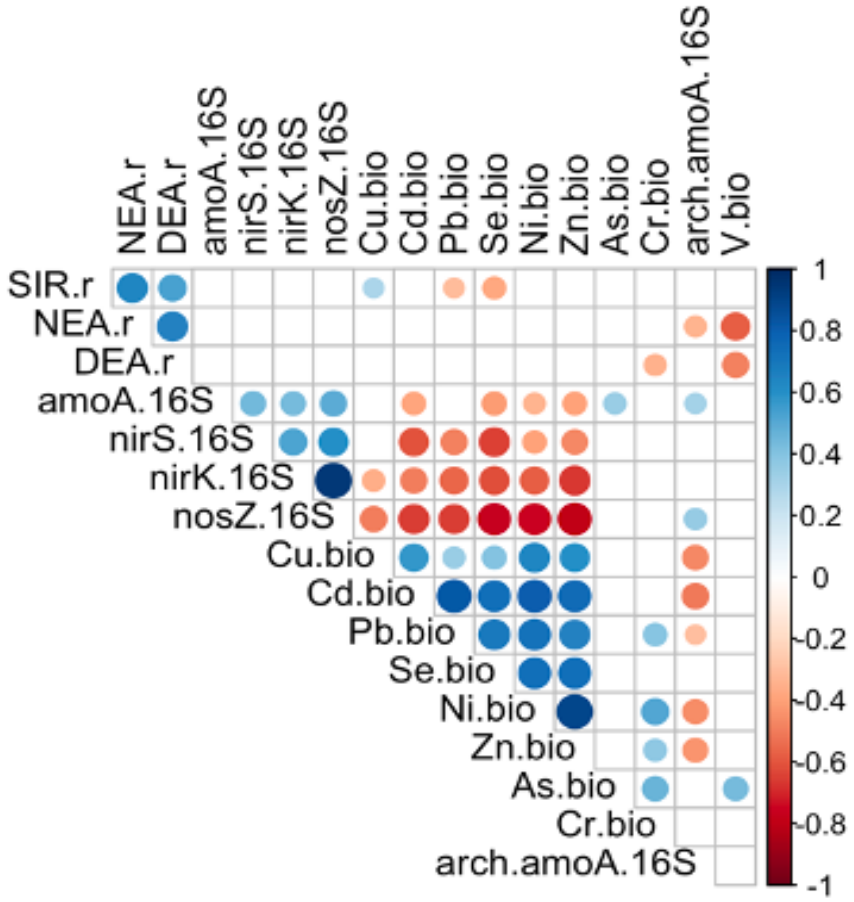

Figure S9. Spearman rank correlations between bacterial parameters normalized to 16S rRNA, and bioavailable metals (As, Cd, Cr, Cu, Ni, Pb, Se, V, Zn) across all sites for Fall and Winter Sampling. The size of the circles is proportional to the correlation coefficient. Bacterial population sizes are represented by log-transformed gene abundances of archaeal and bacterial amoA (nitrifying bacteria), and nirK, nirS, and nosZ (denitrifying bacteria). SIR.r refers to microbial biomass measured via the substrate induced respiration method, while NEA.r and DEA.r refer to the nitrifying, and denitrifying, enzyme activities.

Table S1. Reactions, primers, standards and thermocycling conditions for qPCR.

Target Gene	Primer sequences and references	Reaction mix	Volume (µL)	Thermal profile[(a)]
		Master mix	12.5	40 cycles:
Arch.	F: STAATGGTCTGGCTTAGA	Arch_amoAF (10 µM)	1.5	95 °C - 30 s
amoA	CG	Arch_amoAR (10 µM)	1.5	53 °C - 45 s
	R: GCGGCCATCCATCTGTAT	Nuclease free water	4.5	72 °C - 1 min
	GT	DNA template (3 ng/µL)	5	
	Francis et al. (2005)			
	Santoro et al. (2008)			
		Master mix	12.5	40 cycles:
Bact.	F: GGGGTTTCTACTGGTGGT	amoA1F (10 µM)	1.25	95 °C – 1 min
amoA	R: CCCCTCKGSAAAGCCTTC	amoA2R (10 µM)	1.25	60 °C – 1 min
	TTC	Nuclease free water	5	72 °C - 1 min
	(Rotthauwe et al. 1997)	DNA template (3 ng/µL)	5	
		Master mix	12.5	6 cycles:
nirK	F: ATYGGCGGVAYGGCGA	nirK876C (10 µM)	1.25	95 °C - 15 s
	R: GCCTCGATCAGRTTRTG	nirK1040 (10 µM)	1.25	63-58 °C - 30 s
	GTT	Nuclease free water	5	72 °C - 30 s
		DNA template (3 ng/µL)	5	80 °C - 30 s
				40 cycles:
				95 °C - 15 s
	Henry et al. (2004)			62 °C - 30 s
	Waller et al. (2018)			72 °C - 30 s
				80 °C - 30 s
		Master mix	12.5	40 cycles:
nirS	F: GTSAACGTSAAGGARACS	cd3af (10 µM)	1.5	95 °C - 1 min
	GG	R3cd (10 µM)	1.5	56 °C - 1 min
	R: GASTTCGGRTGSGTCTTG A	Nuclease free water	4.5	72 °C - 1 min
	(Michotey et al. 2000)	DNA template (3 ng/µL)	5	
	(Throback et al. 2004)			
		Master mix	12.5	6 cycles:
nosZ	F: CGCRACGGCAASAAGGTS	nosZ 2F (10 µM)	1.25	95 °C - 15 s
	MSSGT	nosZ 2R (10 uM)	1.25	67-62 °C - 30 s
	R: CAKRTGCAKSGRTGGCAG	Nuclease free water	5	72 °C - 15 s
	AA	DNA template (3 ng/µL)	5	80 °C - 15 s
				40 cycles:
				95 °C - 15 s
	(Henry et al. 2006)			62 °C - 30 s
				72 °C - 15 s
				80 °C - 15 s
		Master mix	12.5	40 cycles:
16S	F: ATGGCTGTCGTCAGCT	16S rRNA-F (12 µM)	1.25	95 °C - 40 s
rRNA	R: ACGGGCGGTGTGTAC	16S rRNA-R (12 µM)	1.25	60 °C - 45 s
		Nuclease free water	8	72 °C - 1 min
	(Pan and Chu 2018)	DNA template (1 ng/µL)	2	

[(a)] All methods include an enzyme activation step consisting of 2 min at 50 °C and 10 min at 95 °C.

Table S2. Soil properties for GSI sites (n = 72, 24 per sampling time). Values represent mean and standard deviation, in parentheses (n=4), measured on a dry soil basis.

Fall 2018 Sampling

Site ID	MZ (UCSB)	SM (UCSB)	CUL (UCI)	VER (UCI)	ACT (UCSD)	SAN (UCSD)
Sand (%)	59 (1)	60 (3)	71 (13)	74 (7)	76 (6)	81 (1)
Silt (%)	28 (1)	19 (2)	10 (7)	15 (3)	13 (3)	10 (1)
Clay (%)	13 (1)	21 (2)	19 (6)	11 (4)	11 (3)	9 (1)
Moisture (%)	18.5 (11.2)	22.2 (3.0)	18.0 (6.2)	14.5 (4.6)	17.4 (2.0)	10.6 (2.1)
SOM (%)	5.1 (1.1)	7.0 (1.6)	6.7 (5.9)	4.0 (0.6)	2.0 (0.3)	2.2 (0.4)
DOC ug C/ g soil)	23.7 (6.0)	30.7 (18.1)	42.8 (9.6)	22.5 (7.7)	14.8 (6.1)	10.9 (5.6)
Bulk density (g/cm3)	1.2 (0.1)	1.2 (0.2)	1.3 (0.1)	1.4 (0.2)	1.6 (0.0)	1.5 (0.1)
pH (-)	7.7 (0.2)	8.0 (0.1)	7.8 (0.4)	7.2 (0.2)	8.1 (0.3)	7.0 (0.3)
CEC (meq/100g)	17.6 (4.5)	19.6 (2.1)	24.6 (6.0)	17.0 (3.5)	12.4 (1.1)	9.0 (1.4)
Total C (%)	2.3 (0.7)	2.1 (0.3)	1.9 (0.8)	1.2 (0.1)	0.5 (0.3)	0.6 (0.3)
Total N (%)	0.2 (0.06)	0.13 (0.03)	0.14 (0.05)	0.09 (0.02)	0.02 (0.01)	0.03 (0.01)
PO_4-P (ppm)	4.4 (1.5)	8.1 (2.0)	50.5 (13.8)	15.9 (0.9)	8.6 (1.7)	2.7 (0.9)
NO_3-N (ppm)	23.1 (13.1)	4.3 (4.8)	81.0 (53.7)	38.8 (1.5)	4.5 (5.2)	4.9 (2.9)
NH_4-N (ppm)	1.0 (0.9)	2.5 (0.9)	1.0 (0.2)	3.1 (0.9)	1.0 (0.4)	0.9 (0.1)

Winter 2019 Sampling

Site ID (Campus)	MZ (UCSB)	SM (UCSB)	CUL (UCI)	VER (UCI)	ACT (UCSD)	SAN (UCSD)
Sand (%)	58 (4)	59 (4)	65 (10)	70 (5)	74 (5)	80 (1)
Silt (%)	28 (3)	21 (3)	16 (6)	17 (3)	14 (3)	12 (1)
Clay (%)	14 (2)	20 (2)	19 (5)	13 (2)	12 (3)	8 (0)
Moisture (%)	33.2 (4.9)	28.1 (2.3)	23.6 (6.8)	18.9 (3.8)	16.9 (2.1)	14.4 (2.8)
SOM (%)	4.4 (0.6)	5.0 (1.3)	6.6 (3.1)	4.0 (1.2)	1.7 (0.3)	2.0 (0.5)
DOC ug C/ g soil)	35.8 (5.8)	24.0 (4.0)	39.9 (6.8)	30.5 (7.8)	40.3 (8.8)	27.8 (6.5)
Bulk density (g/cm3)	1.1 (0.1)	1.1 (0.1)	1.3 (0.1)	1.2 (0.1)	1.6 (0.0)	1.5 (0.0)
pH (-)	8.0 (0.2)	8.6 (0.3)	8.3 (0.3)	7.9 (0.3)	8.8 (0.2)	7.5 (0.5)
PO_4-P (ppm)	3.1 (2.4)	3.6 (2.6)	11.5 (5.9)	1.9 (0.6)	3.9 (1.6)	1.7 (0.7)
NO_3-N (ppm)	5.4 (3.1)	4.8 (2.6)	11.6 (6.0)	5.3 (0.9)	4.7 (2.7)	4.1 (0.3)
NH_4-N (ppm)	2.7 (1.7)	1.8 (1.0)	1.4 (0.7)	2.5 (0.7)	1.0 (0.8)	1.0 (0.3)

Table S2. (Cont.)

Spring 2019 Sampling

Site ID (Campus)	MZ (UCSB)	SM (UCSB)	CUL (UCI)	VER (UCI)	ACT (UCSD)	SAN (UCSD)
Sand (%)	58 (2)	64 (5)	70 (11)	74 (1)	75 (7)	78 (1)
Silt (%)	29 (2)	18 (3)	14 (8)	16 (1)	14 (4)	13 (1)
Clay (%)	13 (1)	18 (2)	16 (4)	10 (1)	11 (3)	9 (1)
Moisture (%)	10.4 (1.5)	16.5 (7.4)	11.7 (5.3)	9.9 (3.4)	13.6 (4.3)	10.8 (0.6)
SOM (%)	5.5 (0.8)	7.3 (1.8)	8.1 (5.1)	3.8 (5.1)	1.6 (0.3)	2.2 (0.3)
DOC (ug C/g soil)	103 (20.0)	81.6 (30.5)	125 (50.8)	79.7 (22.1)	51.4 (7.3)	24.6 (6.5)
pH (-)	8.1 (0.2)	8.2 (0.2)	8.1 (0.3)	7.6 (0.3)	8.7 (0.3)	7.3 (0.2)
CEC (meq/100g soil)	18.7 (3.1)	20.6 (1.0)	26.7 (10.5)	14.5 (1.2)	11.3 (1.5)	8.7 (0.8)
Total C (%)	2.5 (0.3)	3.1 (0.6)	3.8 (2.4)	1.5 (0.6)	0.3 (0.1)	0.7 (0.2)
Total N (%)	0.20 (0.04)	0.19 (0.02)	0.28 (0.17)	0.10 (0.04)	0.02 (0.00)	0.05 (0.01)
PO_4-P (ppm)	4.9 (1.7)	6.0 (2.1)	28.3 (25.2)	2.9 (1.7)	5.7 (2.7)	1.7 (0.5)
NO_3-N (ppm)	15.0 (6.8)	8.1 (4.6)	64.5 (62.7)	6.4 (1.2)	5.3 (2.8)	5.3 (1.0)
NH_4-N (ppm)	1.3 (0.6)	2.5 (0.8)	1.7 (0.9)	5.7 (2.3)	1.1 (0.3)	1.9 (0.3)

Abbreviations: UCSB, University of California, Santa Barbara; UCI, University of California, Irvine; UCSD, University of California, San Diego MZ, Manzanita; SM, Sierra Madre; CUL, Culver; VER, Verano, ACT, Altman Clinical and Translational Research Institute; SAN, Sanford; SOM, soil organic matter; DOC, dissolved organic carbon; CEC, cation exchange capacity.
Note: CEC, Total C and Total N were not measured during winter sampling; bulk density was not measured during fall sampling.

Table S3. Bioavailable and total metal concentrations (mg/kg dry soil) for GSI sites (n = 72).

	Bioavailable metal concentrations (mg/kg dry soil)								
	As	**Cd**	**Cr**	**Cu**	**Ni**	**Pb**	**Se**	**V**	**Zn**
Mean	0.332	0.0246	0.47	0.127	1.11	0.418	0.0326	4.63	0.154
Median	0.23	BDL	0.06	0.08	BDL	0.0156	BDL	2.26	BDL
Min	BDL	BDL	BDL	BDL	BDL	BDL	BDL	BDL	BDL
Max	3.05	0.438	3.85	1.46	5.54	2.82	0.281	79.5	2.08
	Total metal concentrations (mg/kg dry soil)								
	As	**Cd**	**Cr**	**Cu**	**Ni**	**Pb**	**Se**	**V**	**Zn**
Mean	5.72	0.328	17.3	17.5	15	6.06	0.335	31.1	52.5
Median	4.68	0.173	12.7	14.1	12.6	5.71	0.283	20.5	48.6
Min	0.37	BDL	0.45	0.238	2.01	BDL	BDL	2.64	BDL
Max	28.8	5.09	96.8	78.8	83.5	40.9	1.3	150	207
	Method detection limits and reference values (mg/kg dry soil)								
	As	**Cd**	**Cr**	**Cu**	**Ni**	**Pb**	**Se**	**V**	**Zn**
Method detection limit (total metals)	0.013	0.013	0.013	0.013	0.013	0.013	0.013	0.013	0.025
Residential soil screening levels [a]	0.41	71	230	NA	820	80	NA	NA	NA
Ecological soil screening levels [b]	18	32	26	70	38	120	0.52	7.8	120
Background levels in California soils [b]	3.5	0.36	122	28.7	57	23.9	0.058	112	149
Background levels in US soils d	6.4	0.3	36	17.9	17.7	25.8	0.3	60	66

a. Residential soil screening levels (DTSC HERO, 2020).
b. Ecological soil screening levels for invertebrates, plants, or birds (lowest value) from US EPA (https://www.epa.gov/chemical-research/interim-ecological-soil-screening-level-documents)
c. Background metal levels in California soils (Bradford et al., 1996).
d. Background metal levels in soils of the United States (Smith et al., 2013).
Abbreviations: BDL, below detection limit; NA, not available

Table S4. N_2O sampling details and fluxes for GSI sites at three Southern CA campuses (UCSB: MZ and SM; UCI: CUL, VER; UCSD: ACT, SAN) (n = 36).

Season	Campus	Site ID	Sample time	Chamber height (m)	Plant cover	Moisture	Soil temperature (°C)	Flux N_2O (μg N/m^2 h)
Fall	UCSB	MZ1	10:05	0.50	100%	0.46	19.8	28.4
		MZ2	8:45	1.50	100%	0.19	16.8	BDL
		SM1	12:00	0.50	100%	0.10	27.3	15.8
		SM3	13:30	0.50	100%	0.09	30.8	5.6
	UCI	CUL2	7:30	0.50	80%	0.23	18.7	49.1
		CUL3	8:30	0.50	5%	0.34	19.2	32.9
		VER1	10:35	0.50	100%	0.23	24.4	37.9
		VER2	11:20	0.50	60%	0.06	27.8	60.0
	UCSD	ACT2	8:35	1.00	80%	0.24	18.9	61.8
		ACT3	9:15	0.50	20%	0.29	18.1	22.1
		SAN2	11:25	1.00	100%	0.09	24.0	BDL
		SAN4	12:15	0.50	90%	0.05	26.1	BDL
Winter	UCSB	MZ1	10:30	0.50	100%	0.48	15.5	11.4
		MZ2	9:30	1.50	100%	0.48	17.8	16.0
		SM1	12:10	0.50	100%	0.48	13.5	24.7
		SM3	13:15	0.50	100%	0.22	18.1	7.4
	UCI	CUL2	7:10	0.50	75%	0.37	9.5	40.3
		CUL3	8:40	0.50	100%	0.39	12.6	16.6
		VER1	10:15	0.50	100%	0.28	17.8	23.6
		VER2	11:00	0.50	90%	0.18	18.2	19.7
	UCSD	ACT2	7:20	1.00	80%	0.20	11.6	5.4
		ACT3	8:30	0.50	5%	0.33	12.7	BDL
		SAN2	10:30	0.50	80%	0.13	20.2	26.7
		SAN4	11:15	0.50	75%	0.17	20.4	33.3

Table continues in the next page

Table S4. (Cont.) N_2O sampling details and fluxes for GSI sites at three Southern CA campuses (UCSB: MZ and SM; UCI: CUL, VER; UCSD: ACT, SAN).

Season	Campus	Site ID	Sample time	Chamber height (m)	Plant cover	Moisture	Soil temperature (°C)	Flux N_2O (μg N/m^2 h)
Spring	UCSB	MZ1	9:30	0.50	100%	0.10	21.7	27.1
		MZ2	8:20	1.50	80%	0.16	17.7	18.7
		SM1	11:15	0.50	80%	0.03	25.4	38.3
		SM3	12:10	0.50	100%	0.03	29.5	9.4
	UCI	CUL2	7:20	0.50	90%	0.10	17.0	BDL
		CUL3	8:05	0.50	0%	0.20	18	24.4
		VER1	9:40	0.50	100%	0.19	19.7	31.0
		VER2	10:30	0.50	90%	0.03	21.5	6.8
	UCSD	ACT2	7:40	1.00	80%	0.23	16.2	46.6
		ACT3	8:35	0.50	5%	0.31	16.05	BDL
		SAN2	10:10	0.50	40%	0.04	18.65	40.9
		SAN4	11:20	0.5	80%	0.07	24.15	BDL

Sampling occurred in October/November 2018 (Fall), February/March of 2019 (Winter), and April 2019 (Spring). Vegetation cover was visually assessed within the chamber base area.
Abbreviations: UCSB, University of California, Santa Barbara; UCI, University of California, Irvine; UCSD, University of California, San Diego.
BDL: below detection limit

Table S5. Multiple linear regression models for absolute abundances of functional genes in biofilter soils based on three GSI systems (MZ, CUL, ACT). Starting models included soil properties, and concentrations of total and bioavailable metals. A stepwise method was used to select the final models. Prior to MLR analysis, all variables were log-transformed to better approximate normal distributions.

Gene	Equation	R^2	Adj. R^2	p-value
amoA_a	Log (amoA_a) = 2.79 + 2.56 Log (Moisture) + 2.79 Log (Clay) – 1.83 Log(Silt) – 0.39 Log (Pb) – 0.56 Log (V)	0.66	0.55	0.002
amoA_b	Log (amoA_a) = 17.51 – 16.73 Log (pH) + 2.67 Log (Moisture) – 0.36 Log (Pb)	0.72	0.68	< 0.0001
nirK	Log (nirK) = 11.50 – 9.31 Log (pH) + 1.54 Log (Moisture) + 1.90 Log (Clay) – 0.26 Log (Pb)	0.70	0.64	< 0.0001
nirS	Log (nirS) = 4.54 + 2.57 Log (Moisture) – 0.14 Log (Zn) – 0.23 Log (Pb)	0.80	0.77	< 0.0001
nosZ	Log (nosZ) = 15.26 – 14.30 Log (pH) + 1.93 Log (Clay) + 1.57 Log (Moisture) + 0.71 Log (V) – 0.40 Log (Pb)	0.79	0.73	0.001
16S rRNA	Log (nosZ/16S) = 16.19 – 10.23 Log (pH) + 1.69 Log (Moisture) + 1.47 Log (Clay) – 0.12 Log (Pb)	0.77	0.72	< 0.0001

3.9. Additional References

Francis, C. A., Roberts, K. J., Beman, J. M., Santoro, A. E., and Oakley, B. B. (2005). Ubiquity and diversity of ammonia-oxidizing archaea in water columns and sediments of the ocean. *Proc. Natl. Acad. Sci*., 102, 14683-14688.

Henry. S., Baudoin, E., López-Gutiérrez, J. C., Martin-Laurent, F., Brauman, A., and Philippot, L. (2004). Quantification of denitrifying bacteria in soils by nirK gene targeted real-time PCR. *J. Microbiol. Methods*, 59(3), 327-335.

Henry, S., Bru, D., Stres, B., Hallet, S., and Philippot, L. (2006). Quantitative detection of the nosZ gene, encoding nitrous oxide reductase, and comparison of the abundances of 16S rRNA, narG, nirK, and nosZ genes in soils. *Appl. Environ. Microbiol.*, 72(18), 5181-5189.

Michotey V., Mejean V., and Bonin P. (2000). Comparison of methods for quantification of cytochrome cd1-denitrifying bacteria in marine samples. *Appl. Environ. Microbiol*., 66(4), 1564-1571.

Pan, M., and Chu, L.M. (2018). Occurrence of antibiotics and antibiotic resistance genes in soils from wastewater irrigation areas in the Pearl River Delta region, southern China. *Sci. Total Environ.,* 624, 145-152.

Rotthauwe, J. H., Witzel, K. P., and Liesack, W. (1997). The ammonia monooxygenase structural gene amoA as a functional marker: molecular fine-scale analysis of natural ammonia-oxidizing populations. *Appl. Environ. Microbiol*., 63(12), 4704-4712.

Santoro A. E., Francis, C. A., De Sieyes, N. R., and Boehm, A. B. (2008). Shifts in the relative abundance of ammonia-oxidizing bacteria and archaea across physicochemical gradients in a subterranean estuary. *Environ. Microbiol.*, 10(4), 1068-1079.

Waller, L. J., Evanylo, G. K., Krometis, L-A. H., Strickland, M., Wynn-Thompson, T. M., and Badgley, B. D. (2018). Engineered and environmental controls of microbial denitrification in established bioretention cells. *Environ. Sci. Technol*., 52(9), 5358-5366.

Chapter 4. Stormwater biofilter response to high nitrogen loading under transient flow conditions: ammonium and nitrate fates, and N_2O emissions

Abstract

N in urban runoff is often managed by green infrastructure including biofilters. However, N fates in biofilters are insufficiently understood since neither laboratory "steady-state" flow conditions nor field-scale studies with low N loading have differentiated influent versus internal N processing over realistic timescales. We tested biofilter responses to high N loading during simulated transient flow storms. The times for N reaction (days to weeks) relative to N residence time (7 to 30 hours) suggested limited N processing during storms, but outflow ammonium (NH_4^+) was 60.7 to 92.3 % lower relative to the inflow. Soil denitrifying gene abundances (*nir*K + *nir*S: 3.0×10^6 to 1.8×10^7; *nos*Z: 5.0 to 2.2×10^6 gc g $soil^{-1}$), and a ratio of $\delta^{18}O\text{-}NO^{3-}$ to $\delta^{15}N\text{-}NO_3^-$ of 1.83 in soil eluates implied N assimilation, remineralization, and denitrification. However, nitrous oxide (N_2O) emissions (13.5 to 84.3 μg N m^{-2} h^{-1}) and N_2O export (14.4 mg $N\text{-}N_2O$) were low, and soil nitrification potentials (0.45 to 1.63 mg N kg $soil^{-1}day^{-1}$) exceeded those for denitrification (0.17 to 0.49 mg N kg $soil^{-1}$ day^{-1}). Similarly, archaeal, and bacterial amoA gene abundances (1.7×10^5 to 1.2×10^6 gc g $soil^{-1}$), nitrifier presence by16S rRNA gene sequencing, and outflow $\delta^{18}O\text{-}NO_3^-$ values (-3.0 to 17.1 ‰) were characteristic of nitrification. Nitrate (NO_3^-) export exceeded (3100 to 3900 %) that explainable by inflow NO_3^-, or nitrification of inflow NH_4^+, indicating nitrification in between storms. Mass balance of $NH_4^+$and NO_3^-, indicated similar amounts of aqueous export (4.3×10^3 mg N) and soil storage (1.2×10^3 mg N). A comprehensive

analysis of chemical, bacterial, and isotopic metrics indicated that stormwater biofiltration resulted in net N export, with an NO_3^- mass balance reinforcing net nitrification. Implications on biofilter design for N removal are discussed.

4.1 Introduction

Anthropogenic inputs of nitrogen (N) to the environment are currently well beyond sustainability targets as outlined in the planetary boundaries framework (Steffen et al. 2015), indicating a critical need for practices and technologies that enhance N removal. Excess N in water can result in ecosystem disruption and hypoxia, while high levels of nitrate in drinking water can be toxic. Urban stormwater runoff contains elevated levels of N and other pollutants that can impact the trophic status and quality of receiving waters (Walsh et al. 2004). To address these concerns, green stormwater infrastructure (GSI) approaches such as biofilters are often used. Biofilters capture and treat stormwater runoff, removing suspended solids (Bratières et al. 2008, Hatt et al. 2008), heavy metals (Davis et al. 2001, Hatt et al. 2008), and fecal bacteria (Liu et al. 2014, Li et al. 2021). However, N removal in biofilters varies (Davis et al. 2001) due to multiple transformations that can generate the mobile, and critical pollutant, nitrate (NO_3^-) (Payne et al. 2014 a). While biofilters may reduce outflow concentrations of total N by more than 70% (Bratières et al. 2008, Payne et al. 2014 b), in many instances as runoff flows through a biofilter it leaches nitrate from biofilter soil (Bratières et al. 2008) and may result in net N export (Davis et al. 2001, Hatt et al. 2007).

N removal across biofilters depends on biofilter design factors including soil depth, inflow characteristics, and plant species (Davis et al. 2001, Bratières et al. 2008, Li and Davis 2009, Read et al. 2010); removal often improves when biofilters are saturated, since saturation promotes denitrification of NO_3^- to gaseous forms (Zinger et al. 2013). Biofilter designs may therefore include a saturated zone amended with organic carbon sources such as

biochar to enhance N removal (Zinger et al. 2013, Boehm et al. 2020. Yet many established biofilters do not have such design features, so that denitrification is not a major pathway for N removal and N export may occur.

N entering a biofilter may be filtered and adsorbed by soils, taken up by plants, transform abiotically, or be immobilized and transformed by microbes (Payne et al. 2014 a). In a field-scale biofilter, an N mass balance suggested that the dominant pathways of N transformation were transfer between particulate organic N (PON) and dissolved inorganic N (DON) pools, DON mineralization to ammonium (NH_4^+), plant assimilation of NH_4^+ and nitrate (NO_3^-), and nitrification of NH_4^+ to NO_3^- (Li and Davis 2014). In small-scale biofilter mesocosms, ^{15}N labeling showed that influent N was rapidly assimilated by plants and was but minimally denitrified (Payne et al. 2014 b). Denitrification in biofilter columns was infrequent and removed only 1.4% of influent NO_3^- (Burgis et al. 2020).

Prior biofilter N processing studies, however, generally do not emulate realistic biofilter hydrology due to their small scales and use of relatively steady state conditions, versus more realistic transient flow conditions (Hsieh and Davis 2005, Davis et al. 2007, Hatt et al. 2009, Brown and Hunt 2011, Li and Davis 2014, Burgis et al. 2020). Under transient flow, soils are not saturated to the same extent as they are in steady-state flow; the wetter soils under steady-state flow may promote denitrification and overestimate N removal. Field studies may provide better N removal estimates, but often only include single storms (Brown and Hunt 2011, Hatt et al. 2009, Hunt et al. 2006), which overlooks the effects of drying and rewetting cycles on C and N processing (Fierer and Schimel 2002), and the potential influence of the

antecedent dry period on nitrate formation. Further, N exported during one storm depends on prior storm event characteristics, and weather conditions between storm events (Brown et al. 2013). A detailed understanding of N processing requires studying consecutive storm events. Studies on multiple storm events show that nitrate is formed and accumulates during dry periods (Hatt et al. 2007, Brown et al. 2013, Li and Davis 2014). N loading in these studies, however, represents median runoff concentrations. Higher N loading may export more N in subsequent storms due to internal nitrate formation (Brown et al. 2013, Payne et al. 2014). Due to prior study limitations, we have an incomplete understanding for how GSI systems process N when they receive polluted flow from a large storm under realistic transient flow conditions. How these nutrient inputs could prime biofilter N processing in subsequent storms, and influence N treatment variability, are also unknown. Such knowledge is needed to precisely examine the role of biofilters as sources of aqueous and gaseous N, and to what extent typical biofilter designs support N removal.

Our objectives were to evaluate N export in biofilters by (1) assessing the fates of NH_4^+ and NO_3^-, and the fluxes of N_2O under realistic temporal and spatial conditions, (2) identifying predominant transformation processes within and between storms through dual nitrate isotope analysis, (3) quantifying genes encoding bacterial 16S rRNA, nitrifying (archaeal and bacterial *amo*A) genes, and denitrifying (*nir*K, *nir*S, *nos*Z) genes, and (4) evaluating the importance of *in situ* NH_4^+, and NO_3^- generation (via mineralization and nitrification) versus influent inputs. We met those objectives by challenging full scale biofilters with transient stormflow events, including one where runoff was highly N-

contaminated. The findings point to an overall dominance of nitrification occurring between storms, regardless of how influent N is processed within a storm. The results of this study are interpreted for future considerations of how to mitigate N export from biofilters.

4.2. Methods

4.2.1. Experimental design and hydrology

Experiments were conducted on two full-scale biofilters (control biofilter "C2" and test biofilter "C4") at the Orange County Public Works (OCPW) Glassell campus (Orange, CA). Climate at this site has warm, dry summers and mild, winters. Annual precipitation is 37 cm and occurs mostly during winter (December – March) (NOAA, 2021). The biofilters were 2.4 m long, 1.5 m wide, and 1.8 m deep (Figure S1 and Table S1) and were planted with *Carex spissa*. Soil depth was approximately 0.6 m, consisting of a sandy loam with 85−88% sand, 8−12% fines, and 3−5% organic matter. The biofilters were dosed with influents consisting of unspiked, or sewage-spiked (50% by volume) stormwater, and their soil, effluent, and atmospheric gas emissions were studied.

Transient flow conditions were imposed through the biofilters following a hydrograph constructed from storms observed in Orange County and adjusted to represent an 85^{th} percentile storm (Figure S2). Time series of infiltration, gravitational discharge, and soil saturation were obtained by solving the one-dimensional Richards equation (Hydrus 1D, Version 4.17.0140, PC-Progress), using measured inflows and potential evapotranspiration estimates, as described previously (Parker et al. 2021).

Stormwater runoff or mixed influent were dosed under transient flow conditions in several experimental storms. Runoff from an adjacent parking lot and a treatment wetland were collected and stored in an underground cistern for less than 6 months. A mixed influent was prepared by combining approximately 750 L of raw sewage from the Orange County Sanitation District wastewater treatment plant with 750 L of stormwater runoff. Further experimental details are published (Parker et al. 2021). The biofilters were conditioned with runoff (storms S1-2), after which biofilter C2 was sacrificed to collect baseline soil cores. Biofilter C4 then received 1:1 mixed influent (storm S3) and was then flushed with runoff (storms S4-7). Following flushing, endpoint soil cores were collected (Figure S3).

4.2.2. Water and soil sampling

Influent stormwater runoff or mixed influent were sampled from an inflow tank 2 to 4 times per storm, while biofilter effluent was sampled every 10 minutes. For storms 1 and 2, ten effluent samples were collected from the shared (C2 and C4) biofilter underdrain (Figure S1) using a peristaltic pump (flow rate 0.23 L/min). For storms S3-7, 21 to 28 effluent water samples were collected per storm, from a sump located at the end of a manifold through which biofilter C4 effluent drained. Biofilter effluent was pumped (Model 98 Sump Pump, Zoeller Pump Company, Louisville, KY) from the sump into a continuously overflowing 5L bucket, which was sub-sampled by a peristaltic pump (20 mL/min) (BioLogic LP, Bio-Rad, Hercules, CA) and fractionated every 5 minutes until outflow ceased. Water samples were filtered through a 0.45 μm PES syringe filter (Whatman Uniflo, GE Healthcare, Chicago, IL), collected into 50 mL conical tubes and refrigerated (4 °C) until analysis.

Soil samples at depths of 0 to 10 cm, 10 to 20 cm, 30 to 40 cm, and 50 to 60 cm were collected via coring in the C2 and C4 biofilters; cored soils were sieved through a brass 2-mm mesh (No. 10) (Advantage Manufacturing, Inc., New Berlin, WI), subsampled, transported, and stored (4 °C) until analysis, as detailed in the Supplemental Methods. Soil eluents were generated onsite (Supplemental Methods).

4.2.3. Biofilter soil, aqueous influent and effluent, and soil eluate analyses

Analysis of soil gravimetric moisture content, organic matter via loss on ignition (SOM-LOI), pH, bulk density, and concentrations of NH_4^+, NO_3^-, and dissolved organic carbon (DOC) followed standard or published methods (Supplemental Methods). A 500 g soil subsample was shipped to the UC Davis Analytical Lab (https://anlab.ucdavis.edu/) for total carbon (TC), total nitrogen (TN), cation exchange capacity (CEC), and particle size analyses. Soil microbial biomass was assessed by the substrate induced respiration (SIR) method. Nitrification enzyme activity (NEA), and denitrification enzyme activity (DEA) were assessed via the chlorate inhibition method, and acetylene reduction method, following standard methods (Supplemental Methods).

NH_4^+ and NO_3^- concentrations in aqueous samples were analyzed within 14 days. Nitrite concentrations were negligible and were not considered further. NH_4^+ concentrations were assessed using a colorimetric method (EPA Method 350.1). Briefly, samples were buffered at a pH of 9.5 and ammonia (NH_3) in the sample was reacted with alkaline phenol and hypochlorite to form indophenol blue. Sample absorbance was read at 640nm on a Dual Fluorometer UV-visible spectrometer (HORIBA Scientific, Piscataway, NJ). NO_3^-

concentrations were measured using a Dionex DX-120 ion chromatograph (Thermo Fisher Scientific, Waltham, MA) (EPA Method 300.0). Detection limits were 0.1 mg /L of either NH_4^+ or NO_3^-. Mass flow rate (Supplemental Methods, eq. S1 and eq. S2) and percent relative mass removal (Supplemental Methods, eq. S3) were computed. Aqueous samples and soil eluates were analyzed for dual NO_3^- isotope ratios (see Section 4.2.5).

4.2.4. CO_2, CH_4 and N_2O fluxes

Surface emissions (from soil to air) of CO_2, CH_4, and N_2O in biofilter C4 were assessed using the closed chamber method (Hutchinson and Mosier, 1981) as detailed in the Supplemental Methods (Soil, and gas sampling; Gas flux calculations; eq. S4 to eq. S6). CO_2 fluxes were used to estimate C mineralization rates, while CH_4 fluxes were used to indicate anoxic conditions in the biofilter. Daily N_2O fluxes for storms S3-7 were used to compute the mass of N_2O-N emissions across these storms. The daily N_2O fluxes were calculated as the average of three daily measurements for each storm dosing day (Table S4). There is one average daily flux for storm S3, one for storms S4-5, and one for storms S6-7.

4.2.5. Dual nitrate isotope analyses

Dual NO_3^- isotopes (δ^{15}N-NO_3^- and δ^{18}O-NO_3^-) (Supplemental Methods, eq. S7, eq. S8) were measured in biofilter C4 for inflows and outflows of storms S3-7, and soil eluates from endpoint soil cores. Sample aliquots (10 to 40 mL) were filtered through a 0.2 µm Isopore polycarbonate filters (Millipore Sigma, Burlington, MA) into acidified 40 mL amber vials. $NO_3^-$was measured using an AQ300 Discrete Analyzer (Seal Analytical, Inc., Mequon, WI) (EPA Method 353.2) and samples with greater than 0.08 mg N/L were analyzed for dual

NO_3^- isotopes on a GasBench II system Spectrometer fitted with a denitrification kit and a Delta V Isotope Ratio Mass Spectrometer (Thermo Fisher Scientific, Waltham, MA) (Supplemental Methods).

4.2.6. Soil DNA extraction, qPCR, and 16S rRNA gene sequencing

Soil DNA was extracted in duplicate using the DNeasy PowerSoil Kit (Qiagen, Hilden, Germany). One extraction blank was included per batch. Extracted DNA was pooled, quantified (Quant-iT dsDNA Broad-Range Assay Kit, Invitrogen Co., Waltham, MA), and archived (-20 °C) until analysis. Genes encoding bacterial 16S rRNA, as well as nitrifying (archaeal and bacterial *amo*A) and denitrifying (*nir*K, *nir*S, *nos*Z) functional genes were evaluated via quantitative polymerase chain reaction (qPCR) assays in 25 µL reactions using the PowerUp SYBR Green Master Mix (Thermo Fisher Scientific, Waltham, MA) on a CFX96 real-time PCR detection system (Bio-Rad Laboratories, Hercules, CA). Further details, including standard curve generation, qPCR reactions, thermocycling conditions, inhibition testing, and product specificity analysis, are in the Supplemental Materials (Supplemental Methods, Table S3, eq. S9). All qPCR assays had amplification efficiencies between 85.2% and 103.1% with an average R^2 greater than 0.99.

For 16S rRNA gene sequencing, extracted DNA was amplified using primers 27F and 534R, targeting the V1-V3 region of genes encoding 16S rRNA. Amplicons were sequenced on an Illumina MiSeq platform with a MiSeq v3 600 cycle kit (2 by 300 bp), as published (Li et al. 2020). Sequences were grouped into operational taxonomic units (OTUs) at 97% sequence similarity. Representative OTU sequences were compared to the Greengenes

aligned reference database (http://greengenes.secondgenome.com/) to assign taxonomic data. Sequencing data were deposited in NCBI SRA with the BioProject ID PRJNA723423 (Li et al. 2020).

4.2.7. Biological reaction and transport timescales, and N species mass balances

Transport times were established by the age of the water in storage (c.f., Figure 6, Parker et al. 2021). Biological reaction rates and characteristic times for N mineralization were estimated from organic C mineralization rates (Supplemental Methods, eq. S10, eq. S11). In absence of field measures of nitrification or denitrification, a range of *in-situ* reaction rates were obtained from biofilters (Chen et al. 2019, Fan et al. 2019, Wang et al. 2021).

The mass balances for NH_4^+, NO_3^-, and N_2O were calculated for storms S3-7, and considered storm inputs, changes in biofilter storage from initial (prior to storm S3) to final conditions (after storm S7), and aqueous flows and gaseous N emissions as outputs. Evapotranspiration had previously been determined to represent less than 0.3 % of storm inflows (Parker et al. 2021) and so was neglected. NH_4^+ and NO_3^- inputs and outputs were calculated using formulas eq. S1 and eq. S2 in the Supplemental Methods. Cumulative mass N_2O-N emissions were calculated as described in Section 4.2.4. N_2 emissions were not measured since they do not pose an environmental concern, and assessing NO emissions was beyond the scope of this study. Instead, we focused on N_2O emissions as a metric for nitrification and denitrification. NH_4^+ and NO_3^- masses in soil were calculated as the products of dry soil mass and soil concentrations for each depth section.

4.2.8. Data analysis

One-way analysis of variance (Kruskal-Wallis) and post-hoc Dunn's tests ($p < 0.05$) was used to assess differences across storms for analyte concentrations, mass flow rates, N_2O emissions, and effluent $\delta^{15}N\text{-}NO_3^-$ and $\delta^{18}O\text{-}NO_3^-$. Pearson product-moment correlations were used to assess the relationship between soil saturation, ADP, and GHG fluxes, since these variables were normally distributed (Shapiro-Wilk test). Spearman rank-order correlations and linear regression were used to assess the relationships between soil physicochemical characteristics and bacterial parameters. Statistical analysis was performed with R (version 4.0.1) at a level of significance of $\alpha = 0.05$.

4.3. Results and Discussion

4.3.1. Biofilter soil properties in control and test biofilters

Soil properties are presented to contextualize overall environmental conditions and to assess changes imposed on test biofilter C4 by the high nutrient storm (S3) and following flushing storms (S4-7). Soil pH was neutral to alkaline, ranging from 7.5 to 7.7. Gravimetric moisture content ranged from 14.7 to 17.7% in C2, and 14.3 to 24.9% in C4, and increased with depth in C4 (Table S2). Soil organic matter (SOM) ranged from 1.71 to 4.19 % in C2, and from 2.92 to 3.18% in C4 (Table S2). Additional storms in C4 may have caused differences in SOM distribution, such that in C4, leaching of dissolved organic fractions resulted in lower SOM near the surface, but higher SOM in deeper soils relative to C2. Similarly, the higher DOC in C2 (14.07 to 17.09 %) than in C4 (7.39 to 11.05 %) suggested

that DOC was leached by the influent storms (Table S2). Similar trends were observed for TC, except in the bottom soil layer, while TN was relatively uniform. Molar C:N ratios were similar in C2 and C4, except near the surface (higher in C2) and at depth (higher in C4) (Table S2). These differences may have resulted from higher C losses in C4 due to microbial processing and leaching of DOC, and higher N loading due to the sewage inputs in storm S3. This N loading was evidenced in the higher surface concentrations of NH_4^+ and NO_3^- in C4, relative to C2 (Table S2). In contrast, the storm inputs did not significantly change soil texture, and the percentages of sand, silt and clay were relatively uniform with depth (Table S2). CEC also showed no depth differences, suggesting a relatively uniform capacity to sorb pollutants. The similar CEC values in C2 and C4 (Table S2) also suggested that storm inputs did not significantly diminish the biofilter's ability to sorb pollutants. In contrast, microbial biomass (assessed via SIR) decreased with depth, with means ranging from 0.74 to 7.56 mg C/kg dry soil/day. SIR was significantly correlated with SOM ($\rho = 0.71$, $p = 0.05$), DOC ($\rho = 0.75$, $p = 0.03$), TC ($\rho = 0.83$, $p = 0.01$), and TN ($\rho = 0.72$, $p = 0.04$). Overall, biofilter soil properties suggested that N processing might decrease with soil depth, since microbial biomass, and nutrients were highest near the surface. In contrast, the relatively uniform CEC and soil texture suggested that the biofilter might be able to sorb pollutants and positively charged chemical species such as NH_4^+ throughout its soil depth.

4.3.2. Biofilter infiltration, gravitational discharge, and soil saturation

Biofilter hydrology was assessed to determine over which timescales the soils were close to saturation, and thus likely to support denitrification, versus relatively unsaturated and more

likely to promote nitrification. Infiltration for storms S1-7 ranged from 0 to 19.4 L/min, while discharge ranged from 0 to 16.2 L/min (Figure S5). Biofilter soil saturation ranged from 0.22 to 1, with full saturation reached (for 43 to 90 min) during dosing, and rapidly declining after infiltration ceased. Due to consecutive storms, soil saturation preceding a new storm increased with time (Figure S5), such that environmental conditions may have become more favorable to denitrification as stormwater dosing progressed. However, soils were mostly unsaturated, indicating that nitrification might be favored.

4.3.3. NH_4^+ and NO_3^- concentrations, mass flow rates, and relative mass removal

NH_4^+ and NO_3^- concentrations, and mass flow rates in inflows and outflows were assessed to preliminarily infer N fates within and in between storms, and to compute relative percent mass removals. Within the context of biofilters, NH_4^+ retention or removal refers to removal within one storm event, with the understanding that this N removal is temporary since NH_4^+ may be nitrified in between storms, and leach from the biofilter as NO_3^- with subsequent storms. Concentration data for NH_4^+ and NO_3^- is presented first, and data for mass flows, and whether they represent removal or export, is subsequently discussed.

NH_4^+ outflow concentrations in biofilter C4 ranged from 0.1 to 2.1 mg N/L, and were lower than inflow concentrations, which ranged from 0.6 to 15.6 mg N/L (Figure 1a), likely due to adsorption and assimilation processes in biofilter soil, and possibly some nitrification (Payne et al. 2014). NH_4^+ outflow event mean concentrations (EMCs) ranged from 0.1 to 1.2 mg N/L; the highest EMC occurred in storm S3 (Table 1), and generally decreased thereafter. There were significant differences in outflow NH_4^+ concentrations for storms S3 through S7

($\chi 2 = 94.9$, $p<0.0001$), with storm S3 > S4 and S5 > S6 and S7 (Dunn's test). NO_3^- concentrations were low (~0.1mg N/L) in dosing waters, but high in outflows for storms S1 and S2 (6.5 to 75.8 mg N/L), and relatively high in storms S3 through S7 (2.1 to 7.6 mg N/L), with EMCs ranging from 3.0 to 48.0 mg N/L (Figure 1b, Table 1). The increase in outflow NO_3^-concentrations suggested that previously formed NO_3^-, or NO_3^- formed within a storm, were leaching. Over time, NO_3^-outflow concentrations decreased, so that concentrations in storm S3 > S4 through S7 ($\chi 2 = 76.3$, $p < 0.0001$), with storms S4 and S6 > S5 and S7 (Dunn's test, $p = 0.011$) (Figure 1b). The decrease in NO_3^- concentrations between storms S4 and S5, and storms S6 and S7, could have been due to increased outflow volumes and related dilution. During storm S1, a substantial amount of water was expended to increase biofilter water storage; in storm S2, more water was routed to outflow (Figure S5, c). Mass flow rates were calculated to estimate the relative removal or export of NH_4^+ and NO_3^-, and how these varied across storm events.

NH_4^+ mass flow rates exiting biofilter C4 peaked (22.1 mg N/min) after the high NH_4^+ input from storm S3 (Figure 2, a and b), while large NO_3^- mass flow rates in biofilter output for storms S1 and S2, suggested NO_3^- formation during the antecedent dry period. NO_3^- mass flow rates ranged from 0 to 1224 mg N/min, and 0 to 2.0 mg N/min, in biofilter outputs and inputs, respectively (Figure 2, c and d). Relative percent removal for NH_4^+ mass within a storm was high, ranging from 60.7 to 92.3 %. NH_4^+removal capacity was lowest in storms S4 and S5. Possibly, organic N mineralization within the biofilter contributed additional NH_4^+. Also, NH_4^+ introduced with storm S3 may have been initially retained in a surficial organic

layer that was observed after the sewage-contaminated water drained from the biofilter. We observed that subsequent sewage-free storms washed out this surface layer, possibly introducing NH_4^+ into the soil profile. Unlike NH_4^+, NO_3^- export occurred for storms S1-7 (Figure 2, c and d), with export exceeding 3000 % (Table 1).

In all storms, except storm S3, the amount of NO_3^- exported was an order of magnitude greater than either NO_3^- or NH_4^+ inputs (Table 1) and could not be explained by nitrification of influent NH_4^+. More likely, the exported NO_3^- during storms S3-7 corresponded to NO_3^- that was formed in between storm events following the nigh nutrient inputs in storm S3, or to NO_3^- that already existed in the biofilter soil, perhaps prior to our simulated storm experiments (note the highest NO_3^- concentrations and leaching occurred at the beginning of the first storm). NO_3^- export increased for consecutive storms S4 and S5 (ADP < 2 h) but decreased for storms S6 and S7 (ADP < 2h), which may have indicated less NO_3^- leaching from the soil or more denitrification occurring. NO_3^- mass export exceeded values reported for bioretention in the stormwater BMP database (Clary et al. 2011), with indicate median and maximum exports of 25 % and 1500%, respectively (Valenca et al. 2021). NO_3^- export herein may have resulted from leaching of pre-existing NO_3^- (prior to storm S1), as well as high hydraulic loading and nutrient content in storm S3, and internal N processing. Overall, concentration and mass flow data suggested that the biofilter was temporarily retaining NH_4^+within a storm, but that this $NH_4^+$was likely being nitrified in between storms and substantially leaching in subsequent storms. The declining NO_3^- export after consecutive storms may have indicated some denitrification around storms S6 and S7. To further

elucidate N fates and their relationship to biofilter soil saturation, we assessed CO_2, CH_4 and N_2O emissions. Partial mass balances for storms S3 through S7, including ammonium, nitrate and N_2O emissions, are discussed in section 4.9.

4.3.4. Emissions of CO_2, CH_4 and N_2O in test biofilter C4

Biofilter C4 emitted CO_2 in the range of 79.5 to 239.7 mg C/m^2 h, while mean values of 142.2 ± 44.4 mg C/m^2 h (Table S4, Figure S6 a) were comparable to other biofilter studies (88.3 to 367.9 mg C/m^2 h) (Grover et al. 2013, McPhilips et al. 2017). However, our measurements were made with fully shaded chambers, which precluded photosynthetic activity and CO_2 uptake by plants within the chamber, potentially inflating CO_2 emissions. Plant root respiration may have also significantly contributed to CO_2 emissions (Baggs 2006). Highest CO_2 emissions occurred after storm S3, which delivered high amounts of organic N and C to biofilter soil. CO_2 emissions were related to temperature (R^2 = 0.39, p = 0.02), which is consistent with increased microbial respiration with rising temperatures. There were no measurable CH_4 emissions prior to wetting, which may have indicated that biofilters were a small CH_4 sink when soils were relatively dry, as observed in other biofilters (Grover et al. 2013). After dosing, the biofilter became a CH_4 source, with emissions ranging from 10.2 to 205.5 µg C/m^2 h (Figure S6 b, Table S4). Mean CH_4 emissions of 116.3 ± 83.1 µg C/m^2 h were higher than other biofilters (-11.1 to 45.5 µg C/m^2 h) (Grover et al. 2013, McPhilips et al. 2017), which could be due to differences in inflows and draining times, and in how CH_4 emissions were measured in this study. Specifically, sewage addition in storm S3 may have introduced large amounts of decomposable C, which positively relates to CH_4 production

(Cao et al. 1996). In fact, mean DOC concentration in S3 inflow was 40.5 mg C/L, compared to 11.8 to 19.2 mg C/L in storms S4 through S7. CH_4 emissions increased as wetting progressed (Figure S6 b) and were positively related to soil saturation ($r = 0.84$, $p = 0.0001$) and negatively related to ADP ($r = -0.71$, $p = 0.006$). CH_4 emissions indicated that soils were at least partially anoxic, supporting methanogenesis and other processes needing low O_2 levels, such as denitrification. Further, methanogenesis typically proceeds under deeply reducing conditions, which only occur once NO_3^- has been depleted (Achtnich et al. 1995). CH_4 emissions thus suggest some degree of NO_3^- depletion.

The C4 biofilter was a N_2O source, with mean emissions of 48.7 ± 25.4 μg N/m^2 h, and values ranging from 12.8 to 84.3 μg N/m^2 h (Table S4, Figure 3), which were higher than grass-covered detention basins (0.5 to 9.5 μg N/m^2 h) (McPhillips and Walter 2015) and dry and wet basins (means of 1.1 and 34.3 μg N/m^2 h) (Morse et al. 2017), and comparable to emissions from parking lot biofilters (13.7 to 65.6 μg N/m^2 h) (Grover et al. 2013). There were no significant differences in average N_2O emissions between storms, and average N_2O emissions from storms were similar to baseline measurements (Figure 3a). However, we may not have fully captured the N_2O peaks after a storm event, because these may have occurred when there was standing water in the biofilter, which did not allow us to sample. Also, N_2O emissions vary greatly during the day, due to diurnal temperature fluctuations (Shurpali et al. 2016). Higher temperatures increase microbial activity, and photosynthetic activity, and hence likely C supply via root exudates. Further, increasing temperatures also decrease N_2O solubility, so that higher temperatures should accelerate denitrification and N_2O emissions.

N_2O emissions were larger prior to stormwater runoff dosing and declined after wetting, when biofilter saturation was higher (Figure 3 b). This trend was confirmed by the positive correlation between N_2O emissions with ADP ($r = 0.61$, $p = 0.027$) and the negative relationship with soil saturation ($r = -0.59$, $p = 0.027$). The biofilter was only briefly waterlogged and saturation was mostly below 70% (for 92 h of the 110 h timeseries) (Figure S5 c), so N_2O emissions were likely from nitrification (Bateman and Baggs 2005) plus denitrification in anaerobic microsites (Parkin 1987). A dampening of N_2O emissions following stormwater runoff dosing may have been caused by diffusional constraints, where an increased transport time due to higher biofilter saturation allowed for more conversion of N_2O to N_2. Furthermore, the enzymes catalyzing N_2O reduction to N_2 are sensitive to soil O_2 levels, such that as soil dries and O_2 levels increase N_2O reduction may be inhibited (Philippot et al. 2007). As the biofilter soil dries, gas transport to the surface may accelerate and cause N_2O emissions to increase, as observed in between dosing days. N_2O emissions following storm S3, the high nutrient loading storm, remained relatively high (Figure 3a), likely due to higher nitrification and denitrification rates from the processing of added NH_4^+, NO_3^- and organic C. Also, increased soil respiration due to C inputs from sewage-contaminated runoff (storm S3) may have created localized anaerobic microsites and promoted denitrification (Parkin 1987).

Overall, CO_2, CH_4 and N_2O emissions and biofilter soil saturation suggested that nitrification and denitrification were taking place, with a timing and magnitude that was

influenced by soil water content, soil temperature, and C and N supply. To further investigate the timing and prevalence of N processes we evaluated dual NO_3^- isotopes.

4.3.5. NO_3^- isotope analysis and source tracking

Dual NO_3^- isotopes ($\delta^{18}O\text{-}NO_3^-$ and $\delta^{15}N\text{-}NO_3^-$) were determined for inflows and outflows of storms 3 through 7, and soil eluates of biofilter C4. Outflow samples were the most depleted $\delta^{18}O\text{-}NO_3^-$ and $\delta^{15}N\text{-}NO_3^-$, ranging from -1.71 to 3.66 ‰, and -9.76 to 9.72 ‰, respectively, followed by soil eluates, and influent samples, which were very enriched relative to outflow samples (+15‰ for $\delta^{15}N\text{-}NO_3^-$, +30% for $\delta^{18}O\text{-}NO_3^-$) (Figure 4, Table S5). The $\delta^{18}O\text{-}NO_3^-$ and $\delta^{15}N\text{-}NO_3^-$ of inflows, outflows, and soil eluates were compared against common NO_3^- sources (Kendall et al., 2007, Hastings et al. 2013). Inflow storm samples had enriched $\delta^{15}N\text{-}NO_3^-$ consistent with values for septic waste. Soil eluates were half-way in between inflow samples and septic waste, consistent with NO_3^- sources from a mix of stormwater and septic waste. Outflow samples plotted in the range of $\delta^{18}O\text{-}NO_3^-$ values corresponding to NO_3^- sources from nitrification (Figure 4) (Kendall et al. 2007), indicating that nitrification was a dominant process This isotopic evidence for nitrification is consistent with the decrease in NH_4^+ concentrations, and increase in NO_3^- concentrations observed between inflows and outflows (Figure 1, Table 1). The depletion in $\delta^{18}O\text{-}NO_3^-$ and $\delta^{15}N\text{-}NO_3^-$ from inflow (top right, in Figure 4) to outflow samples (bottom left, in Figure 4) is also consistent with nitrification. Nitrifying bacteria derive their N isotopic values from NH_4^+ and their O isotopic values from water and atmospheric O_2 at a ratio of 2/3 H_2O to 1/3 O_2 (Kendall and McDonnell 2012). Overall, nitrification depletes $\delta^{18}O\text{-}NO_3^-$ because ^{18}O is

more depleted in water than in the atmosphere; nitrification depletes δ^{15}N-NO_3^- because molecules with the lighter isotope react more readily than heavier molecules. An analysis of average δ^{15}N-NO_3^- between storms S3 through S7, showed that δ^{15}N-NO_3^- values decreased between S3 and S5 ($\chi 2 = 35.48$, $p < 0.001$; Dunn's test, $p < 0.001$), and were similar for storms S5 through S7 (Figure S7 a) likely indicating competing processes such as N assimilation and denitrification (Sigman et al. 2005). Average δ^{18}O-NO_3^- in storms S3 through S7 were different ($\chi 2 = 24.29$, $p < 0.001$), due to enrichment from storms S3 to S4 (Dunn test, $p < 0.01$) (Figure S7 b) likely due to the combined effects of ^{18}O enrichment during evaporation in upper soil layers, and preferential consumption of ^{16}O when plants and microbes respire (Spoelstra et al. 2007). The longer draining time between storms S3 and S4, and the increased respiration following high nutrient inputs in storm S3 supports these outcomes since incoming water would flush out NO_3^- that is enriched in δ^{18}O-NO_3^-.

In the later storms, there was evidence of denitrification. Outflow δ^{18}O-NO_3^- and δ^{15}N-NO_3^- for storms S6 and S7 were linearly related, with slopes between 0.5 and 1, indicative of denitrification (Sigman et al. 2005). However, this relationship was only significant in storm S7 ($R^2 = 0.84$, $p = 0.002$) (Figure S7 c). Denitrification was also investigated in eluates of endpoint soil cores. Since new infiltration partially pushes out stored water, younger and more oxygenated water would likely be near the soil surface, and older and less oxygenated water would be in deeper soils, so that denitrification would be favored in deeper soils. This would result in enriched δ^{18}O-NO_3^- and δ^{15}N-NO_3^- with depth, as confirmed by the positive relationship ($R^2 = 0.68$, slope = 1.83, $p = 0.18$) (Figure S7 d). The slope > 1 implied that

other processes intervened in NO_3^- removal, such as N assimilation, which has a similar isotopic signature to denitrification (Sigman et al. 2005). N assimilation by biofilter plants, a common fate for NO_3^- (Payne et al. 2014) may explain the observed slope value between $\delta^{18}O\text{-}NO_3^-$ and $\delta^{15}N\text{-}NO_3^-$. If assimilated N is remineralized to NH_4^+ and then nitrified, the $\delta^{18}O\text{-}NO_3^-$ values increase further (Sigman et al. 2005).

Taken together, isotopic data suggested that, under the studied conditions, nitrification was dominant, while denitrification was becoming more relevant in later storms. Another suggested N fate was assimilation coupled with subsequent remineralization. To provide quantitative evidence for nitrification and denitrification, we evaluated the abundance of nitrifying and denitrifying bacteria and examined their distribution through the soil profile.

4.3.6. qPCR and 16S rRNA gene sequencing

Overall, nitrifiers and denitrifiers co-existed throughout the soil profile, showing depth-dependent enrichment. This may have resulted from nutrients delivered by the storm inputs, and water flow through the biofilter, as detailed below.

The 16S rRNA gene abundance were comparable to other biofilters (Chen et al. 2013), with values ranging from 9.2×10^8 to 5.7×10^9 gene copies per gram of dry soil (gc/g dry soil) (Fig. 5 a and b, Table S6). Gene copies of 16S rRNA appeared to increase between the surface (0-10 cm) and the 10 to 20 cm soil section and decrease with soil depth thereafter (Fig. 5a and Table S6). Due to lack of replication, the significance of these trends could not be determined.

Bacterial and archaeal ammonia oxidizing (*amo*A) gene abundances ranged from 1.2×10^3 to 2.3×10^4 and 2.1×10^5 to 1.2×10^6 gc/g dry soil, respectively (Figure 5, a and b, Table S6). Bacterial *amo*A gene abundance was smaller than in other bioretention systems—for example field-based bioretention systems average 10^4 to 10^6 copies while biofilter columns typically have 10^6 to 10^8 *amo*A gene copies (Chen et al. 2013; Chen et al. 2019). However, our values are within the range of pristine and agricultural soils (~10^3 to 10^7; Leininger et al. 2006). Archaeal *amo*A gene abundances were comparable to values reported in agricultural soils (10^4 to 10^8) (Leininger et al. 2006). At every sampled depth, archaeal *amo*A genes were 10 to 900 times more abundant than bacterial *amo*A, consistent with previous findings (Leininger et al. 2006). Archaeal *amo*A gene prevalence suggests that ammonia oxidizing archaea may contribute significantly to biofilter nitrification, however they are rarely characterized. Copies of *amo*A gene normalized to 16S rRNA gene copies, showed an apparent increase with depth for archaeal *amo*A in C2, and bacterial *amo*A in C4 (Figure S9), possibly indicating different niche preferences, likely due to the differing dosing regimens that influenced nutrient profiles (Table S2). However, the significance of these trends could not be verified, since analysis was based on one composite sample for each soil depth.

Denitrifiers were assessed via the *nir*K, *nir*S, and *nos*Z genes, whose abundances ranged from 4.5×10^5 to 3.1 to 10^6, 1.8×10^6 to 1.5×10^7, and 5.0×10^5 to 2.2×10^6 gc/g dry soil, respectively (Figure 5 a and b, Table S6), and were comparable to other biofilters (*nir*K: 10^4 to 10^8; *nir*S*:* 10^5 to 10^8; *nos*Z: 10^5 to 10^8 gc/g dry soil) (Chen et al. 2013, Waller et al. 2018, Chen et al. 2019). The general trend was that these denitrifier gene abundances increased

from the 0 to10 cm down to the 10 to 20 cm soil sections, and decreased with depth thereafter (Figure 5, a and b), paralleling overall 16s rRNA copies. This increase with depth may have been due to washing out of attached bacterial populations from surface soils due to storm inputs; this trend was more apparent in C4, which received more storms than C2. When normalized to 16S rRNA gene copies, denitrifying genes increased with depth for C2; this trend was apparent for *nir*K in C4 (Figure S9).

Results from previously reported (Li et al. 2021) 16S rRNA gene sequencing in biofilter soils from this set of experiments were used to estimate the relative abundance of autotrophic nitrifiers in biofilter soil. Major assigned bacterial phyla were α-, β-, γ-, and δ-Proteobacteria, Acidobacteria Actinobacteria, Bacteroidetes, Chloroflexi, and Nitrospirae (Figure S10). Denitrifiers are included in Bacteroidetes, and α-, β-, γ- and ε-Proteobacteria (Philippot et al. 2007). The *Nitrospira* genus includes soil nitrite-oxidizing bacteria (NOB) and was relatively abundant in biofilter soil, ranging from 0.80 to 2.10 % in C4, and 0.57 to 1.50 % in C2. *Nitrospira* relative abundance increased with soil depth in C2 and C4 (results reproduced in Figure S10 of this paper). Other identified genera were *Nitrosomonas*, and *Nitrobacteria* for NOB, and *Nitrosopumilus* for ammonia oxidizing archaea.

4.3.7. Nitrifying and denitrifying enzyme activities

Potential enzyme activities were used as measures of the population sizes of potentially active nitrifying and denitrifying bacteria. NEA in C2 and C4 ranged from 0.45 to 1.63 µg N/g dry soil/day (Figure 5 c) and decreased with soil depth. NEA was similar in C2 and C4 (Kruskal-Wallis, $p > 0.05$). When NEA results were normalized to SIR, nitrification

potentials were uniform in C2, and increased with depth in C4 (Figure 5 d), indicating higher relative abundance of nitrifiers with depth, consistent with qPCR results (Figure S9 b). However, NEA, and archaeal and bacterial *amo*A were not significantly related. Near the surface, NEA was larger than DEA, but in the 30 to 40 cm and 50 to 60 cm soil sections, NEA and DEA were similar, likely indicating comparable nitrification and denitrification potentials as soil depth increased. DEA ranged from 0.17 to 0.59 µg N/g dry soil/day (Figure 5d) and was on the lower end of biofilter values (0.24 to 16.8 µg N/g dry soil/day) (Morse et al 2017, Waller et al. 2018, Kavehei et al. 2021). DEA was relatively unchanged with soil depth but, when normalized to SIR, increased with depth in C4, likely indicating more favorable conditions for denitrification, consistent with NO_3^- isotope results. DEA was negatively correlated to *nir*K ($\rho = -0.72$, $p = 0.054$) and *nir*S ($\rho = -0.70$, $p = 0.042$), possibly indicating a disconnect between the abundance and activity of denitrifiers.

4.3.8 Transport times and biological reaction rates

Transport timescales and biological reaction rates were compared to evaluate if residence time in the biofilter allowed significant biological transformation. Although standing water in biofilters drains relatively quickly, water held in pore spaces may persist in the biofilter for much longer times, and incoming water flows may only partially flush out older water, as observed previously (Parker et al. 2021). Transport times were determined from the mean age of water in storage, as developed previously (Parker et al. 2021). Mean water ages ranged from 7.3 to 29.5 h for storms 1 through 7, and 9.3 to 27.1 h between storms (Figure S8). To estimate biological reaction rates, reaction times for N mineralization were estimated, and

reaction times for nitrification and denitrification were obtained from published literature. Ecosystem respiration rates (Figure S6 a, Table S4) and soil data, using formulas eq. S10 and eq. S11 (Supplemental Methods) were used to derive N mineralization reaction constants, k_{min}, and reaction times, τ_{min}. We assumed that total mineralizable N ranged from 5 to 20% of total N. For the 5% assumption, k_{min} was $0.002 \pm 5.71 \times 10^{-4}$ day^{-1}, while for the 20% assumption k_{min} was $0.008 \pm 2.43 \times 10^{-4}$ day^{-1}. Both ranges were comparable to k_{min} for soil studies (0.001 to 0.004 day^{-1}) (Lotse et al. 1992). The reaction times for N mineralization ranged from 18 to 100 weeks. For nitrification, reaction rate constants derived from soil and bioretention studies ranged from 0.02 to 0.5 day^{-1} (reaction times: 2 to 50 days) (Lotse et al. 1992, Sogbedji et al. 2001, Chen et al. 2019, Fan et al. 2019, Wang et al. 2021). These reaction rates and times were similar or faster than those reported for denitrification, which ranged from 0.01 to 0.2 day^{-1} (reaction time: 5 to 100 days) (Lotse et al. 1992, Sogbedji et al. 2001, Chen et al. 2019, Fan et al. 2019, Wang et al. 2021, Kavehei et al. 2021). Denitrification reaction times may be slower than nitrification times in aerated soils because O_2 levels may at least partially inhibit denitrification, given that denitrifiers are facultative anaerobes and preferentially use O_2, over NO_3^-, as a terminal electron acceptor (Schlesinger et al. 2009). The range of water ages (hours to days) and biological reaction times (days to months) confirmed the N processing dynamics expected for fast draining biofilters: dominance of transport processes during storms, and an increase in significance of biogeochemical reactions during drying periods. However, denitrification during dry periods would likely be limited due to inhibitory O_2 concentrations.

4.3.9. Mass balance of NH_4^+, NO_3^- and N_2O emissions

A partial mass balance of NH_4^+, NO_3^-, and N_2O emissions for storms S3 through S7 suggested that biofilter C4 was mineralizing N and acting as a net nitrifier (Figure 6). When considering NH_4^+ and NO_3^- together, the balance resulted in a slight increase of stored N in the biofilter (1.16 g N), and export of 4.26 g N. The NH_4^+ balance in C4 soils was positive, suggesting that N mineralization and adsorption of NH_4^+ from influent stormwater dominated over plant uptake, microbial immobilization, and bacterial and archaeal nitrification. This suggested, that although nitrification was a more dominant process than denitrification, it may not have been as significant as N mineralization and NH_4^+ adsorption, likely because nitrifiers only represent a small fraction of total bacteria.

The NH_4^+ mass introduced with storm 3 (21.0 g N, Table 1) was an order of magnitude greater than soil NH_4^+ mass prior to storm S3 (3.66 g N, Table S7), while soil NO_3^- (7.93 g N, Table S7) was an order of magnitude greater than NO_3^- inputs in storm S3 (0.18 g N, Table 1). NH_4^+ temporarily retained during storm S3 (subtracting output from input: 19.4 g N, Table 1) was similar to the excess NO_3^- leaving the biofilter during storms S4 through S7 (subtracting input from output:19.4 g N, Table 1). These results suggested that NH_4^+initially retained within a storm was nitrified in between storms (ca. 1 day herein), and almost completely released as NO_3^- in subsequent storms. We must also acknowledge that most NO_3^- export occurred during the conditioning storms (S1-2) (Figure 2), due to previously formed NO_3^-. The relatively low N_2O emissions (14.4 mg N) suggested minimal denitrification or a prevalence of complete denitrification.

When considering NO_3^-only, storage increased by 0.28 g N in the soil, while the balance of aqueous flows created an export of 26.2 g N, suggesting that assimilation and denitrification were not as significant as nitrification. In between storms, nitrification of influent and stored NH_4^+ may have contributed to NO_3^- formation. When the soils were re-wet after a dry period, NO_3^- leaching occurred and persisted in subsequent storms. These results highlight the importance of monitoring the storms that follow a high-flow, and high-loading event, since export may persist even for short ADPs. The magnitude and persistence of this export would likely vary depending on influent characteristics, soil properties, biofilter vegetation, and biofilter designs. Still, our results show that typical biofilters which rapidly infiltrate stormwater runoff are almost certain to be overloaded when they experience big, pulsed storms, and that they do not support N removal.

4.4. Conclusion and Recommendations

A full-scale biofilter was challenged with a large pulse of N (mainly NH_4^+) and other sewage-associated nutrients (e.g., organic C) during a realistic simulated storm. Successive storms delivered unpolluted stormwater that leached NO_3^- from the biofilter. The influent NH_4^+ pulse was subject to all expected fates in a soil system: adsorption, assimilation by plants, immobilization by microbes, and nitrification. However, the mass of NO_3^- released from the biofilter exceeded what could have been formed by nitrification of the NH_4^+ added during storm 3, in part due to NO_3^- that had already accumulated in the pore fluids of the biofilter prior to our experiment, for example from fertilizer added when the biofilter was

first planted. Our estimates for mineralization and N-cycling reaction times were longer than biofilter residence times, favoring NO_3^- production between storms and NO_3^- leaching during storms. By using a comprehensive analysis of chemical, bacterial, and isotopic metrics, we showed that denitrification was limited even for high-frequency, large storms, and that the biofilter was a net NO_3^- exporter.

Taken together, our results show that typical biofilter designs perform very poorly, in terms of removing N, when challenged with large, pulsed storms. To promote denitrification and permanent N removal, storm residence times would have to increase from hours to days, which may be problematic because high hydraulic conductivity is needed for rapid infiltration. A viable way of addressing the mismatch between reaction and residence times identified here, may be a treatment train consisting of a stormwater capture system (e.g., that uses real-time control to optimize runoff capture (Parker et al. 2022), sequentially followed by fast- and slow-draining cells. In this arrangement, the tank reduces stormwater runoff (and associated pollutants) entering streams, the first cell reduces runoff volume (via water storage and lateral exfiltration into adjacent soils), and the second, and slow-draining, cell enhances N removal by providing longer contact times. In this design, influent NH_4^+ may be adsorbed and nitrified in the first cell, while influent NO_3^- and dissolved organic nitrogen (DON) flow through into the second cell, relatively unchanged. The longer residence times of the second cell promote denitrification and NO_3^- removal, while clay minerals in soils sorb DON (Wang et al. 2020). Although DON can then be mineralized and potentially nitrified, by separating influent NH_4^+ and DON, in the first and second cell, respectively, a larger N pulse is

transformed into two smaller and potentially more manageable pulses, supporting better N treatment and lower N export from biofilters.

4.5. Acknowledgements

The performance of this research was supported by funding from by the University of California Office of the President, Multicampus Research Programs and Initiatives, Grant ID MRP-17-455083. EAP and SBG were additionally supported by a NSF Growing Convergence Research (GCR) award (#2021015). We thank Jian Peng, and the Orange County Public Works, CA for use of biofilters and onsite laboratory, logistical support, water filtration, and soil coring. We thank Beta Analytic Inc. and Source Molecular Corporation, particularly Florencia Goren and Thierry Tamers for financial support, as well as Zeneida Cernada and the IRMS team for technical assistance and analysis of nitrate isotopic ratios. Raw sewage was provided by the Orange County Sanitation District, CA. Nitrate analysis was performed at UC Riverside, with assistance from Emily Santiago. Dr. Jen Le assisted with GHG sampling. Plasmid DNA standards were provided by Dr. Alyson Santoro and Dr. Brian Badgley. Financial support from Mr. Henry H. Wheeler, Jr. is acknowledged.

4.6 References

Achtnich, C., Bak, F., and Conrad, R. (1995). Competition for electron donors among nitrate reducers, ferric iron reducers, sulfate reducers, and methanogens in anoxic paddy soil. *Biol. Fertil. Soils*, 19(1), 65-72.

Baggs, E. M. (2006). Partitioning the components of soil respiration: a research challenge. *Plant Soil*, 284, 1-5.

Bateman, E. J., and Baggs, E. M. (2005). Contributions of nitrification and denitrification to N_2O emissions from soils at different water-filled pore space. *Biol. Fertil. Soils* 41, 379-388.

Blackmer, A. M., and Green, C. J. (1995). Nitrogen turnover by sequential immobilization and mineralization during residue decomposition in soils. *Soil Sci. Soc. Am. J.*, 59(3), 1052-1058.

Boehm, A. B., Bell, C. D., Fitzgerald, N. J. M., Gallo, E., Higgins, C. P., Hogue, T. S., Luthy, R. G., Portmann, A. C., Ulrich, A. B., and Wolfand. J. M. (2020). Biochar-augmented biofilters to improve pollutant removal from stormwater - can they improve receiving water quality? *Environ. Sci.: Water Res. Technol*., 6, 1520-1537.

Bratières, K., Fletcher, T. D., Deletic, A., and Zinger, Y. (2008). Nutrient and sediment removal by stormwater biofilters; a large-scale design optimisation study. *Water Res*., 42(14), 3930-3940.

Brown, A. R., and Hunt, W. F. (2011). Impacts of media depth on effluent water quality and hydrologic performance of undersized bioretention cells. *J. Irrig. Drain. Eng*., 137(3), 132-143.

Brown, R. A., Birgand, F., and Hunt, W. F. (2013). Analysis of consecutive events for nutrient and sediment treatment in field-monitored bioretention cells. *Water Air Soil Pollut.*, 224(6), 1-14.

Burgis, C. R., Hayes, G. M., Zhang, W., Henderson, D. A., Macko, S. A., and Smith, J. A. (2020). Tracking denitrification in green stormwater infrastructure with dual nitrate stable isotopes. *Sci. Total Environ.*, 747, 141281.

Casciotti, K. L. (2009). Inverse kinetic isotope fractionation during bacterial nitrite oxidation. *Geochim. Cosmochim. Acta, 73*(7), 2061-2076.

Chen, X., Peltier, E., Sturm, B. S., and Young, C. B. (2013). Nitrogen removal and nitrifying and denitrifying bacteria quantification in a stormwater bioretention system. *Water Res*., 47(4), 1691-1700.

Chen, T., Liu, Y., Zhang, B., and Sun, L. (2019). Plant rhizosphere, soil microenvironment, and functional genes in the nitrogen removal process of bioretention. *Environ. Sci. Process. Impacts*, 21(12), 2070–2079.

Clary, J., Leisenring, M., Poresky, A., Earles, A., and Jones, J. (2011). BMP performance analysis results for the international stormwater BMP database. In Proc., World Environmental and Water Resources Congress. Reston, VA: ASCE.

Davis, A. P., Shokouhian, M., Sharma, H., and Minami, C. (2001) Laboratory study of biological retention for urban stormwater management. *Water Environ. Res.*, 73, 5-14.

Davis, A. P. (2007). Field performance of bioretention: water quality. *Environ. Eng. Sci*., 24 (8), 1048-1064.

Fierer, N. and Schimel, J.P., 2002. Effects of drying–rewetting frequency on soil carbon and nitrogen transformations. *Soil Biol. Biochem.*, 34(6), 777-787.

Fierer, N., Colman, B. P., Schimel, J. P., and Jackson, R. B. (2006), Predicting the temperature dependence of microbial respiration in soil: A continental-scale analysis, *Global Biogeochem. Cycles*, 20, GB3026.

Grover, S. P. P., Cohan, A., Chan, H. S., Livesley, S. J., Beringer, J., and Daly, E. (2013). Occasional large emissions of nitrous oxide and methane observed in stormwater biofiltration systems, *Sci. Total. Environ*., 465, 64-71.

Hastings, M. G., Casciotti, K. L., and Elliott, E. M. (2013). Stable isotopes as tracers of anthropogenic nitrogen sources, deposition, and impacts. *Elements*, 9(5), 339-344.

Hatt, B. E., Fletcher, T. D., and Deletic, A. (2007). Hydraulic and pollutant removal performance of stormwater filters under variable wetting and drying regimes. *Water Sci. Technol*., 56(12), 11-19.

Hatt, B. E., Fletcher, T. D., and Deletic, A. (2008). Hydraulic and pollutant removal performance of fine media stormwater filtration systems. *Environ. Sci. Technol.*, 42(7), 2535-2541.

Hatt, B. E., Fletcher, T. D., and Deletic, A. (2009). Hydrologic and pollutant removal performance of stormwater biofiltration systems at the field scale. *J. Hydrol*, 365(3), 310-321.

Hsieh, C. H., and Davis, A. P. (2005). Evaluation and optimization of bioretention media for treatment of urban storm water runoff. *J. Environ. Eng.*, 131(11), 1521-1531.

Hunt, W. F., Jarrett, A. R., Smith, J. T., and Sharkey, L. J. (2006). Evaluating bioretention hydrology and nutrient removal at three field sites in North Carolina. *J. Irrig. Drain. Eng.*, 132(6), 600-608.

Hutchinson, G. L., and Mosier, A. R. (1981). Improved soil cover method for field measurement of nitrous oxide fluxes. *Soil Sci. Soc. Am. J.*, 45, 311-316.

Kavehei, E., Farahani, B. S., Jenkins, G., Lemckert, C., and Adame, M. (2021). Soil nitrogen accumulation, denitrification potential, and carbon source tracing in bioretention basins. *Water Res*., 116511.

Kendall, C., Elliott, E. M., Wankel, S. D. (2007). Chapter 12, Tracing Anthropogenic Inputs of Nitrogen to Ecosystems. In: Stable Isotopes in Ecology and Environmental Science, 2nd ed., Lajtha, K., and Michener, R.H. (Eds.), Blackwell Scientific Publications, Oxford, UK.

Kendall, C., and McDonnell, J. J. (Eds.) (2012). Isotope Tracers in Catchment Hydrology. Elsevier Science, Amsterdam, The Netherlands.

Leininger, S., Urich, T., Schloter, M., Schwark, L., Qi, J., Nicol, G. W., Prosser, J. I., Schuster, S. C., and Schleper, C. (2006). Archaea predominate among ammonia-oxidizing prokaryotes in soils. *Nature*, 442, 806-809.

Li, D., Van De Werfhorst, L. C., Rugh, M. B., Feraud, M., Hung, W-C, Jay, J., Cao, Y, Parker, E. A., Grant, S. B., and Holden, P. A. (2021). Limited bacterial removal in full-scale stormwater biofilters as evidenced by community sequencing analysis. *Environ. Sci. Technol.* 55(13), 9199-9208.

Li, H., and Davis, A. P. (2009). Water quality improvement through reductions of pollutant loads using bioretention. *J. Environ. Eng*., 135(8), 567-576.

Li, L. and Davis, A. P. (2014). Urban stormwater runoff nitrogen composition and fate in bioretention systems. *Environ. Sci. Technol*. 48(96), 3403-3410.

Liu, J., Sample, D. J., Bell, C., and Guan, Y. (2014). Review and research needs of bioretention used for the treatment of urban stormwater. *Water*, 6(4), 1069-1099.

Lotse. E. G., Jabro, J. D., Simmon, K. E., and Baker, D. E. (1992). Simulation of nitrogen dynamics and leaching from arable soils. *J. Contam. Hydrol.*, 10, 183-196.

McPhillips, L., and Walter, M. T. (2015). Hydrologic conditions drive denitrification and greenhouse gas emissions in stormwater detention basins. *Ecol. Eng*., 85, 67-75.

McPhillips, L., Goodale, C., and Walter, M. T. (2017). Nutrient leaching and greenhouse gas emissions in grassed detention and bioretention stormwater basins. *J. Sustainable Water Built Environ.*, 4(1), 04017014.

Morse, N. R., McPhillips, L. E., Shapleigh, J. P., and Walter, M. T. (2017). The role of denitrification in stormwater detention basin treatment of nitrogen. *Environ. Sci. Technol.*, 51(14), 7928-7935.

National Oceanographic and Atmospheric Administration, 2021. California Nevada River Forecast Center: Observed Precipitation.

Parker, E. A., Rippy, M. A., Mehring, A. S., Winfrey, B. K., Ambrose, R. A., Levin, L. A., and Grant, S. B. (2017). Predictive power of clean bed filtration theory for fecal indicator bacteria removal in stormwater biofilters. *Environ. Sci. Technol.*, 51(10), 5703-5712.

Parker, E. A., Grant, S. B., Cao, Y., Rippy, M. A., McGuire, K. J., Holden, P. A., Feraud, M., Avasarala, S., Liu, H., Hung, W. C., Rugh, M., Jay, J., Peng, J., Shao, S., and Li, D. (2021). Predicting solute transport through green stormwater infrastructure with unsteady transit time distribution theory. *Water Resour. Res.*, 57, e2020WR028579.

Parker, E.A., Grant, S. B., Sahin, A., Vrugt, J. A., and Brand, M. W. (2022). Can smart stormwater systems outsmart the weather? Stormwater capture with real-time control in Southern California. *ACS ES&T Water*, 2(1), 10-21.

Parkin, T. B. (1987). Soil microsites as a source of denitrification variability, *Soil Sci. Soc. Am. J.*, 51, 1194-1199.

Payne, E. G., Fletcher, T. D., Cook, P. L., Deletic, A., and Hatt, B. E. (2014 a). Processes and drivers of nitrogen removal in stormwater biofiltration. *Crit. Rev. Env. Sci. Tech*., 44(7), 796-846.

Payne E.G., Fletcher T.D., Russell D.G., Grace M.R., Cavagnaro T.R., Evrard V., Deletić A., Hatt B.E., and Cook P.L. (2014 b). Temporary storage or permanent removal? The division of nitrogen between biotic assimilation and denitrification in stormwater biofiltration systems. *PloS One*, 9, e90890.

Philippot, L., Hallin, S., and Schloter, M. (2007). Ecology of denitrifying prokaryotes in agricultural soil. *Adv. Agron.*, 96, 249-305.

Read, J., Fletcher, T. D., Wevill, T., and Deletic, A. (2010). Plant traits that enhance pollutant removal from stormwater in biofiltration systems. *Int. J. Phytorem.*, 12, 34-53.

Schlesinger, W. H. (2009). On the fate of anthropogenic nitrogen. *Proc. Natl Acad. Sci.*, 106, 203-208.

Sigman, D. M., Granger, J., DiFiore, P. J., Lehmann, M. M., Ho, R., Cane, G., and van Geen, A. (2005). Coupled nitrogen and oxygen isotope measurements of nitrate along the eastern North Pacific margin. *Global Biogeochem. Cy.*, 19(4), GB4022.

Sogbedji, J. M., van Es, H. M., and Hutson, J. L. (2001). N fate and transport under variable cropping history and fertilizer rate on loamy sand and clay loam soils: I. Calibration of the LEACHMN model. *Plant Soil*, 229, 57-70.

Spoelstra, J., Schiff, S. L., Hazlett, P. W., Jeffries, D. S., and Semkin, R. G. (2007). The isotopic composition of nitrate produced from nitrification in a hardwood forest floor. *Geochim. Cosmochim. Acta*, 71, 3757-3771.

U.S. EPA. (1997). Method 300.1: Determination of inorganic anions in drinking water by ion chromatography, Revision 1.0. Cincinnati, OH.

U.S. EPA. (1993). Method 350.1: Nitrogen, ammonia (colorimetric, automated phenate), Revision 2.0. Cincinnati, OH.

Valenca, R., Le, H., Zu, Y. Y., Dittrich, T. M., Tsang, D.C.W., Datta, R., Sarkar, D., and Mohanty, S. K. (2020). Nitrate removal uncertainty in stormwater control measures: is the design or climate a culprit? *Water Res.*, 190, 116781.

Walsh, C.J., Leonard, A.W., Ladson, A.R., and Fletcher, T.D. (2004). Urban stormwater and the ecology of streams. Cooperative Research Centre for Freshwater Ecology and Cooperative Research Centre for Catchment Hydrology, Canberra, Australia.

Wang, L., Xin, J., Nai, H., Zheng, T., Tian, F., and Zheng, X. (2020). Sorption of DONs onto clay minerals in single-solute and multi-solute systems: Implications for DONs mobility in the vadose zone and leachability into groundwater. *Sci. Tot. Environ.*, 712, 135502.

Zinger, Y., Blecken, G. T., Fletcher, T. D., Viklander, M., and Deletic, A. (2013). Optimising nitrogen removal in existing stormwater biofilters: benefits and tradeoffs of a retrofitted saturated zone. *Ecol. Eng.*, 51, 75-82.

4.7 Figures and Tables

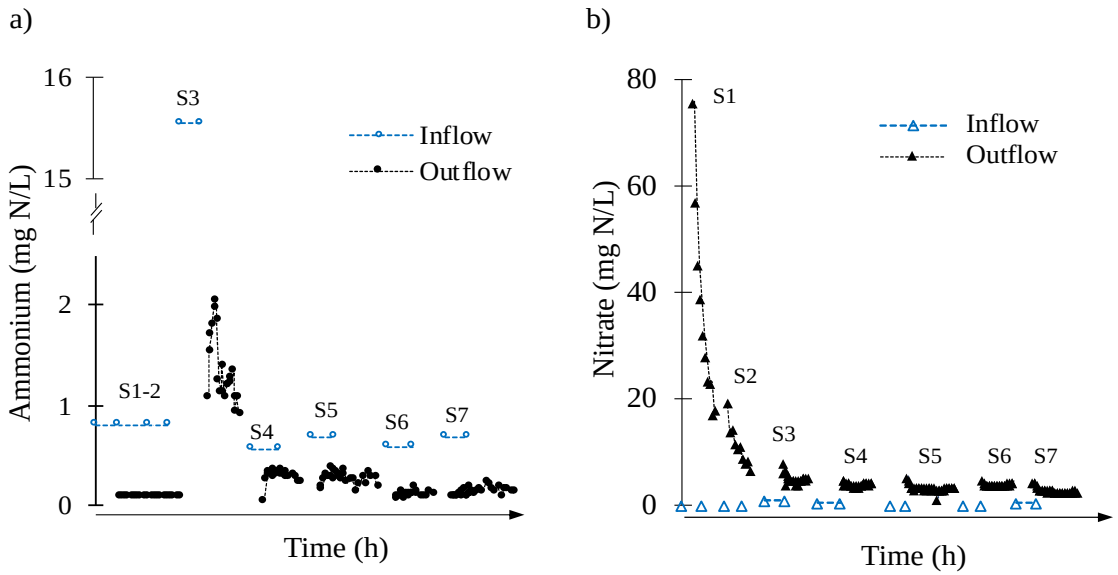

Figure 1. Inflow and outflow concentration profiles for ammonium (a) and nitrate (b) in test biofilter C4 during storms 1 through 7 (S1-7). The time between storms has been shortened for visualization purposes; actual timing for storm events is shown in Figure 2. The break in the y-axis in panel (a) from 2 mg N/L to 15 mg N/L accommodates the high inflow ammonium concentration during storm 3, corresponding to a 1:1 mix of sewage and stormwater runoff.

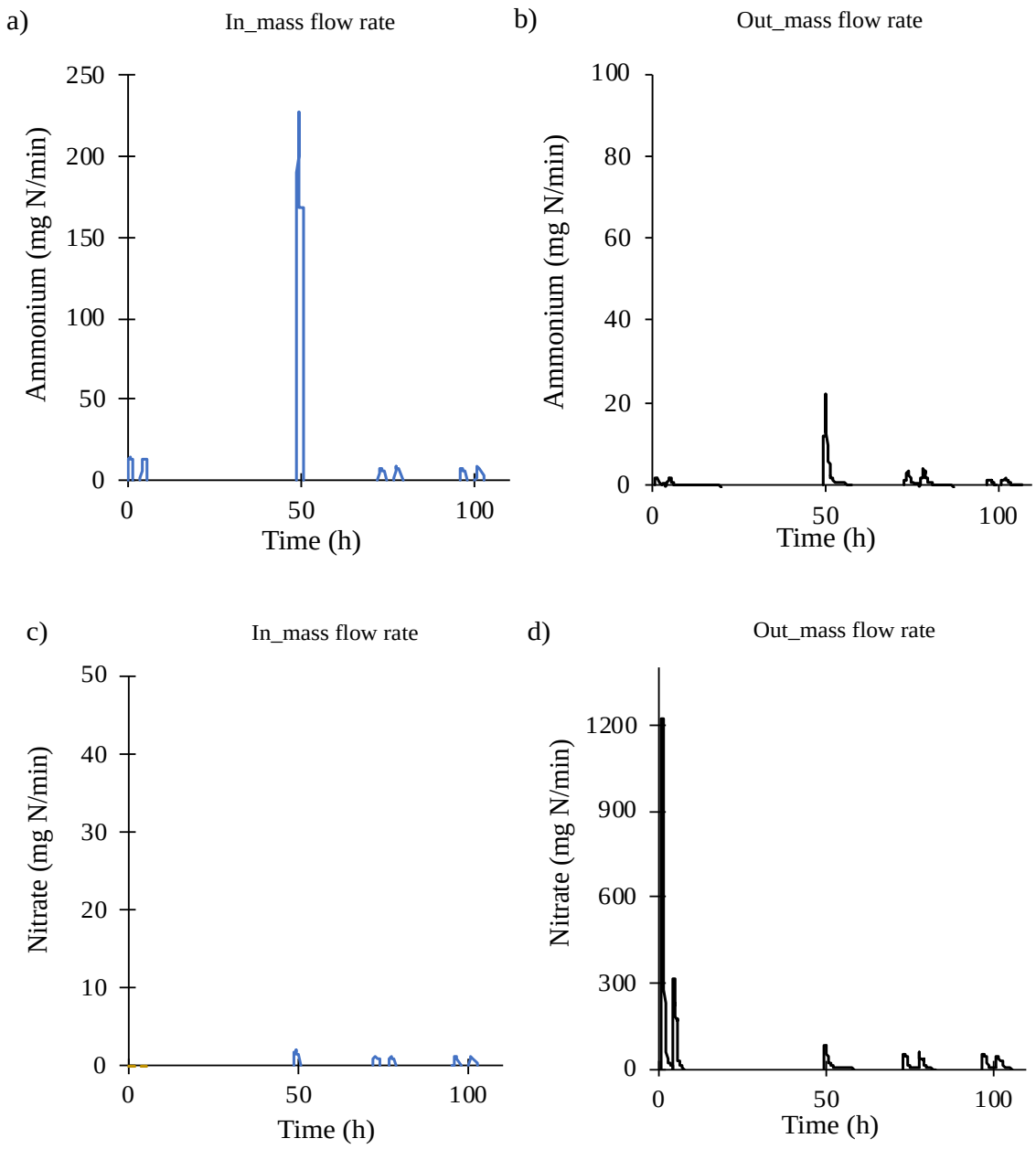

Figure 2. Mass flow rates for ammonium inflow (a) and outflow (b) and nitrate inflow (c) and outflow(d) in test biofilter C4 for storms S1-7. Note scale differences on y-axis for all panels. In (c), there was no measurable nitrate in the inflows of storms S1 and S2.

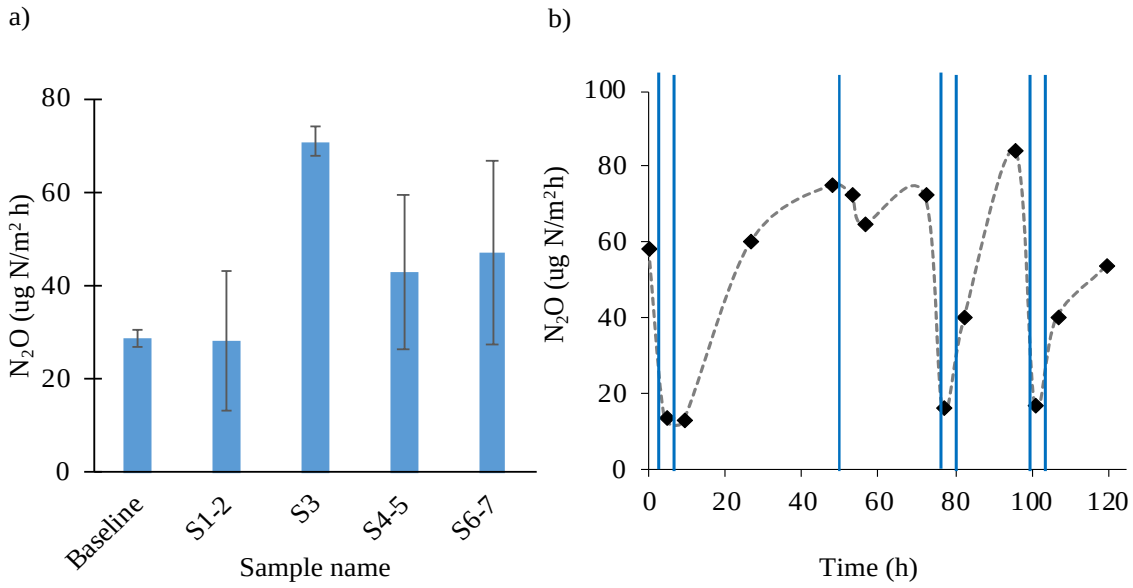

Figure 3. a) N_2O emissions (mean ± 1 standard deviation) for baseline and storms S1 through S7 in test biofilter C4. N_2O emissions were similar (Kruskal-Wallis, $p > 0.05$). b) N_2O emissions trends for storms S1-7 (in blue lines). Time zero corresponds to the first N_2O sampling prior to storm S1 dosing. There were three measurements per dosing day, and one measurement in between storms S2 and S3, and the day after storm S7. Trends in between measurements were inferred (dashed lines) but suggested dampened N_2O emissions following a storm, except for storm S3.

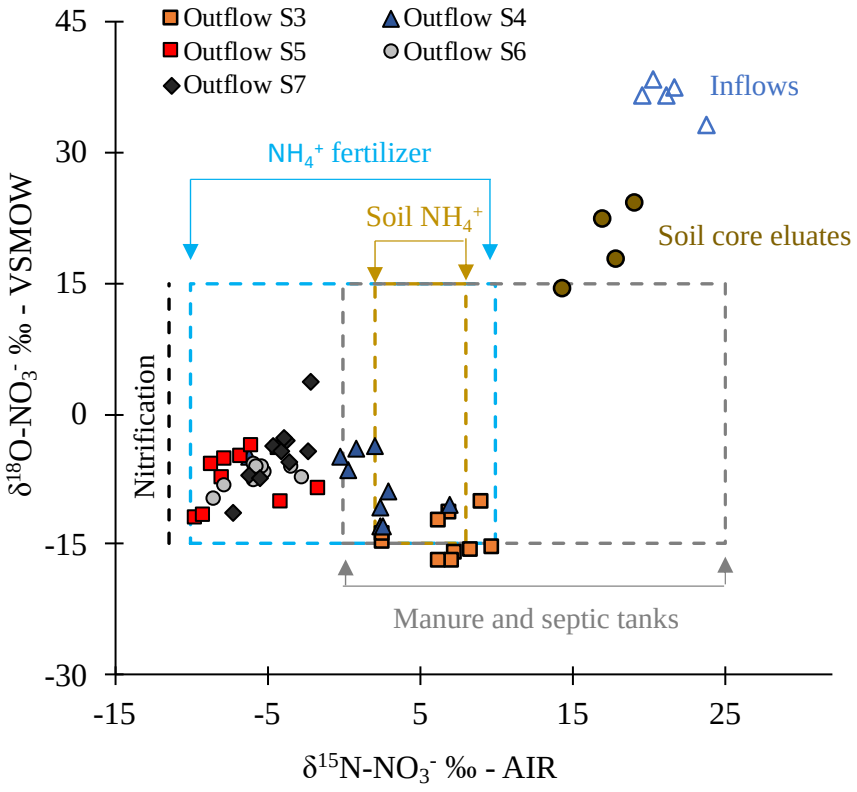

Figure 4. Nitrate isotopes (δ^{18}O-NO_3^- and δ^{15}N-NO_3^-) for inflows and outflows (storms S3 through S7), and soil eluents for test biofilter C4. Also shown are isotopic composition areas of nitrate sources, including ammonium fertilizers, soil ammonium, and manure and septic waste (Kendall et al., 2007; Hastings et al., 2013). Typical δ^{18}O-NO_3^- for nitrification of ammonium are denoted by "Nitrification". δ^{18}O-NO_3^- and δ^{15}N-NO_3^- are reported relative to Vienna Standard Mean Ocean Water (VSMOW), and N_2 in air (AIR), respectively.

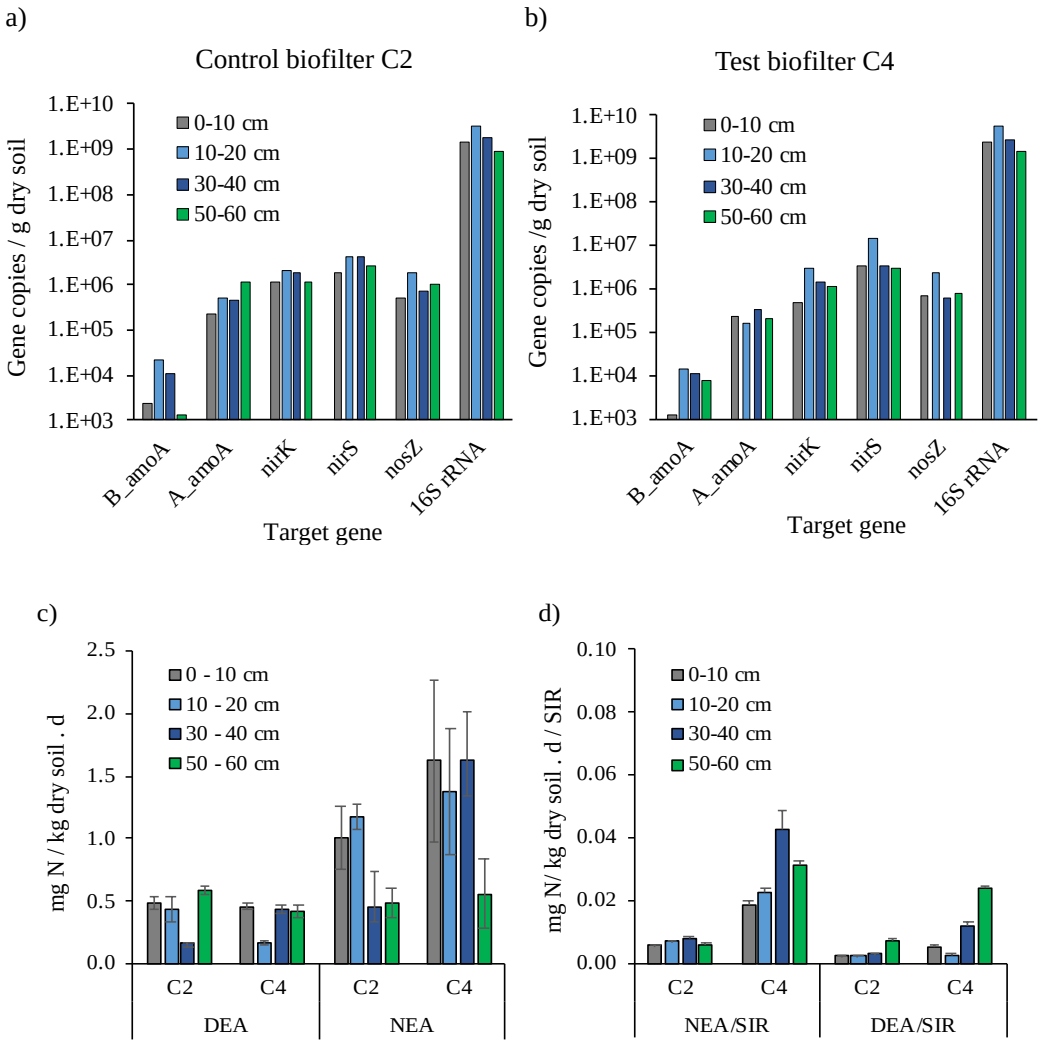

Figure 5. Gene copies of 16S rRNA, bacterial (B_*amo*A) and archaeal (A-*amo*A) *amo*A, *nir*K, *nir*S, and *nos*Z for control C2 (a) and test C4 (b) biofilters. Each composite sample was sectioned at 0 to 10 cm, 10 to 20 cm, 30 to 40 cm, and 50 to 60 cm, and analyzed in triplicate. Also shown, the nitrifying (NEA) and denitrifying (DEA) enzyme activities (c) for duplicate samples (mean and standard error), and the NEA and DEA normalized to microbial biomass estimated via the substrate induced respiration (SIR) (d).

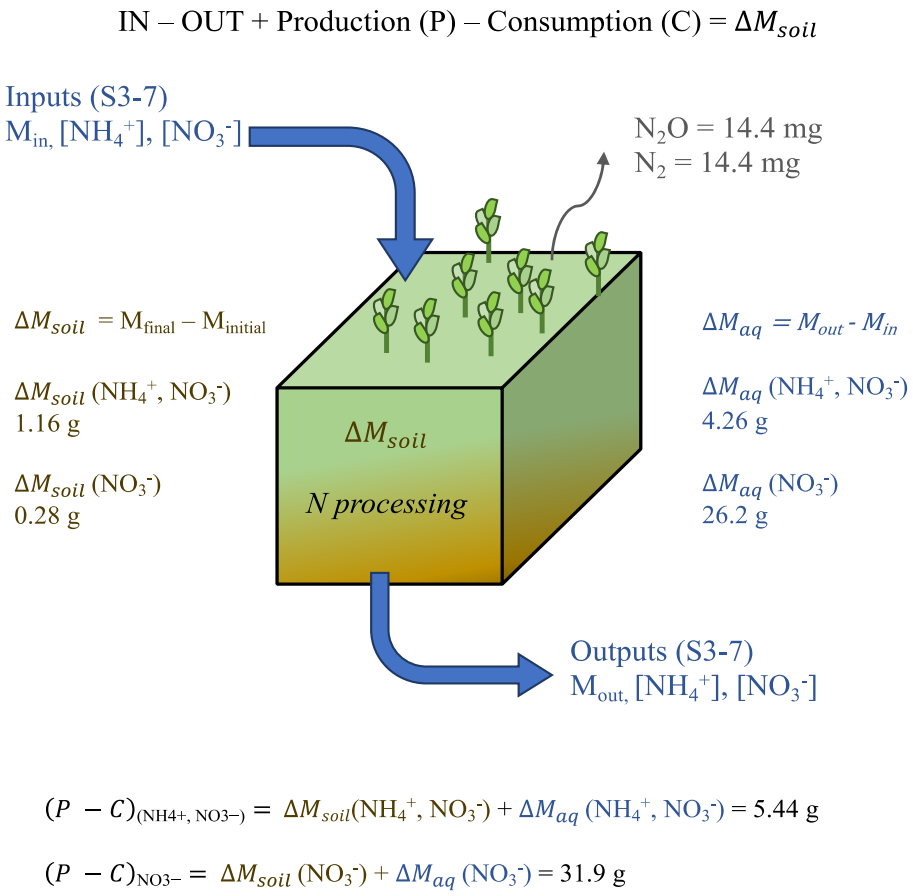

Figure 6. Conceptual diagram and equations for a partial mass balance of ammonium, nitrate and N_2O in test biofilter C4 for storms S3 through S7. The control volume accounted for 54% lateral aqueous exfiltration (Parker et al. 2021). Soil masses were approximated from C2 soils prior to storm S3 (initial), and from C4 cores after storm S7 (final). The positive balance of production and consumption processes for ammonium and nitrate suggested that mineralization dominated over ammonium or nitrate removal processes, while the positive balance for nitrate suggested the biofilter was a net nitrifier.

Table 1. Ammonium and nitrate event mean concentrations, masses, and relative removal in inflows and outflows of test biofilter C4 for storms S1 through S7.

	S1	**S2**	**S3**	**S4**	**S5**	**S6**	**S7**
Ammonium							
EMC Inflow (mg N/L)	0.79	0.79	15.6	0.55	0.69	0.58	0.68
EMC Outflow (mg N/L)	0.1	0.1	1.21	0.21	0.24	0.1	0.13
Reduction (%)	87.5	89.4	92.2	58.2	64.9	81.6	80.3
Mass input (mg)	1.1E+03	1.1E+03	2.1E+04	7.8E+02	9.6E+02	8.2E+02	9.3E+02
Mass output (mg)	1.1E+02	1.3E+02	1.6E+03	2.8E+02	3.8E+02	1.3E+02	2.0E+02
Removal (%)	90.0	87.7	92.3	64.1	60.7	84.1	78.4
Nitrate							
Inflow (mg N/L)	BDL	BDL	0.13	0.10	0.10	0.10	0.10
Outflow (mg N/L)	47.98	11.82	5.39	4.06	3.56	4.06	2.97
Reduction (%)	na	na	-3920	-3961	-3461	-3960	-2874
Mass input (mg)	0.0E+00	0.0E+00	1.8E+02	1.4E+02	1.4E+02	1.4E+02	1.4E+02
Mass output (mg)	5.5E+04	1.8E+04	7.0E+03	5.0E+03	5.5E+03	5.0E+03	4.4E+03
Removal (%)	na	na	-3880	-3470	-3820	-3480	-3080

Note: EMC is the event mean concentration, equivalent to the total mass divided by the total volume. Reductions in EMC, and mass removal are calculated relative to the inflow. For nitrate in S1-2, calculations were not performed because inflows were BDL (0.1 mg N/L). Abbreviations: BLD, below detection limit; na, not available.

4.8. Supplemental Materials

4.8.1. Supplemental Methods

Soil, and gas sampling

Six, evenly spaced soil samples were collected via clean stainless-steel corers (7.6 cm diameter, 45.7 cm long) lined with brass rings, which were pushed into the ground with a sledgehammer. Prior to coring, surface vegetation was manually removed. The cores were cut between the brass rings with clean metal scrapers at intervals corresponding to depths of 0 to 10 cm, 10 to 20 cm, 30 to 40 cm, and 50 to 60 cm. Each depth sample from 6 to 8 replicate cores was composited in a resealable bag and sieved (2 mm pore size) fresh on site. A subsample (50 g) of sieved soil was stored (-80 °C) prior to transport on dry ice to UCSB and maintained at −20 °C until DNA extraction. Soil eluents were generated on site following a published method (Boehm et al. 2009), and 30 mL of the eluent filtered through 0.22 μm PES Micro Funnel filters (PALL Co., Port Washington, NY) for nitrate isotope ratio analysis. The remaining sieved soil was stored (4 °C) prior to transport on ice to UCSB and maintained at 4 °C until physicochemical analysis.

For gas sampling, a week prior to measurements a metal base (50 cm x 50 cm) was pushed flush into the ground. The surface within the metal base consisted of patches of soil with plants. Percent vegetation cover was visually estimated inside each metal base. During sampling, a chamber (50 cm x 50 cm x 50 cm) was secured over the metal base to create a gas-tight enclosure (Figure S4) and shaded fully using reflective material to minimize temperature changes. Thus, CO_2 fluxes represented ecosystem respiration since

photosynthesis was excluded. On stormwater runoff dosing days, CO_2, CH_4 and N_2O fluxes were measured around 7 am, noon, and 4 pm. In between storms, fluxes were measured once daily between 10:00 am and 12:30 pm. Ancillary field measurements included air temperature and relative humidity measured with a HOBO® logger (Onset, Bourne, MA). Further details for gas fluxes are in "Gas flux calculations" (below).

Biofilter soil characterization

Soil gravimetric moisture was determined in triplicate on 3 g subsamples of sieved soil as the mass difference before and after drying (105 °C, 24 h) (Gardner, 1986). To determine soil organic matter via loss on ignition (LOI), dried soils (3 g) were combusted at 550°C for 4 hours (Nelson and Sommers, 1996). Soil pH was measured for a slurry (10 g soil, 10 g deionized water) using a pH meter (Oakton Ion 700 benchtop meter; Cole Parmer, Vernon Hills, IL) according to standard methods (Thomas 1996). Soil bulk density was measured on triplicate soil cores (10.0 cm depth, 5.1 cm diameter), after drying the soil (105 °C, 24 h), by dividing the dry soil mass by the soil core volume. For ammonium and nitrate analysis, 3g of sieved soil were extracted with 30 mL of 2M KCl solution (Mulvaney 1996); the extracts were filtered using grade 42 Whatman filters (Sigma-Aldrich, St. Louis, MO), and the filtrates stored (-20°C) until flow injection analysis (QuikChem8500 Series 2; Lachat Instruments, Milwaukee, WI) at the Marine Science Institute Analytical Lab at UCSB. For DOC analysis, slurries of 15 g of sieved soil and 15 mL of deionized water were prepared in acid-washed 50 mL conical tubes and mixed on a reciprocal shaker (2 hours, 4 °C). The slurry was centrifuged, and the supernatant vacuum filtered using pre-combusted 0.45 µM

GF/F filters (Advantec MFS, Inc., Dublin, CA). Filtrates were diluted 30× with deionized water and stored (-20 °C) until analysis on a Shimadzu TOC-V Analyzer (Shimadzu Corporation, Tokyo, Japan) at the Carlson Lab at UCSB. Microbial biomass was assessed via the substrate induced respiration (SIR) assay, modified from West and Sparling (1986) and Fierer et al. (2003). Briefly, triplicate subsamples of 10 g sieved soil were weighed into 250 mL amber Boston Rounds fitted with Mininert caps, and 10 mL of sterile yeast extract solution (1.2% w/w) were added to each bottle. The bottles were capped and incubated at room temperature (20 °C) on a horizontal roller table. Gas samples (5 mL) were collected after capping, and at 2 and 4 hours via a syringe fitted with a stopcock valve. The CO_2 content was measured using an infrared gas analyzer (EGM-4; PP Systems, Amesbury, MA), and SIR was obtained from the slope of CO_2 concentrations versus time.

Ammonium and nitrate mass flow rates

Mass flow rates were estimated by multiplying volumetric flow rates by concentrations. Ammonium or nitrate mass entering (in) or leaving (out) the biofilter between two times was the average mass flow rate multiplied by the elapsed time, thus total N mass (in) or (out) was:

$$\text{Mass N (in)} = \sum_{i=0}^{n} \frac{J(t)_{i-1} \times C_{in}(t)_{i+1} + J(t)_i \times C_{in}(t)_i}{2} \times \left(t_{i+1-t_i}\right) \qquad \text{(eq. S1)}$$

$$\text{Mass N (out)} = \sum_{i=0}^{n} \frac{Q(t)_{i-1} \times C_{out}(t)_{i+1} + Q(t)_i \times C_{out}(t)_i}{2} \times \left(t_{i+1-t_i}\right) \qquad \text{(eq. S2)}$$

Where: $J(t)_i$ and $Q(t)_i$ were the infiltration and discharge rates, and $C_{in}(t)_i$ and $C_{out}(t)_i$ were the concentrations of ammonium or nitrate in dosing waters and effluent, respectively, for time

"i", and "n" was the number of measurements. Event mean concentrations (EMCs) are total mass divided by total volume. Percent relative mass removals were:

$$\text{Relative removal } \% = \frac{\text{Mass}_{in} - \text{Mass}_{out}}{\text{Mass}_{in}} \times 100 \quad \text{(eq. S3)}$$

Nitrifying and denitrifying enzyme activities

Nitrifying enzyme activity (NEA) was assessed via the chlorate inhibition method, which blocks nitrite conversion to nitrate, following others (Belser and Mays 1980, Hart et al. 1994). Duplicate soil slurries of 4 g sieved soil and 35 mL nitrification potential solution (0.1 mM KH_2PO4, 0.8 mM K_2HPO_4, 0.5 mM $(NH_4)_2SO_4$, and 10 mM $NaClO_3$) were prepared in 125 mL Erlenmeyer flasks and incubated on a reciprocal shaker (20 °C). Aliquots (5 mL) were removed at 15 min, 2 h, and 4 h, centrifuged, and 1 mL supernatant transferred to a cuvette containing 1 mL Nanopure water and 0.5 mL nitrite color reagent (Sulfanilamide/N-Naphthyl Reagent, LabChem, Inc., Zelienople, PA). Sample absorbance was read at 543 nm with a UV spectrophotometer (UV-1800, Shimadzu Co., Kyoto, Japan). Calibration curves were developed daily using nitrite standards (0.01, 0.05, 0.1, and 0.5 ppm, ACS Analytical grade); good linearity ($R^2 > 0.99$) was verified. The rate of nitrate production was the slope of time versus nitrite concentration.

The denitrifying enzyme activity (DEA) assay was adapted from others (Tiedje and Smith 1979; Barnard et al. 2006). Duplicate samples of 2 g sieved soil and 20 mL denitrification potential media (0.72 g KNO_3, 2.5g glucose, 2.2 g glutamic acid in 1 L deionized water) were dispensed into amber 250 mL Boston rounds fitted with Mininert caps. The bottles were capped, and an anaerobic atmosphere obtained by repeated evacuation (4

min) and flushing (1 min) cycles with ultra-high purity (UHP) nitrogen gas. Acetylene was added at 10% v/v, and the bottles incubated at room temperature on a tabletop shaker (20 °C). Headspace samples (15 mL) were removed immediately, at 30 min, and 1 hour, with a syringe fitted with a stopcock valve, dispensed into evacuated Exetainers (Labco Ltd., Lampeter, UK), and analyzed using a GC (8610C gas chromatograph (SRI Instruments)) fitted with an ECD. The N_2O production rate was the slope of time versus N_2O concentration.

Gas flux calculations

Concentrations of CH_4 and CO_2 (ppm) in the chamber headspace were measured using an Ultraportable Greenhouse Gas Analyzer (Los Gatos Research, San Jose, CA) connected to a CR1000X DataLogger (Campbell Scientific, North Logan, UT). CO_2 and CH_4 concentration measurements for a chamber closure of 2 to 3 min were plotted against time to obtain CO_2 and CH_4 production rates (ppm/min), from which the respective fluxes (ug C / m^2 h) were calculated (eq. S4 and eq. S5 below). Only data points with good linearity ($R^2 > 0.8$) were selected. To measure N_2O concentrations, 20 mL chamber headspace samples were collected from a sampling port at 0, 6, 12, 18, 24, and 30 min, and injected into 12-mL pre-evacuated Exetainers (Labco Ltd., Lampeter UK) using a 20 mL syringe fitted with a stopcock valve. Samples were stored in a cool, dark place until analysis within four weeks using an 8610C gas chromatograph (SRI Instruments, Torrance, CA) fitted with an electron capture detector (ECD). Gas calibration curves were obtained by triplicate injection of N_2O standards at 1 ppm, 0.1 ppm (Matheson Tri-Gas, Inc., Irving, TX), and 0 ppm (UHP N_2, Praxair, Inc., Danbury, CT). To correct for instrument drift, N_2O standards were included every 8

injections. N_2O concentrations (ppm) were plotted against time to obtain N_2O production rates (ppm/min), from which N_2O fluxes (ug N / m^2 h) were calculated (eq. S6 below). Only data with good linearity ($R^2 > 0.6$) were selected. The lowest flux detected (detection limit) was 6 ug N/m^2 h. Fluxes were expressed as ug C / m^2 h or ug N / m^2 h:

$$\text{Flux } CO_2 = \text{Rate } CO_2 \left[\frac{\text{ppm}}{\text{min}}\right] \times \frac{60 \text{ min}}{1 \text{ h}} \times H \times \frac{P}{RT} \times MW_C \quad \text{(eq. S4)}$$

$$\text{Flux } CH_4 = \text{Rate } CH_4 \left[\frac{\text{ppm}}{\text{min}}\right] \times \frac{60 \text{ min}}{1 \text{ h}} \times H \times \frac{P}{RT} \times MW_C \quad \text{(eq. S5)}$$

$$\text{Flux } N_2O = \text{Rate } N_2O \left[\frac{\text{ppm}}{\text{min}}\right] \times \frac{60 \text{ min}}{1 \text{ h}} \times H \times \frac{P}{RT} \times MW_{NC} \quad \text{(eq. S6)}$$

Where: P was the ambient pressure in Pa, R is the universal gas constant, 8.314 J mol^{-1} K^{-1}, T was the air temperature, H was the chamber height in m, MW_C is the molecular weight of carbon in mol/g, and MW_N is the molecular weight of nitrogen in mol/g.

Dual isotope analysis for nitrate

Samples were analyzed for stable nitrate isotopes ($\delta^{15}N\text{-}NO_3^-$ and $\delta^{18}O\text{-}NO_3^-$) via a chemical reduction method (Casciotti et al. 2002)**.** Briefly, nitrate in samples was chemically reduced to nitrous oxide (N_2O), and the produced N_2O was then analyzed via continuous flow (CF) Isotope Ratio Mass Spectrometry (IRMS) (Casciotti et al. 2002, Foreman et al. 2016, Altabet et al. 2019). Each sample analysis was referenced to 10 injections of pure N_2O, which had a standard deviation of <0.1‰ for $\delta^{18}O$ and $\delta^{15}N$. This reference N_2O gas was standardized with international nitrate isotopic reference materials USGS-32, USGS-34, and

USGS-35 (Coplen 2021). Method uncertainty was ±2‰ (1 RSD) for $\delta^{18}O$ and ±0.5‰ (1 RSD) for $\delta^{15}N$, comparable to previous analyses (Sigman et al. 2005).

Stable nitrate isotopes $\delta^{15}N\text{-}NO_3^-$ and $\delta^{18}O\text{-}NO_3^-$ were reported as delta (δ) values in units of parts per thousand (per mill or ‰) (Coplen 2011), relative to N_2 in air, and Vienna Standard Mean Ocean Water (VSMOW) reference water, respectively, and were:

$$\delta^{18}O\text{-}NO_3^-‰ = \left(\frac{\frac{O^{18}_{sample}}{O^{16}_{sample}}}{\frac{O^{18}_{vsmow}}{O^{16}_{vsmow}}} - 1 \right) \times 1000 \qquad \text{(eq. S7)}$$

$$\delta^{15}N\text{-}NO_3^- ‰ = \left(\frac{\frac{N^{15}_{sample}}{N^{14}_{sample}}}{\frac{N^{15}_{air}}{N^{14}_{air}}} - 1 \right) \times 1000 \qquad \text{(eq. S8)}$$

qPCR assays

Reactions were prepared in 25 µL volumes in 96-well plates and included 12.5 µL of PowerUp SYBR Green Master Mix (Thermo Fisher Scientific, Waltham, MA), 1.25 to1.5 µL each of forward and reverse primers (500 to 600 nM), 4.5 to 8 µL molecular grade water, and 2 to 5 µL DNA template (Table S3). To avoid inhibition, DNA templates were diluted with nuclease free water to 3.0 ng/µL; DNA for 16S rRNA qPCR was diluted to 1.0 ng/µL. Assays were done in triplicate and included positive, and no template, controls. All qPCR reactions per gene were performed in a single plate. All qPCR thermal profiles included an enzyme activation step (2 minutes at 50 °C, followed by 10 minutes at 95 °C). Subsequent

steps are detailed in Table S3. Melt curves were obtained for a temperature range of 60 to 95 °C, at 0.2 °C increments every 15 s. Product specificity was evaluated via melt curve analysis. A subset of PCR products was verified via gel electrophoresis on FlashGel DNA Cassettes run with a DNA Marker (100 bp - 4 kb; Lonza Group AG, Basel, Switzerland).

Standard curves were generated by serial dilution of linearized plasmid DNA. Standards were run in serial dilutions from 1 x 10^7 to 1 x 10^1 copies/µL for 16S rRNA, and 1 x 10^6 to 1 x 10^1 copies/µL for all other target genes. Samples with two or more replicates amplifying within the range of the standard curve were within the range of quantification, and thus quantified. Samples with only one or no replicates amplifying were considered not detected, and the sample's gene quantity was set at ½LOD, where LOD was 3 gene copies per reaction, following MIQE guidelines for qPCR (Bustin et al., 2009).

Standards for 16S rRNA were constructed from gBlocks® Gene Fragments (Integrated DNA technologies, Coralville, IA) and were 351 base pairs in length. Standards for the remaining target genes were obtained from competent *E. coli* cells containing plasmids with the target genes, produced using the TOPO® TA Cloning® Kit (Invitrogen, Co., Waltham, MA) following the manufacturer's instructions, as performed by Waller et al. (2018) for bacterial *amoA*, *nirK*, *nirS*, and *nosZ*, and by Santoro et al. (2008) for archaeal *amoA*. A glycerol stock of *E. coli* cells containing the target plasmid DNA was prepared by transferring a single isolated colony from a streak plate (Luria broth or LB with agar, and 50 ug/mL ampicillin) into 2 mL of LB containing 50 µg/mL ampicillin, growing the culture

overnight, and mixing 1 mL of culture and 0.15 mL filter-sterilized (0.22 µm) glycerol in a 2 mL cryovial. The qPCR standards were obtained from the frozen stocks as follows:

1) *E. coli* cells containing the plasmids with the target genes (frozen stock at – 80 °C) were streaked on an LB plate containing 50 µg/mL ampicillin and grown overnight (16 h).
2) A few colonies (2 to 6) were transferred to a sterile glass tube with 5 mL of LB broth with 50 µg/mL ampicillin, capped and incubated (16 h) at 38 °C in a reciprocal shaker.
3) A volume of 1 mL of the culture was transferred to a 15-mL conical tube and centrifuged at 6800g for 15 minutes to pellet the bacterial cells.
4) The supernatant was discarded, and the pellet was resuspended with 44 µL nuclease free water in a 200 µL microcentrifuge tube for plasmid linearization.
5) The plasmid was linearized by adding 5 µL buffer, and 1 µL NotI-HF restriction enzyme (New England Biolabs, Ipswich, MA) to the resuspended plasmid, and digesting for 1 h at 37 °C, and 20 min at 65 °C.
6) The linearized plasmid was purified using a QIAprep Spin Miniprep Kit (Qiagen, Co., Hilden, Germany) following manufacturer's instructions, and DNA was quantified in triplicate using a Cytation3 microplate reader (BioTek Instruments, Winooski, VT).
7) The number of target gene copies of the stock standards was calculated as:

$$\text{No. of copies} = \frac{C_s\left(\frac{ng}{\mu L}\right) \times 6.022E23\left(\frac{copies}{mol}\right)}{MW_s\left(\frac{g}{mol}\right) \times 1E09\left(\frac{ng}{g}\right)} \quad \text{(eq. S9)}$$

Where: Cs was the concentration of the standard, and MWs was the molecular weight of the standard, obtained by multiplying the base pair length of the plasmid (TOPO® TA vector +

PCR insert of target gene) by the molecular weight of a base pair, estimated at 650 g per mol. Gene base pair lengths were 635, 491, 164, 425, and 267 for archaeal and bacterial *amo*A, *nir*K, *nir*S, and *nos*Z, respectively.

Inhibition testing was performed on a subset of samples by creating a DNA template consisting of a 1:1 mix of sample and standard of a known concentration and comparing the observed quantitation cycle (Cq) with the predicted Cq, determined from the standard curve (Cq = slope x (Log Concentration) + y-intercept) assuming a perfect mix. A sample was considered inhibited if the variation between the predicted and observed Cq was larger than 1 cycle, since the difference between sample replicates is not expected to be larger than 1 cycle, assuming a 0.5 cycle variability between replicates (Cao et al. 2012). In all cases measured Cq values were within less than 1 cycle of the predicted Cq.

Biological Reaction Rates and Times

N mineralization rate (N_{min}, μN/ m^3h) was estimated as a fixed fraction (1 mol N per 14 mol C) of the organic C mineralization rate (C_{min}) (Azizian et al. 2017), equivalent to a mass ratio of 1:12 N to C. N_{min} and its characteristic reaction time (τ_{min}) were:

$$N_{min} = \frac{1}{12}\left[\frac{\mu g\ N}{\mu g\ C}\right] \times C_{min} = \frac{1}{12}\left[\frac{\mu g\ N}{\mu g\ C}\right] \times \frac{\text{Flux } CO_2\left[\frac{\mu g\ C}{m^2\ h}\right]}{\text{biofilter depth [m]}} \quad \text{(eq. S10)}$$

$$\tau_{min}\ [h] = \frac{1}{k_{min}} = \frac{\text{OrgN}\left[\frac{\mu g\ N}{g\ dry\ soil}\right] \times \text{Bulk density}\left[\frac{g\ dry\ soil}{m^3}\right]}{N_{min}\left[\frac{\mu g\ N}{m^3 h}\right]} \quad \text{(eq. S11)}$$

Where OrgN was mineralizable N, equal to 5 to 20% of TN given minimum and average values for soils (Stanford et al. 1972), and k_{min} was the mineralization rate constant. Nitrification (N_{nit}) and denitrification (N_{den}) rates were obtained from published soil studies, since the NEA and DEA assays, which are a measure of potential activity, are not representative of actual environmental nitrification and denitrification rates.

4.9. Additional Figures and Tables

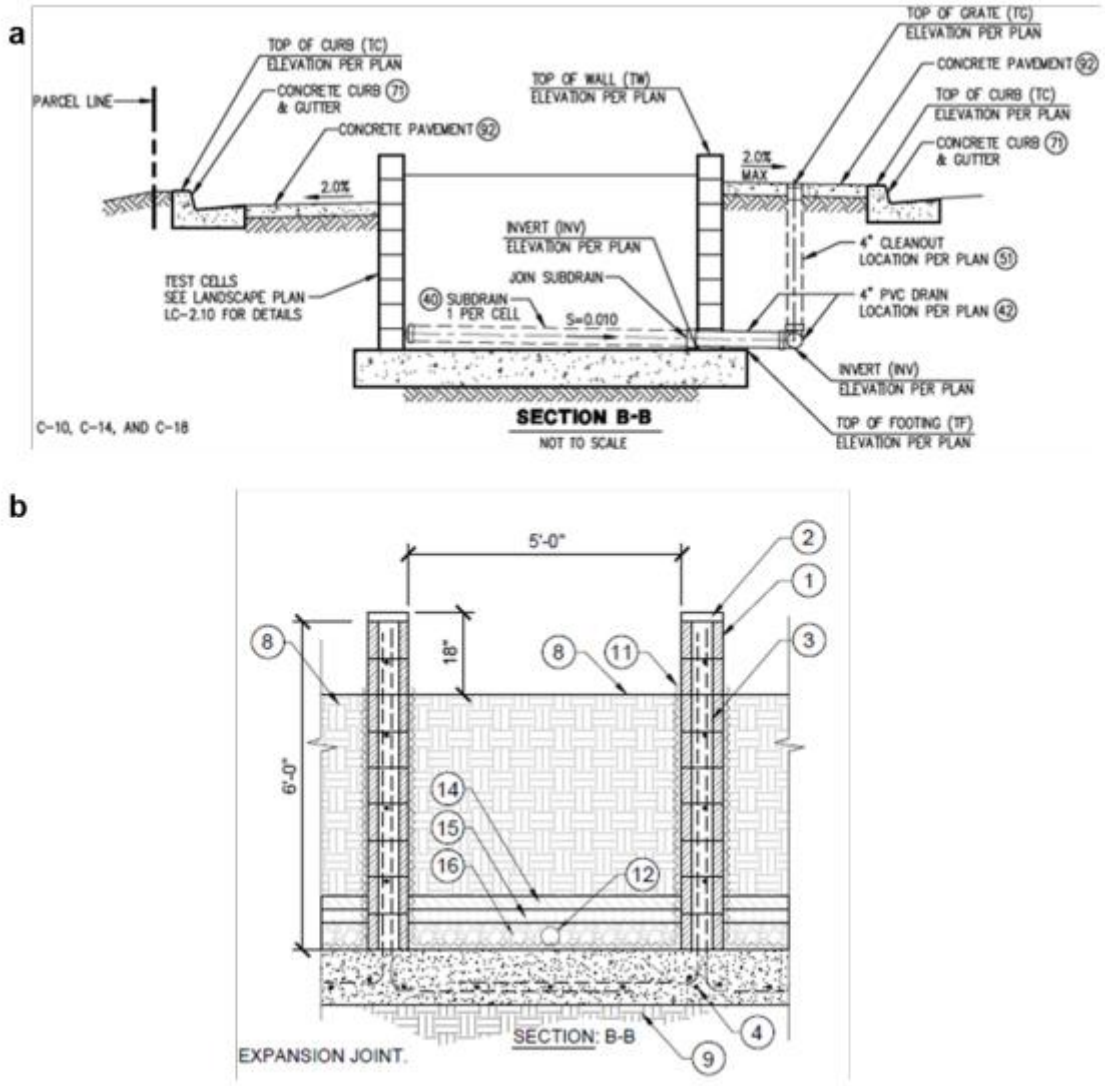

Figure S1. Cross-sectional design drawings of the study biofilters (a, and b). Key components in b are: (8) soil surface (the 6 ft depth refers to the wall height); (14) sand layer; (15) #8 Choke stone layer; (16) coarse aggregate layer; (12) perforated underdrain; (9) compacted subgrade to 90%; (11) Polycoat-Aquaseal 5000 waterproofing.

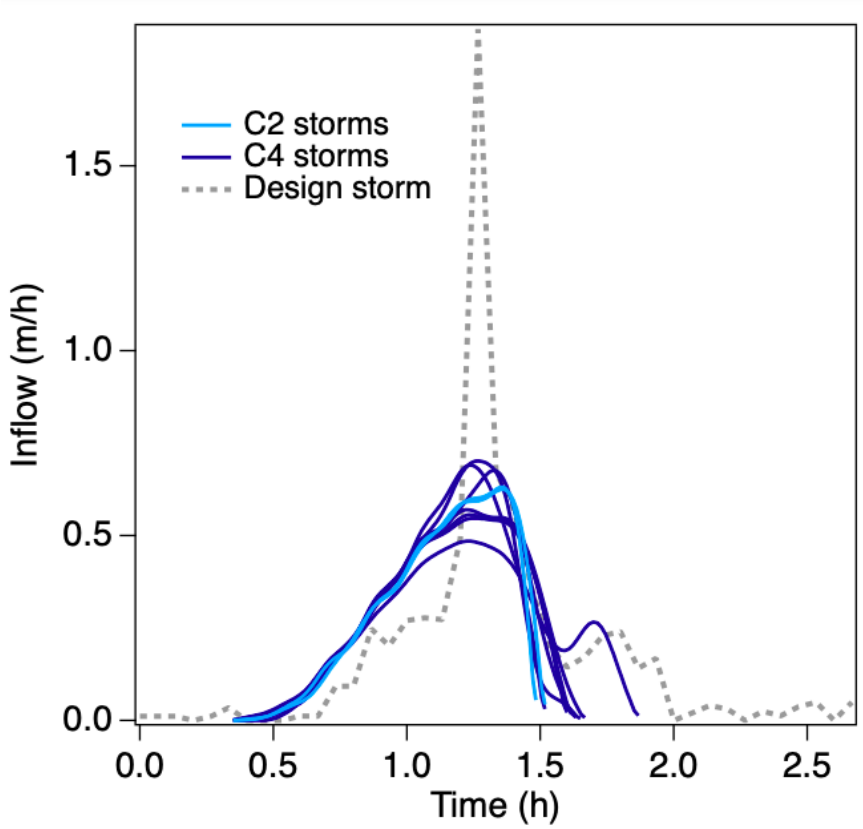

Figure S2. Hydrographs of design storm and storms S1 through S7, under transient flow conditions, in control (C2) and test (C4) biofilters (modified from Parker et al. 2021).

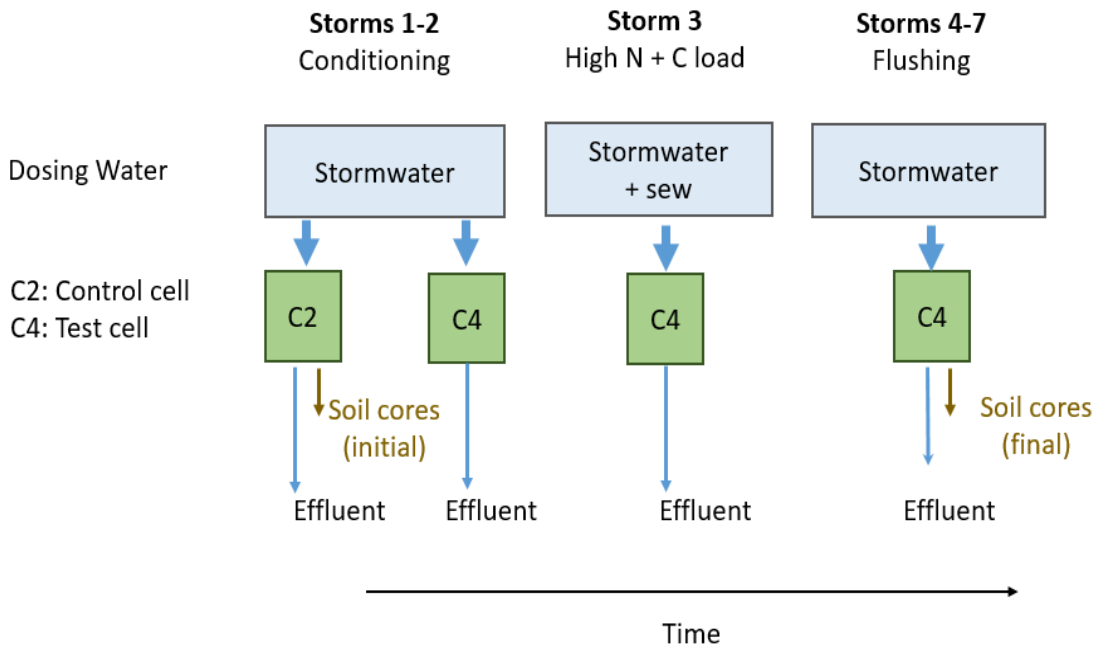

Figure S3. Stormwater runoff dosing and water and soil sampling schematic. There were three experimental phases: conditioning (storms 1-2) in control (C2) and test (C4) biofilters; stormwater runoff and sewage 1:1 mix dosing in C4; and flushing of C4 (storms 4 through 7). Core samples collected in C2 after the conditioning storms represented initial conditions, and core samples collected in C4 at the end of the experiment represented final conditions.

Figure S4. Chamber and metal base setup for CO_2, CH_4, and N_2O sampling. The chamber was shaded with reflective material prior to gas flux measurements, which were taken for 2 to 3 minutes for CO_2 and CH_4, and over a 30-minute period for N_2O. Due to chamber shading, CO_2 emissions corresponded to ecosystem respiration since photosynthetic activity was excluded.

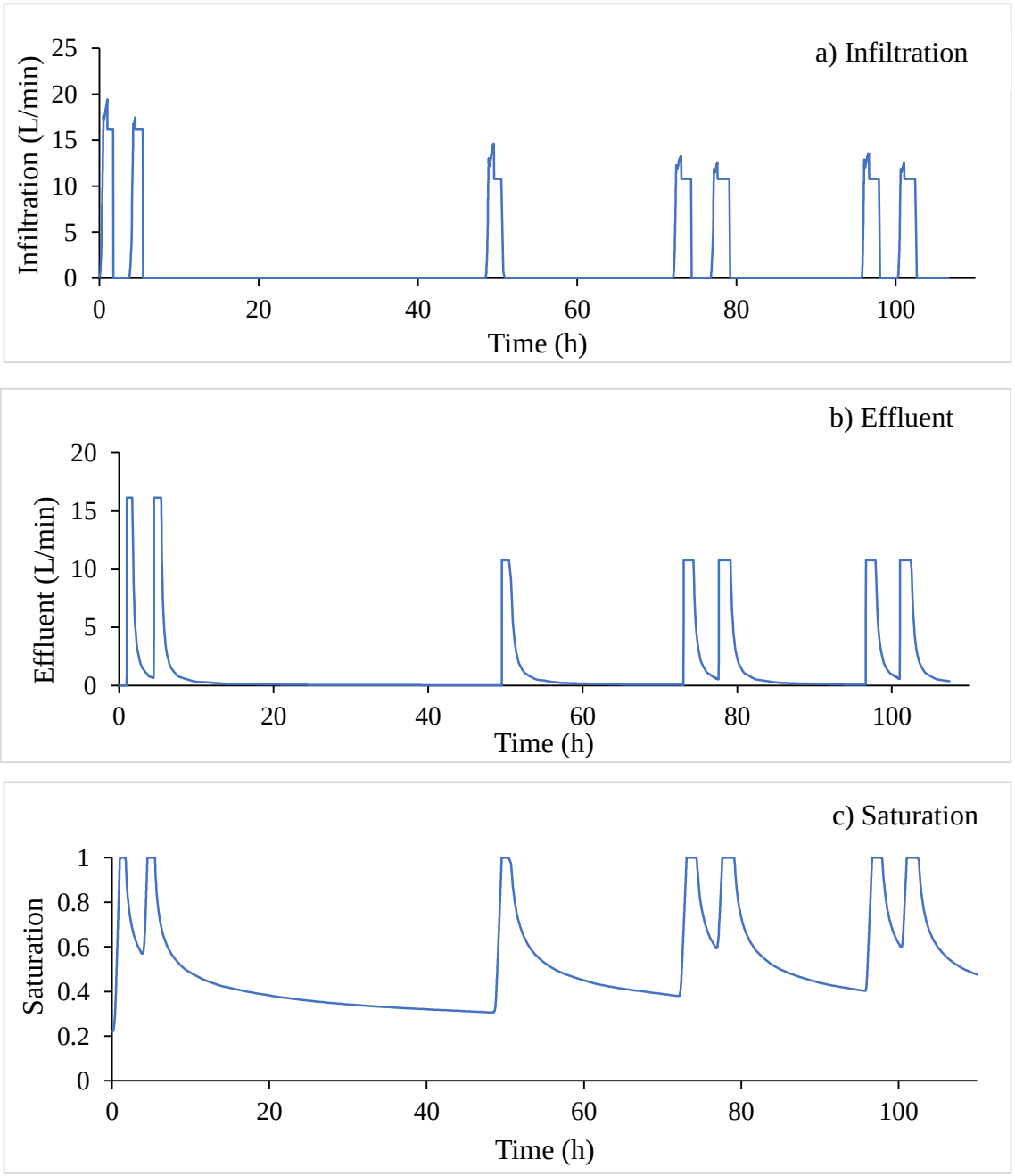

Figure S5. Infiltration (a) and discharge (b) flows, and soil saturation (c) in test biofilter C4 for storms S1 through S7, modeled via Hydrus 1D (in Parker et al. 2021) using field collected data for inflow and effluent flows. Saturation in between storm events increased with time.

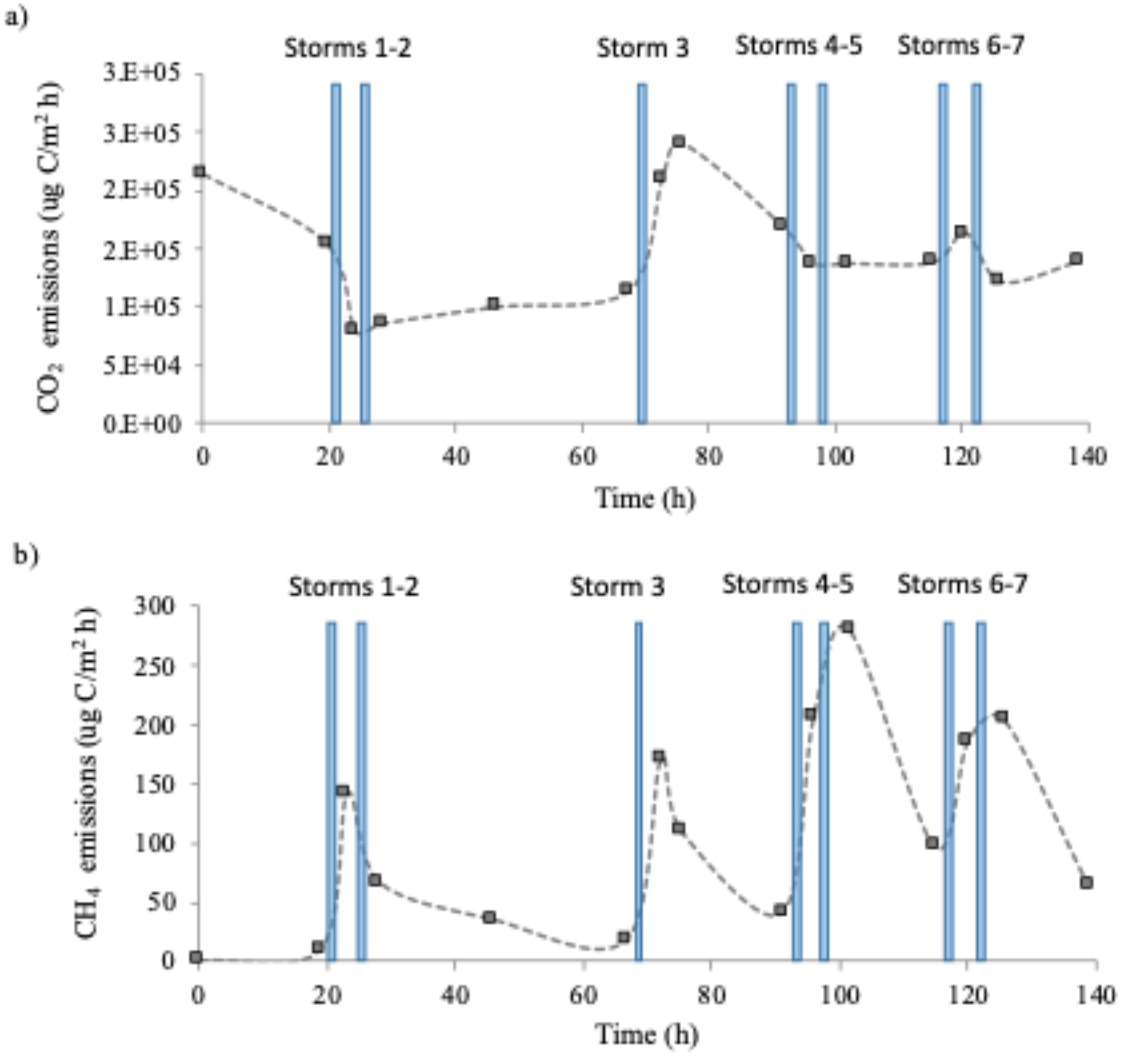

Figure S6. Emissions of CO_2 (a) and CH_4 (b) in test biofilter C4 for storms S1 through S7. Trends in between measured time points are inferred (dashed lines) but suggest a large peak in CO_2 emissions following storm 3, and an increase in average CH_4 emissions with time, as the biofilter becomes more saturated. Time zero corresponds to a baseline measurement.

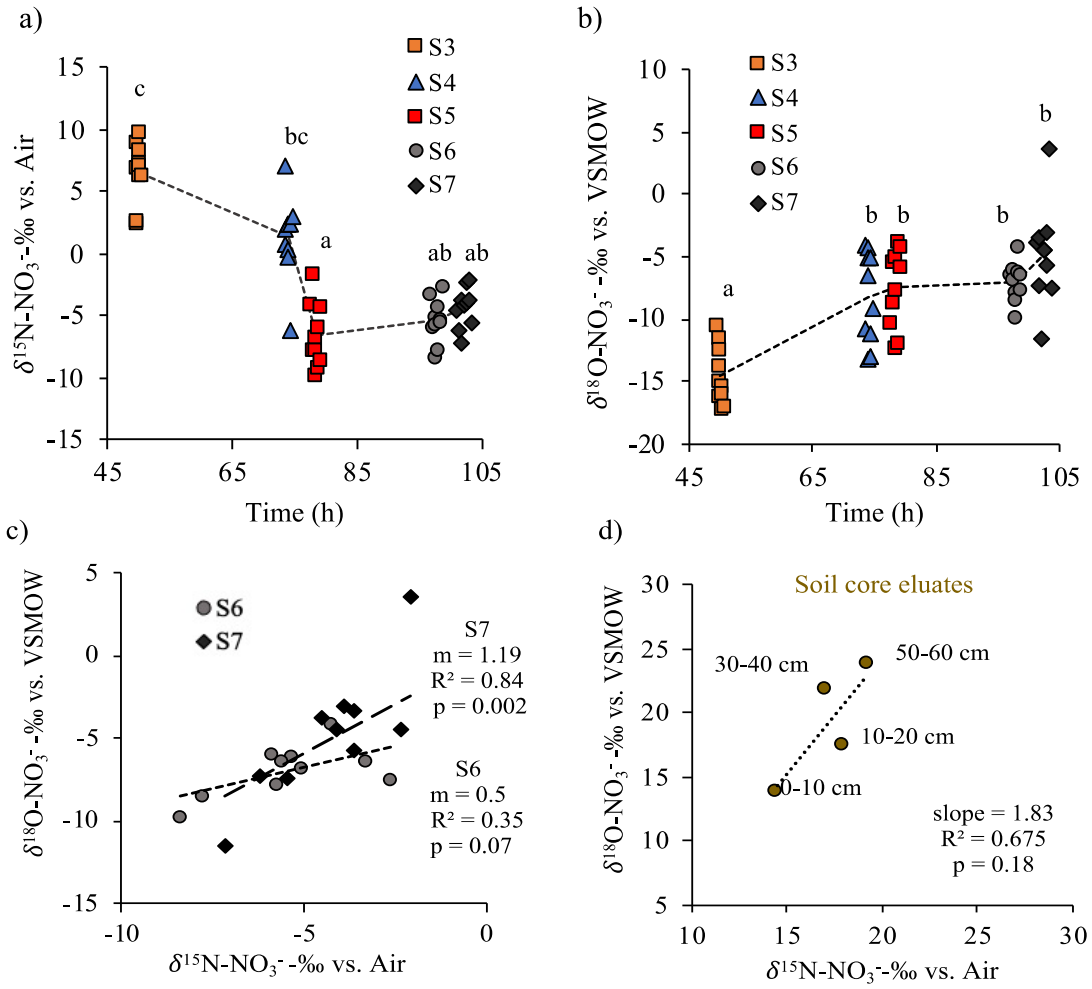

Figure S7. Evidence for nitrification and denitrification from dual nitrate isotope analysis. Depletion (decreasing trend) in õ^{15}N-NO_3^- from storms 3 to 5 (S3-5) (a), and enrichment (positive trend) for õ^{18}O-NO_3^- (b) in outflows of biofilter C4 during storms S3-7. Significant differences are denoted by letters a, b, and c, for Kruskal-Wallis and Dunn tests. Temporal trend in õ^{15}N-NO_3^- for outflows of storms 6 (S6) and 7 (S7), with slopes of 0.5 and 1.19 (c), and positive relationship with slope > 1 between õ^{15}N-NO_3^- and õ^{18}O-NO_3^- in soil eluate samples of biofilter C4 (d), suggest denitrification may be occurring.

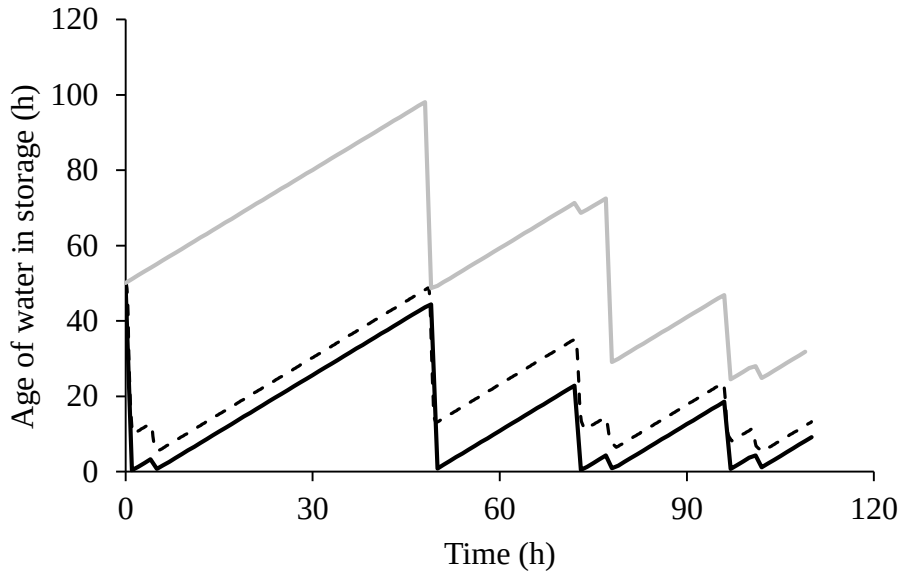

Figure S8. Age of water in storage for relevant sampling times, determined in (see Figure 5 in Parker et al. 2021). The mean age is shown in black dashed lines, the median age in continuous black lines, and the 95th percentile data in gray lines. The 5th percentile and median data overlap. When the biofilter receives storm inputs, the age of water in storage rapidly drops; age increases during draining periods in between storms. Initial water age (time zero) was assumed to be 50 h.

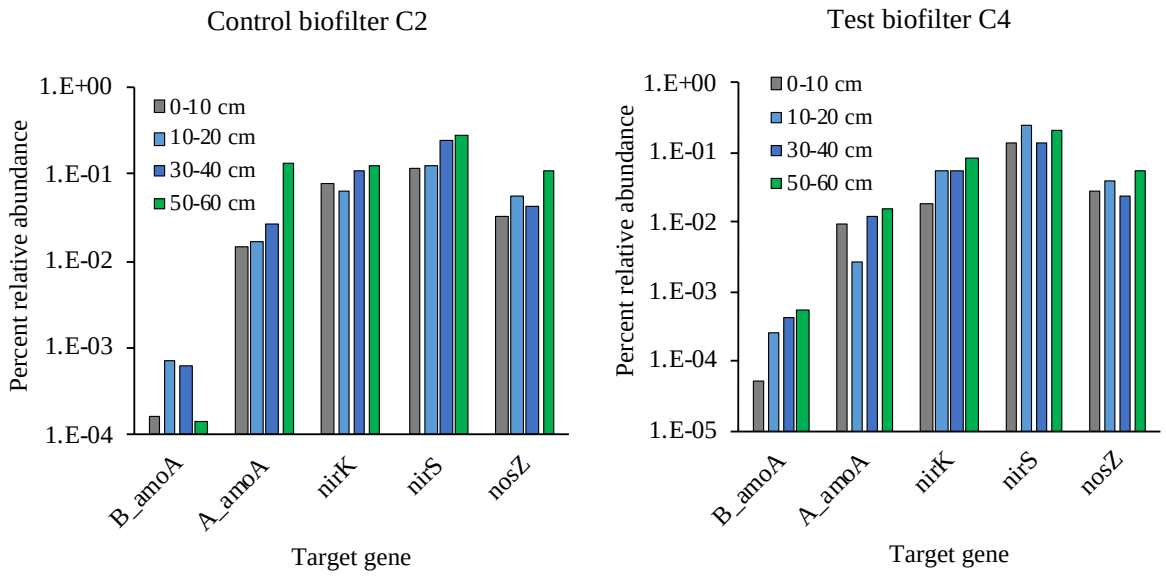

Figure S9. Relative abundances, normalized to 16S rRNA, of archaeal *amoA* (B_amoA) and bacterial *amoA* (B_amoA), *nirK*, *nirS*, and *nosZ* genes in control (C2) and test (C4) biofilter soil samples at depths of 0 to 10 cm, 10 to 20 cm, 30 to 40 cm, and 50 to 60 cm. Bars represent mean value of three analytical replicates. There are no significant differences between C2 and C4.

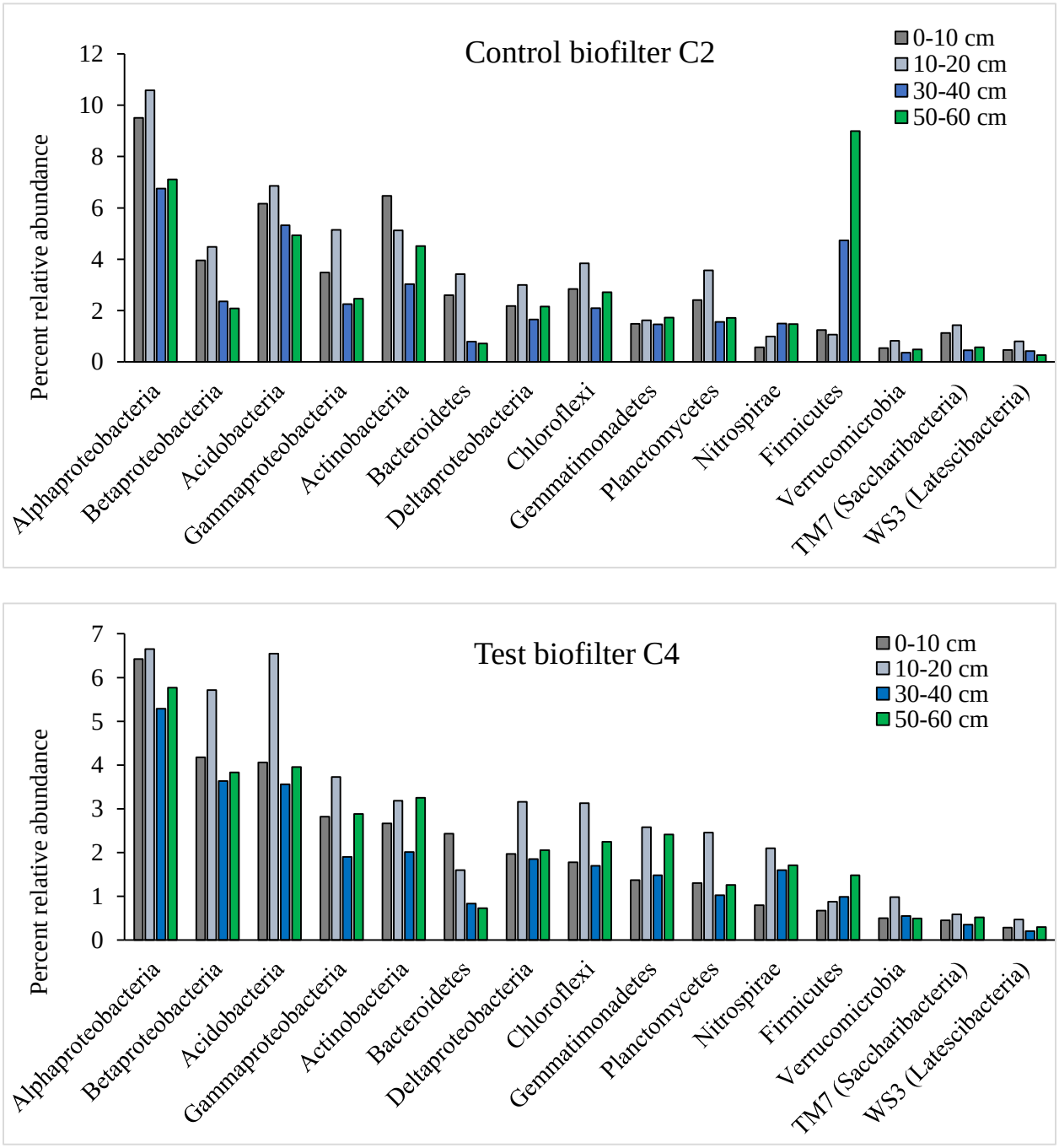

Figure S10. Top 15 assigned bacterial phyla in soils of control C2 (a) and test C4 (b) biofilters based on 16S rRNA gene sequencing results.

Table S1. Biofilter design specifications.

Parameter	**Specification**
Length (m)	2.4
Width (m)	1.5
Surface area (m^2)	3.6
Soil depth (m)	0.6
Freeboard (m)	0.5
Porosity	0.41
Design infiltration rate (m/h)	0.13
Hydraulic loading rate (m/h)	0.5

Table S2. Soil characterization for control (C2) and test (C4) biofilters. Soil samples are for depths 1) 0-10 cm, 2) 10-20 cm, 3) 30-40 cm, and 4) 50-60 cm. Values are on a dry soil basis, and for single measurements, except for moisture, SOM, and SIR (n = 3) (mean and standard deviation in parentheses).

Sample ID	Moisture (%)	pH	SOM [a] (%)	DOC (mg C/kg soil)	SIR [b] (mg C/kg soil .d)	TC (%) [c]	TN (%) [c]	C:N (mol basis)	NH_4^+ mg N/kg soil	NO_3^- (mg N/kg soil)	CEC [d] (meq/ 100g soil)	Sand (%) [c]	Silt (%) [c]	Clay (%) [c]
C2-1	15.0 (0.69)	7.65	4.19 (0.78)	15.69	7.56 (0.16)	1.73	0.09	21.7	1.30	3.52	11.9	81	9	10
C2-2	17.0 (0.19)	7.57	4.11 (0.26)	17.09	7.08 (0.05)	1.60	0.12	16.1	1.05	4.61	13.0	81	9	10
C2-3	14.7 (0.24)	7.71	2.74 (0.10)	16.16	2.36 (0.09)	1.08	0.09	13.9	1.17	1.72	10.5	79	9	12
C2-4	17.7 (0.44)	7.65	1.71 (NA)	14.07	3.30 (0.11)	1.02	0.08	14.9	1.71	1.98	11.9	80	8	12
C4-1	14.3 (0.37)	7.65	3.18 (0.05)	10.58	3.61 (0.21)	1.03	0.09	14.1	1.87	4.68	11.1	85	8	7
C4-2	14.8 (0.07)	7.67	2.93 (0.03)	11.05	2.56 (0.14)	1.07	0.08	16.0	1.70	4.14	11.2	85	7	8
C4-3	19.5 (0.25)	7.70	2.96 (0.03)	9.60	1.59 (0.26)	0.81	0.07	13.7	1.68	1.63	11.2	83	9	8
C4-4	24.9 (0.75)	7.54	2.92 (0.05)	7.39	0.74 (0.04)	1.37	0.06	25.0	0.49	0.81	11.3	81	10	9

[a] SOM is the soil organic matter.

[b] SIR is the substrate induced respiration method, used as a proxy for microbial biomass.

[c] Percentages are given on a mass basis.

[d] CEC is the cation exchange capacity.

Table S3. Reactions, primers, standards and thermocycling conditions for qPCR.

Target Gene	Primer sequences and references	Reaction mix	Volume (µL)	Thermal profile[(a)]
		Master mix	12.5	40 cycles:
Arch.	F: STAATGGTCTGGCTTAGA	Arch_amoAF (10 µM)	1.5	95 °C - 30 s
amoA	CG	Arch_amoAR (10 µM)	1.5	53 °C - 45 s
	R: GCGGCCATCCATCTGTAT	Nuclease free water	4.5	72 °C - 1 min
	GT	DNA template (3 ng/µL)	5	
	Francis et al. (2005)			
	Santoro et al. (2008)			
		Master mix	12.5	40 cycles:
Bact.	F: GGGGTTTCTACTGGTGGT	amoA1F (10 µM)	1.25	95 °C – 1 min
amoA	R: CCCCTCKGSAAAGCCTTC	amoA2R (10 µM)	1.25	60 °C – 1 min
	TTC	Nuclease free water	5	72 °C - 1 min
	(Rotthauwe et al. 1997)	DNA template (3 ng/µL)	5	
		Master mix	12.5	6 cycles:
nirK	F: ATYGGCGGVAYGGCGA	nirK876C (10 µM)	1.25	95 °C - 15 s
	R: GCCTCGATCAGRTTRTG	nirK1040 (10 µM)	1.25	63-58 °C - 30 s
	GTT	Nuclease free water	5	72 °C - 30 s
		DNA template (3 ng/µL)	5	80 °C - 30 s
				40 cycles:
				95 °C - 15 s
	Henry et al. (2004)			62 °C - 30 s
	Waller et al. (2018)			72 °C - 30 s
				80 °C - 30 s
		Master mix	12.5	40 cycles:
nirS	F: GTSAACGTSAAGGARACS	cd3af (10 µM)	1.5	95 °C - 1 min
	GG	R3cd (10 µM)	1.5	56 °C - 1 min
	R: GASTTCGGRTGSGTCTTG	Nuclease free water	4.5	72 °C - 1 min
	A	DNA template (3 ng/µL)	5	
	(Michotey et al. 2000)			
	(Throback et al. 2004)			
		Master mix	12.5	6 cycles:
nosZ	F: CGCRACGGCAASAAGGTS	nosZ 2F (10 µM)	1.25	95 °C - 15 s
	MSSGT	nosZ 2R (10 uM)	1.25	67-62 °C - 30 s
	R: CAKRTGCAKSGRTGGCAG	Nuclease free water	5	72 °C - 15 s
	AA	DNA template (3 ng/µL)	5	80 °C - 15 s
				40 cycles:
				95 °C - 15 s
	(Henry et al. 2006)			62 °C - 30 s
				72 °C - 15 s
				80 °C - 15 s
		Master mix	12.5	40 cycles:
16S	F: ATGGCTGTCGTCAGCT	16S rRNA-F (12 µM)	1.25	95 °C - 40 s
rRNA	R: ACGGGCGGTGTGTAC	16S rRNA-R (12 µM)	1.25	60 °C - 45 s
		Nuclease free water	8	72 °C - 1 min
	(Pan and Chu 2018)	DNA template (1 ng/µL)	2	

a) All methods include an enzyme activation step consisting of 2 min at 50 °C and 10 min at 95 °C.

Table S4. CO_2, CH_4, and N_2O emissions from test biofilter C4 and sampling details.

Sample description	Sampling date	Time (h)	Sampling time	Temp (°C)	Flux N_2O (ug N/m^2h)	Flux CO_2 (mg C/m^2h)	Flux CH_4 (ug C/m^2h)
Baseline 1	5/30/19	0	11:03 am	26.7	30.94	NA	NA
Baseline 2	5/30/19	0	12:25 pm	32.9	26.44	213.83	ND
Prior to S1	6/1/19	18.9	7:20 am	21.2	58.17	154.34	10.19
After S1	6/1/19	23.1	11:29 am	22.0	13.50	79.47	141.98
After S2	6/1/19	28.0	4:24 pm	25.0	12.80	86.04	66.76
Day after S1-2	6/2/19	45.6	10:01 am	21.7	60.33	100.07	35.32
Prior to S3	6/3/19	66.6	7:01 am	20.8	75.20	113.48	17.59
After S3 (1)	6/3/19	72.0	12:24 pm	30.1	72.34	210.00	170.00
After S3 (2)	6/3/19	75.3	3:41 pm	30.5	64.91	239.73	109.38
Prior to S4	6/4/19	91.0	7:24 am	20.9	72.84	169.43	40.57
After S4	6/4/19	95.8	12:33 pm	24.6	15.93	137.91	205.52
After S5	6/4/19	101.4	6:09 pm	26.3	40.12	137.38	280.11
Prior to S6	6/5/19	114.8	7:12 am	21.8	84.30	138.33	96.23
After S6	6/5/19	120.0	12:22 pm	28.3	17.05	163.78	185.83
After S7	6/5/19	125.6	6:03 pm	28.5	40.16	121.61	203.87
Day after S6-7	6/6/19	138.7	7:05 m	22.5	53.77	139.46	64.45

Notes: S1-S7 refer to storms S1 through S7. Baseline samples were taken prior to stormwater runoff dosing, which commenced on June 1st, 2019, at 9:16 am. The timing of "Baseline 2" (measured on test biofilter C4) was used as time zero, and time for "Baseline 1" (collected in control C2) was also set to zero for N_2O emissions. ND indicates emissions were not detectable, and NA (not available) indicates measurement was not performed.

Table S5. Dual nitrate isotope analysis for inflow and outflows in storms 1 through 7 (S1-7), and soil eluates from cored samples in the test biofilter C4. The $\delta^{18}O\text{-}NO_3^-$ values are reported relative to Vienna Standard Mean Ocean Water (VSMOW), and $\delta^{15}N\text{-}NO_3^-$ is reported relative to N_2 in air (AIR).

Sample Name	NO_3^- (mg N/L)	$\delta^{18}O\text{-}NO_3^-$ ‰ vs. VSMOW	$\delta^{15}N\text{-}NO_3^-$ ‰ vs. Air
Inflows			
S3, sewage	1.3	29.7	18.4
S3, stormwater runoff	0.1	38.3	19.7
S3 (1:1 mix)	0.1	37.3	21.7
S4	0.0	33.0	23.7
S5	0.0	36.4	19.6
S6	0.0	36.3	21.2
S7	0.0	38.2	20.2
Outflows			
S3-1	2.9	-10.4	9.1
S3-2	1.2	-14.9	2.5
S3-3	1.8	-13.8	2.6
S3-4	3.5	-11.5	6.9
S3-5	3.4	-12.4	6.3
S3-6	2.8	-16.2	7.3
S3-7	2.4	-15.4	9.7
S3-8	2.0	-15.9	8.3
S3-9	2.3	-17.1	7.1
S3-10	1.8	-17.0	6.4
S4-1	1.7	-10.6	7.0
S4-2	1.7	-4.0	2.1
S4-3	1.8	-4.1	0.8
S4-4	1.8	-6.5	0.3
S4-5	1.8	-5.1	-0.2
S4-6	1.9	-13.1	2.4
S4-7	1.8	-12.9	2.5
S4-8	1.7	-5.0	-6.2
S4-9	1.7	-11.0	2.4
S4-10	1.5	-9.1	3.0

Table S5. (Continued)

Sample Name	NO_3^- (mg N/L)	$\delta^{18}O\text{-}NO_3^-$ ‰ vs. VSMOW	$\delta^{15}N\text{-}NO_3^-$ ‰ vs. Air
Outflows			
S5-1	1.1	-10.3	-4.1
S5-2	1.3	-8.6	-1.6
S5-3	1.3	-5.4	-7.7
S5-4	1.6	-7.6	-7.9
S5-5	1.3	-5.0	-6.7
S5-6	0.8	-12.2	-9.8
S5-7	1.4	-11.9	-9.2
S5-8	1.3	-3.8	-6.0
S5-9	1.7	-4.2	-4.3
S5-10	0.9	-5.9	-8.6
S6-1	1.3	-6.4	-3.3
S6-2	1.6	-6.0	-5.9
S6-3	1.6	-6.8	-5.1
S6-4	1.9	-7.7	-5.8
S6-5	1.3	-9.8	-8.4
S6-6	1.5	-8.4	-7.8
S6-7	1.3	-4.2	-4.3
S6-8	1.2	-6.2	-5.4
S6-9	0.8	-6.3	-5.6
S6-10	1.8	-7.5	-2.6
S7-1	1.1	-3.7	-4.5
S7-2	1.8	-7.3	-6.2
S7-3	1.1	-3.3	-3.7
S7-4	1.9	-11.4	-7.2
S7-5	1.2	-4.4	-4.1
S7-6	1.1	-4.4	-2.3
S7-7	1.2	-3.0	-3.9
S7-8	1.5	-5.7	-3.6
S7-9	1.1	3.7	-2.1
S7-10	1.4	-7.4	-5.5
Soil eluates (cores)			
C4-1 (0-10 cm)	0.1	13.9	14.5
C4-2 (10-20 cm)	0.2	17.5	18.0
C4-3 (30-40 cm)	0.2	21.9	17.1
C4-4 (50-60 cm)	0.2	23.8	19.2

Table S6. qPCR results for 16S rRNA, nitrifying, and denitrifying genes in biofilter soils. Values are reported as gene copy numbers per gram of dry soil.

Biofilter	Sample section	Bacterial *amo*A	Archaeal *amo*A	*nir*K	*nir*S	*nos*Z	16S rRNA
C2	0-10 cm	2.4E+03	2.1E+05	1.2E+06	1.8E+06	5.0E+05	1.5E+09
	10-20 cm	2.3E+04	5.3E+05	2.0E+06	4.0E+06	1.8E+06	3.2E+09
	30-40 cm	1.1E+04	4.5E+05	1.9E+06	4.2E+06	7.2E+05	1.7E+09
	50-60 cm	1.3E+03	1.2E+06	1.1E+06	2.6E+06	1.0E+06	9.2E+08
C4	0-10 cm	1.2E+03	2.3E+05	4.5E+05	3.4E+06	6.6E+05	2.4E+09
	10-20 cm	1.4E+04	1.6E+05	3.1E+06	1.5E+07	2.2E+06	5.7E+09
	30-40 cm	1.1E+04	3.2E+05	1.5E+06	3.5E+06	6.2E+05	2.7E+09
	50-60 cm	7.5E+03	2.1E+05	1.1E+06	2.9E+06	7.6E+05	1.4E+09

Table S7. Mass balance in soil compartment of test biofilter C4 for storms S1 through S7. Calculation details are included in Methods, section 4.2.7.

Sampling details	Soil section	Ammonium (mg)	Nitrate (mg)	Total N (mg)
Initial conditions (prior to storm 3, sampled in control cell C2)[a]	0-10 cm	6.11E+02	1.66E+03	4.23E+07
	10-20 cm	4.94E+02	2.17E+03	5.64E+07
	20-30 cm	5.22E+02	1.49E+03	4.94E+07
	30-40 cm	5.50E+02	8.09E+02	4.23E+07
	40-50 cm	6.77E+02	8.70E+02	4.00E+07
	50-60 cm	8.04E+02	9.31E+02	3.76E+07
	Total	3.66E+03	7.93E+03	2.68E+08
Final conditions (after storm 7, sampled in test cell C4)	0-10 cm	9.98E+02	2.50E+03	4.80E+07
	10-20 cm	9.07E+02	2.21E+03	4.27E+07
	20-30 cm	9.02E+02	1.54E+03	4.00E+07
	30-40 cm	8.97E+02	8.70E+02	3.74E+07
	40-50 cm	5.79E+02	6.51E+02	3.47E+07
	50-60 cm	2.62E+02	4.32E+02	3.20E+07
	Total	4.55E+03	8.20E+03	2.35E+08
Total balance (final - initial)	0-60 cm	8.85E+02	2.77E+02	-3.33E+07

[a] Soil nutrient status in control biofilter C2 after the conditioning storms 1-2 was used to approximate initial nutrient concentrations in test biofilter C4.

4.10. Additional references

Altabet, M.A., Wassenaar, L.I., Douence, C., and Rupsa, R. (2019). A Ti(III) reduction method for one-step conversion of seawater and freshwater nitrate into N2O for stable isotopic analysis of 15N/14N, 18O/16O and 17O/16O. *Rapid Commun. Mass Spectrom.*, 33, 1227-1239.

Azizian, M., Boano, F., Cook, P. L. M., Detwiler, R. L., Rippy, M. A., and Grant, S. B. (2017). Ambient groundwater flow diminishes nitrate processing in the hyporheic zone of streams. *Water Resour. Res.*, 53, 3941-3967.

Barnard, R., Le Roux, X., Hungate, B. A., Cleland, E. E., Blankinship, J. C., Barthes, L., and Leadley, P. W. (2006) Several components of global change alter nitrifying and denitrifying activities in an annual grassland. *Funct. Ecol.*, 20, 557-564.

Belser, L. W., and Mays, E. L. (1980). Specific inhibition of nitrite oxidation by chlorate and its use in assessing nitrification in soils and sediments. *Appl. Environ. Microbiol*., 39, 505-510.

Boehm, A. B., Griffith, J., McGee, C., Edge, T. A., Solo-Gabriele, H. M., Whitman, R., Cao, Y., Getrich, M., Jay, J. A., Ferguson, D., Goodwin, K. D., Lee, C. M., Madison, M., and Weisberg, S. B. (2009) Faecal indicator bacteria enumeration in beach sand: a comparison study of extraction methods in medium to coarse sands. *J. Appl. Microbiol*., 107, 1740-1750.

Bustin, S.A., Benes, V., Garson, J.A., Hellemans, J., Huggett, J., Kubista, M., Mueller, R., Nolan, T., Pfaffl, M.W., Shipley, G.L., Vandesompele, J., and Wittwer, C.T. (2009). The MIQE guidelines: Minimum information for publication of quantitative real-time PCR experiments. *Clin. Chem.*, 55, 611-622.

Cao, Y., Griffith, J. F., Dorevitch, S., and Weisberg, S. B. (2012). Effectiveness of qPCR permutations, internal controls and dilution as means for minimizing the impact of inhibition while measuring Enterococcus in environmental waters. *J. Appl. Microbiol*., 113(1), 66-75.

Casciotti, K. L., Sigman, D. M., Hastings, M. G., Böhlke, J. K., and Hilkert, A. (2002). Measurement of the oxygen isotopic composition of nitrate in seawater and freshwater using the denitrifier method. *Anal. Chem*., 74(19), 4905-4912.

Coplen, T. B. (2011). Guidelines and recommended terms for expression of stable-isotope-ratio and gas-ratio measurement results. *Rapid Comm. Mass Spectrom.*, 25, 2538-2560.

Coplen, T.B. (2021). Report of stable isotopic composition. Reference Materials USGS32, USGS34, and USGS35 (nitrogen and oxygen isotopes in nitrate).

Ervin, J. S., Van De Werfhorst, L. C., Murray, J. L. S., and Holden, P. A. (2014). Microbial source tracking in a coastal California watershed reveals canines as controllable sources of fecal contamination. *Environ. Sci. Technol.*, 48, 9043-9052.

Fierer, N., Schimel, J. P., and Holden, P. A. (2003). Variation in microbial community composition through two soil depth profiles. *Soil Biol. Biochem.* 35, 167-176.

Foreman, R. K., Segura-Noguera, M., and Karl, D. M. (2016). Validation of Ti (III) as a reducing agent in the chemiluminescent determination of nitrate and nitrite in seawater. *Mar. Chem.*, 186, 83- 89.

Francis, C. A., Roberts, K. J., Beman, J. M., Santoro, A. E., and Oakley, B. B. (2005). Ubiquity and diversity of ammonia-oxidizing archaea in water columns and sediments of the ocean. *Proc. Natl Acad. Sci.*, 102, 14683-14688.

Gardner, W. H. (1986). Water content, In: Methods of soil analysis, part 1- Physical and mineralogical methods (2nd edition), Klute, A. (Ed.), American Society of Agronomy, Agronomy Monographs 9(1), Madison, WI, 493-544.

Hart, S. C., Stark, J. M., Davidson, E. A. and Firestone, M. K. (1994). Nitrogen mineralisation, immobilisation, and nitrification. In: Methods of soil analysis: part 2 - Microbiological and biochemical properties, Bezdiecek, D. (Ed.), Soil Science Society of America, Madison, WI, 985-1018.

Henry. S., Baudoin, E., López-Gutiérrez, J. C., Martin-Laurent, F., Brauman, A., and Philippot, L. (2004). Quantification of denitrifying bacteria in soils by nirK gene targeted real-time PCR. *J. Microbiol. Methods*, 59(3), 327-335.

Henry, S., Bru, D., Stres, B., Hallet, S., and Philippot, L. (2006). Quantitative detection of the nosZ gene, encoding nitrous oxide reductase, and comparison of the abundances of 16S rRNA, narG, nirK, and nosZ genes in soils. *Appl. Environ. Microbiol.*, 72(18), 5181-5189.

International Atomic Energy Agency (IAEA) (2017). Reference sheet for international measurement standards. Available at: https://nucleus.iaea.org/sites/ReferenceMaterials/Shared%20Documents/ReferenceMaterials/StableIsotopes/VSMOW2/VSMOW2_SLAP2.pdf

Kalbitz K, Solinger S, Park J-H, Michalzik B, Matzner E (2000) Controls on the dynamics of dissolved organic matter in soils: a review. *Soil Sci*., 165, 277-304. Available at: https://journals.lww.com/soilsci/Fulltext/2000/04000/CONTROLS_ON_THE_DYNAMICS_OF_DISSOLVED_ORGANIC.1.aspx

Michotey V., Mejean V., and Bonin P. (2000). Comparison of methods for quantification of cytochrome cd1-denitrifying bacteria in marine samples. *Appl. Environ. Microbiol*., 66(4), 1564-1571.

Mulvaney, R. L. (1996). Nitrogen - inorganic forms, In: Methods of Soil Analysis, Part 3 - Chemical Methods. SSSA Book Series No. 5. Sparks D. L. (Ed.), Soil Science Society of America, Madison, WI, 1129-1131.

Nelson, D. W., and Sommers, L. E. (1996). Total carbon, organic carbon, and organic matter, In: Methods of Soil Analysis, Part 3 - Chemical Methods. SSSA Book Series No. 5. Sparks D. L. (Ed.)., Soil Science Society of America, Madison, WI, 1002-1005.

Pan, M., and Chu, L.M. (2018). Occurrence of antibiotics and antibiotic resistance genes in soils from wastewater irrigation areas in the Pearl River Delta region, southern China. *Sci. Total Environ.,* 624, 145-152.

Rotthauwe, J. H., Witzel, K. P., and Liesack, W. (1997). The ammonia monooxygenase structural gene amoA as a functional marker: molecular fine-scale analysis of natural ammonia-oxidizing populations. *Appl. Environ. Microbiol*., 63(12), 4704-4712.

Santoro A. E., Francis, C. A., De Sieyes, N. R., and Boehm, A. B. (2008). Shifts in the relative abundance of ammonia-oxidizing bacteria and archaea across physicochemical gradients in a subterranean estuary. *Environ. Microbiol.*, 10(4), 1068-1079.

Sigman, D. M., Casciotti, K. L., Andreani, M., Barford, C., Galanter, M., and Böhlke, J. K. (2001). A bacterial method for the nitrogen isotopic analysis of nitrate in seawater and freshwater. *Anal. Chem*., 73(17), 4145-4153.

Stanford, G., and Smith, S. J. (1972). Nitrogen mineralization potential of soils. *Soil Sci. Soc. Am. Proc*. 36, 465-472.

Tiedje, J. M. and Smith, and M. S. (1979). Phases of denitrification following oxygen depletion in soil. *Soil Biol. Biochem.*, 11(3), 261-267.

Thomas, G. W. (1996). Soil pH and soil acidity, In: Methods of Soil Analysis, Part 3 - Chemical Methods. SSSA Book Series No. 5. Sparks D. L. (Ed.), Soil Science Society of America Madison, WI, 475-490.

Throback, I. N., Enwall, K., Jarvis, A., and Hallin, S. (2004). Reassessing PCR primers targeting nirS, nirK and nosZ genes for community surveys of denitrifying bacteria with DGGE. *FEMS Microbiol. Ecol.*, 49(3), 401-417.

Waller, L. J., Evanylo, G. K., Krometis, L-A. H., Strickland, M., Wynn-Thompson, T. M., and Badgley, B. D. (2018). Engineered and environmental controls of microbial denitrification in established bioretention cells. *Environ. Sci. Technol*., 52(9), 5358-5366.

West, A., and Sparling, G. (1986). Modifications to the substrate-induced respiration method to permit measurement of microbial biomass in soils of differing water contents. *J. Microbiol. Methods*, 5(3-4), 177-189.

Chapter 5. Conclusions and Future Research

5.1 Conclusions

This doctoral dissertation research has provided insights into the effects of soil accumulated metals on soil nitrifying and denitrifying bacteria, and N cycling in stormwater biofilters. Further, this research has contributed to the increased understanding of N processing under dynamic flow conditions, and how biofilters respond to high nutrient loading and high-flow events.

The first study (Chapter 2) shows that metals can accumulate in biofilter soils in residential areas, but that concentrations are similar to background soil metal concentrations, and below screening levels. Yet, the positive relationship between soil metal concentrations and metrics that combine biofilter properties, and drainage area characteristics, indicates that easily computed metrics may be used to guide monitoring and risk assessment efforts. The good agreement between measured metal concentrations, and concentrations predicted through annual metal loads is also promising. Results suggest that in more polluted watersheds, simple calculations may be used to estimate metal concentrations. Only readily accessible data is needed, such as runoff volume estimates, drainage area to biofilter area ratios, and runoff metal concentrations. The proposed approach may help stormwater managers prioritize monitoring efforts in sites with higher expected metal pollution.

The positive relationships between biofilter drainage area and metal accumulation, observed even in lightly contaminated watersheds motivated further investigation of metal accumulation in biofilters that were experiencing a broader range of metal pollution.

Overlaid onto this study, was the potential interaction between accumulated metals and soil nitrifying and denitrifying bacteria. This study (Chapter 3) shows that soil properties predominantly influence functional gene abundance of nitrifying and denitrifying bacteria, but that metals also influence nitrifying and denitrifying functional gene abundances.

The final study (Chapter 4) indicates that typical biofilter designs predominantly nitrify influent or existing NH_4^+ in the dry periods in between storms, and that the biofilter persistently exports NO_3^- in subsequent storms. Denitrification is occurring, but it is limited. Results showed that the biofilter was a net NO_3^- exporter, with potential consequences to groundwater contamination and water quality in receiving surface waters. To promote denitrification, I propose to increase residence times by using a treatment train consisting of a stormwater capture system, followed by slow- and fast- draining cells.

Taken together, this doctoral research has advanced the understanding of potential interactions between soil accumulated metals and nitrifying and denitrifying bacteria in bioretention soils. This research has also shown the extent to which biofilters may export N under current designs, which may have been previously underestimated. The discrepancy between biofilter water residence times, and times needed for reaction, can only support limited N processing during storm events. The major N fate is nitrification of initially retained ammonium, in between storms. Biofilters appear to be net mineralizers and net nitrifiers under high loading events, which highlight the need for special consideration for large storms. Although biofilters may be able to fully capture a large storm event and meet hydrologic goals, this will be at the expense of persistent nitrate export in subsequent storms.

5.2 Future Research

A few questions emerge from this dissertation work and motivate future research.

1. To what extent is total metal accumulation in biofilters determined by system age, and the ratio of impervious drainage area to biofilter area, vs. soil properties?

In Chapter 2, total Zn and the ratio of the directly connected impervious area to the biofilter area (impervious ratio) were positively related, so that calculations of annual metal loads were suitable to predict metal concentrations. This simple approach was tested in similarly designed biofilters exposed to limited metal contamination; a logical next step is to test this approach over a broader range of biofilter designs and metal contamination. Exploring this question requires sampling biofilter soils, assessing metals and relevant soil properties, evaluating model fit, and refining modeling efforts using measured soil properties.

Preliminary exploration of the biofilters included in the second study (Chapter 3) suggests that this approach may be valid, but that introducing soil properties improves model results. Further, results depend on the metal species, so that how metals fractionate between insoluble, dissolved, or particulate forms may be important considerations. Identifying which metals may best indicate metal accumulation and establishing useful models for how metals accumulate in biofilter soils is especially relevant for more contaminated watersheds.

2. How do accumulated soil metals, and soil properties jointly affect the gene expression of nitrifiers and denitrifiers in bioretention soils?

In chapter three, metals appeared to have either a positive or negative effect on functional gene abundances, depending on their biological role, and on their availability, i.e., total vs.

bioavailable metals. However, the presence of functional genes is not always connected to their expression levels, or real process activity. MLR analysis on functional gene transcripts may help to elucidate how metals affect nitrifying and denitrifying bacteria. To explore this question, a combination of field and lab approaches could be used. Field sampling would be as described in Chapter 3 but include sites with low and high metal pollution. An MLR approach would be used to relate functional gene transcripts with soil properties, and soil metals. Field measurements would also include process rates measured on intact soil cores. Mesocosm lab experiments could be used to evaluate potential metal toxicity thresholds, to inform MLR analysis and evaluate the evidence for positive or negative metal effects.

3. To what extent does a treatment train approach, combining a stormwater capture system followed by fast- and slow- draining cells, improve N treatment? What are the implications for NO_3^- and DON removal?

In the third study (Chapter 4), I proposed an alternative configuration for biofilters that might be better suited to remove N, particularly for large, polluted storms. How does a treatment train approach to stormwater biofiltration, combining a stormwater capture system followed by a fast- and slow- draining cells improve N treatment? What are the implications for NO_3^- and DON removal? I hypothesized that separating influent NH_4^+ and DON in the fast- and slow- draining cells, respectively, might provide better treatment. To test the proposed design, lab mesocosms of a traditional vs. a treatment train configuration could be built and similar analysis as in Chapter 4 performed. Additional analysis could include using an ^{15}N isotope-dilution method and labeled NO_3^- and NH_4^+ to estimate N processing rates.